Development of a Model for Estimation of Buried Large Diameter Thin-Walled Steel Pipe

Deflection due to External Loads


By


JWALA RAJ SHARMA


Presented to the Faculty of the Graduate School of

The University of Texas at Arlington in

Partial Fulfillment of Requirements

for the Degree of


DOCTOR OF PHILOSOPHY


THE UNIVERSITY OF TEXAS AT ARLINGTON

MAY 2013

wife Ms. Srishti Pathak, and my sisters Ms. Jyotshna Sharma Tiwari, Ms. Jyoti Sharma Pudasaini, Ms. Jayanti Sharma Rijal, and Ms. Jaya Sharma.

April 16, 2013

Abstract

Development of a Model for Estimation of Buried Large Diameter Thin Walled Steel Pipe

Deflection due to External Loads

Jwala Raj Sharma, Ph.D.

The University of Texas at Arlington, 2013

Supervising Professor: Dr. Mohammad Najafi

Design of buried pipeline systems involves solution of geotechnical and structural problems in addition to the hydraulics and mechanical issues. Just like any buried structure, it is of utmost importance to understand how the pipe interacts with the soil when subjected to external and internal loads. Based on the mode of withstanding loads, pipes are classified into two major categories, which are rigid and flexible pipes. Pipe material is the major factor governing the classification of a pipe being rigid or flexible. Rigid pipe is a pipe which is designed to withstand external dead and live loads and internal pressure loads without deformation. Flexible pipe on the other hand is designed with allowance to deform within a specified limit depending upon the pipe material and type of coatings and linings on the pipe. Designs of flexible pipes are generally based on hydraulic criteria of the pipeline, also known as Hydraulic Design Basis (HDB). Side soil column plays a pivotal role in flexible pipe's ability to withstand external loads.

Pipe diameters and pipe wall thicknesses of flexible pipes are usually designed as per hydraulic requirements, such as, flow capacity, internal fluid pressure, pipe material strength and elasticity, and so on. Analysis of flexible pipe for response to external loads is commonly carried out with proper embedment rather than to increase pipe structural capacity. This approach is rightly adopted because it is much more economical to provide good embedment rather than increasing stiffness of the pipe with increased thickness. Most common methods for flexible pipe analyses to predict pipe deflecions include the Modified Iowa and the Bureau of Reclamation equations.

The Modified Iowa formula and the Bureau of Reclamation equations are semi-empirical methods to predict flexible pipe deflections. The pipe material properties used in these equations are engineering properties. However, the Modulus of soil reaction (E') which is a key property in determining the predicted long term deflection of pipe is an empirical value.

One of the key assumptions in Spangler's (1941) soil pipe interaction model is that the passive soil resistances offered by embedment soil above and below the pipe springline are symmetric. This assumption is addressed in this dissertation, especially for the case of large diameter pipes. It is a widely accepted principle in geotechnical engineering that lateral pressure (active, at-rest or passive) from soil is dependent on depth, with deeper soils with higher lateral forces potential due to greater overburden pressures and also in cases where two different embedment materials are used. The Spangler's model does not consider peaking behavior (increase of vertical diameter) of pipe during embedment construction. There is a need to develop a model to predict pipe behavior due to embedment construction. This model needs to consider the cycle that embedment soil goes through from at-rest conditions (at the time of placement of layer), to active conditions (during peaking deflection), and finally to passive conditions (due to deflection of pipe).

The objectives of this research are to consider engineering properties of embedment soils in analysis of flexible pipe-soil system for external load conditions and develop a new model for prediction of deflection of flexible steel pipe. Full scale laboratory tests were perfomed to develop the new model and finite element models were analysed to validate the test results. In this research, finite element method was effectively used to model the soil pipe interaction for five full scale laboratory tests conducted on a steel pipe. Such models can be used for analysis of flexible pipe embedment design for layered embedment conditions. The results of finite element analysis showed that the squaring of the pipe occurs when haunch soil is weak compared to the side column. Another critical observations made during the tests were stresses at the bottom of pipe and bedding angle. It is desirable that the stress due to surcharge load on top of the pipe, weight of the pipe, and water inside the pipe be distributed uniformly across width of the bedding.

Best results against peaking deflection were obtained with crushed limestone (Test 3) due to lesser lateral earth pressure coefficient and lesser energy required for compaction. Perhaps, that is the reason why peaking deflections in flexible pipe have not been studied extensively in the past. However, if clayey materials are considered, peaking deflections need to be examined closely.

Best results against deflection due to surcharge load were obtained in Test 4 with mixed embedment of crushed limestone and native clay. This was the only case when horizontal deflection due to surcharge load was observed to be approximately equal to vertical deflection in magnitude. This only echoes the importance of haunch area in behavior of pipe. The haunch area consisted of flow-able crushed limestone which was also subjected to compaction energy from compaction of clay embedment above 0.3 diameter. Also, the bedding angle for Test 4 was highest of all tests. The stress at top of pipe was well distributed along the bedding of pipe which is a favorable condition for integrity of bedding.

Table of Contents

List of Illustrations

List of Tables

Chapter 1

Introduction

1.1 General

Not considering effects of internal pressures and/or vacuum loads, the design of buried pipeline systems mainly involves solution of geotechnical and structural problems in addition to the hydraulics and mechanical issues. Just like any buried structure, it is of utmost importance to understand how the pipe interacts with the soil when subjected to external and internal loads (Najafi, 2010). A typical layout of a buried pipe construction is illustrated in Figure 1.1. A trench is excavated and a layer of "bedding" is provided for support at the trench bottom. The bedding is instrumental in uniformly supporting the weight of the pipe, which is loaded internally with fluid and externally with surcharge loads from the top. It is desirable that the bedding does not settle under application of those loads. After the pipe is placed in the trench, different layers of "embedment" are placed above the bedding. Depending upon the type and diameter of the pipe, embedment may be placed up to 30% diameter, 50% of diameter, 70% of diameter, or even one foot above the "crown" of pipe. The area under the pipe springline and above the bedding is known as "haunch," and is the main part of embedment support. It is important to recognize the importance of the haunch area, because during pipeline construction, it is generally difficult to achieve desired compaction and resulting soil properties in this section of embedment. Also, the haunch area and bedding must work together to distribute the load of the pipe to minimize concentrated loading at the bedding and the pipe invert. The soil placed above the embedment to fill the trench is known as "backfill." In this research, the terms "crown", "springline," "invert," "bedding," "haunch," "embedment," and "backfill," will refer to components of a typical buried pipe trench layout as illustrated in Figure 1.1.

Buried pipe is also subjected to dead load of backfill on top of the pipe and, dependent on the backfill depth, the live loads from the ground surface. Buried pipe must be designed to withstand these dead and live loads to maintain the structural integrity of the pipeline. The primary determinant of such structural design is usually the pipe material, soil conditions, and construction method. Based on the mode of withstanding loads, pipes are classified into two major categories, rigid and flexible. Pipe material is the governing factor in rigid or flexible pipeline design and construction.

1
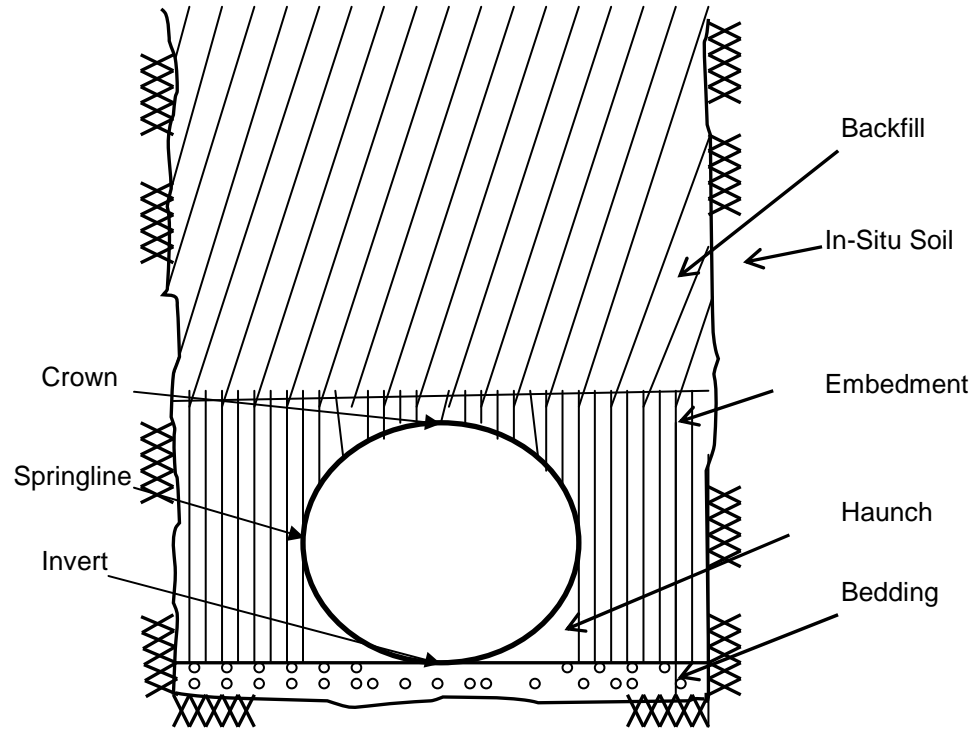
Figure 1.1: Typical Buried Pipe Trench Layout

Rigid pipe is designed to withstand external dead and live loads as well as internal pressure loads with minimum deformation. Primarily, concrete-based pipes, such as Reinforced Concrete Pipe (RCP) and Pre-stressed Concrete Cylinder Pipe (PCCP), Vitrified Clay Pipe (VCP), and Cast Iron (CI) Pipe are classified in this category. Deformation may cause crack in the pipe material and impinge on the structural integrity of the pipe. Generally, rigid pipes are designed to adequately withstand internal and external loads with minimum support of the side soil column (Sharma et al., 2012).

Flexible pipes on the other hand are designed with allowance to deform within a specified limit dependent on the pipe material and type of coatings and linings. Examples of flexible pipes are Steel, High Density Polyethylene (HDPE), Polyvinyl Chloride (PVC), Ductile Iron Pipe (DI), Bar-Wrapped Cylinder Concrete, and Fiberglass Pipes. Design of flexible pipes are generally based on hydraulic criteria of the pipeline, also known as Hydraulic Design Base (HDB). Side soil column plays a pivotal role in flexible pipe's ability to withstand external loads. The allowable deformations for flexible pipes are governed by their respective standards published by American Water Works Association (AWWA). For example, AWWA M11 for steel pipe, AWWA M55 for HDPE pipe, AWWA M41 for DI pipe, AWWA M45 for

fiberglass pipe provide limits on change in diameter, which is termed as deflection. Table 1.1 presents allowable vertical deflection for steel pipe.

Table 1.1: Allowable Deflections for Steel Pipe

| Pipe Material | Allowable Horizontal Deflection | Reference |
|---|---|---|
| Steel: Mortar-lined and coated | 2% of pipe diameter | |
| Steel: Mortar-lined and flexible coated | 3% of pipe diameter | AWWA M11 (2004) |
| Steel: Flexible lined and coated | 5% of pipe diameter | |

1.2 Research Needs and Objectives

Pipe diameters and pipe wall thicknesses of flexible pipes are usually designed per hydraulic requirements, such as flow capacity, internal fluid pressure, pipe material strength and elasticity, and so on. Analysis of flexible pipe for response to external loads is commonly carried out with an objective to use proper embedment rather than to increase pipe structural capacity and stiffness. This approach is rightly adopted because it is much more economical to provide good embedment rather than increasing stiffness of the pipe with increased thickness. Most common methods for flexible pipe analyses to predict pipe deflecions include the Modified Iowa and the Bureau of Reclamation equations. The Steel Pipe Design Manual (AWWA M11, 2004) recommends use of the Modified Iowa Formula presented in Equation 1.1.

$$\Delta x = D_L \left( \frac{K W r^3}{EI + 0.061 E' r^3} \right) \dots\dots\dots\dots\dots\dots\dots\dots\dots\dots\dots\dots\dots\dots\dots\dots\dots\dots\dots(1.1)$$

Where:

$\Delta x$ = Predicted long term horizontal deflection of pipe (in.)

$D_L$ = Deflection lag factor (non-dimensional)

$K$ = Bedding constant (non-dimensional, typically 0.1)

$W$ = Load per unit of pipe (lb/in.)

$r$ = Pipe radius (in.)

$E$ = Modulus of elasticity (psi) of pipe material

$I$ = Moment of inertia of pipe wall per unit length of pipe (in$^4$/in)

$E'$ = Modulus of soil reaction (psi)

Similarly, Bureau of Reclamation equation is presented in Equation 1.2.

3

$$\Delta Y\ (\%)\ =\ T_F\ \frac{0.07\,\gamma\,h}{EI/r^3 + 0.061\,Fd\,E'} \dotfill (1.2)$$

Where,

      $\Delta Y$ = Predicted vertical deflection of pipe (%)

      $T_F$ = Time lag factor (unit-less)

      $\gamma$ = Density of Soil (pcf)

      $h$ = Height of cover (ft)

      $r$ = Pipe radius (in.)

      $E$ = Modulus of elasticity (psi) of pipe material

      $I$ = Moment of inertia of pipe wall per unit length of pipe (in.$^4$/in)

      $F_d$ = Design Factor  (unit-less)

      $E'$ = Modulus of soil reaction (psi)

The Modified Iowa formula and the Bureau of Reclamation equations are semi-empirical methods to predict flexible pipe deflections. The pipe material properties used in these equations are engineering properties. However, the Modulus of soil reaction (E') which is a key property in determining the predicted long-term deflection of pipe is an empirical value. Most commonly used E' values for embedment soils are the ones proposed by Hartley and Duncan (1987) that are based on classification of embedment soils, degree of compaction relative to maximum Proctor density, and the height of backfill. The ones proposed by Howard (1976) and later revised in Howard (2006) are based on classification of embedment soils, and the degree of compaction. The E' values proposed by both Hartley and Duncan (1987) and Howard (1976) are based on statistical analyses of data gathered from a number of flexible pipe installations.

Problem with the use of E' values is that they are obtained by using the original Iowa Model proposed by Spangler (1941). The original Iowa formula published by Spangler (1941) was derived by combining the elastic ring theory and "fill-load hypothesis." Three components of fill-load hypothesis included:

    a. Vertical load on top of pipe can be determined by Marston's theory and is distributed approximately uniformly over the breadth (diameter, see Figure 1.2) of the pipe at the top of the pipe.

b. Vertical reaction at the bottom of pipe is equal to the vertical load on top of the pipe and is distributed uniformly over the bedding width at the contact surface between bedding and the pipe (Figure 1.2).

c. Horizontal pressure on the sides of the pipe are distributed parabolically over the middle of the pipe as shown in Figure 1.2, and the maximum unit pressure is equal to the Modulus of passive pressure of embedment material multiplied by one-half of the horizontal deflection of the pipe.
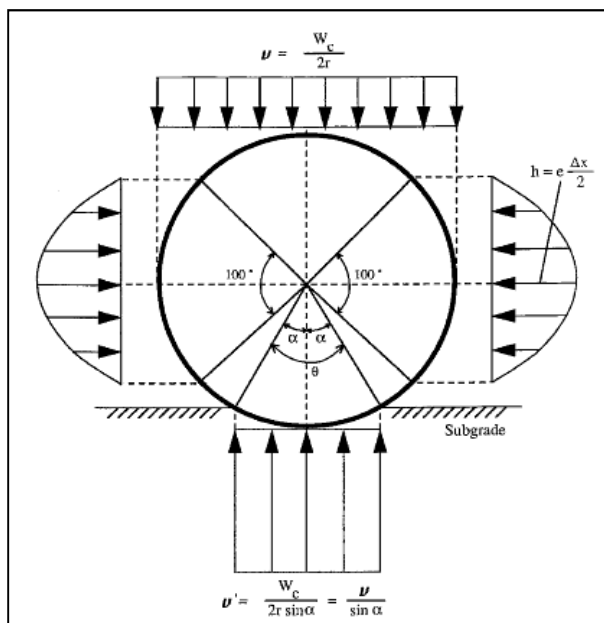


Figure 1.2: Spangler's Hypothesis on Stress Distribution on Flexible Pipe.
Adapted from Masada (2000)

Equation 1.8 presents the original Iowa formula derived by Spangler (1941) .

$$\Delta x = \frac{D_l W_c r^3 K}{EI + 0.061 \, e \, r^4} \dots \dots (1.8)$$

Where,

$\Delta x$ = Horizontal diameter change (in.)

$D_l$ = Time lag factor  (unit-less)

$W_c$ = Vertical load on pipe (lb/in.)

r = Radius of un-deformed pipe (in.)

K = Bedding constant (unit-less)

5

E = Modulus of elasticity of pipe material (psi)

I = Moment of inertia of pipe wall section (in.$^4$/in.)

e = Modulus of passive soil resistance (psi/in.)

Modified Iowa formula replaces product of Modulus of passive soil resistance (e) and radius of pipe (r) by Modulus of soil reaction (E'). Empirical values of E' have been published by Howard (1976), Hartley and Duncan (1987), and Howard (2006).

One of the key assumptions in Spangler's soil pipe interaction model is that the passive soil resistances offered by embedment soil above and below the pipe springline are symmetric. This assumption is questionable from geotechnical engineering point of view, especially in case of large diameter pipes. It is widely accepted principle in geotechnical engineering that lateral pressure (active, at-rest or passive) from soil is dependent on depth, with deeper soils potentially offering higher lateral forces due to greater overburden pressures. This assumption is invalidated in the cases where two different embedment materials are used in layers. Modified Iowa formula and Bureau of Reclamation Equation are based on Spangler's model with Modulus of soil reaction (E') values being fitted to Spangler's model. Two key concerns in using E' values in soil pipe interaction modeling are: (1) validity of Spangler's model to large diameter pipes (more than 24 in.), and (2) subjective results from fitted E' values, since E' values are found based on soil classification rather than soil strength.

Spangler's model does not consider peaking behavior (an increase in pipe's vertical diameter) during embedment construction. Therefore, there is a need to develop a model to predict pipe behavior due to embedment construction. This model needs to consider the cycles that embedment soil goes through, from at-rest conditions (at the time of placement of layer), to active conditions (during peaking deflection), and finally to passive conditions (due to deflection of pipe).

Based on the current models used for prediction of flexible pipe deflection, Howard (1996) ranked embedment material types in the order presented in Table 1.2.

It is a standard practice to use crushed rock as embedment material for large diameter steel pipes. Crushed rocks are expensive and consume a lot of resources to be produced and transported. Design and construction with crushed rock not only increases the project costs, but also increases the

carbon footprint of the project due to energy consumed and $CO_2$ emissions during production and transportation. Therefore, re-using the native material as embedment and backfill can provide great cost savings and a sustainable solution.

Table 1.2: Ordered Ranking of Embedment Materials (Howard 1996)

| Best | Crushed rock with 100% passing the 3 inch sieve, less than 25% passing the 3/8 inch sieve, and less than 12% passing No. 200 Sieve |
| | Well graded gravel (GW), Poorly graded gravel (GP), well graded sand (SW), poorly graded sand (SP), and poorly graded granular soils containing fines (GP-GM, and SP-SC) |
| | Silty gravel (GM), clayey gravel (GC), silty sand (SM) and clayey sand (SC) |
| | Sandy lean clay (CL), sandy silt (ML), or sandy silty clay (CL-ML) or combination of CL/ML or ML/CL containing 30% or more sand and/or gravel |
| | Lean clay (CL)*, silt (ML), or sandy silty clay (CL-ML) or combination of CL/ML or ML/CL containing 30% |
| Worst | Elastic silt (MH), fat clay (CH), organic silt (OL, OH), organic clay (OL, OH), peat (PT) |

* Soil type used for laboratory tests for this research.

It should be noted that the native material used as embedment soil must not compromise strctural integrety of the pipe. Embedment design that is inadequate for the given site conditions can lead to pipe failure. Talesnich and Baker (1999) presented a case of a large diameter steel pipeline failure in Israel due to inadequate design of embedment. In fact, the failure was due to cracking of concrete liner rather than failure of steel. In this case, the alowable deflection of concrete-lined steel pipe was exceeded. Lining strength is a determining factor to limit the allowable deflection of flexible steel pipe as presented in Table 1.1. For previous case, the pipe outer diameter was 47.75 in. and wall thickness was 0.252 in. Figure 1.3 illustrates pipe embedment for this case.

Talesnich and Baker (1999) attributed the failure of the soil under the pipe as the cause of excessive deflection of the pipe. Figure 1.4 illustrates failure of haunch and bedding soil after excavation to investigate the causes of failure.

As listed in Table 1.2, clayey materials are not considered as suitable for embedment construction and sometimes are used as backfill above pipe. Therefore, the main objective of current research is to investigate potential methods to maximize the re-use of native clayey materials as embedment design. To maximize such re-use, strengthening clay by lime stabilization was also investigated. Five full scale laboratory tests were performed to facilitate such investigation and the results

7

were analyzed comparing with current models. Finite element analysis were performed using engineering properties of embedment soils for validation and sensitivity analysis.
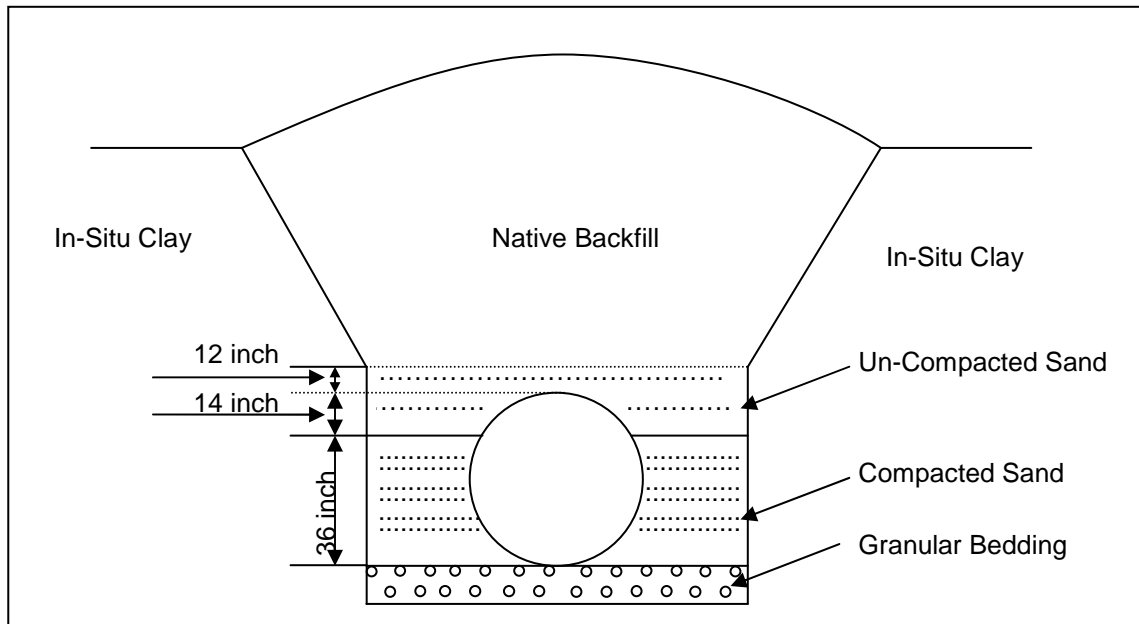


Figure 1.3: Embedment Design Layout of Failed Pipeline
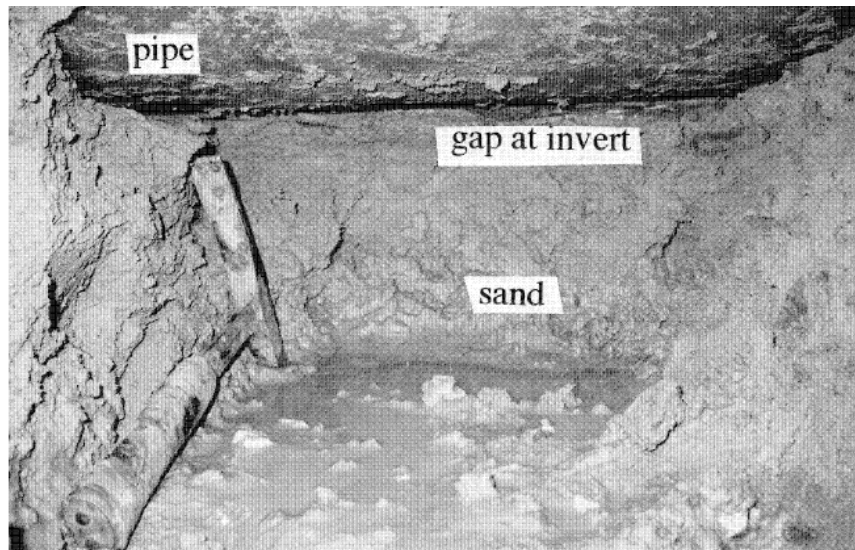


Figure 1.4: Failure of Soil under Pipe
Source: Talesnich and Baker (1999)

1.3 Dissertation Organization

There are 7 chapters following Chapter 1 (Introduction) as described below:

Chapter 2 presents the basic concepts about the role of embedment soils in resistance of external forces in buried flexible pipes. It also consists of a comprehensive literature review conducted as a part of this research. The topics searched include design of flexible pipes, finite element modeling of pipes, constitutive modeling of soils, lateral earth pressure of cohesive soils, and so on. The concepts currently used for flexible pipe design for external loads are discussed and the concepts from geotechnical and structural engineering that are useful for development of a constitutive model for flexible pipe-soil system is reviewed.

Chapter 3 presents the detailed procedure and methodology adopted for the laboratory tests performed for the research. It describes the details of the soil box test, pipe specimen, embedment soil properties, instrumentation details for data acquisition, test setup and step-by-step procedures for each of the five tests performed.

Chapter 4 presents the results of the full scale laboratory tests. The data acquired and the key observations from the tests are presented. The key data include deflection results, earth pressure readings, and pipe wall strains.

Chapter 5 presents the discussion of the laboratory test results. The key observations including deflection ratio (ratio of horizontal deflection to vertical), bedding angle (as described in Spangler's model), lateral earth pressure coefficients and Modulus of soil reaction values obtained by fitting test parameters to modified Iowa and Bureau of reclamation equations are discussed. The calculations of these values are also shown.

Chapter 6 presents the calibration of laboratory testing for the unconsolidated undrained soil test using the Duncan hyperbolic model parameter. The procedure for such calibration is detailed and the calibrated values are presented.

Chapter 7 presents the methodology and description of finite element models (FEM) developed to model the behavior of steel pipe embedded in various soils. The finite element models are analyzed by using PLAXIS 2D software. The results of the analysis are compared to the actual test results validation. This validation facilitates use of finite element method to do further analyses without having to perform the actual laboratory tests. Numerous models were executed with various soil properties and changes in

configurations of the laboratory test. The properties and of soil and pipe parameters are described and the results are presented.

Chapter 8 presents the conclusions and recommendations for future research based on the findings of this research.

<u>1.4 Summary</u>

This chapter presented an introduction to rigid and flexible pipe classification based on how they react to the external loads. Importance of embedment design for flexible pipes as well as current practice for flexible pipe design was discussed. The research needs and objectives were presented. The contents of this dissertation and their organization were summarized.

Chapter 2

Fundamental Concepts and Literature Review

2.1 Introduction

This chapter presents the basic concepts about the role of embedment soil in resisting external forces in buried flexible pipes. It also consists of a comprehensive literature review conducted as a part of this research. The subjects searched include design of flexible pipes, finite element modeling, constitutive modeling of soils, lateral earth pressure of cohesive soils, and so on. The geotechnical and structural engineering concepts currently used for flexible pipe design for external loads are discussed.

2.2 Flexible Pipe Design Concept

Figure 2.1 illustrates the concept for flexible pipe behavior under external loads. Figure 2.1 (a) represents the flexible pipe with spring stiffness of 2k. To take advantage of the two-fold symmetry, the pipe is represented by a quadrant arc. Figure 2.1 (b) illustrates flexible pipe response to lateral embedment pressure, where vertical elongation is equal to vertical deflection. Figure 2.1 (c) illustrates typical behavior of a flexible pipe under application of a load F. Deflections are observed in both horizontal and vertical springs and are equal in magnitude of $U_1$. Equation 2.1 presents the energy state of the pipe quadrant when force F is applied.

$$\text{Total Energy, } E = F \times U_1 - k \times U_1^{\,2} \dots\dots\dots\dots\dots\dots\dots\dots\dots\dots\dots\dots\dots\dots\dots(2.1)$$

Because change in energy is zero, $U_1$ can be calculated by differentiating total energy with respect to $U_1$. The calculated deflection is given in Equation 2.2.

$$U_1 = F/2k \dots\dots\dots\dots\dots\dots\dots\dots\dots\dots\dots\dots\dots\dots\dots\dots\dots\dots\dots\dots\dots\dots\dots(2.2)$$

Figure 2.1 (d) illustrates a case where soil spring stiffness of $(k_s/a^2)$ is added as side support such that magnitude of deflection of vertical spring is $U_2$ and that of horizontal spring is $(a \times U_2)$. Constant a is introduced to acknowledge the fact that when side support is provided, change in horizontal and vertical diameters are not equal in magnitude. The practical value of constant a is less than 1. Equation 2.3 represents energy state of the system corresponding to Figure 2.1 (d).

$$\text{Total Energy, } E = F \times U_2 - k/2 \times U_2^{\,2} - (k + k_s/a^2)/2 \times a^2 \times U_2^{\,2} \dots\dots\dots\dots\dots(2.3)$$
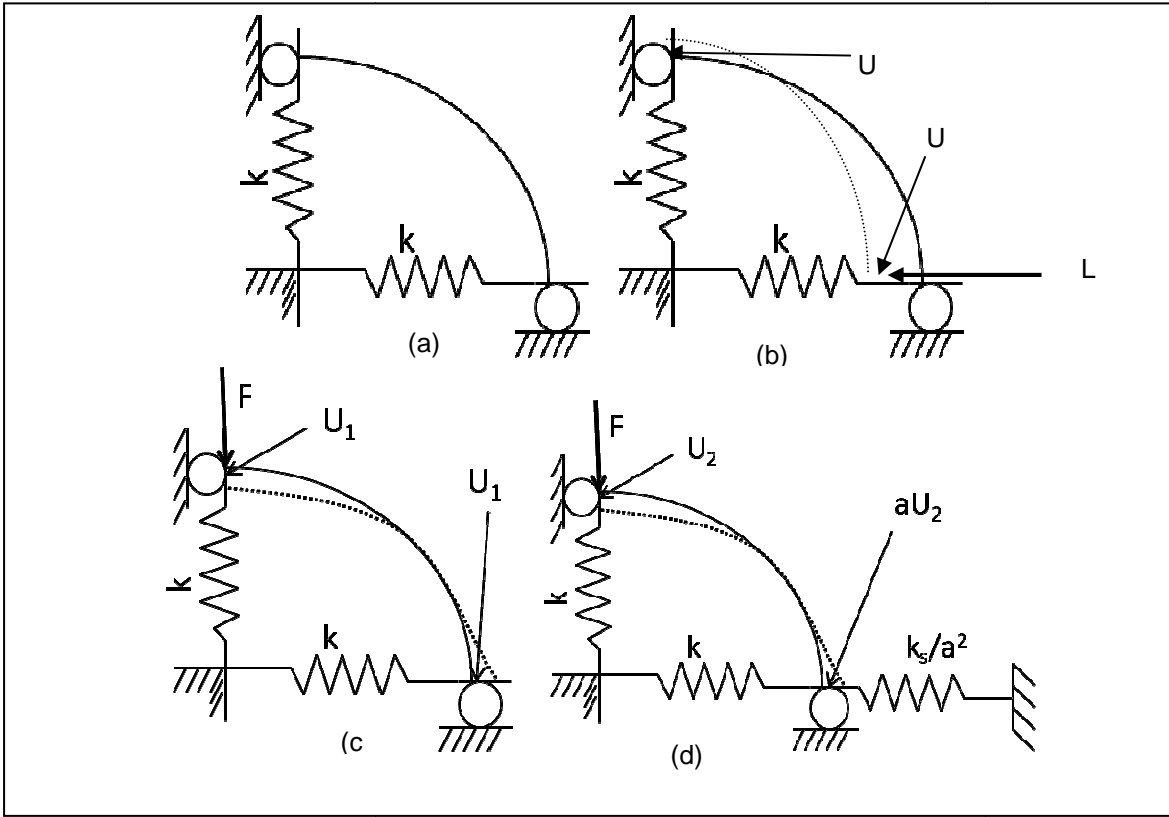
Figure 2.1: (a) Flexible Pipe Represented with Spring Stiffness; (b) Flexible Pipe under Lateral Soil Load; (c) Flexible Pipe under Backfill Load, (d) Flexible Pipe with Added Soil Spring Stiffness

Again, the result of differentiating total energy with respect to deflection is given in Equation 2.4.

$$U_2 = F/(k + a^2k + k_s) \dots\dots\dots\dots\dots\dots\dots\dots\dots\dots\dots\dots\dots\dots\dots\dots\dots\dots\dots\dots\dots (2.4)$$

Assuming a to be equal to 1, Equations 2.2 and 2.4 can be used to derive Equation 2.5 which shows the significance of soil stiffness in reducing deflection of pipe diameter.

$$U_2 = U_1/(1 + k_s/2k) \dots\dots\dots\dots\dots\dots\dots\dots\dots\dots\dots\dots\dots\dots\dots\dots\dots\dots\dots\dots\dots\dots (2.5)$$

### 2.3 Vertical Soil Load on Buried Pipe

Marston and Anderson (1913) developed methods for calculating earth load on buried pipe (Moser, 2001). The equation for calculating earth load on the crown of the pipe proposed by Marston and Anderson (1913) is known as Marston Load and is presented in Equation 2.6.

$$W_c = \gamma\, B_d^{\,2}\, (1 - e^{-2K\mu'(H/Bd)})/2K\mu' \dots\dots\dots\dots\dots\dots\dots\dots\dots\dots\dots\dots\dots\dots\dots\dots\dots\dots (2.6)$$

Where,

$W_c$ = Load on top of pipe (lb/ft)

12

γ = Unit weight of backfill material (lb/ft$^3$)

$B_c$ = Diameter of Pipe (ft)

$B_d$ = Horizontal width of trench at top of the pipe (ft)

H = Height of backfill (ft)

K = Rankine's active lateral earth pressure coefficient (unit-less)

μ' = Coefficient of friction between backfill and trench wall (unit-less)

e = Base of natural logarithms (unit-less)

Equation 2.7 is based on arching theory which calculates vertical pressure on voids. On undeformed pipe, there is no void between top of the pipe and the backfill soil. Therefore, it is a common practice to analyze flexible pipe with soil prism load, as recommended by AWWA M11 (2004), as presented by Equation 2.7.

$$W_c = γ \, B \, H \dotfill (2.7)$$

Where,

$W_c$ = Load on pipe (lb/ft)

γ = Unit weight of backfill material (lb/ft$^3$)

B = Diameter of Pipe (ft)

H = Height of backfill (ft)

Final pressure on top of a flexible pipe, after void is induced due to deflection of pipe, may be calculated by Equation 2.3 presented by Marston, Anderson and Terzhagi (After McKelvey III, 1994).

$$ρ_a = B \, (γ − 2c/B) \, (1 − e^{-2Kμ'(H/Bd)})/2Kμ' \dotfill (2.8)$$

Where,

$ρ_a$ = Earth pressure on top of pipe (lb/ft$^2$)

γ = Unit weight of backfill material (lb/ft$^3$)

B = Width of void (for rectangular void) or radius of void (for circular void) (ft)

c = Cohesive strength of backfill soil (lb/ft$^2$)

H = Height of backfill (ft)

K = Rankine's active lateral earth pressure coefficient (unit-less)

μ' = Coefficient of friction between backfill and trench wall (unit-less)

e = Base of natural logarithms (unit-less)

<u>2.4 Lateral Earth Pressures</u>

Lateral earth pressures on retaining earth structures have been studied since Coulomb presented his theory in 1973 (Das, 2004). Lateral earth pressures on large diameter pipe are important in the behavior of pipe-soil system. However, study on such pressures during pipe installation is limited. In comparison, retaining earth structures are generally straight in shape with vertical or inclined alignment, and without any curvature. The question is whether lateral pressure theories that are used in retaining earth structures design are applicable in estimating earth pressures on buried pipeline. Available lateral earth pressure theories are discussed in this section.

Robinson (1982) listed four categories for determination of lateral force or pressure on retaining earth structures:

a) Static limit equilibrium methods based on equilibrium of a failure wedge (Rankine and Coulomb lateral earth pressure theories, and membrane method),

b) Static limit equilibrium methods based on finite slice elements, or method of slices (Methods developed by Janbu (1957), Shields and Tolunay (1973), and Basudhar and Madhav (1980),

c) Methods based on constitutive laws of stress strain in soil, and

d) Methods based on constitutive laws of stress and strain applied at design stress levels.

Methods in categories (c) and (d) above are not widely used in engineering practice due to requirement of complete numerical solutions with significant computational difficulties (Robinson, 1982). In static equilibrium methods, assumptions concerning the shape of failure surface, stress at wall, how friction is developed in soil, and how vertical shear stress is dissipated are made. Most common method used in design of earth retaining structures is Rankine earth pressure theory according to which lateral earth pressure on earth retaining structure is given by Equation 2.9.

$$\sigma_{a/p} = \sigma_v \, K_{a/p} \pm 2 \, c \, \sqrt{K_{a/p}} \quad\text{................................................................................(2.9)}$$

Where,

$\sigma_{a/p}$ = Active or passive lateral earth pressure (lb/ft$^2$)

$\sigma_v$ = Vertical earth pressure (lb/ft$^2$)

$K_{a/p}$ = Rankine active or passive earth pressure coefficient (unit-less)

c = Cohesive strength of soil (lb/ft$^2$)

± = Positive for passive and negative for active

Active and passive lateral pressure coefficients represent the limit (or yielding) states in soil and are functions of strength of soil represented in Mohr-Coulomb yielding criteria (Michalowski, 2005). It is important to study lateral pressure on pipe at rest condition. Lateral pressure at rest falls between active and passive lateral pressures and can be used as initial stress condition for evaluation of final stresses. In flexible pipe, it becomes more important in order to predict pipe elongation due to embedment. Jaky (1944) derived coefficient of lateral earth pressure at rest as a function of angle of internal friction of soil, which is presented in Equation 2.10.

$$K_0 = 1 - \sin \varphi \quad \text{..............................................................................................(2.10)}$$

Where,

$K_0$ = Lateral earth pressure coefficient at rest  (unit-less)

$\varphi$ = Angle of internal friction of soil (degrees)

Brooker and Ireland (1965), after a set of tests, confirmed that the expression for lateral earth coefficient at rest presented in Equation 2.10 was useful, although they found that expression in Equation 2.11 matched better to their results. Brooker and Ireland (1965) also proposed Equation 2.12 as lateral earth coefficient at rest for plastic soils.

$$K_0 = 0.95 - \sin \varphi \quad \text{.........................................................................................(2.11)}$$

$$K_0 = 0.4 + 0.007 \, (PI) \quad \text{...................................................................................(2.12)}$$

Where,

PI = Plasticity Index of soil (%)

In addition to active, passive and at-rest pressures, it is also imperative to study the effects of compaction forces. According to Ingold (1980), Sowers et al published the first quantitative work on effects of compaction on lateral earth pressures in 1957. The study, carried out on compacted clay behind 6 ft high retaining wall, and compacted sand behind 5 ft deep concrete lined pit, showed that measured

earth pressures were considerably higher than those predicted by classical earth pressure theory. Ingold (1980) proposed Equation 2.13 to quantify the maximum lateral pressure due to compaction.

$$\sigma'_{hm} = \sqrt{\frac{2P\gamma}{\pi}} \quad\text{.............................................................................................(2.13)}$$

Where,

$\sigma'_{hm}$ = Maximum lateral pressure (psi) due to compaction at critical depth $z_c$

P = Infinitely long surface line load (lb/in.)

$\gamma$ = Density of soil (lb/in.$^3$)

$$z_c = K_a \sqrt{\frac{2P}{\pi\gamma}}$$

$K_a$ = Active earth pressure coefficient (unit-less)

Lateral earth pressure theories will not only be useful to evaluate the stress at the pipe, but also to evaluate the strength of trench wall support and its overall influence on soil pipe interaction.

## 2.5 Soil Constitutive Models

Soils are heterogeneous materials with behaviors that are strongly influenced by grain size, mineralogy, structure, pore water pressure, initial stress state, etc. and are also characterized by time dependent modifications (creep) (Popa and Batali, 2010). There are numerous constitutive laws associated to soils which are used in modeling of soil behavior based on type of soil, nature of the problem, etc. A list of popular soil constitutive models is presented below:

a. Mohr-Coulomb elastic-perfectly plastic model,

b. Drucker-Prager plasticity model (Drucker and Prager, 1952),

c. Cam-clay model (Roscoe et al., 1963),

d. Modified Cam-clay model (Roscoe and Burland, 1968),

e. Duncan hyperbolic model (Duncan et al., 1980),

f. Vermeer nonlinear elastic - hardening plastic model (Vermeer, 1982),

g. Hardening soil model (Schanz et al., 1999),

h. Undrained soft clay model (Hsieh et al., 2010), etc.

## 2.5.1 Duncan Hyperbolic Model

Selig (1988) recommended use of Duncan hyperbolic model for design and analysis of buried pipelines. Duncan hyperbolic model is a nonlinear elastic model which represents the stress-strain behavior (both axial and volumetric) of the soil before failure by Mohr-Coulomb yield criteria. Duncan hyperbolic model is appropriate to employ in buried flexible pipeline design because priority is to model the movement in soil (that results in movement of pipe) before failure, rather than to a model soil behavior post failure. Duncan hyperbolic model and method to calibrate its model parameter is described below.

Duncan hyperbolic model uses five parameters to define Young's Modulus of elasticity at any given stress state. The parameters are listed and defined in Table 2.1. These parameters must be calibrated based on the triaxial test results on test samples. During triaxial test, soil is placed in the cylindrical triaxial cell and confined by a hydrostatic pressure of $\sigma_3$. Then, the soil is subject to a deviator stress, q, until shear failure of the sample occurs. This is illustrated in Figure 2.2. The hyperbolic function representing the stress-strain relationship from the triaxial test is given by Equation 2.14.

Table 2.1: Parameters for Duncan and Selig Model for Modulus of Elasticity

| Parameter | Definition |
|---|---|
| $R_f$ | Failure Ratio (Unit-less) |
| K | Dimensionless Parameter (Unit-less) |
| N | Dimensionless Parameter (Unit-less) |
| C | Cohesive Strength (psi) |
| Φ | Internal Angle of Friction (degrees) |

$$q = \varepsilon/(1/E_i + \varepsilon/q_u) \quad \text{.............................................................................(2.14)}$$

Where,

$E_i$ = Initial tangential Modulus (psi)

$q_u$ = Ultimate deviator stress at large strain (psi)

$\varepsilon$ = Axial strain (unit-less)

Equation 2.15 can be written in the form:

$$\varepsilon/q = 1/E_i + \varepsilon/q_u \quad \text{.............................................................................(2.15)}$$
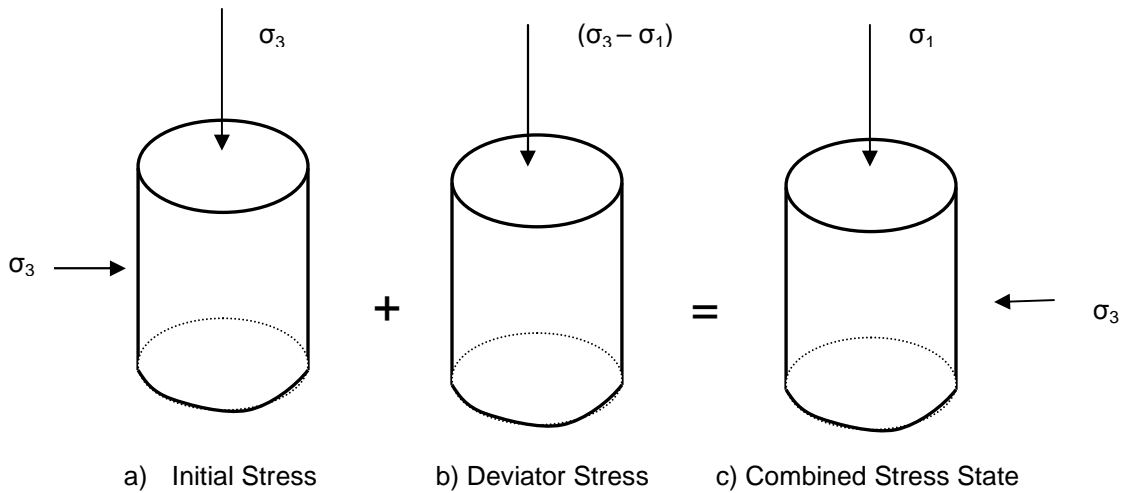
Figure 2.2: Triaxial Test Stresses

Equation 2.6 represents equation of the straight line when $\varepsilon/q$ is plotted against $\varepsilon$. To calibrate $q_u$ and $E_i$, $\varepsilon/q$ for each load increment is plotted against axial strain as illustrated in Figures 2.3.

The failure ratio, $R_f$ is given by Equation 2.16.

$$R_f = q_f/q_u \dotfill (2.16)$$

Where,

$q_f$ = deviator stress at failure obtained from the triaxial test (psi)
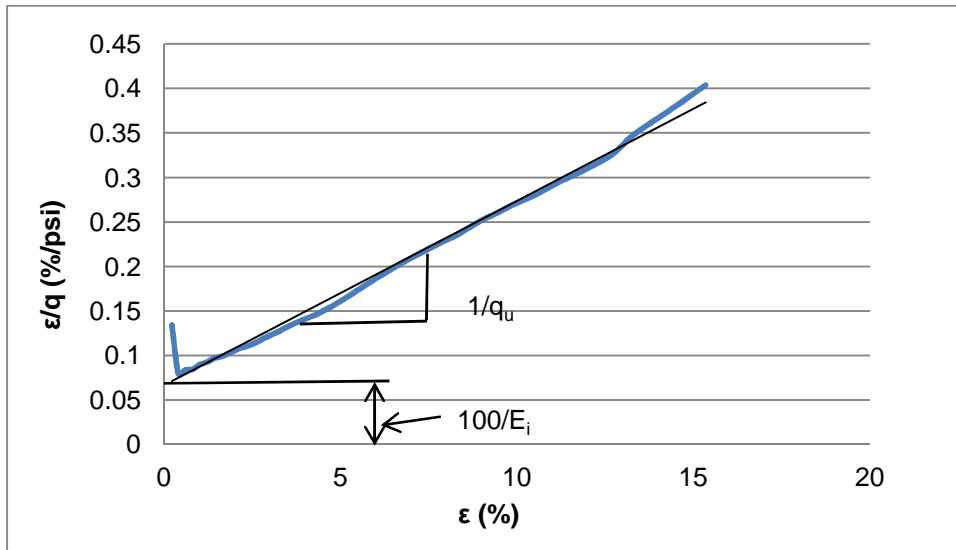


Figure 2.3: Calibration of $E_i$ and $q_u$

Duncan hyperbolic model assumes that the initial tangential Modulus of elasticity increases with confining pressure and this increase is represented by Equation 2.17.

$$E_i = K \, P_a \, (\sigma_3/P_a)^n \dots\dots\dots\dots\dots\dots\dots\dots\dots\dots\dots\dots\dots\dots\dots\dots\dots(2.17)$$

Where,

$E_i$ = Initial Tangential Modulus of Elasticity (psi)

K and n are model parameters

$\sigma_3$ = Confining pressure (psi)

$P_a$ = Atmospheric pressure (psi)

Equation (2.17) can be simplified as:

$$\ln (E_i/P_a) = \ln K + n \ln (\sigma_3/P_a) \dots\dots\dots\dots\dots\dots\dots\dots\dots\dots\dots\dots\dots(2.18)$$

Equation (2.18) is an equation of a straight line in slope-intercept form. Parameters K and n can be calibrated by plotting $\ln (E_i/P_a)$ vs. $\ln (\sigma_3/P_a)$ as illustrated in Figure 2.4.

Internal angle of friction and cohesive strength of soil are related to the Mohr-Coulomb failure criteria and can be calibrated by drawing Mohr circle from the triaxial tests. Once all five parameters are calibrated, stress-strain behavior of soil can be predicted by Young's Modulus of elasticity at any given stress state in soil represented by Equation 2.19.
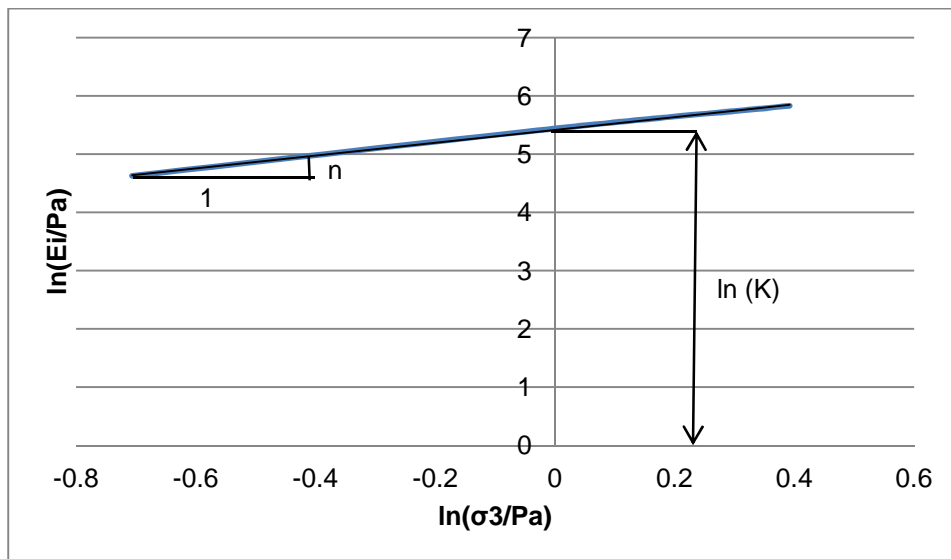


Figure 2.4: Calibration of K and n

$$E_t = [1 - R_f (1 - \sin \Phi) \, q/(2 \, C \cos \Phi + 2 \, \sigma_3 \sin \Phi)]^2 \, K \, P_a \, (\sigma_3/P_a)^n \quad \text{...................(2.19)}$$

Where,

$E_t$ = Young's Modulus of Elasticity (psi)

Volumetric stress-strain behavior of soil is modeled by using soil bulk Modulus, B, represented in Equation 2.20.

$$B = \frac{\Delta \sigma_m}{\Delta \varepsilon_{vol}} \quad \text{...................................................................................(2.20)}$$

Where,

$\Delta \sigma_m$ = Change in mean stress (psi)

$\Delta \varepsilon_{vol}$ = Change in volumetric strain (psi)

Equation 2.21 represents the variation of B with $\sigma_3$.

$$B = K_b \, P_a \, (\sigma_3/P_a)^m \quad \text{.........................................................................(2.21)}$$

Where,

B = Bulk Modulus of Elasticity (psi)

$K_b$ and m are model parameters

$\sigma_3$ = Confining pressure (psi)

$P_a$ = Atmospheric pressure (psi)

Equation 2.21 can be represented as Equation 2.22, and therefore, $K_b$ and m are calibrated by plotting ln (B/Pa) against ln ($\sigma_3/P_a$) as illustrated in Figure 2.5.

$$\ln (B/P_a) = \ln K_b + m \ln (\sigma_3/P_a) \quad \text{...................................................(2.22)}$$

Selig (1988) carried out consolidated drain triaxial tests on different types of soils at different compaction levels and recommended the model parameters for those soils at provided compaction levels through consolidated drained triaxial tests. Selig (1988) also provided lateral earth pressure coefficient ($K_o$) and wet unit weight for the soils. The $K_o$ and wet unit weight are important to quantify initial stress state of the soil. Selig (1988) recommended consolidated drained triaxial tests to calibrate model parameters for embedment soils.
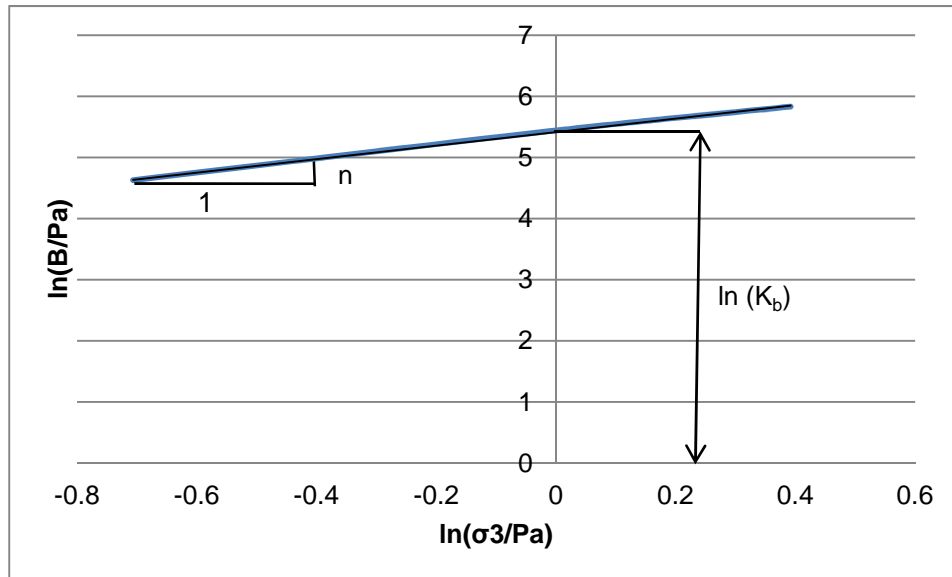
Figure 2.5: Calibration of $K_b$ and n

2.5.2 Hardening Soil Model

The Hardening soil model is a hypo-elastic model developed by Schanz et al. (1999). It is very similar to Duncan Hyperbolic Model in terms of modeling the loading curve. However, hardening soil model adds unloading criteria to the constitutive model. The failure criteria for hardening soil model are same as Duncan hyperbolic model. Hardening soil model uses secant Modulus to model the stress strain relationship. This relation is given by Equations 2.23.

$$E_{50} = E_{50}{}^{ref} \{(\sigma_3 + c.cot\varphi)/(\sigma^{ref} + c.cot\varphi)\}^m \text{.....................................................(2.23)}$$

Where,

$E_{50}$ = Confining stress dependent stiffness of primary loading (psi)

$E_{50}{}^{ref}$ = A reference stiffness Modulus corresponding to $\sigma^{ref}$ (psi)

$\sigma^{ref}$ = Reference stress (psi)

$\sigma_3$ = Confining pressure (psi)

m = Amount of stress dependency (unit-less)

2.6 Previous Tests on Large Diameter Steel Pipe

Webb et al. (2002) and Kawabata et al. (2006) presented results of tests on thin walled steel pipes of diameters comparable to selected tests for this research and conducted at CUIRE Laboratory.

However, previous tests were performed in the field, but the results of the field tests can be compared to that of the laboratory tests.

Webb et al. (2002) presented test results on 123–in. outer diameter steel pipe with wall thickness of 0.394 in. (D/t of 313). Webb et al. (2002) also reported on test results on stiffened 123 in. outer diameter steel pipe with wall thickness of 0.236 in. (D/t of 522). The tests carried out on unstiffened steel pipes consisted of 20 ft deep trenches with 12 in. bedding, 20 in. flowable fill embedment, and weathered granite (8–in. layers) embedment up to one foot above pipe compacted to 90% and 80% Modified AASHTO (T-180) maximum dry density. Pipe deformation result was that the peaking deflection occurred due to compaction of embedment soil. Webb et al. (2002) concluded that well compacted embedment provided better support to the pipe but had larger peaking deformations due to compaction.

Kawabata et al. (2006) presented test results on 138–in. diameter steel pipe with a wall thickness of 1.024 in. (D/t of 135). Two tests as illustrated in Figure 2.6 were conducted. In both tests, initial elongations of pipes were observed. Compressive strains were measured at crown and invert of the pipe while tensile strains were observed at the springlines of the pipe. Horizontal pressure at springline of the pipe exceeded the vertical pressure at top of the pipe in both cases.
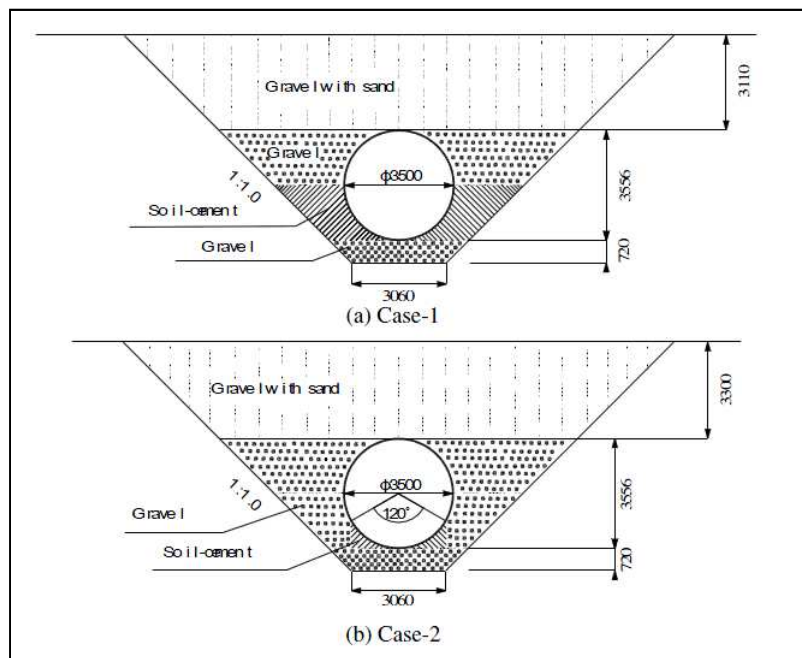


Figure 2.6: Field Tests by Kawabata et al. (2006) (Dimensions are in mm)

<u>2.7 Soil-Pipe Interaction</u>

Original Iowa formula published by Spangler (1941) was derived by combining the elastic ring theory and "fill-load hypothesis." The assumptions and description of this model were presented in Section 1.2 and Figure 1.2.

The Modified Iowa formula, also discussed in Chapter 1, replaces product of Modulus of passive soil resistance (e) and radius of pipe (r) by Modulus of soil reaction (E'). As said earlier, Empirical values of E' have been published by Howard (1976), Hartley and Duncan (1987), and Howard (2006).

The Iowa formula in its original and modified forms predicts the change in horizontal diameter of pipe. Howard (1976) proposed Bureau of Reclamation equation to predict vertical deflection of flexible pipe. Bureau of Reclamation equation was discussed in Chapter 1. Masada (2000) derived relation between horizontal and vertical diameter changes, presented in Equation 2.24, based on original work by Spangler (1941) without any changes to the assumptions made to derive the Iowa equation.

$$\left|\frac{\Delta y}{\Delta x}\right| \approx 1 + \frac{0.0094\, E'}{(PS)} \quad\text{................................................................................................(2.24)}$$

Where

Δx = Horizontal diameter change (in.)

Δy = Vertical diameter change (in.)

E' = Modulus of soil reaction (psi)

(PS) = Pipe stiffness (psi)

Masada (2000) reported strong correlation of deflection ratio (Δy/Δx) to bedding angle (θ in Figure 1.2). The deflection ratio decreased with increase in bedding angle.

Based on methodology similar to Spangler (1941), Masada and Sargand (2007) derived formulas to predict peaking deflections of thermoplastic flexible pipe. Peaking deflections are defined as diametric changes due to vertical elongation during embedment process. Peaking of flexible pipe is illustrated in Figure 2.7. In order to derive peaking deflection formula, Masada and Sargand (2007) made assumptions similar to Spangler (1941). These assumptions are illustrated in Figure 2.8. Equation 2.25 is derived for peaking deflection by Masada and Sargand (2007).

23
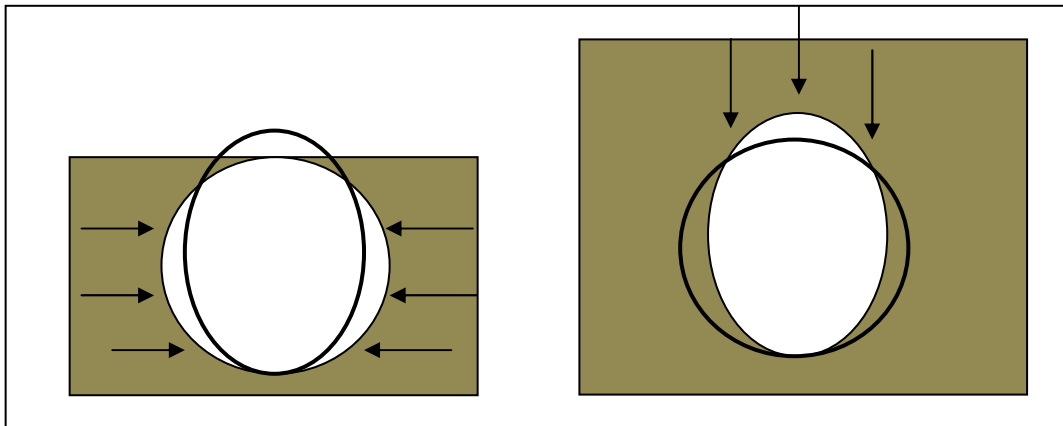
Figure 2.7: (a) Peaking due to Lateral Forces of Embedment, (b) Deflection due to
Backfill Cover
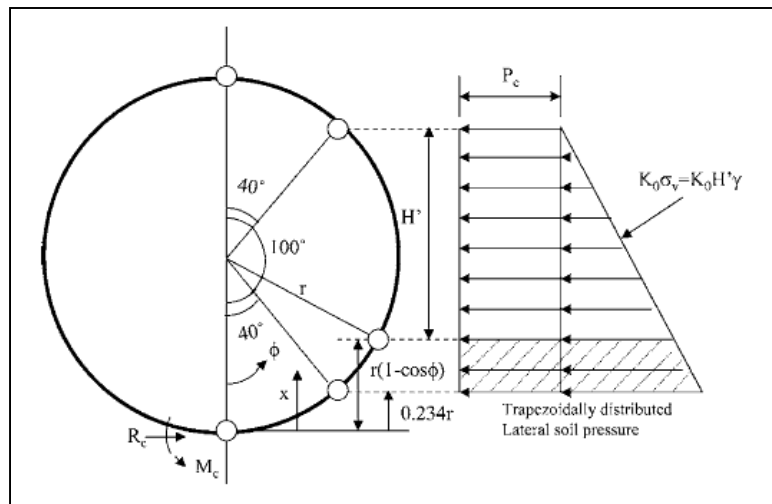


Figure 2.8: Lateral Forces on Pipe During Embedment.
Source: Masada and Sargand (2007)

$$\left|\frac{\Delta y}{D}\right| = \left|\frac{\Delta x}{D}\right| = \frac{4.7\ P_c + K_0 r\ \gamma}{3.874\ (PS)} \dots\dots\dots\dots\dots\dots\dots\dots\dots\dots\dots\dots\dots\dots\dots\dots\dots\dots\dots\dots\dots\dots(2.25)$$

Where

$\Delta x$ = Horizontal diameter change (in.)

$\Delta y$ = Vertical diameter change (in.)

D = Diameter of pipe (in.)

$P_c$ = Lateral force generated by compaction (lb/in.)

$K_0$ = Coefficient of lateral earth pressure (dimensionless)

24

r = Radius of pipe (in.)

γ = Wet density of embedment soil (lb/in.$^3$)

PS = Pipe stiffness (psi)

Other methods to predict vertical deflections of flexible pipes are ones proposed by Greenwood and Lang (1990), and Miles and Schrock (1998). Equations 2.26 and 2.27 are expressions for prediction of vertical deflections as per Greenwood and Lang (1990), and Miles and Schrock (1998) respectively.

$$\delta_{vl} = \frac{k_x\left(\frac{\Delta V}{\Delta H}\right)(C_l\,\gamma\,H + W_l)}{8\frac{C_{TP}EI}{D^3} + 0.061\,(0.6\,\xi)E_s}$$ ....................................................................................(2.26)

Where,

$\delta_{vl}$ = Vertical diameter change (in.)

$k_x$ = Bedding factor (dimensionless)

$\frac{\Delta V}{\Delta H}$ = Deflection ratio (dimensionless)

$C_l$ = Soil arching factor (dimensionless)

γ = Density of backfill soil (lb/in.$^3$)

H = Height of backfill (in.)

$W_l$ = Live load (lb/in.)

$C_{TP}$ = Pipe stiffness retention factor (dimensionless)

E = Modulus of elasticity of pipe material (psi)

I = Moment of inertia of pipe wall section (in.$^4$/in.)

D = Pipe stiffness diameter (in.)

ξ = Leonhardt trench width factor (dimensionless)

$E_s$ = Long term soil creep Modulus (psi)

$$\delta_v = \frac{k_x\left(\frac{dy}{dx}\right)(C_l\,\gamma\,H + W_l)}{S_p + 0.061\,\xi\,C_w C_l E_b}$$ ....................................................................................(2.27)

Where

$\delta_v$ = Vertical diameter change (in.)

$k_x$ = Bedding factor (dimensionless)

$\frac{dy}{dx}$ = Deflection ratio (dimensionless)

$C_l$ = Soil arching factor (dimensionless)

$\gamma$ = Density of backfill soil (lb/in.$^3$)

$H$ = Height of backfill (in.)

$W_l$ = Live load (lb/in.)

$S_P$ = Pipe stiffness (psi)

$\xi$ = Leonhardt trench width factor (dimensionless)

$C_w$ = Construction testing factor (dimensionless)

$E_b$ = Embedment zone soil Modulus (psi)

Leonhardt trench width factor used in Equations 2.26 and 2.27 is given by Equation 2.28.

$$\xi = \frac{1.622 + 0.639\left(\frac{B}{D} - 1\right)}{\left(\frac{B}{D} - 1\right) + \left[1.662 - 0.361\left(\frac{B}{D} - 1\right)\right]\frac{E_b}{E_s}} \dots\dots\dots(2.28)$$

Where,

$\xi$ = Leonhardt trench width factor (dimensionless)

$B$ = Excavation trench width (in.)

$D$ = Pipe diameter (in.)

$E_b$ = Embedment zone soil Modulus (psi)

$E_s$ = In-situ soil Modulus (psi)

### 2.8 Summary

This chapter presented the basic concept about the role of embedment soil in resisting external forces in buried flexible pipe. It also consisted of a comprehensive literature review conducted as a part of this research. The subjects searched included design of flexible pipes, finite element modeling of pipe, constitutive modeling of soils, lateral earth pressure of cohesive soils, and so on. The concepts currently used for flexible pipe design for external loads were discussed and the concepts from geotechnical and structural engineering that are useful for development of constitutive models of flexible pipe-soil system were reviewed.

Chapter 3

Laboratory Tests

3.1 Introduction

This chapter presents the detailed procedure and methodology adopted for the laboratory tests performed for the research. It describes the details of the test soil box, pipe specimen, embedment soil properties, instruments used for data acquisition and their locations, test setup and step by step procedure for each of the five tests performed.

Five full scale tests static load test on a 72-inch diameter steel pipe were conducted inside a unique soil box located at the CUIRE Facility at UT Arlington. The objectives of these tests are:

a) to compare the test results to existing pipe deflection models,

b) to calibrate the finite element model, and

c) to develop a new model for pipe soil interaction based on test results and calibrated finite element model.

Summary of embedment used for the five laboratory tests and their construction durations are listed in Table 3.1.

Table 3.1 Summary of Soil box Tests

| Test | Description | Construction Duration |
|------|-------------|----------------------|
| Test 1 | Pea gravel bedding, native clay (B6) embedment up to 1 foot above pipe, long construction duration | 1/18/2011 – 5/2/2011 (15 Wks) |
| Test 2 | 6% lime treated (B6) bedding, 6% lime treated (B6) embedment up to 0.5 diameter of pipe, native clay (B6) up to 1 foot above pipe | 9/19/2011 – 11/2/2011 (6 Wks) |
| Test 1 (a) | Pea gravel bedding, native clay (B6) embedment up to 1 foot above pipe, short construction duration | 2/27/2012 – 3/2/2012 (5 Days) |
| Test 3 | Crushed limestone bedding, crushed limestone embedment up to 1 foot above pipe, short construction duration | 4/24/2012 – 4/26/2012 (3 Days) |
| Test 4 | Crushed limestone bedding, crushed limestone embedment up to 0.3 Diameter of pipe, native clay (B6) up to 1 foot above pipe, short construction duration | 6/19/2012 – 6/22/2012 (4 Days) |

## 3.2 Test Location

The soil box tests were performed at the laboratory facility of Center for Underground Infrastructure Research and Education (CUIRE) at The University of Texas at Arlington. Figure 3.1 presents the location of the CUIRE lab and the stockpile location for native backfill soil and pea gravel.
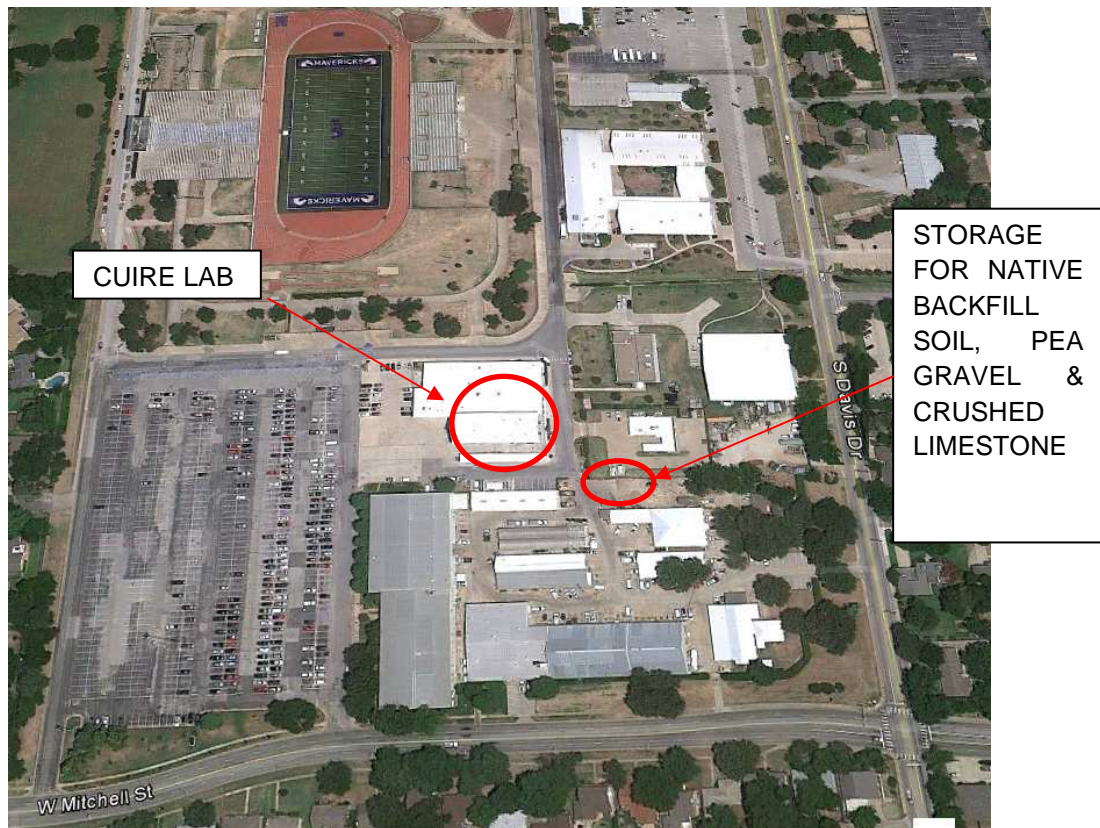


Figure 3.1: Location of CUIRE Lab Facility

## 3.3 Soil Box

The concrete soil box at the CUIRE lab consists of 3,000 psi reinforced concrete walls and floor. It is 25-ft long, 12.5-ft wide and 10-ft high. Based on the requirements of the test, modifications were made to the concrete soil box. A wooden bulkhead was constructed to reduce the length of the concrete load cell to 21 ft. This provided 4 ft of working space at the north side of the load cell. The entry inside the pipe for installation of instruments was made possible due to this modification. A wooden frame was constructed to provide 8-ft high walls on all sides to facilitate additional static load of cover. Figure 3.2

illustrated soil box after placement of bedding layer for Test 1. Figures 3.3 and 3.4 illustrate the dimensions of soil box before and after modifications respectively.



Figure 3.2: Soil Box with Bedding Layer for Test 1
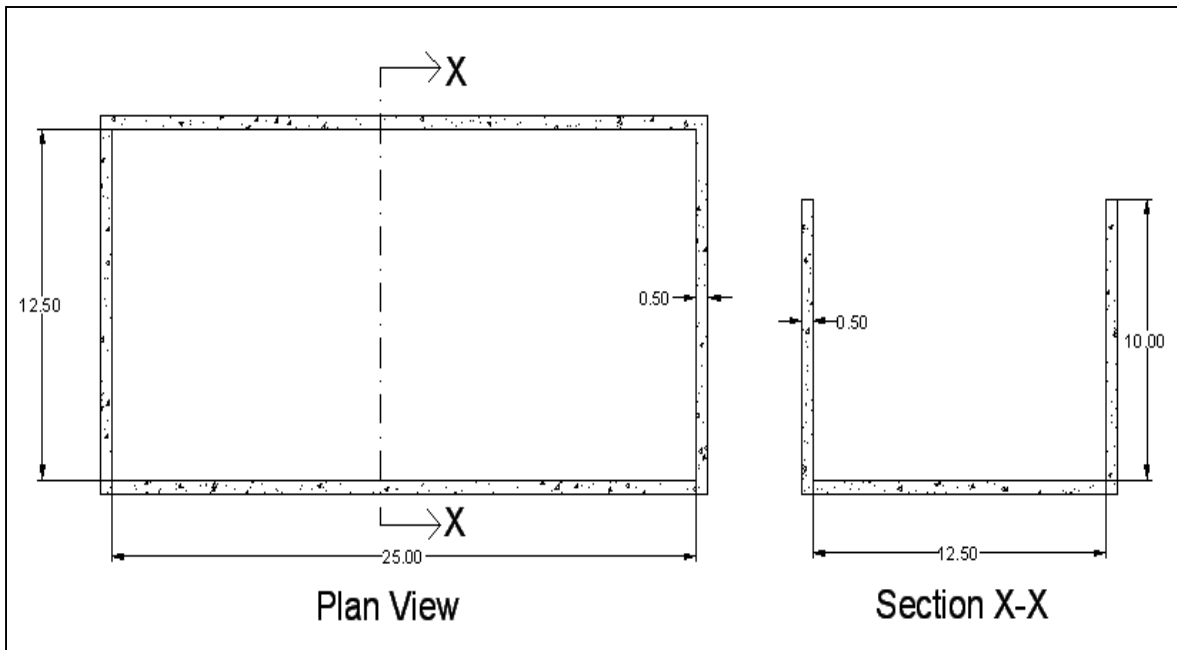
Figure 3.3: Dimensions (in ft.) of Soil Box before Modification
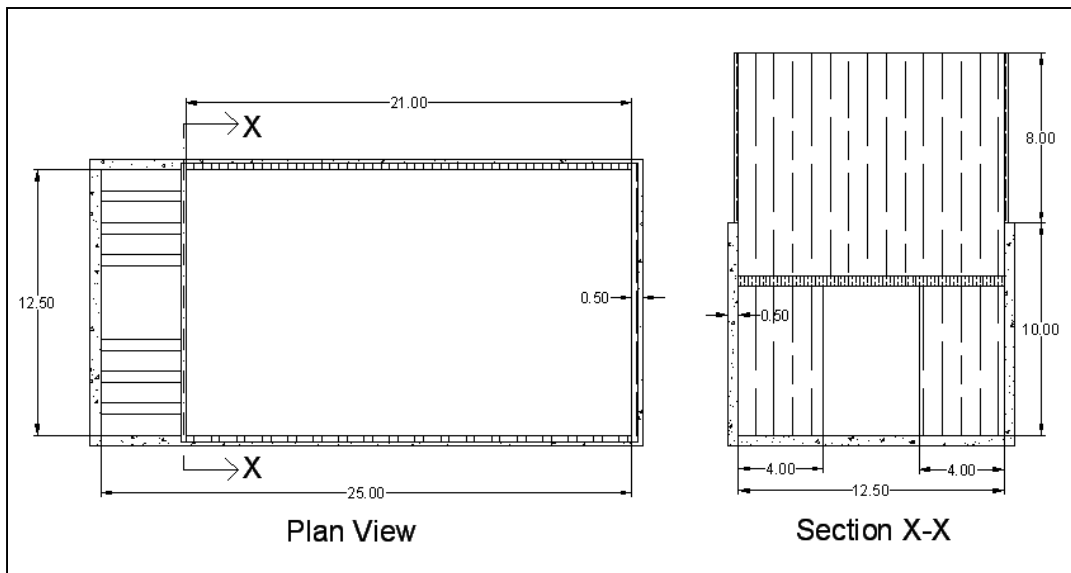


Figure 3.4: Dimensions (in ft.) of Soil Box after Modification

### 3.4 Test Pipe

Steel pipe test piece was provided by a steel pipe manufacturing company in Saginaw, Texas. Same test piece was used for all of the tests because pipe was not tested to failure or yielding stress in all of five cases. Length of the 72 in. nominal diameter test piece was 19-ft and 7.75 in. Outside diameter

was 73.75 in. and wall thickness was 0.313 in. (D/t of 230). Figure 3.5 shows the steel pipe delivery at the CUIRE lab. Total weight of pipe was 4,824 lbs. The test piece was bare without any coating or lining. Hooks as illustrated in Figure 3.6 were prefabricated in order to facilitate installation of measurement instrument (convergence meter).



Figure 3.5: Pipe Delivered to CUIRE Lab



Figure 3.6: Prefabricated Hook

## 3.5 Instrumentation

Earth pressure cells, convergence meters and strain gages were used to acquire data from the tests. These instruments were connected to data loggers and the data loggers were connected to the computer for data recording. The schematic of the instruments is illustrated in Figure 3.7.
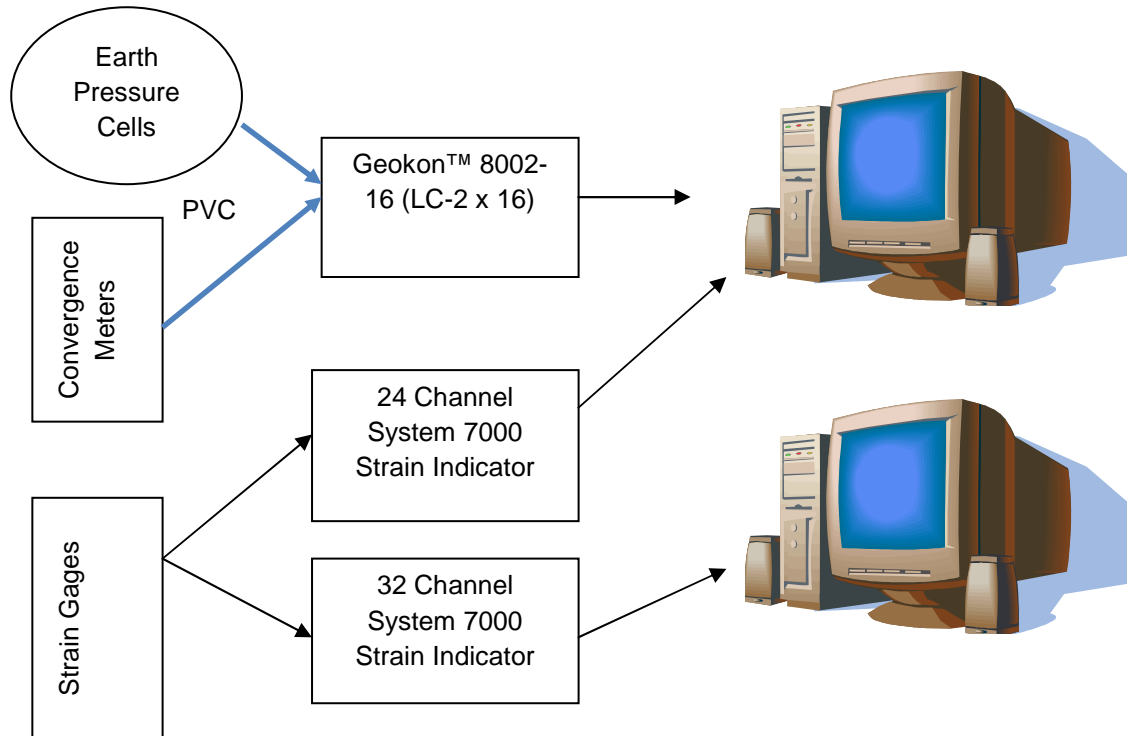


Figure 3.7: Schematic of Instrumentation

### 3.5.1 Earth Pressure Cells

Geokon™ model 4810 vibrating wire earth pressure cells illustrated in Figure 3.8 were used for measurement of horizontal and vertical earth pressures. Earth pressure cells are constructed from two stainless steel plates welded together around their periphery and separated by a narrow gap filled with hydraulic fluid. External pressures squeeze the two plates together creating equal pressure in the internal fluid. A length of stainless steel tubing connects the fluid filled cavity to a pressure transducer that converts the fluid pressure into an electrical signal transmitted by a cable to the readout location (Geokon Datasheet). The range of the pressure cells used was 51 psi with an accuracy of 0.1%.
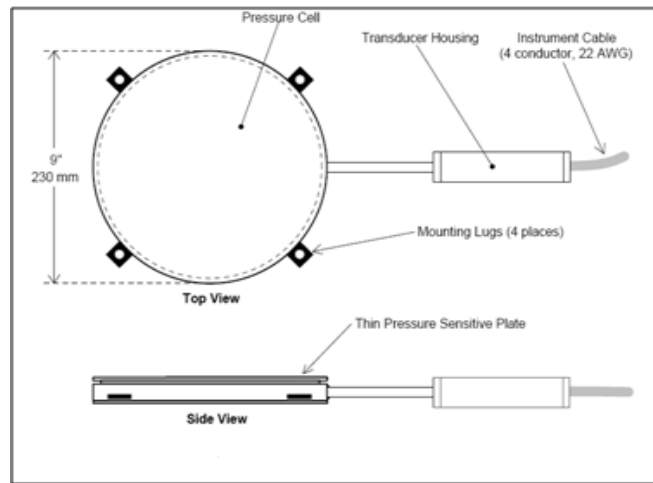
**(a)**



**(b)**

Figure 3.8: (a) Model 4810 Earth Pressure Cell, (b) Earth Pressure Cell used in the Test

3.5.2 Convergence Meters

Geokon™ Model 4425 vibrating wire convergence meters illustrated in Figure 3.9 were used for measurement of horizontal and vertical pipe deflections. As stated by Geokon™ "the Model 4425 convergence meters are designed to detect deformations in tunnels and underground caverns by measuring contraction (or elongation) between two anchor points fixed in walls of the tunnel or cavern. The Model 4425 consists of a spring-tensioned vibrating wire transducer assembly, turnbuckle, 0.24–in. diameter connecting rods (stainless steel, fiberglass or graphite), rod clamp, and a pair of anchor points. Changes in distance between the two anchors are conveyed by the connecting rods and measured by the transducer. The Model 4425 can operate in horizontal, vertical and inclined configurations." The range for convergence meters was four inches of displacement with 0.1% accuracy.
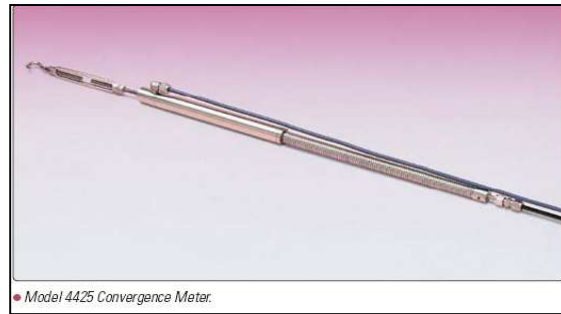
**(a)**
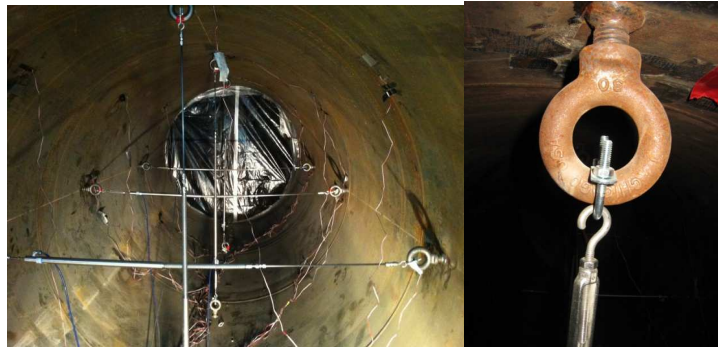

**(b)**                                              **(c)**

Figure 3.9: (a) Model 4425 Convergence Meter, (b) Convergence Meters installed inside the Pipe, (c) Connection of Convergence Meter

### 3.5.3 Strain Gauges

Vishay™ model C2A-06-250LW-350 uniaxial strain gauges illustrated in Figure 3.10 were used for measurement of strains.

### 3.5.4 Geokon™ 8002-16 (LC-2 x 16)

Geokon™ 8002-16 (LC-2 x 16) was used to collect and record data from earth pressure cells and convergence meters. It consisted of sixteen channels availing data collection from six convergence meters and ten earth pressure cells. Figure 3.11 illustrates the data logger used in the tests. The data logger was connected to a desktop computer and data was retrieved by using Geokon™ Logview software.

**(a)** **(b)**
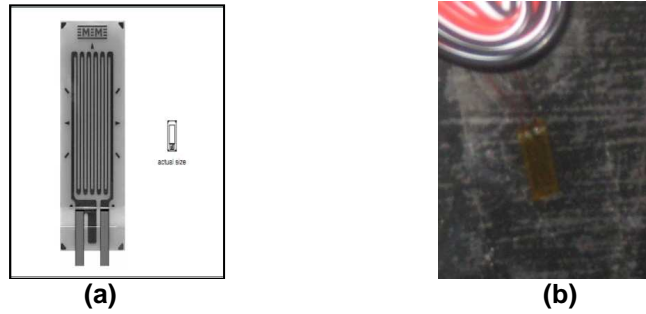
Figure 3.10: (a) C2A-06-250LW-350 Strain Gage, (b) Strain Gage Attached to Pipe



PVC Wires from Earth Pressure Cells and Convergence Meters

Wire to Computer

Figure 3.11: Geokon™ 8002-16 (LC-2 x 16) Data Logger used in the Tests

3.5.5 Vishay™ System 7000 Scanner

Two Vishay™ System 7000 scanner was used to collect and record data from strain gages. For tests 1 and 2, one 24-channel scanner was used. For Tests 1a, 3 and 4, additional scanner with 32 channels was used because more strain gages used in these test. The scanner(s) were connected to desktop computer(s) for data logging. Strain Smart™ version 4.7 was the software used to collect the data recorded by the scanner. Figure 3.12 illustrates a scanner used in the tests.

3.5.6 Calibration of Instruments

The data recording instruments were factory calibrated. The calibration sheets of the instruments are presented in Appendix A.

3.6.1 Test 1

Instrumentation for Test 1 consisted of six convergence meters, six earth pressure cells and twenty-four strain gages. Figure 3.13 illustrates the location of these instruments in the test setup. Data from all of the convergence meters and earth pressure cells were collected and recorded successfully. Data from fifteen out of twenty-four strain gages were collected successfully throughout the duration of the test. Nine strain gages failed during different stages of the test. Possible reason for such failure is loss of adhesion between strain gage and pipe wall with time. Figure 3.13 also illustrates the locations of strain gages that failed.

Wires from Strain gages

Wire to Computer
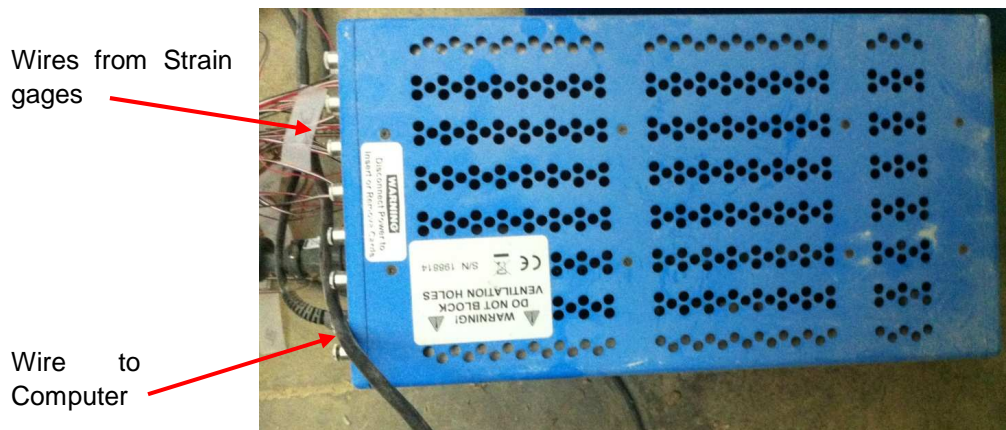


Figure 3.12: System 7000 Scanner used in the Tests

3.6.2 Test 2

After review of Test 1 results, it was deemed necessary to add instruments to measure lateral earth pressure at the soil box walls. This was based on recommendations from IPL design teams' comments and researchers' agreement to requirement of additional instruments. Six convergence meters, ten earth pressure cells and twenty-four strain gages were used for Test 2. Figure 3.14 illustrates the location of these instruments. Data from all of the convergence meters were collected and recorded successfully. Data from eight out of ten earth pressure cells, and eighteen out of twenty-four strain gages were collected successfully throughout the duration of the test. Figure 3.14 also illustrates the locations of earth pressure cells and strain gages that failed.
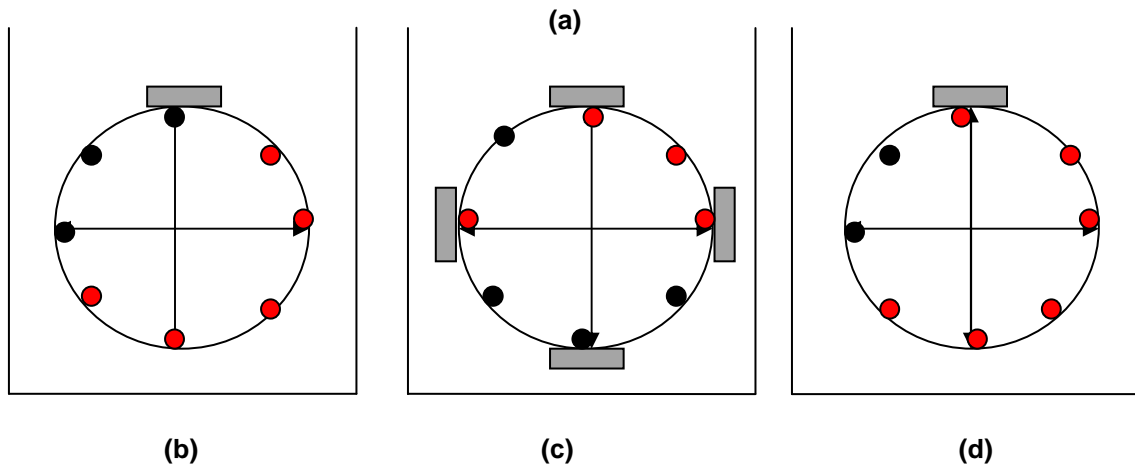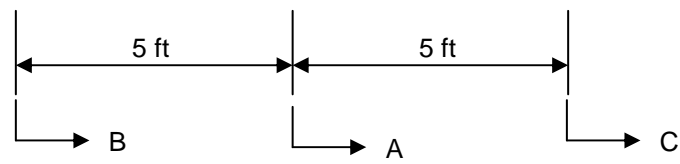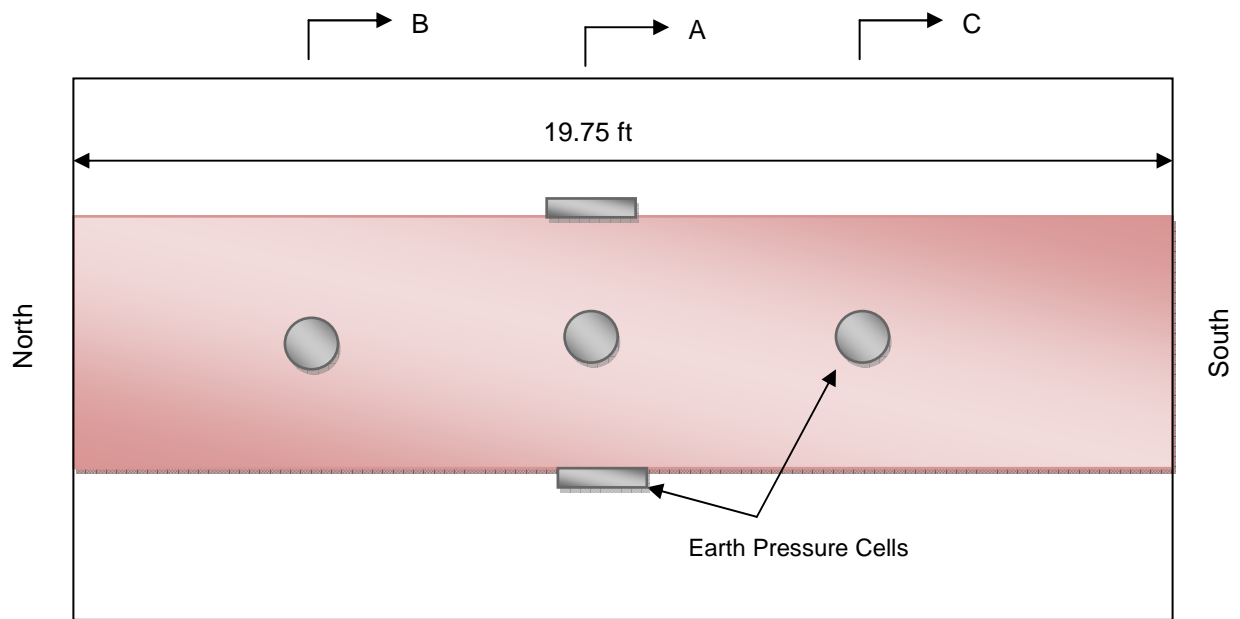
Figure 3.13: Instrument Setup for Test 1: (a) Plan View, (b) Section B-B (North), (c) Section A-A (Center), (d) Section C-C (South)
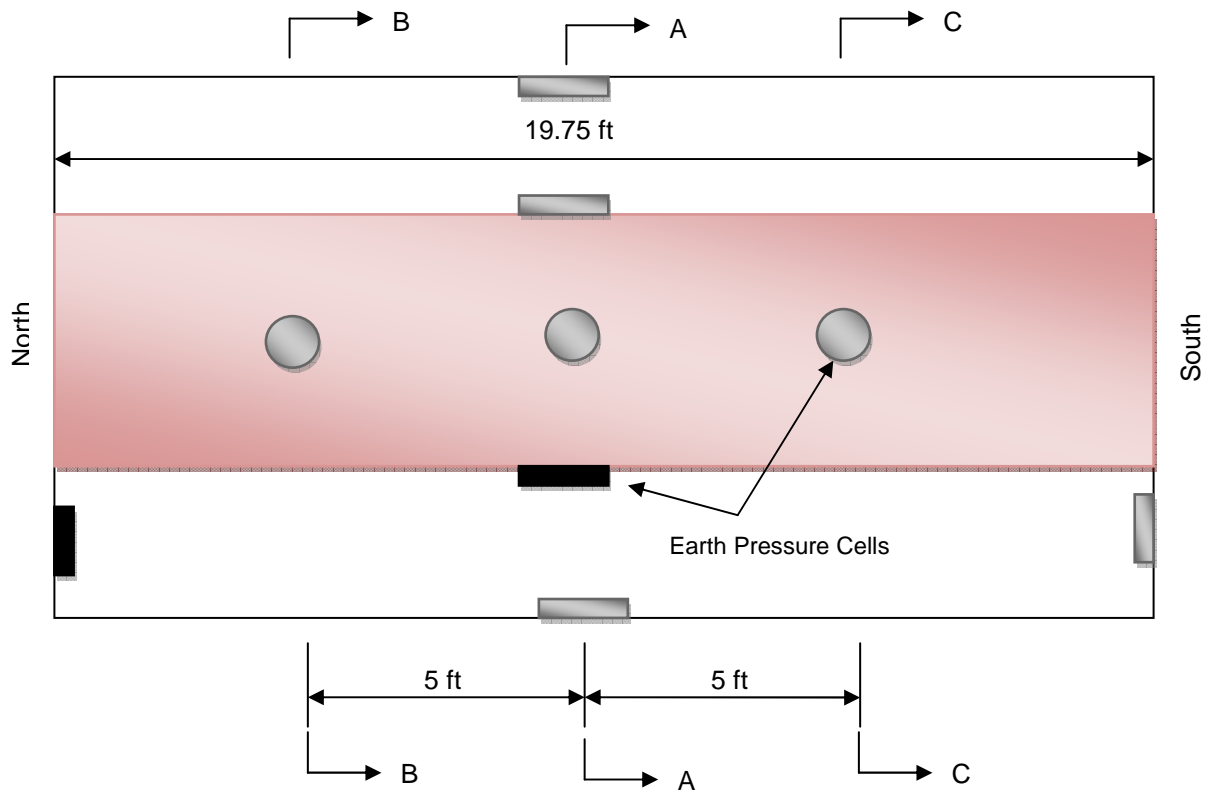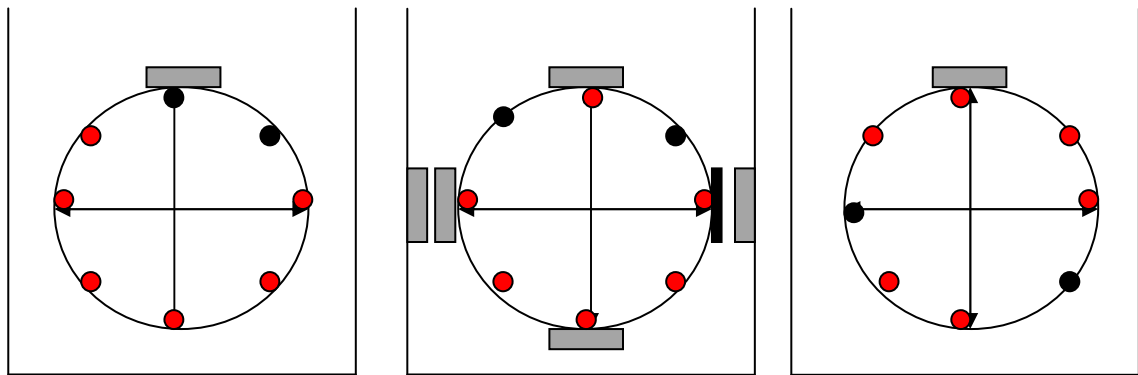
Figure 3.14: Instrument Setup for Test 2: (a) Plan View, (b) Section B-B (North), (c) Section A-A (Center), (d) Section C-C (South)

### 3.6.3 Test 1a

After recommendations from UTA Structural Group, of additional strain gages were added to the test setup. Six convergence meters, ten earth pressure cells and thirty-six strain gages were used for Test 1a. Figure 3.15 illustrates the location of these instruments. Data from all of the convergence meters and earth pressure cells were collected and recorded successfully. Data from thirty-two out of thirty-six strain gages were collected successfully throughout the duration of the test. Figure 3.15 also illustrates the locations of earth pressure cells and strain gages that failed.

### 3.6.4 Test 3

Six convergence meters, ten earth pressure cells and thirty-six strain gages were used for Test 1a. Figure 3.16 illustrates the location of these instruments. Data from all of the convergence meters and earth pressure cells were collected and recorded successfully. Data from thirty-three out of thirty-six strain gages were collected successfully throughout the duration of the test. Figure 3.16 also illustrates the locations of earth pressure cells and strain gages that failed.

### 3.6.5 Test 4

Six convergence meters, ten earth pressure cells and thirty-six strain gages were used for Test 1a. Figure 3.17 illustrates the location of these instruments. Data from all of the convergence meters and earth pressure cells were collected and recorded successfully. Data from twenty-eight out of thirty-six strain gages were collected successfully throughout the duration of the test. Figure 3.17 also illustrates the locations of earth pressure cells and strain gages that failed.

<center>3.7 Soil Properties</center>

Total of four types of soils were used amongst five tests as bedding, embedment and backfills. These soils include pea gravel, native lean clay (low plasticity clay, CL) (native clay), lime stabilized lean clay (Modified clay), and crushed limestone.
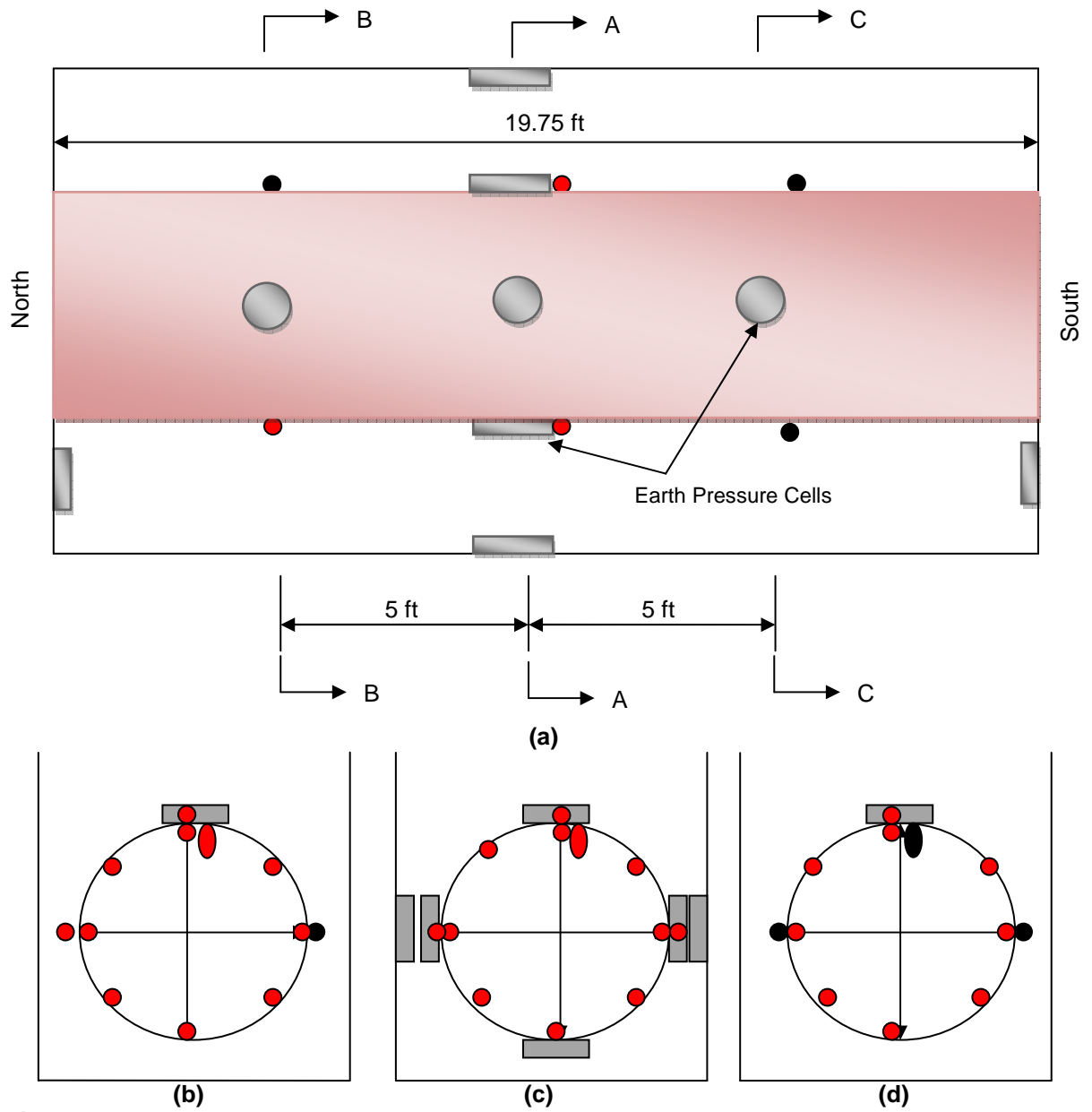
Figure 3.15: Instrument Setup for Test 1a: (a) Plan View, (b) Section B-B (North), (c) Section A-A (Center), (d) Section C-C (South)
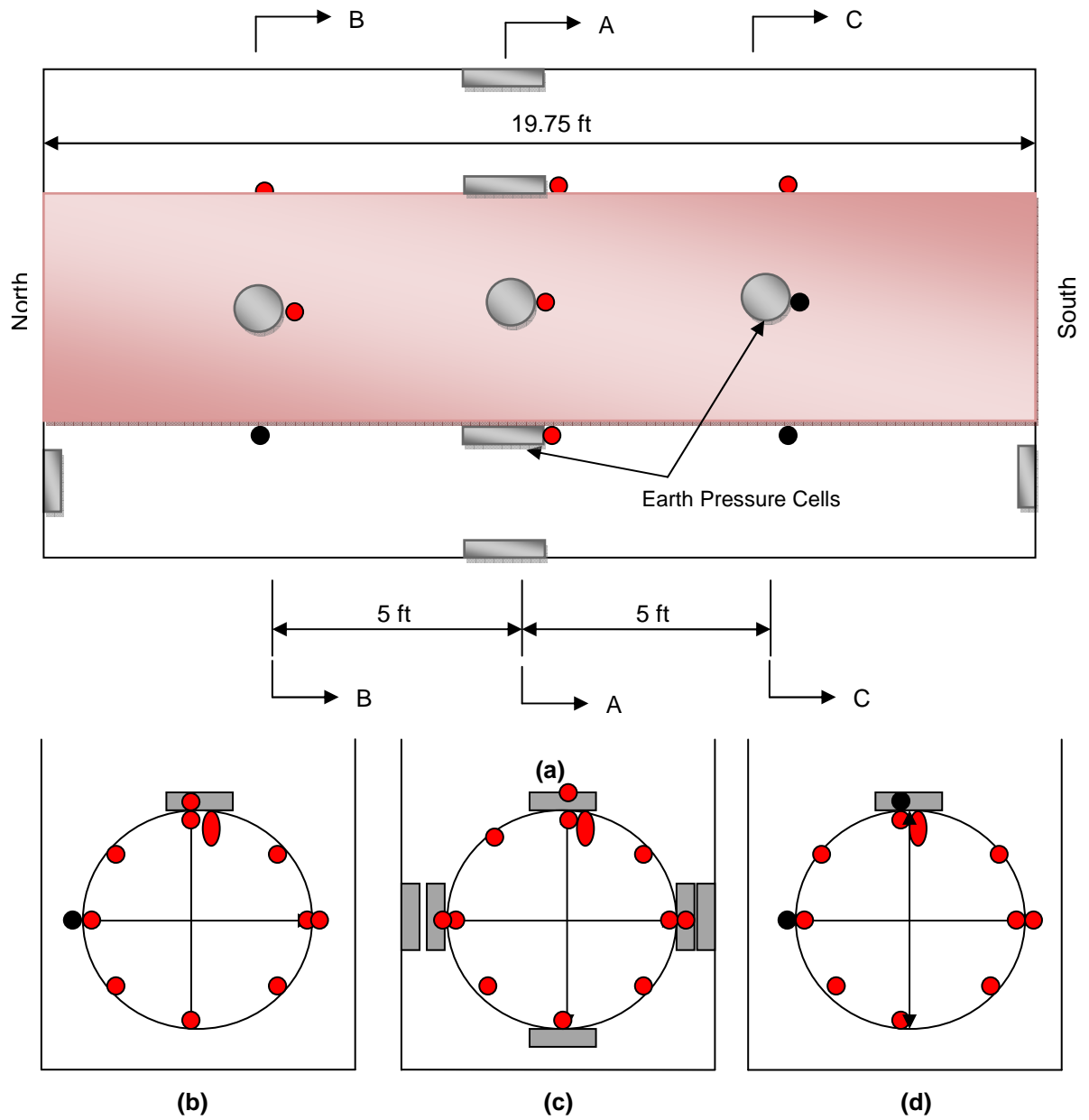
Figure 3.16: Instrument Setup for Test 3: (a) Plan View, (b) Section B-B (North), (c) Section A-A (Center), (d) Section C-C (South)
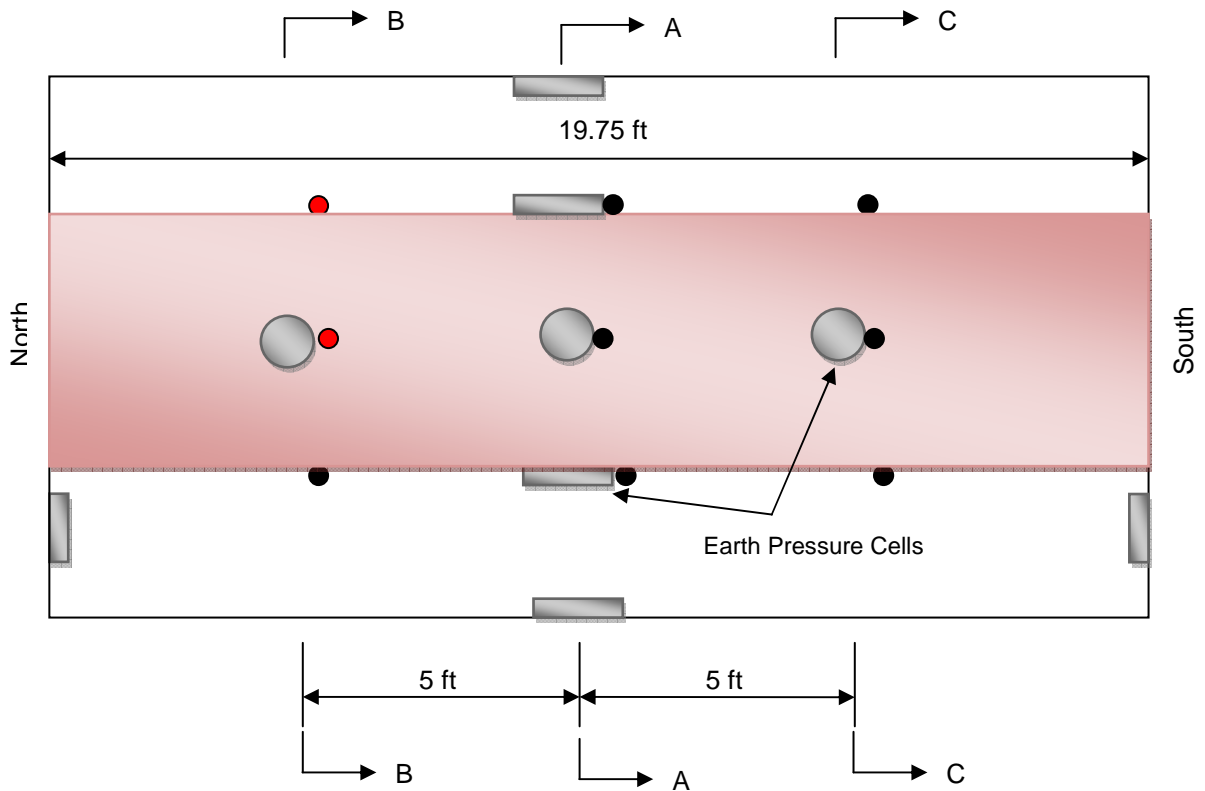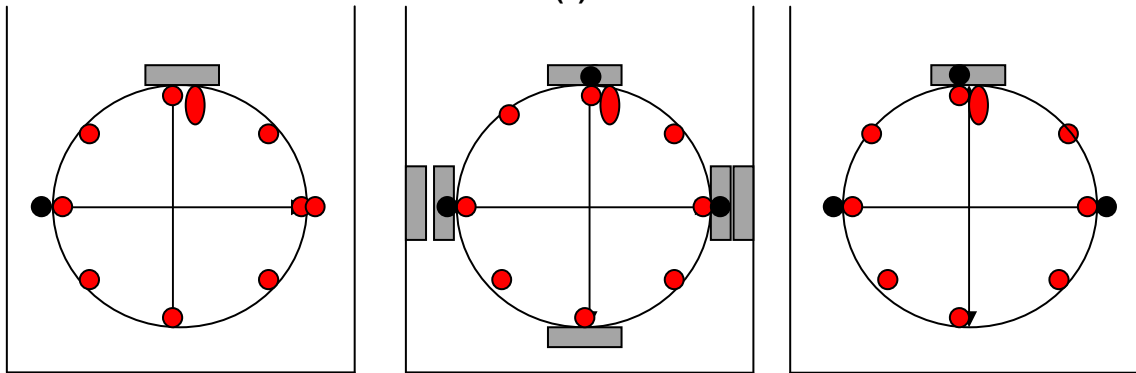
Figure 3.17: Instrument Setup for Test 4: (a) Plan View, (b) Section B-B (North), (c) Section A-A (Center), (d) Section C-C (South)

### 3.7.1 Pea Gravel

Pea gravel used for the tests were provided by a concrete and steel pipe manufacturer located in Grand Prairie, Texas. Sieve analysis of the pea gravel is provided in Table 3.2 showing conformity to specifications for TX367-ASTM #8 (⅜ in. to #4) Washed Pea Gravel. Pea gravel was used as bedding in Tests 1 and 1a and as surcharge load in all of the tests.

Table 3.2: Specifications of Pea Gravel Bedding Material[1]

| Sieve Test | Specification (% Passing) | Tests | Average (% Passing) | Minimum (% Passing) | Maximum (% Passing) | Range | Target |
|---|---|---|---|---|---|---|---|
| ½ in. (12.5mm) | 100 – 100 | 1 | 100 | 100 | 100 | 0 | - |
| ⅜ in. (9.5 mm) | 85 – 100 | 1 | 91 | 91 | 91 | 0 | - |
| ¼ in. (6.3 mm) | - | 1 | 42 | 42 | 42 | 0 | - |
| #4 (4.75 mm) | 10 – 30 | 1 | 15 | 15 | 15 | 0 | - |
| #8 (2.36 mm) | 0 – 10 | 1 | 1 | 1 | 1 | 0 | - |
| #16 (1.18 mm) | 0 – 5 | 1 | 1 | 1 | 1 | 0 | - |
| #200 (75 µm) | 0 – 1.5 | 1 | 0.3 | 0.3 | 0.3 | 0 | 0 – 1 |
| PAN (0 µm) | - | 1 | 0.0 | 0.0 | 0.0 | 0 | - |

### 3.7.1 Native Clay

Native clay was imported from the alignment of IPL project. Native soil from bore location designated as B6 was used in some part in all of the tests except Test 3 (baseline). In Tests 1 and 1a, it was used as embedment from bedding up to one foot above the pipe and also as surcharge load as 2 feet layer of un-compacted backfill. In Test 2, it was used above springline up to one foot above the pipe. In Test 4, it was used above 0.3 times diameter up to one foot above the pipe. The detailed procedures of these tests are provided in section 3.7 below.

Native clay was analyzed and tested by UT Arlington Geotechnical team led by Dr. Anand Puppala. The tests included grain size analysis, index tests, standard proctor test, UU triaxial test, unconfined compressive strength test, chemical tests, and soil mineralogical analysis. The soil sample for

---

[1] Product: TX367-ASTM #8 (⅜ in. to #4) Washed Pea Gravel

these tests were selected from depth of 10 – 15 ft. UU triaxial test and unconfined compressive strength tests were performed on samples remolded to maximum dry density. Table 3.3 presents the summary of test results for B6 native clay presented by UT Arlington Geotechnical Team.

Table 3.3: Summary of Test Results for B6 Native Clay
(Source: UTA Geotechnical Team)

| Sample location ID | | | | B6 |
|---|---|---|---|---|
| Selected sample depth range (ft) | | | | 10 – 15 |
| INDEX TESTS | Grain size analysis | Sieve Analysis | % Gravel | 0 |
| | | | % Sand | 22 |
| | | Hydrometer | % Silt | 62 |
| | | | % Clay | 16 |
| | Atterberg's limits | Liquid Limit (%) | | 40 |
| | | Plastic Limit (%) | | 14 |
| | | PI (%) | | 26 |
| | Soil Classification | | | CL |
| ENGINEERING TESTS | Standard Proctor | MDD* (pcf) | | 108.1 |
| | | OMC** (%) | | 16.2 |
| | UU Triaxial | [+]Undrained Cohesion, $C_u$, Psi | | 14.2 |
| | | [+]Angle of internal friction, $\varphi$ | | 5.7° |
| | | [++]Undrained Cohesion, $C_u$, Psi | | 14.5 |
| | | [++]Angle of internal friction, $\varphi$ | | 8.1° |
| | UCS | Unconfined compression strength, Psi | | 22.8 |
| SOIL MINERALOGY | Monmorillonite | | | 18% |
| | Kaolinite | | | 61% |
| | Illite | | | 21% |
| ELASTIC MODULUS, Psi | Confining pressure = 7.25 psi | | | 1,257 |
| | Confining pressure = 14.50 Psi | | | 3,537 |
| | Confining pressure = 21.75 Psi | | | 6,285 |
| 50% SECANT MODULUS, Psi | Confining pressure = 7.25 psi | | | 968 |
| | Confining pressure = 14.50 Psi | | | 1,380 |
| | Confining pressure = 21.75 Psi | | | 2,114 |

+ 10% Strain; ++ 15% Strain

UU triaxial test data received from the Geotechnical Team was used to calibrate the Duncan hyperbolic model parameters for modeling of native clay behavior. The purpose of this calibration is to avail parameters for FEA of soil pipe interaction in soil-box tests, when Duncan hyperbolic model is preferred. Method described in Section 2.5 was adopted to calibrate three parameters (K, n, and $R_f$) of Duncan model parameter. Remaining two parameters cohesion (c) and angle of friction (Φ) were

provided by UT Arlington Geotechnical Team. Table 3.4 presents calibrated values of Duncan model

parameters for B6 soil. Chapter 6 presents the detailed procedure of the calibration. An excel program

was devised to predict triaxial test results based on five parameters for Duncan hyperbolic model. Figure

3.18 presents the comparison of triaxial test results predicted by calibrated five parameters with the actual

results of the test.

Table 3.4: Duncan Hyperbolic Model Parameters for Native Clay

| Parameter | Value |
|---|---|
| $R_f$ | 0.93 |
| K | 224 |
| N | 1.1024 |
| C | 14.50 |
| Φ | 8.1$^{o}$ |

3.7.1 Modified Clay

The Geotechnical Team investigated the potential of improving the properties of native clay by

treatment with lime and recommended addition of 6% lime by dry weight for optimum stabilization of B6

native soil. As per this recommendation, B6 native soil stabilized with 6% lime was used as bedding and

embedment up to pipe springline in Test 2.
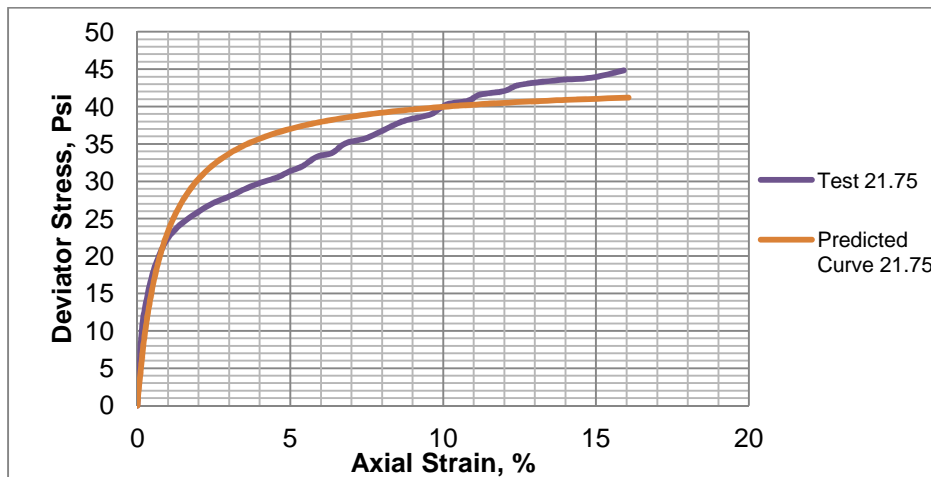


(a)
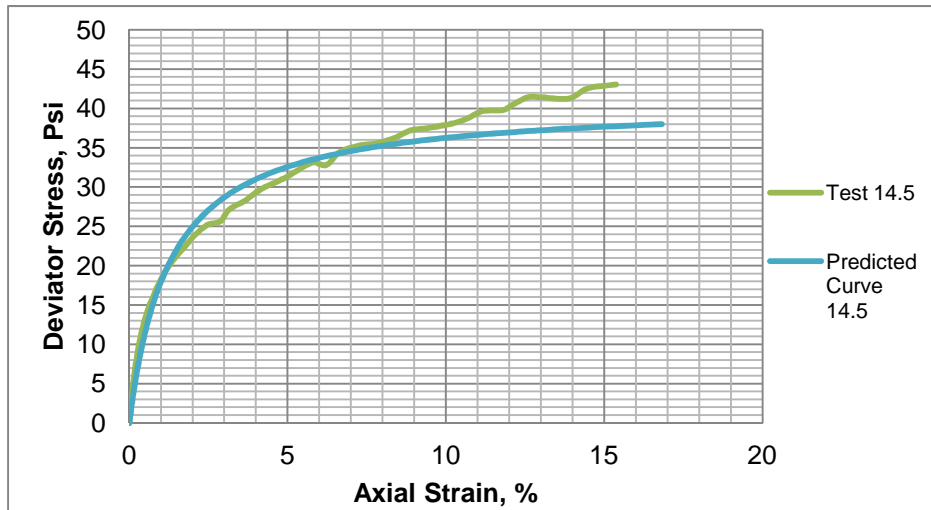
**(b)**
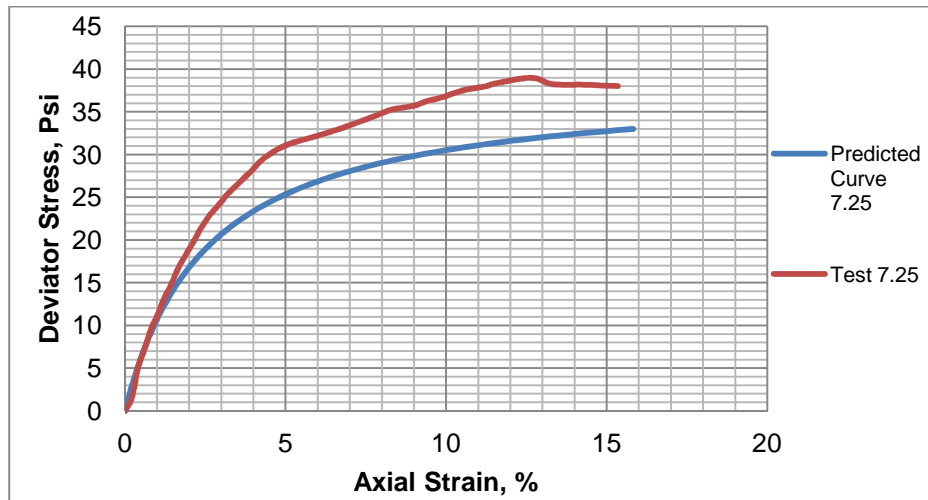


**(c)**

Figure 3.18: Comparison of Duncan-Selig Model Prediction with Actual Test for Native Clay at (a) 21.75 psi confinement, (b) 14.50 psi confinement, (c) 7.25 psi confinement

Modified clay was tested by the Geotechnical Team. The tests included standard proctor test, UU triaxial test, and unconfined compressive strength test. The soil sample taken from depth of 10 – 15 ft, mixed with 6% lime by dry weight of soil and subjected to UU triaxial test and unconfined compressive strength tests at maximum dry density. Table 3.5 presents the summary of test results for B6 native clay provided by the Geotechnical Team.

UU triaxial test data received from the Geotechnical Team was used to calibrate the Duncan hyperbolic model parameters for modeling of modified clay behavior. The purpose of this calibration is to

avail parameters for FEA of soil pipe interaction in soil-box tests, when Duncan hyperbolic model is preferred. Method described in Section 2.5 above was adopted to calibrate three parameters (K, n, and $R_f$) of Duncan model parameter. Remaining two parameters cohesion (c) and angle of friction (Φ) were provided by UT Arlington Geotechnical Team. Table 3.6 presents calibrated values of Duncan model parameters for B6 soil. An excel program was devised to predict triaxial test results based on five parameters for Duncan hyperbolic model. Figure 3.19 presents the comparison of triaxial test results predicted by calibrated five parameters with the actual results of the test.

Table 3.5: Summary of Test Results for B6 Modified Native Clay (Source: UTA Geotechnical Team)

| Sample location ID | | | 6% Lime Treated |
|---|---|---|---|
| Selected sample depth range (ft) | | | 10 – 15 |
| ENGINEERING TESTS | Standard Proctor | MDD* (pcf) | 98.6 |
| | | OMC** (%) | 19.0 |
| | UU Triaxial | Undrained Cohesion, $C_u$, Psi | 23.2 |
| | | Angle of internal friction, φ | 25.8° |
| | UCS | Unconfined compression strength, Psi | 61.7 |
| ELASTIC MODULUS, Psi | Confining pressure = 7.25 Psi | | 3,552 |
| | Confining pressure = 14.5 Psi | | 7,827 |
| | Confining pressure = 27.75 Psi | | 7,702 |
| 50% SECANT MODULUS, Psi | Confining pressure = 7.25 Psi | | 6,424 |
| | Confining pressure = 14.5 Psi | | 14,250 |
| | Confining pressure = 27.75 Psi | | 14,643 |

3.7.1 Crushed Limestone

Crushed limestone was used as bedding in Tests 3 and 4, as embedment in Test 3, and as embedment up to 0.3 times diameter in test 4. The detailed procedures of these tests are described in Section 3.7 below. Crushed limestone was provided by a concrete and steel pipe manufacturer in Grand Prairie, Texas. The specification and some properties of crushed limestone used in the tests, as provided by the supplier, are presented in Table 3.7. Crushed limestone has been considered as the baseline material because this is the standard embedment material used in steel pipe applications.

Table 3.6: Duncan Hyperbolic Model Parameters for 6% Lime Treated Native Soil

| Parameter | Value |
|---|---|
| $R_f$ | 0.7 |
| K | 1319 |
| n | 1.0679 |
| C | 23.2 |
| Φ | $25.8^o$ |

3.8 Test Procedure

3.8.1 Test 1

Test 1 started on January 18, 2011. The construction duration was approximately 15 weeks spanning till May 2, 2011. This test was later repeated as fast construction by a professional contractor with similar test setup. But, this does not take anything away from usefulness of Test 1 data in understanding soil pipe interaction. Figures 3.20 and 3.21 illustrate the setup of Test 1. The procedures involved in construction for Test 1 are described below:

1. Approximately 100 CY of native clay delivered by to the CUIRE lab from B-6 location of the IPL project alignment. At boring site B-6, the first 5 ft of soil was removed first, and soil from between 5 ft -15 in. deep was taken and delivered to CUIRE. This material was stored outside of the CUIRE facility and covered using plastic sheeting.

2. Loose pea gravel bedding of one foot thickness was placed at the floor of the soil box.

3. The center location of the pipe piece was carefully marked and an earth pressure cell was placed at this marked location.

4. Steel pipe test piece was placed longitudinally along the length of the soil box and centrally along the width of the soil box. Along the longitudinal side, a 10-in. gap was provided at the South location and a four-foot gap was provided at the North location. The North gap provided enough work space to work inside the pipe. A wooden frame was constructed at the North side of the load cell to support the embedment at this location. The gap between the wooden frame and the pipe at the North location was approximately two inches.
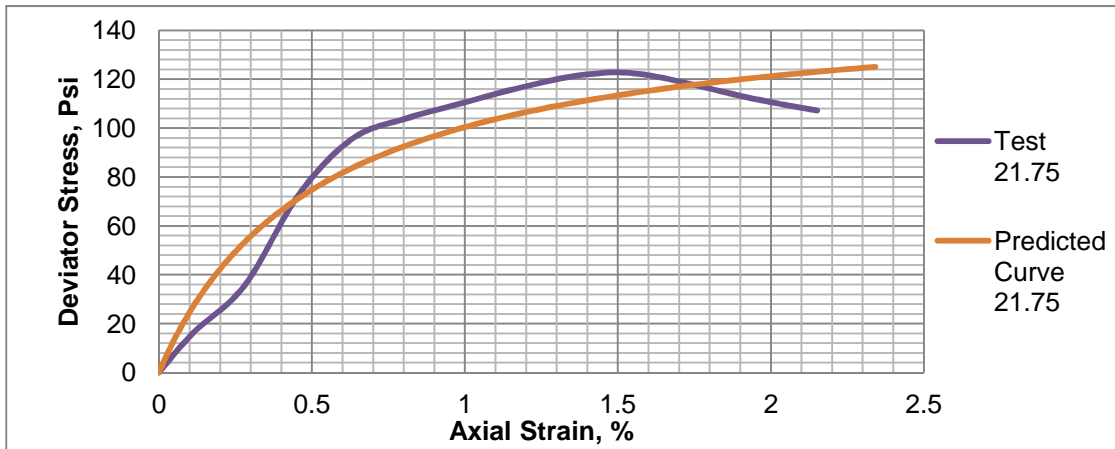
(a)
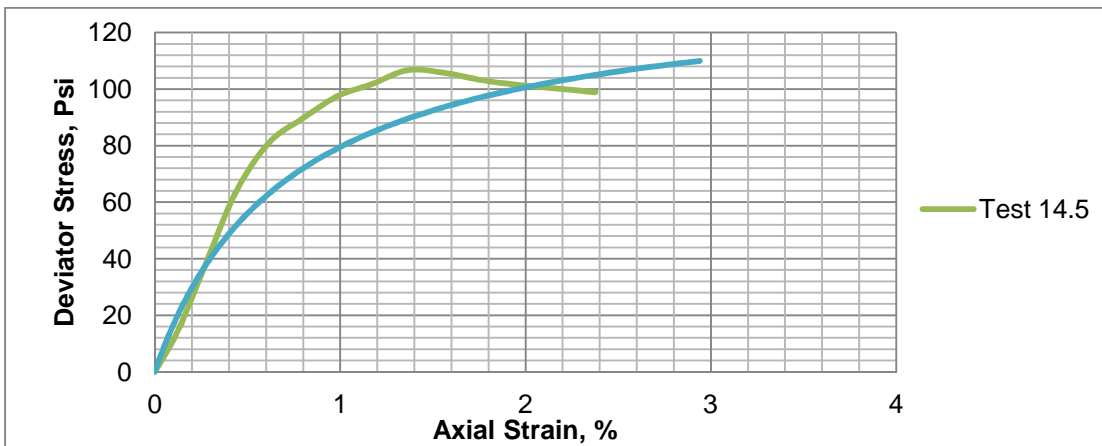
(b)
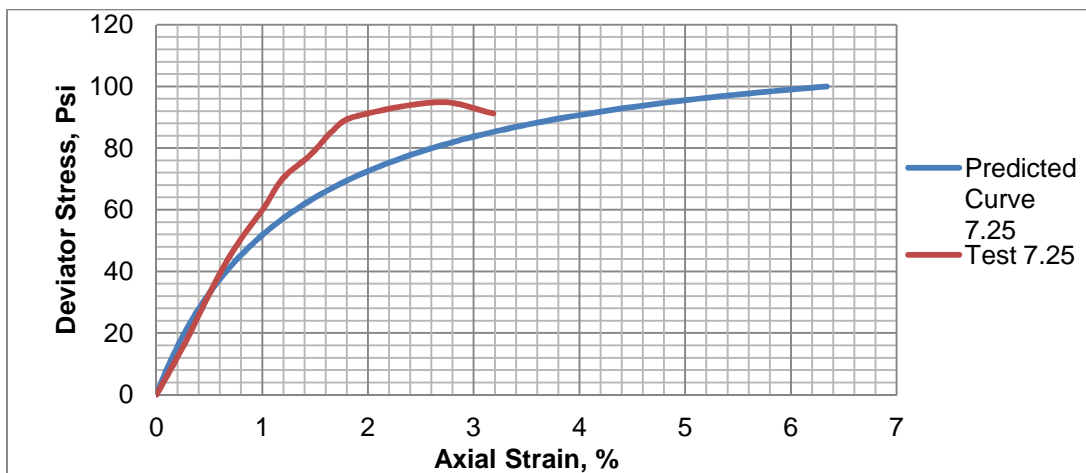
(c)

Figure 3.19: Comparison of Duncan-Selig Model Prediction with Actual Test Modified Native Clay at (a)

21.75 psi confinement, (b) 14.50 psi confinement, (c) 7.25 psi confinement

Table 3.7: Properties of Granular Bedding and Embedment Material

## MATERIALS EVALUATION

### Coarse Aggregates

| | | | |
|---|---|---|---|
| Source: | Hanson @ Bridgeport Perch-Hill Plant #777 | **Technical Services** | |
| Type: | Type "D"    Crushed Lime Stone | Report: **2012-08** | |
| Lab NO: | TS-weekly-12 | Date: 02-28-12 | |
| Date: | Received : 02-01-12 | | |

| ASTM METHOD | TEST DESCRIPTION | TEST RESULTS | | None Specification |
|---|---|---|---|---|
| C-136 | 5/8" Sieve | 100 | % Passing | |
| C-136 | 1/2" Sieve | 99 | % Passing | |
| C-136 | 3/8" Sieve | 93 | % Passing | |
| C-136 | 1/4" Sieve | 68 | % Passing | |
| C-136 | #4 Sieve | 42 | % Passing | |
| C-136 | #8 Sieve | 4 | % Passing | |
| C-136 | #10 Sieve | 3 | % Passing | |
| C-136 | #16 Sieve | 2 | % Passing | |
| C-117 Decant | (- #200 Sieve Washed)         1.45 | % Passing | | |
| C-127 | Bulk Specific Gravity,        SSD | 2.663 | | |
| C-127 | Absorption, | 1.1 | % | |
| C-29 | Unit Weight (Dry Rodded), | 99.4 | Lbs/Cu.Ft. | |
| C-29 | Unit Weight (Dry Loose), | 90.1 | Lbs/Cu.Ft. | |
| C-29 | Voids Content (Dry Rodded), | 40.2 | % | |
| C-131 | L.A. Abrasion, | 26.5 | % Loss | 50%  Max. |
| C-88 | Soundness by Sodium Sulfate (5 cycles),          ………….. | 3.50 | % Loss | 12%  Max. |
| C-88 | Soundness by Magnesium Sulfate (5 cycles),          ………….. | 3.80 | % Loss | 18% Max. |
| C-123 | Light Weight Pieces, | 0.01 | % | 0.5% Max. |
| C-142 | Clay Lumps and Friable Particles, | 0.01 | % | 3.0% Max. |
| C-25 | Calcium Carbonate        EQV, | 95.0 | % | |
| C-25 | Acid Insoluble Residue, | 5.0 | % | |
| G-57 | Soil Resistively, (Tex-129-E Method), | 13000 | ohm-cm | |

5.  The pipe piece was instrumented at three cross sections as explained in Section 3.5.1. These instrumented cross sections will be referred to as North, Center and South cross sections with the North cross section being the cross section with the four foot working space from the concrete wall.

6.  The instrumented pipe was embedded by native clay. The construction was carried out in approximately six-inch layers of native clay compacted to 85-95% of Standard Proctor dry density by use of tamping foot compactor. The layer densities were measured by sand cone in-situ density testing method. The embedment was continued in six-inch layers up to one foot above the pipe.

7. A wooden frame was constructed to provide an additional eight feet of height to the load cell. Additional backfill cover was provided by using pea gravel to achieve average measured load of 8.5 psi at the crown of the pipe.

8. Data recording was continued for nine weeks after completion of backfill.
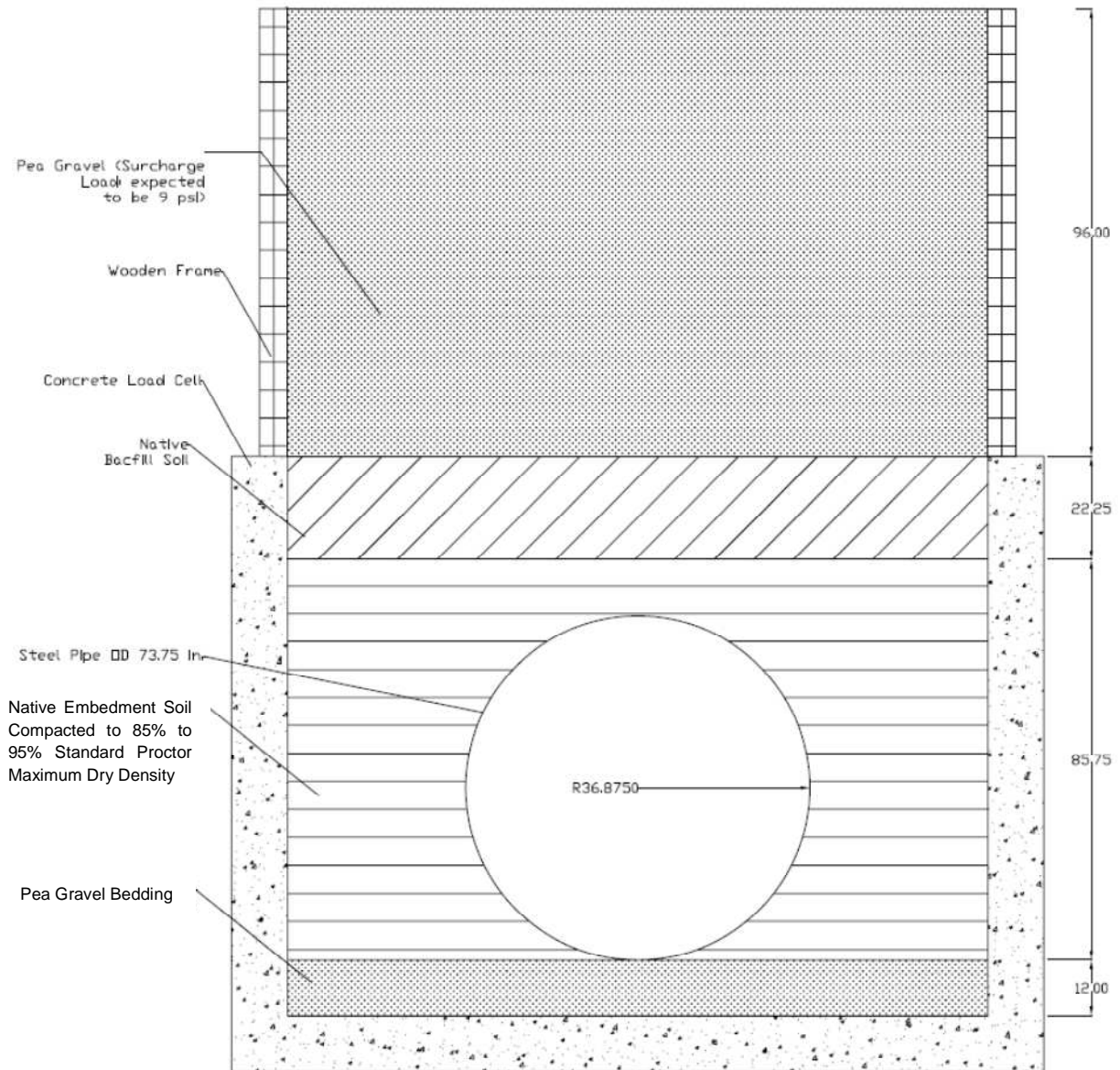


All Dimensions are in Inches

Figure 3.20: Cross Section of the Test 1 Setup
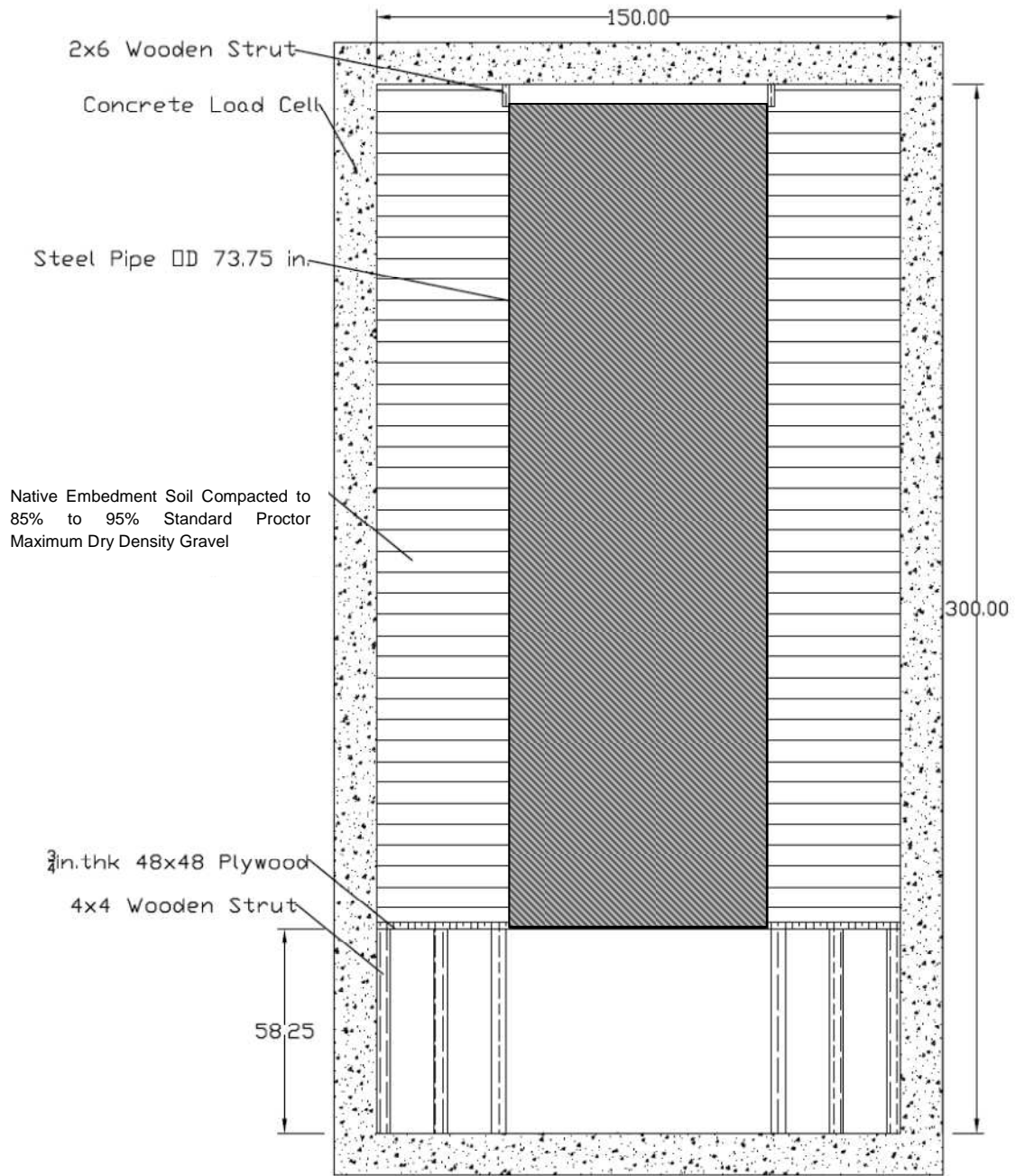
All Dimensions are in Inches

Figure 3.21: Plan View of Test 1 Setup

### 3.8.2 Test 2

Test 2 started on September 19, 2011. The construction duration was approximately 6 weeks spanning till November 2, 2011. Figure 3.22 illustrates cross section of Test 2 setup. Test 2 required

calculations for lime to be added to mix with each layer of soil. Required quantities of lime were calculated as below:

Dry density of loose soil (assumed) = 2000 lb/lcy

Lime per loose cubic yard of soil = 2000 * 6% = 120 lb = 120/50 bags = 2.4 bags

**Bedding Layer (first six inch)**

Compacted volume = 21 * 0.5 * 12.5 / 27 = 4.86 cy

Loose volume = 4.86 * (1.25/0.9) = 6.75 cy

Number of lime bags = 6.75 * 2.4 = 16 bags

**Bedding Layer (second six inch)**

Compacted volume = 21 * 0.5 * 12.5 / 27 = 4.86 cy

Loose volume = 4.86 * (1.25/0.9) = 6.75 cy

Number of lime bags = 6.75 * 2.4 = 16 bags

**Embedment Layer 1 (calculated as six inch)**

Compacted volume = 21 * 0.5 * (12.5 – 0.5) / 27 = 4.67 cy

Loose volume = 4.67 * (1.25/0.9) = 6.48 cy

Number of lime bags = 6.75 * 2.4 = 16 bags

**Embedment Layer 2 (calculated as six inch)**

Compacted volume = 21 * 0.5 * (12.5 – 1.5) / 27 = 4.28 cy

Loose volume = 4.28 * (1.25/0.9) = 5.94 cy

Number of lime bags = 5.94 * 2.4 = 14 bags

**Embedment Layer 3 (calculated as six inch)**

Compacted volume = 21 * 0.5 * (12.5 – 2.5) / 27 = 3.89 cy

Loose volume = 3.89 * (1.25/0.9) = 5.4 cy

Number of lime bags = 5.4 * 2.4 = 13 bags

**Embedment Layer 4 (calculated as six inch)**

Compacted volume = 21 * 0.5 * (12.5 – 3.5) / 27 = 3.5 cy

Loose volume = 3.5 * (1.25/0.9) = 4.86 cy

Number of lime bags = 4.86 * 2.4 = 12 bags

**Embedment Layer 5 (calculated as six inch)**

Compacted volume = 21 * 0.5 * (12.5 – 4.5) / 27 = 3.11 cy

Loose volume = 3.5 * (1.25/0.9) = 4.32 cy

Number of lime bags = 4.32 * 2.4 = 10 bags

**Embedment Layer 5 (calculated as six inch)**

Compacted volume = 21 * 0.5 * (12.5 – 5.5) / 27 = 2.72 cy

Loose volume = 2.72 * (1.25/0.9) = 3.78 cy

Number of lime bags = 3.78 * 2.4 = 9 bags

The procedures involved in construction for Test 2 are described below:

1.  The native clay material used in Test 1 was excavated and stored for re-use in Test 2.

2.  Lime treated native soil bedding of one foot thickness was placed at the floor of the soil box. This was carried out in two layers. First a six inch layer of native soil was place in the soil box and mixed with 6% lime by dry weight. The volumetric batching was carried out with two and a half 50 lb bags of lime mixed with each cubic yard of loose soil (assuming dry unit weight of 2000 lb/lcy, Peurifoy et al., 2005). The mixing was achieved by using garden tiller. After mixing was complete, the mixed soil was allowed to mellow for approximately 24 hours and then compacted to 90% of standard proctor dry density by using a rammer. The mellow time was as suggested by the Geotechnical team. Another six inch layer was placed with same procedure as above to achieve one foot bedding layer.

3.  The center location of the pipe piece was carefully marked and an earth pressure cell was placed at this marked location.

4.  Steel pipe test piece was placed longitudinally along the length of the load cell and centrally along the width of the soil box. A 6-in. gap was provided between the South end of the pipe and load cell wall so that the pipe does not come in contact with soil box wall. Four-foot gap was provided at North end of the pipe to facilitate work space.

5.  Two vertical struts were placed at 3.5 ft from either end of the pipe sample. The purpose was to recover from deformation from self-weight of the pipe and to provide support during test construction.

6.  The pipe piece was instrumented at three cross sections as described in Section 3.5.2.

7.  The instrumented pipe sample was embedded with lime treated native up to the springline. The mixing and compaction of the soil was achieved as described in step 2 above. 90% of Standard Proctor dry density was achieved through compaction in approximately five layers during this installation by use of tamping foot compactor. The embedment above springline was continued with native clay in seven-inch layers up to one foot above the pipe. The untreated native soil layers were also compacted to 90% of standard proctor density.

8.  Surcharge load due to backfill was achieved by 9 ft of pea gravel backfill placed over the embedment.

9.  Data recording was continued for nine weeks after completion of backfill.

Pea Gravel (Surcharge Load: expected to be 9 psi)

Wooden Frame

Concrete Load Cell

Untreated Native Backfill Soil compacted to 90% of standard proctor maximum dry density

Steel Pipe OD 73.75 In.

Embedment

Bedding

R36.8750

116.25

48.75

37.00

12.00
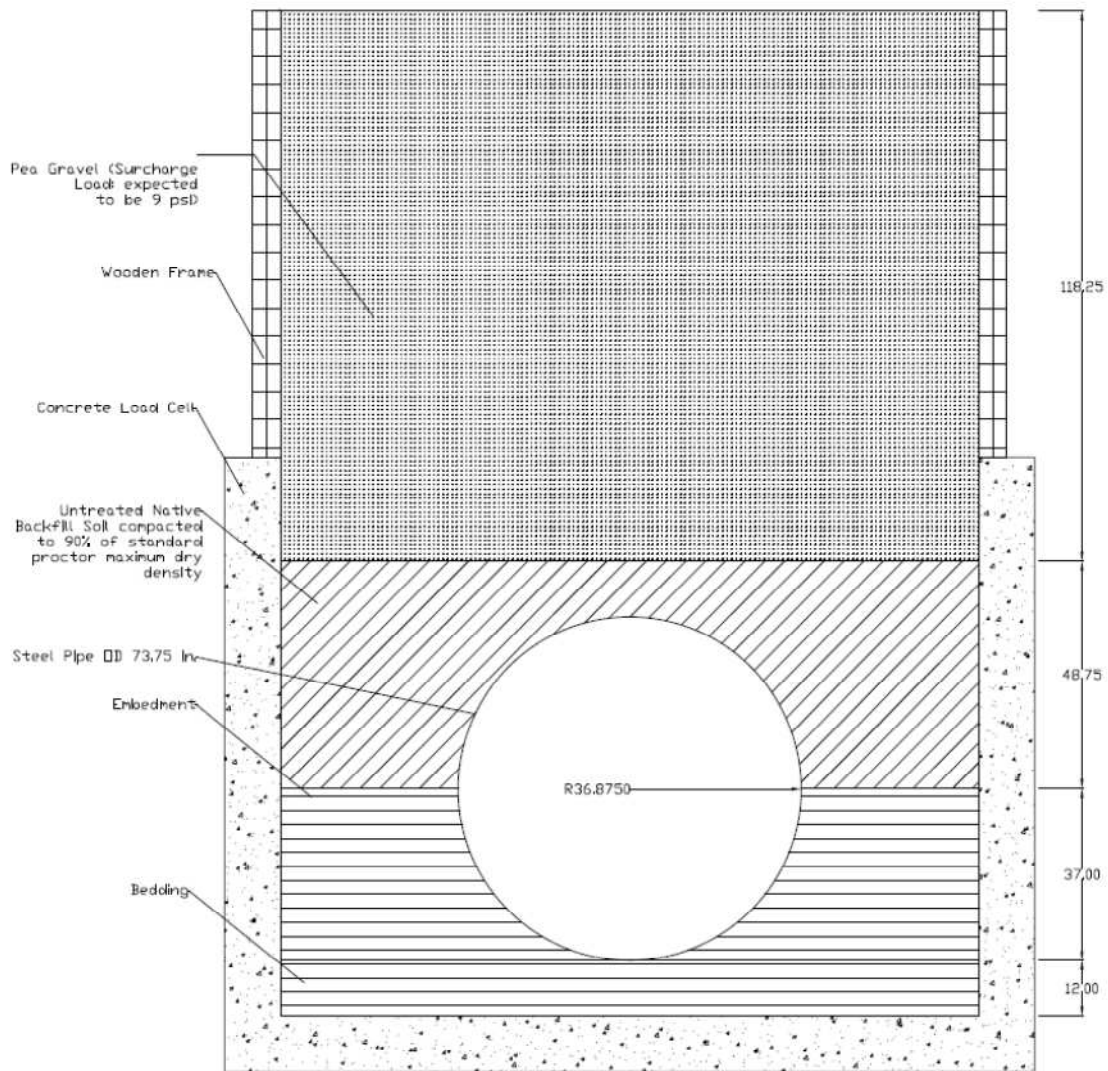
All Dimensions are in Inches

Figure 3.22: Cross-section for Test 2 Setup

3.8.3 Test 1a

Test 1a started on February 27, 2012. The construction duration was 5 days spanning till March 3, 2012. Test 1a is so numbered because of its similarity with Test 1 is general test setup. Figures 3.20 and 3.21 presented setup for Test 1 which is also applicable to Test 1a. The differences between Test 1 and Test 1a are (i) faster pace of construction of Test 1a compared to Test 1, (ii) use of professional contractor (Rudy Renda Contracting) for construction of Test 1a setup, (iii) placement of struts inside the pipe at start of Test 1a construction, and (iv) additional instrumentation in Test 1a as compared to Test 1. The procedures involved in construction for Test 1a are described below:

56

1. Native clay used for Tests 1 and 1a were stored for disposal. Additional 100 CY of embedment soil was delivered by the TRWD to the CUIRE lab from the B-6 location of the IPL project alignment. At boring site B-6, the first 5 ft of soil was removed first, and soil from between 5 ft -15 in. deep was taken and delivered to CUIRE.

2. Pea gravel bedding of one foot thickness was placed at the floor of the soil box.

3. The center location of the pipe piece was carefully marked and an earth pressure cell was placed at this marked location.

4. Steel pipe test piece was placed longitudinally along the length of the load cell and centrally along the width of the soil box. While along the longitudinal side, a 6-in. gap was provided at the South location and a four-foot gap was provided at the North location for work space. The gap between the wooden frame and the pipe at the North location was approximately six inches.

5. The pipe piece was instrumented at three cross sections as described in Section 3.5.3.

6. The vertical struts were placed at four cross-sections at 4 ft c/c.

7. The instrumented pipe sample was embedded with native material as embedment using a professional contractor crew. The crew from Oscar Renda Contracting consisted of two labors, one backhoe operator and one supervisor. The embedment was placed in approximately 8" layers compacted above 90% standard proctor density. Density measurement was taken through nuclear density gage.

8. Surcharge load due to compaction was achieved by two feet of native material and seven feet of pea gravel placed over the embedment.

9. Data recording was continued for four weeks after completion of backfill.

3.8.4 Test 3

Test 3 started on April 24, 2012. The construction duration was 3 days spanning till April 26, 2012. Test 3 was carried out as baseline test with crushed limestone which is standard material used as embedment. The purpose was to compare the results of other tests to this baseline test with an expectation that the best pipe performance will be achieved in this test setup. Figures 3.23 and 3.24 illustrate Test 3 setup. The procedures involved in construction for Test 3 are described below:

1. Approximately 132 tons of crushed limestone was delivered by a concrete and steel manufacturer in Grand Prairie, Texas to the laboratory.

2. One foot bedding of crushed limestone was placed in the soil box.

3. The center location of the pipe piece was carefully marked and an earth pressure cell was placed at this marked location.

4. Steel pipe sample was placed longitudinally along the length of the load cell and centrally along the width of the soil box. While along the longitudinal side, a 6-in. gap was provided at the South location and a four-foot gap was provided at the North location for work space. The gap between the wooden frame and the pipe at the North location was approximately six inches.

5. The pipe piece was instrumented at three cross sections as described in Section 3.5.4.

6. The vertical struts were put in place at four cross-sections at 4 ft center to center.

7. The instrumented pipe sample was embedded with crushed limestone up to one foot above the pipe. The embedment was constructed in lifts of 18 inch thicknesses compacted using vibratory plate compactor.

8. Surcharge load due to backfill was achieved by two feet of crushed limestone and seven feet of pea gravel backfill placed over the embedment.

9. Data recording was continued for four weeks after completion of backfill.
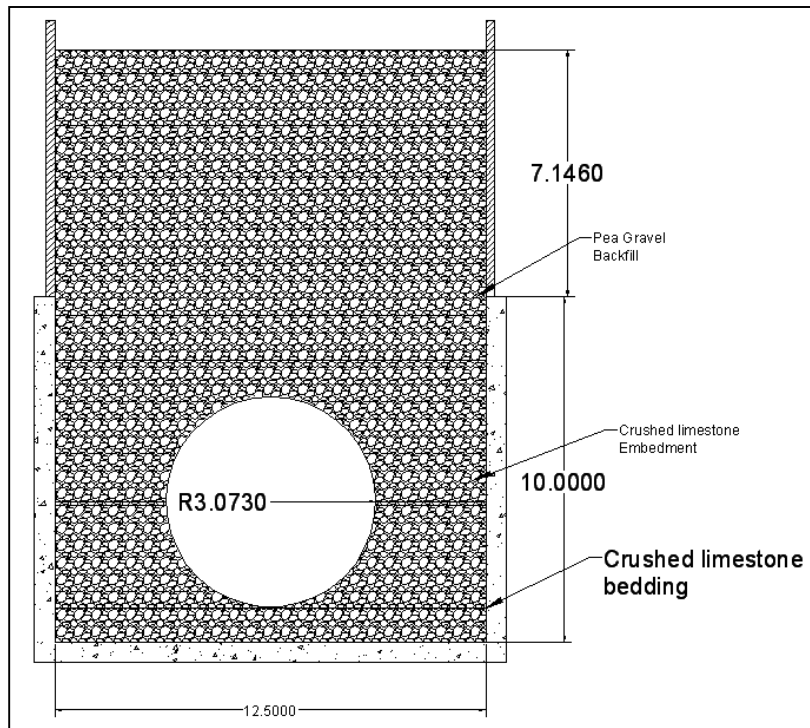
Dimensions are in feet unless specified

Figure 3.23: Cross-section for Test 3 Setup



Dimensions are in feet unless specified

Figure 3.24: Plan View of Test 3 Setup

3.8.5 Test 4

Test 4 started on June 19, 2012. The construction duration was 4 days spanning till June 22, 2012. Figures 3.25 illustrate cross section of Test 4 setup. The procedures involved in construction for Test 4 are described below:



Dimensions are in ft
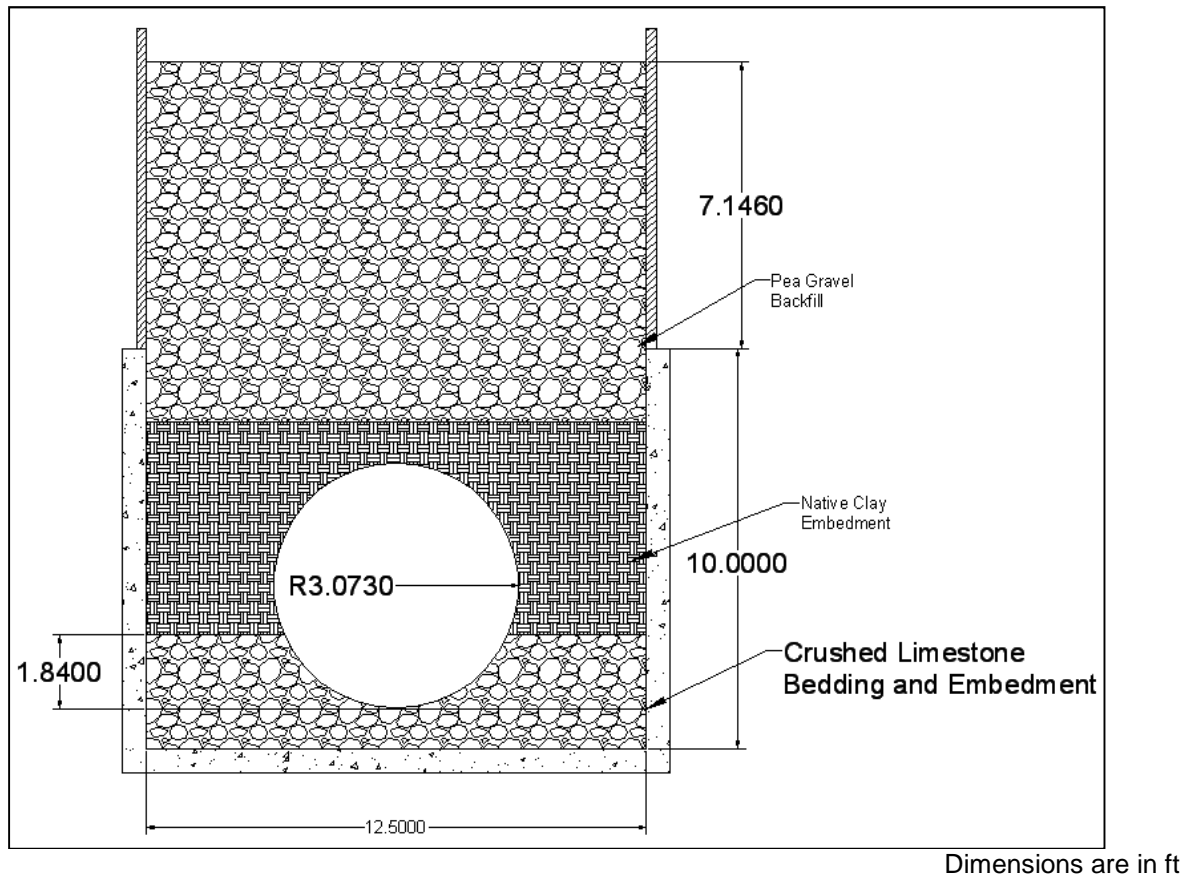
Figure 3.25: Cross-section for Test 4 Setup

1.     Crushed limestone used in Test 3 was stored for re-use in test 4. Excavation of embedment from Test 4 was carried out leaving bedding and pipe test piece inside the pipe.

2.     The pipe piece was instrumented at three cross sections as described in Section 3.5.5.

3.     The vertical struts were put in place at four cross-sections at 4 ft center to center.

4.     The instrumented pipe sample was embedded with crushed limestone up to 0.3 times diameter (22 in.) above the bedding. The embedment was constructed in one lift of 22 inch thickness compacted using vibratory plate compactor.

5.   Embedded was continued with native clay stored from excavation of Test 1a. The crew from Bar Constructors consisting of two labors for compaction of native clay and one backhoe with operator from UT Arlington facilities management completed the embedment construction. The embedment was placed in approximately 8" layers compacted above 90% standard proctor density. Density measurement was taken through nuclear density gage testing by representative from Alliance Geotechnical Group, Inc. Native clay embedment was provided up to one foot above the pipe.

6.   Surcharge load due to backfill was achieved by nine feet of pea gravel backfill placed over the embedment.

7.   Data recording was continued for four weeks after completion of backfill.

## 3.9 Summary

This chapter presented the detailed procedure and methodology adopted for the laboratory tests performed for the research. It described the details of the test soil box, pipe specimen, embedment soil properties, instruments used for data acquisition and their locations, test setup and step by step procedure for each of the five tests performed.

Chapter 4

Laboratory Test Results

4.1 Introduction

This chapter presents the results of the full scale laboratory tests. The data acquired and the key observations from the tests are presented. The key data include deflection results, earth pressure readings, and pipe wall strains.

4.2 Sign Conventions

Presented data for pipe deflections (changes in horizontal and vertical diameters), earth pressure cell, and pipe wall strains require establishment of a sign convention for the presented data. The sign convention followed in this dissertation will be positive for tension and negative for compression. This will translate to any decrease in diameter reported as negative deflection (compression) and any increase in diameter reported as positive deflection (tension). Likewise, when pipe wall strains are reported, compressive strains will be reported as negative and tensile strains will be reported as positive.

4.3 Deflection of Pipe due to Self-Weight

The test pipe (pipe sample) was delivered to the laboratory with two sets of struts placed inside the pipe to provide stiffness against handling stresses. During preparation for Test 1, test pipe was instrumented with the convergence meters with struts inside the pipe. Struts were removed from inside of the pipe to record deflection of pipe due to removal of struts (due to self-weight of pipe). The recorded deflections are presented in the Table 4.1. Two of the convergence meters were dislodged by the dynamic impact of the struts removal. These convergence meter readings are not available and marked with N/A in Table 4.1.

Table 4.1: Deflections Immediately after Removal of Struts

| Vertical Deflections (in.) | | | Horizontal Defection (in.) | | |
|---|---|---|---|---|---|
| **South** | **Center** | **North** | **South** | **Center** | **North** |
| N/A | - 0.517 | - 0.620 | 0.534 | N/A | 0.517 |

Expected pipe deflection due to self-weight was calculated by using modified Iowa equation. This calculation is presented in Chapter 5. In this calculation, value of E' was used as zero, deflection lag factor as 1, bedding constant as 0.1, and weight on top of pipe as 20.462 lb/in., which is self-weight of

pipe. This resulted in expected deflection of 1.34 in. Calculated expectation deflection due to self-weight was more than two times the deflection actually observed due to removal of struts. Therefore, there is need to evaluate shape that pipe is molded during manufacture in order to evaluate deflection due to self-weight of pipe. However, argument can be made that bedding constant is reduced when there is no soil around the pipe, hence reducing predicted pipe deformation due to self-weight.

In further presentation of data, initial shape of the pipe will be assumed to be that after deformation due to self-weight of pipe. This translates to zero deflection of horizontal and vertical diameters being the state when pipe has already deformed due to self-weight. This provides advantage in evaluating lateral pressure due to embedment soil because weight of pipe will no longer be needed to be considered in such evaluation.

<u>4.4 Test 1 Results</u>

4.4.1 Embedment Layers

Twelve layers of native clay were placed as embedment for Test 1. The thickness and densities of these layers are presented in Table 4.2.

4.4.2 Pipe Deflection

Pipe deflection during Test 1 is summarized in Table 4.3. Figure 4.1 illustrates graphical representation of deflection during Test 1. Peaking deflection (increase in vertical diameter) was observed up to layer 12. Surcharge load of cover added after layer 12 caused deflection in pipe. During peaking deflection, horizontal and vertical deflections were approximately equal in magnitude. Horizontal deflection due to surcharge load was less than 40% of vertical deflection.

4.4.3 Earth Pressure

Earth Pressures were measured at six locations described in Section 3.6.1. Vertical pressures at center under the pipe and three locations (south, center, and north) on top of pipe and horizontal pressures at pipe springlines were measured. Table 4.4 presents recorded pressures at these locations at different stages of the test. Figure 4.2 illustrates graphical representation of earth pressure cell data.

Table 4.2: Layer Densities for Test 1

| Layer No. | Thickness (in.) | Cumulative Thickness (in.) | Dry Density (pcf) | Moisture Content (%) | Wet Density (pcf) | Percentage Compaction (%) |
|---|---|---|---|---|---|---|
| 1 | 6 | 6 | 102.2 | 21.4 | 124.0 | 94.5 |
| 2 | 7 | 13 | 97.2 | 18.6 | 115.3 | 90.0 |
| 3 | 7 | 20 | 97.9 | 18.1 | 115.7 | 90.6 |
| 4 | 7 | 27 | 97.2 | 16.4 | 113.1 | 90.0 |
| 5 | 8 | 35 | 94.3 | 12.5 | 106.1 | 87.3 |
| 6 | 6 | 41 | 93.7 | 17.5 | 110.1 | 86.8 |
| 7 | 6 | 47 | 92.4 | 18.1 | 109.1 | 85.6 |
| 8 | 6 | 53 | 93.3 | 14.0 | 106.3 | 86.4 |
| 9 | 6 | 59 | 92.0 | 10.3 | 101.5 | 85.2 |
| 10 | 6 | 65 | 91.9 | 10.2 | 101.2 | 85.1 |
| 11 | 6 | 71 | 91.9 | 11.0 | 102.0 | 85.1 |
| 12 | 6 | 77 | 90.5 | 11.4 | 100.8 | 83.8 |

Table 4.3: Pipe Deflection in Test 1

| Description | Vertical Deflection (inches) | | | Horizontal Deflection (inches) | | |
|---|---|---|---|---|---|---|
| | South | Center | North | South | Center | North |
| Layer 1 | 0.21 | 0.16 | 0.08 | − 0.22 | − 0.14 | − 0.09 |
| Layer 2 | 0.28 | 0.23 | 0.16 | − 0.28 | − 0.20 | − 0.13 |
| Layer 3 | 0.76 | 0.71 | 0.57 | − 0.73 | − 0.62 | − 0.49 |
| Layer 4 | 0.99 | 0.86 | 0.68 | − 0.98 | − 0.79 | − 0.62 |
| Layer 5 | 1.16 | 1.07 | 0.93 | − 1.24 | − 1.08 | − 0.96 |
| Layer 6 | 1.14 | 1.05 | 0.91 | − 1.20 | − 1.03 | − 0.92 |
| Layer 7 | 1.19 | 1.10 | 0.96 | − 1.26 | − 1.09 | − 0.97 |
| Layer 8 | 1.21 | 1.11 | 0.97 | − 1.27 | − 1.10 | − 0.98 |
| Layer 9 | 1.27 | 1.17 | 1.02 | − 1.30 | − 1.13 | − 0.99 |
| Layer 10 | 1.28 | 1.18 | 1.04 | − 1.31 | − 1.14 | − 0.99 |
| Layer 11 | 1.31 | 1.20 | 1.07 | − 1.33 | − 1.15 | − 0.99 |
| Layer 12 | 1.32 | 1.19 | 1.07 | − 1.33 | − 1.14 | − 0.99 |
| Surcharge Load | 0.85 | 0.54 | 0.45 | − 1.21 | − 0.97 | − 0.77 |
| Week 1 | 0.83 | 0.52 | 0.43 | − 1.19 | − 0.95 | − 0.75 |
| Week 2 | 0.81 | 0.50 | 0.41 | − 1.20 | − 0.96 | − 0.75 |
| Week 3 | 0.80 | 0.49 | 0.40 | − 1.19 | − 0.95 | − 0.75 |
| Week 4 | 0.79 | 0.48 | 0.39 | − 1.19 | − 0.95 | − 0.75 |
| Week 5 | 0.78 | 0.47 | 0.38 | − 1.19 | − 0.95 | − 0.74 |
| Week 6 | 0.77 | 0.46 | 0.37 | − 1.19 | − 0.94 | − 0.74 |
| Week 7 | 0.76 | 0.45 | 0.36 | − 1.19 | − 0.94 | − 0.74 |
| Week 8 | 0.75 | 0.45 | 0.36 | − 1.18 | − 0.94 | − 0.72 |
| Week 9 | 0.75 | 0.44 | 0.35 | − 1.18 | − 0.94 | − 0.72 |
| **Immediate Deflection Due to Surcharge load** | **− 0.47** | **− 0.65** | **− 0.62** | **0.12** | **0.17** | **0.22** |
| **Total Deflection Due to Surcharge load** | **− 0.57** | **− 0.75** | **− 0.72** | **0.15** | **0.20** | **0.27** |
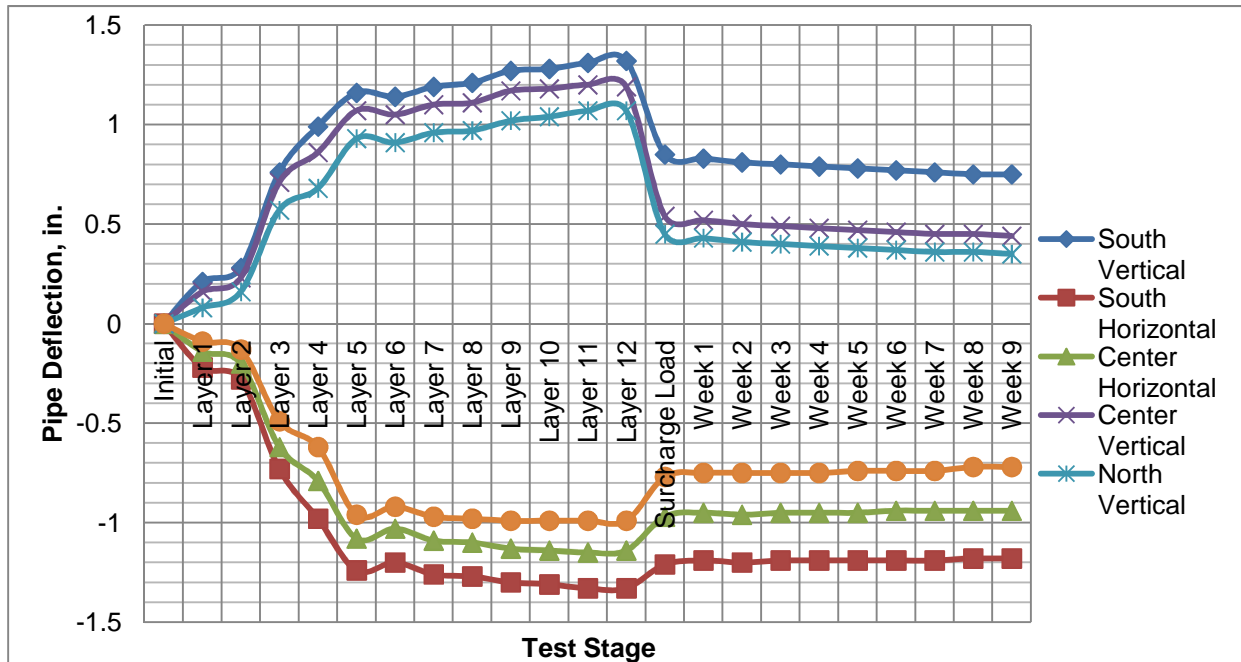
Note: Refer to Figure 3.13 for North, Center, and South Locations

Figure 4.1: Deflection of Pipe in Test 1

Table 4.4: Earth Pressure Cell Data for Test 1

| Description | Horizontal/Vertical (Springline) Loads, psi | | | | | |
|---|---|---|---|---|---|---|
| | South | Center | | | | North |
| | Top | Bottom | Springline East | Springline West | Top | Top |
| Initial | N/A | 24.5 | N/A | N/A | N/A | N/A |
| Layer 1 | N/A | 27.4 | N/A | N/A | N/A | N/A |
| Layer 2 | N/A | 26.8 | N/A | N/A | N/A | N/A |
| Layer 3 | N/A | 23.0 | N/A | N/A | N/A | N/A |
| Layer 4 | N/A | 24.8 | N/A | N/A | N/A | N/A |
| Layer 5 | N/A | 29.9 | N/A | N/A | N/A | N/A |
| Layer 6 | N/A | 28.9 | 0.7 | 0.4 | N/A | N/A |
| Layer 7 | N/A | 29.2 | 0.8 | 0.6 | N/A | N/A |
| Layer 8 | N/A | 29.4 | 0.8 | 0.7 | N/A | N/A |
| Layer 9 | N/A | 29.9 | 0.8 | 0.7 | N/A | N/A |
| Layer 10 | N/A | 30.2 | 0.8 | 0.6 | N/A | N/A |
| Layer 11 | N/A | 30.6 | 0.7 | 0.6 | N/A | N/A |
| Layer 12 | N/A | 31.0 | 0.8 | 0.8 | N/A | N/A |
| Surcharge Loading Complete | 8.0 | 45.7 | 5.3 | 5.4 | 7.6 | 9.8 |
| Week 1 | 7.8 | 45.6 | 5.2 | 5.0 | 7.4 | 9.4 |

Table 4.4 (Continued)

| Description | Horizontal/Vertical (Springline) Loads, psi | | | | | |
| --- | --- | --- | --- | --- | --- | --- |
| | South | Center | | | | North |
| | Top | Bottom | Springline East | Springline West | Top | Top |
| Week 2 | 8.0 | 45.6 | 5.2 | 5.2 | 7.5 | 9.5 |
| Week 3 | 7.9 | 45.5 | 5.1 | 5.0 | 7.4 | 9.4 |
| Week 4 | 8.0 | 45.5 | 5.1 | 5.1 | 7.3 | 9.4 |
| Week 5 | 8.0 | 45.3 | 5.1 | 5.1 | 7.5 | 9.3 |
| Week 6 | 8.0 | 45.2 | 5.1 | 5.0 | 7.3 | 9.2 |
| Week 7 | 7.8 | 45.1 | 4.8 | 4.8 | 7.2 | 9.1 |
| Week 8 | 7.9 | 45.1 | 5.0 | 5.0 | 7.3 | 9.1 |
| Week 9 | 7.9 | 45.0 | 5.0 | 5.0 | 7.3 | 9.0 |

N/A represents the stages of the test when the referred earth pressure cell was not installed yet.

Note: Refer to Figure 3.13 for North, Center, and South Locations
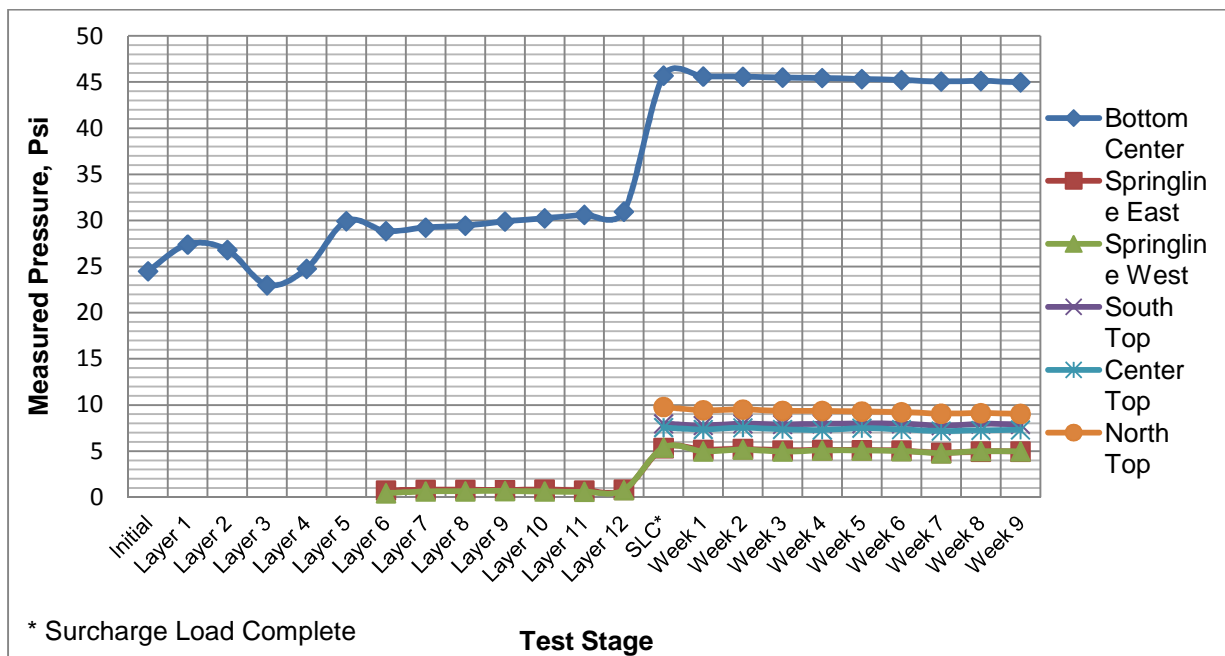


Note: Refer to Figure 3.13 for North, Center, and South Locations

Figure 4.2: Earth Pressures at Different Stages of Test 1

4.4.4 Pipe Wall Strains

Strain gages were installed at twenty-four points circumferentially, as described in Section 3.6.1; strains were measured successfully at fifteen points. Tables 4.5, 4.6 and 4.7 present strains on pipe walls

at different stages of the test. Figures 4.3, 4.4 and 4.5 illustrate graphical representation of pipe wall strain data. The strain data are so plotted in order to show exaggerated shape of pipe deformation.

Table 4.5: Circumferential Strains at South Cross Section in Test 1

| Description | Strain (Micro Strain, με) | | | | | | | |
|---|---|---|---|---|---|---|---|---|
| | Crown | 45 | SL | 135 | Invert | 225 | SL | 315 |
| Layer 5 | -9 | -25 | 15 | 13 | -2 | 13 | N/A | -34 |
| Layer 6 | 6 | 19 | 27 | 17 | 17 | 26 | N/A | 11 |
| Layer 7 | -27 | 14 | -5 | -3 | 3 | 4 | N/A | -6 |
| Layer 8 | 11 | 18 | 2 | 0 | 6 | 13 | N/A | 0 |
| Layer 9 | -45 | 53 | -22 | -5 | 7 | -4 | N/A | -6 |
| Layer 10 | -25 | 20 | -6 | -2 | 4 | 1 | N/A | -2 |
| Layer 11 | -19 | 11 | 3 | -5 | 13 | 16 | N/A | -7 |
| Layer 12 | -33 | -18 | -10 | -18 | -1 | -5 | N/A | -14 |
| Surcharge Loading Complete | 160 | -70 | 160 | -150 | 274 | -110 | N/A | N/A |
| Week 1 | 10 | -4 | -13 | -8 | 72 | -3 | N/A | N/A |
| Week 2 | 2 | -2 | -2 | -11 | 10 | -7 | N/A | N/A |
| Week 3 | 4 | 1 | -1 | -2 | 1 | 0 | N/A | N/A |
| Week 4 | 3 | -1 | -5 | -6 | 1 | -3 | N/A | N/A |
| Week 5 | 2 | -1 | 0 | -6 | 4 | -2 | N/A | N/A |
| Week 6 | 2 | 0 | 1 | -8 | 8 | -2 | N/A | N/A |
| Week 7 | 2 | -1 | 4 | -7 | 8 | -2 | N/A | N/A |
| Week 8 | 5 | 1 | 3 | 24 | 11 | 0 | N/A | N/A |
| Week 9 | 1 | 0 | -4 | -9 | 8 | -4 | N/A | -6 |
| **Total During Embedment** | **-131** | **124** | **0** | **-6** | **59** | **63** | **N/A** | **-47** |
| **Total Due to Surcharge Load** | **313** | **-128** | **174** | **-162** | **1201** | **-210** | **N/A** | **N/A** |
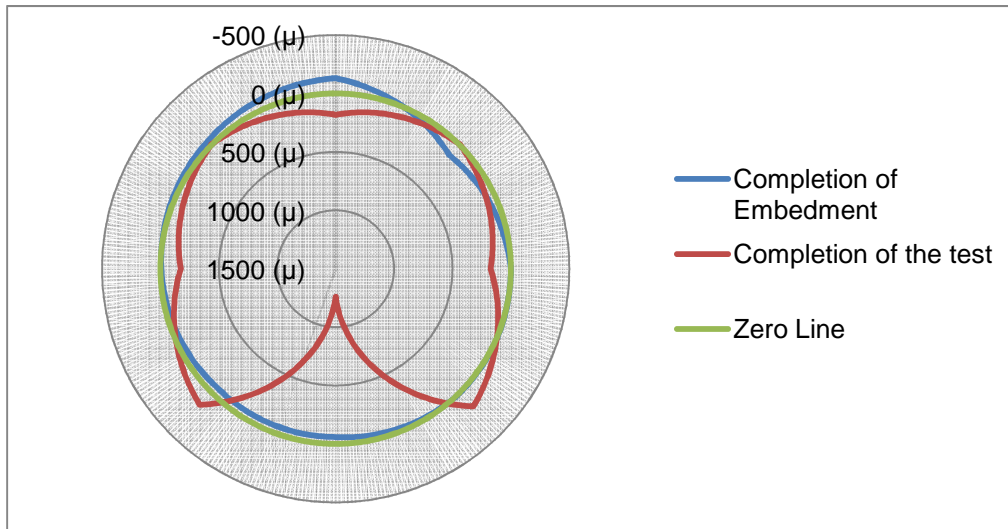
Figure 4.3: Plotted Strain Data for South Cross Section in Test 1

Table 4.6: Circumferential Strains at Center Cross Section in Test 1

| Description | Strain (Micro Strain, με) | | | | | | | |
|---|---|---|---|---|---|---|---|---|
| | Crown | 45 | SL | 135 | Invert | 225 | SL | 315 |
| Layer 5 | -22 | -14 | 3 | 8 | N/A | 4927 | 61 | N/A |
| Layer 6 | 7 | 15 | 29 | 39 | N/A | 577 | -7 | N/A |
| Layer 7 | -26 | 15 | -1 | -6 | N/A | -46 | 25 | N/A |
| Layer 8 | -4 | 12 | 2 | 5 | N/A | -105 | 10 | N/A |
| Layer 9 | -27 | 49 | -29 | -8 | N/A | -29 | -16 | N/A |
| Layer 10 | -28 | 22 | -4 | -4 | N/A | 373 | 11 | N/A |
| Layer 11 | -19 | 10 | 3 | 0 | N/A | -252 | -3 | N/A |
| Layer 12 | -21 | -25 | -15 | -41 | N/A | -78 | 23 | N/A |
| Surcharge Loading Complete | 127 | -90 | 4 | 187 | N/A | -133 | 0 | N/A |
| Week 1 | 5 | -5 | 3 | N/A | N/A | 6 | 0 | N/A |
| Week 2 | 12 | -4 | 0 | N/A | N/A | -16 | 0 | N/A |
| Week 3 | -10 | -2 | 4 | N/A | N/A | 5 | 0 | N/A |
| Week 4 | 15 | -3 | 0 | N/A | N/A | -6 | 0 | N/A |
| Week 5 | 7 | -2 | 2 | 0 | N/A | -6 | 0 | N/A |
| Week 6 | 3 | -2 | 1 | 0 | N/A | -3 | 0 | N/A |
| Week 7 | 0 | -1 | 2 | N/A | N/A | -3 | 0 | N/A |
| Week 8 | -64 | -1 | 1 | N/A | N/A | -2 | 0 | N/A |
| Week 9 | -4 | -2 | 0 | N/A | N/A | -7 | 0 | N/A |
| **Total During Embedment** | **-134** | **114** | **-20** | **-8** | **N/A** | **-138** | **-33** | **N/A** |
| **Total Strain Due to Surcharge Load** | **233** | **-168** | **34** | **N/A** | **N/A** | **N/A** | **-815** | **N/A** |

68
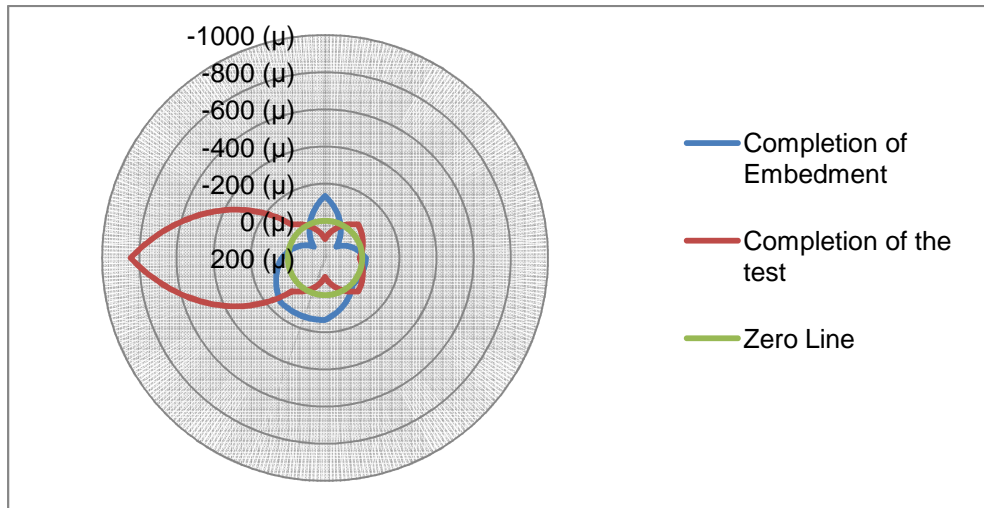
Figure 4.4: Plotted Strain Data for Center Cross Section in Test 1

Table 4.7: Circumferential Strains at North Cross Section in Test 1

| Description | Strain (Micro Strain, µε) | | | | | | | |
|---|---|---|---|---|---|---|---|---|
| | Crown | 45 | SL | 135 | Invert | 225 | SL | 315 |
| Layer 5 | N/A | -8 | 26 | 11 | -3 | -49 | 54 | 17 |
| Layer 6 | N/A | 13 | 113 | 16 | 12 | 9 | 22 | 19 |
| Layer 7 | N/A | 13 | 9 | -8 | 3 | -4 | 15 | 64 |
| Layer 8 | N/A | 10 | 4 | 1 | 4 | -2 | 13 | -16 |
| Layer 9 | N/A | 53 | -32 | -9 | 4 | -7 | 6 | 16 |
| Layer 10 | N/A | 32 | 3 | -1 | 2 | -3 | -7 | 9 |
| Layer 11 | N/A | 10 | 10 | -4 | 11 | -7 | 2 | 9 |
| Layer 12 | N/A | -23 | -80 | -17 | 1 | -16 | -12 | -19 |
| Surcharge Loading Complete | N/A | -82 | -71 | -130 | 271 | -159 | N/A | N/A |
| Week 1 | N/A | 3 | 51 | 1 | 5 | -3 | 37 | N/A |
| Week 2 | N/A | 2 | -56 | -6 | 4 | -7 | 6 | N/A |
| Week 3 | N/A | 3 | 27 | 0 | 7 | -1 | 33 | N/A |
| Week 4 | N/A | 1 | -9 | -3 | 3 | -3 | 7 | -976 |
| Week 5 | N/A | 2 | -11 | -2 | 5 | -5 | 3 | -145 |
| Week 6 | N/A | 3 | 1 | -1 | 6 | -4 | 7 | 7 |
| Week 7 | N/A | 2 | 4 | 0 | 5 | -4 | 15 | 29 |
| Week 8 | N/A | -10 | 1 | 69 | 84 | -3 | -235 | N/A |
| Week 9 | N/A | 2 | -11 | 6 | 3 | -4 | -3 | -7 |
| Total After Layer 5 | N/A | 80 | -64 | 38 | 523 | -275 | N/A | N/A |
| **Total During Embedment** | **N/A** | **133** | **-3** | **-5** | **40** | **-60** | **124** | **379** |
| **Total Due to Surcharge Load** | **N/A** | **-53** | **-61** | **43** | **483** | **-215** | **N/A** | **N/A** |
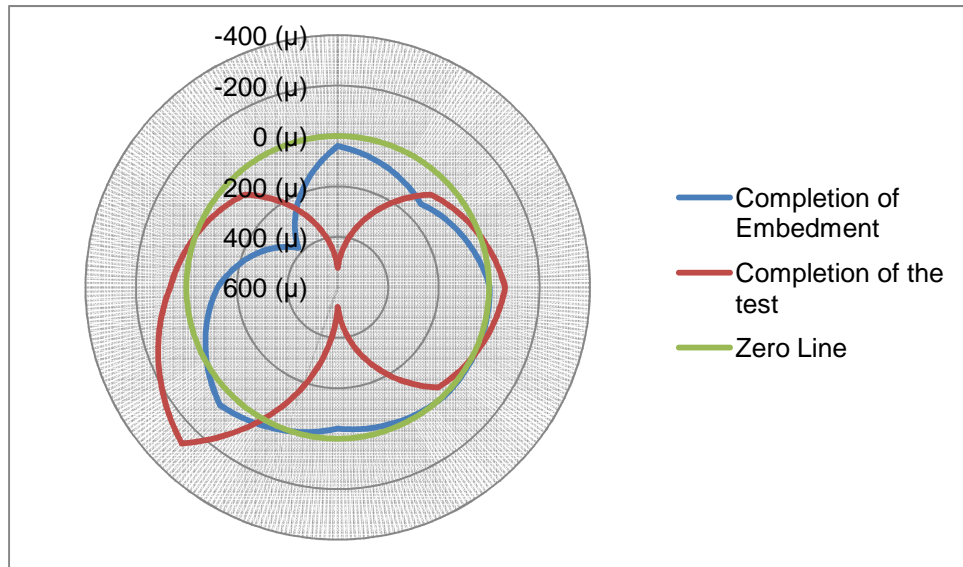
Figure 4.5: Plotted Strain Data for Center Cross Section in Test 1

### 4.5 Test 2

#### 4.5.1 Embedment Layers

Two layers of bedding and ten layers of embedment were placed during Test 2. Table 4.8 presents thicknesses, compaction densities, and soil type of these layers.

#### 4.5.2 Pipe Deflection

Pipe deflection during Test 2 is summarized in Table 4.9. Figure 4.6 illustrates graphical representation of deflection during Test 2. Peaking deflection (increase in vertical diameter) was observed up to layer 10. Surcharge load of cover added after layer 10 caused deflection in pipe. During peaking deflection, horizontal and vertical deflections were approximately equal in magnitude. Horizontal deflection due to surcharge load was less than 40% of vertical deflection.

#### 4.5.3 Earth Pressure

Earth Pressures were measured at ten locations described in Section 3.5.2. The vertical pressures were measured at center under the pipe and three locations (south, center, and north) on top of pipe. Horizontal pressures were measured at pipe springline and soil box walls. Table 4.10 presents the recorded pressures at these locations at different stages of the test. Figure 4.7 illustrates graphical representation of earth pressure cell data.

Table 4.8: Bedding and Embedment Layers Densities for Test 2

| Layer No. | Layer Thickness (in.) | Embedment Depth (in.) | Average Dry Density (pcf) | Average Water Content (%) | Average wet Density (pcf) | Percent Compaction (%) | Soil Type |
|---|---|---|---|---|---|---|---|
| **Bedding** | | | | | | | |
| 1 | 6 | N/A | 91.2 | 21.5 | 110.8 | 92.5 | Lime Stabilized |
| 2 | 6 | N/A | 90.9 | 22.1 | 111.0 | 92.2 | Lime Stabilized |
| **Embedment** | | | | | | | |
| 1 | 8 | 8 | 90.5 | 20.4 | 109.0 | 91.8 | Lime Stabilized |
| 2 | 7 | 15 | 90.3 | 19.5 | 107.9 | 91.6 | Lime Stabilized |
| 3 | 8 | 23 | 90.3 | 21.2 | 109.4 | 91.6 | Lime Stabilized |
| 4 | 7 | 30 | 89.6 | 19.3 | 106.9 | 90.9 | Lime Stabilized |
| 5 | 7 | 37 | 89.7 | 21.6 | 109.1 | 91.0 | Lime Stabilized |
| 6 | 7 | 42 | 98.1 | 17.2 | 115.0 | 90.7 | Untreated Native |
| 7 | 7 | 49 | 97.6 | 16.1 | 113.3 | 90.3 | Untreated Native |
| 8 | 7 | 56 | 96.9 | 17.6 | 113.9 | 89.6 | Untreated Native |
| 9 | 8 | 64 | 96.8 | 15.5 | 111.8 | 89.5 | Untreated Native |
| 10 | 8 | 72 | 97.1 | 17.3 | 113.9 | 89.8 | Untreated Native |

Table 4.9: Vertical and Horizontal Deflection of Pipe in Test 2

| Description | Vertical Deflection (in.) | | | Horizontal Deflection (in.) | | |
|---|---|---|---|---|---|---|
| | South | Center | North | South | Center | North |
| Strut Placement* | 0.52 | 0.52 | 0.52 | -0.52 | -0.52 | -0.52 |
| Layer 1 | 0.52 | 0.52 | 0.52 | -0.52 | -0.52 | -0.52 |
| Layer 2 | 0.52 | 0.52 | 0.52 | -0.52 | -0.52 | -0.52 |
| Layer 3 | 0.60 | 0.56 | 0.54 | -0.57 | -0.62 | -0.54 |
| Layer 4 | 0.70 | 0.62 | 0.59 | -0.67 | -0.62 | -0.62 |
| Layer 5 | 0.76 | 0.72 | 0.73 | -0.82 | -0.75 | -0.75 |
| Layer 6 | 0.94 | 0.95 | 0.88 | -0.91 | -0.88 | -0.84 |
| Layer 7 | 1.00 | 1.00 | 0.93 | -1.12 | -1.14 | -1.04 |
| Layer 8 | 1.05 | 1.20 | 1.10 | -1.21 | -1.24 | -1.11 |
| Layer 9 | 1.12 | 1.24 | 1.13 | -1.22 | -1.26 | -1.12 |
| Layer 10 | 1.14 | 1.24 | 1.13 | -1.24 | -1.26 | -1.13 |
| Backfill Complete | 0.94 | 0.99 | 0.94 | -1.16 | -1.09 | -1.04 |
| Week 1 | 0.93 | 0.97 | 0.93 | -1.16 | -1.13 | -1.04 |
| Week 2 | 0.92 | 0.96 | 0.92 | -1.16 | -1.13 | -1.04 |
| Week 3 | 0.92 | 0.95 | 0.91 | -1.16 | -1.13 | -1.04 |

Table 4.9 (Continued)

| Description | Vertical Deflection (in.) | | | Horizontal Deflection (in.) | | |
|---|---|---|---|---|---|---|
| | South | Center | North | South | Center | North |
| Week 4 | 0.91 | 0.95 | 0.91 | -1.16 | -1.13 | -1.03 |
| Week 5 | 0.90 | 0.95 | 0.91 | -1.16 | -1.13 | -1.03 |
| Week 6 | 0.90 | 0.95 | 0.90 | -1.16 | -1.13 | -1.03 |
| Week 7 | 0.90 | 0.95 | 0.90 | -1.16 | -1.13 | -1.03 |
| Week 8 | 0.90 | 0.94 | 0.90 | -1.16 | -1.13 | -1.03 |
| Week 9 | 0.89 | 0.94 | 0.90 | -1.16 | -1.13 | -1.03 |
| **Immediate Deflection Due to Surcharge Load** | **-0.20** | **-0.25** | **-0.19** | **0.08** | **0.13** | **0.09** |
| **Total Deflection Due to Surcharge Load** | **-0.25** | **-0.3** | **-0.23** | **0.08** | **0.13** | **0.10** |

* Assumed value

Note: Refer to Figure 3.14 for North, Center, and South Locations
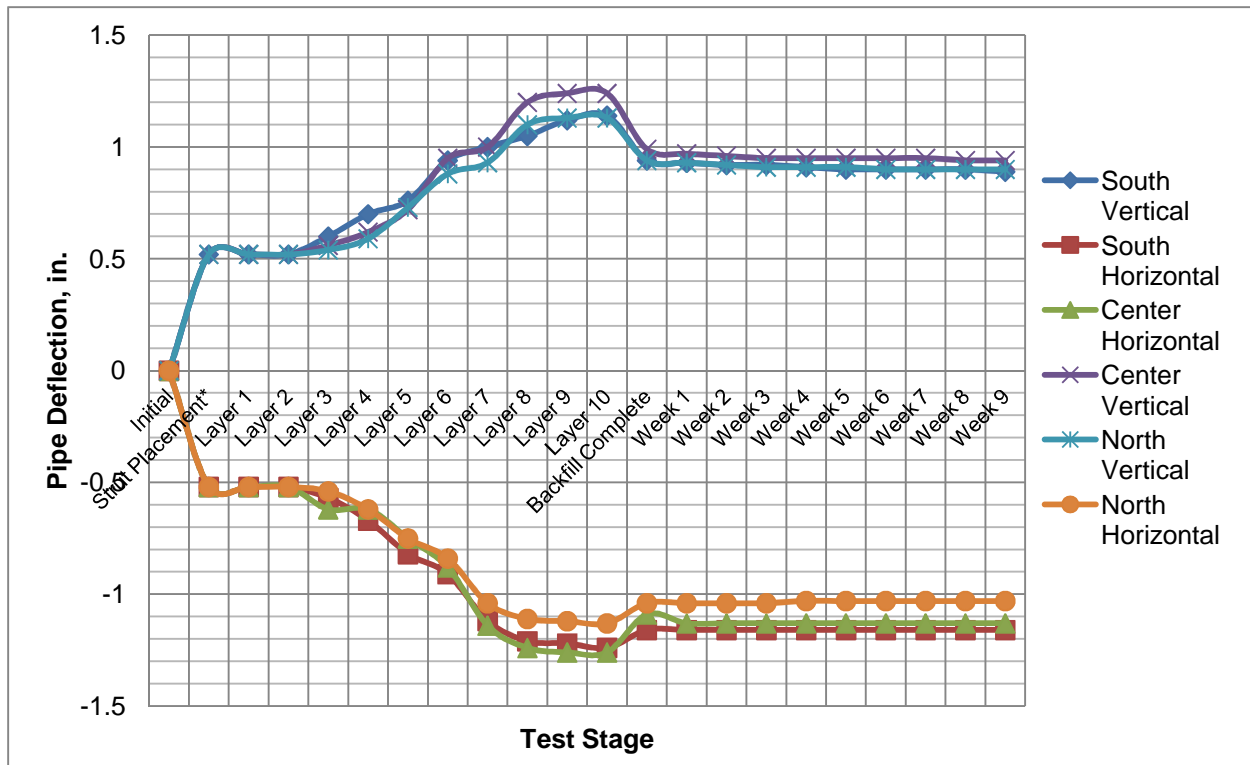


Figure 4.6: Deflection of Pipe in Test 2

Table 4.10: Earth Pressure Cell Data for Test 2

| Description | Horizontal/Vertical (Springline) Loads, psi | | | | | | | | | |
| | South | Center | | | | | | North | Walls | |
| | Top | Bottom | Springline East | East Wall | Springline West | West Wall | Top | Top | South | North |
| --- | --- | --- | --- | --- | --- | --- | --- | --- | --- | --- |
| Initial | N/A | 6.8 | N/A | N/A | N/A | N/A | N/A | N/A | N/A | N/A |
| Layer 1 | N/A | 7.1 | N/A | N/A | N/A | N/A | N/A | N/A | N/A | N/A |
| Layer 2 | N/A | 6.8 | N/A | N/A | N/A | N/A | N/A | N/A | N/A | N/A |
| Layer 3 | N/A | 5.2 | N/A | N/A | N/A | N/A | N/A | N/A | N/A | N/A |
| Layer 4 | N/A | 5.1 | N/A | N/A | N/A | N/A | N/A | N/A | N/A | N/A |
| Layer 5 | N/A | 5.9 | 3.5 | 0.7 | N/A | 0.4 | N/A | N/A | 0.3 | N/A |
| Layer 6 | N/A | 9.8 | 3.0 | 1.0 | N/A | 1.1 | N/A | N/A | 0.6 | N/A |
| Layer 7 | N/A | 9.6 | 1.7 | 1.3 | N/A | 0.8 | N/A | N/A | 0.6 | N/A |
| Layer 8 | N/A | 11.9 | 3.1 | 0.9 | N/A | 0.7 | N/A | N/A | 0.8 | N/A |
| Layer 9 | N/A | 17.3 | 0.4 | 0.8 | N/A | 0.8 | N/A | N/A | 1.1 | N/A |
| Layer 10 | N/A | 18.5 | 0.3 | 0.6 | N/A | 0.7 | N/A | N/A | 1.1 | N/A |
| Backfill Complete | 6.8 | 51.1 | 3.5 | 1.8 | N/A | 2.6 | 5.4 | 7.5 | 1.8 | N/A |
| Week 1 | 7.2 | 53.7* | 3.7 | 1.9 | N/A | 2.3 | 4.9 | 7.6 | 2.0 | N/A |
| Week 2 | 6.9 | 53.7* | 3.3 | 1.7 | N/A | 1.8 | 4.7 | 7.0 | 1.7 | N/A |
| Week 3 | 7.1 | 53.7* | 3.4 | 1.8 | N/A | 1.7 | 4.6 | 7.2 | 1.8 | N/A |
| Week 4 | 6.6 | 53.7* | 3.0 | 1.8 | N/A | 1.6 | 4.3 | 7.2 | 1.9 | N/A |
| Week 5 | 6.8 | 53.7* | 3.2 | 1.6 | N/A | 1.6 | 4.3 | 7.5 | 1.8 | N/A |
| Week 6 | 6.5 | 53.7* | 2.9 | 1.7 | N/A | 1.7 | 4.1 | 7.3 | 1.7 | N/A |
| Week 7 | 6.4 | 53.7* | 3.1 | 1.8 | N/A | 1.5 | 4.0 | 7.1 | 1.8 | N/A |
| Week 8 | 6.2 | 53.7* | 2.6 | 1.8 | N/A | 1.5 | 3.9 | 6.9 | 1.8 | N/A |
| Week 9 | 6.2 | 53.7* | 2.8 | 1.7 | N/A | 1.5 | 3.6 | 7.2 | 1.8 | N/A |

* Out of the range of the instrument

4.5.4 Pipe Wall Strains

Strain gages were installed at twenty-four points circumferentially, as described in Section 3.5.2; strains were measured successfully at eighteen points. Tables 4.11, 4.12 and 4.13 present strains on pipe wall at different stages of Test 2. Figures 4.8, 4.9 and 4.10 illustrate graphical representation of pipe wall strain data. The strain data are so plotted in order to show exaggerated shape of pipe deformation.
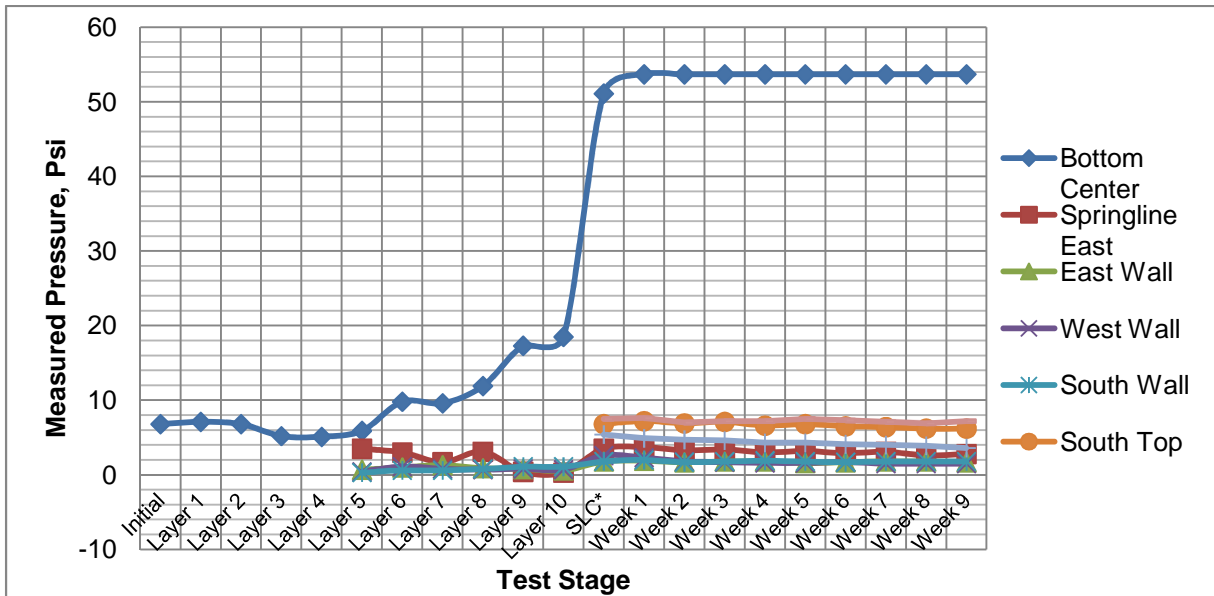
Figure 4.7: Earth Pressures at Different Stages of Test 2

Table 4.11: Circumferential Strains at South Cross Section in Test 2

| Description | Strain (Micro Strain, µε) | | | | | | | |
|---|---|---|---|---|---|---|---|---|
| | Crown | 45 | SL | 135 | Invert | 225 | SL | 315 |
| Initial | 0 | 0 | 0 | 0 | 0 | 0 | 0 | 0 |
| Layer 1 | 12 | 10 | 13 | N/A | 7 | 7 | N/A | 13 |
| Layer 2 | 7 | -29 | -4 | N/A | -45 | -2 | N/A | -19 |
| Layer 3 | -132 | -49 | 51 | N/A | -40 | 12 | N/A | 0 |
| Layer 4 | -185 | 5 | 54 | N/A | -48 | 18 | N/A | -21 |
| Layer 5 | -230 | 96 | 73 | N/A | -54 | -3 | N/A | -48 |
| Layer 6 | -392 | 156 | 82 | N/A | -59 | -32 | N/A | -70 |
| Layer 7 | -309 | 262 | 81 | N/A | -69 | -58 | N/A | -100 |
| Layer 8 | -367 | 228 | 93 | N/A | -73 | -60 | N/A | 30 |
| Layer 9 | -418 | 223 | 87 | N/A | -87 | -64 | N/A | 48 |
| Layer 10 | -387 | 232 | 62 | N/A | -89 | -62 | N/A | 15 |
| Backfill Complete | -370 | 144 | 80 | N/A | -41 | -105 | N/A | -35 |
| Week 1 | -375 | 135 | 83 | N/A | -45 | -108 | N/A | -32 |
| Week 2 | -377 | 129 | 74 | N/A | -48 | -115 | N/A | -47 |
| Week 3 | -368 | 119 | 82 | N/A | -36 | -114 | N/A | -34 |
| Week 4 | -375 | 107 | 69 | N/A | -39 | -132 | N/A | -3 |
| Week 5 | -389 | 106 | 58 | N/A | -57 | -139 | N/A | -18 |
| Week 6 | -392 | 100 | 54 | N/A | -56 | -142 | N/A | -21 |
| Week 7 | -395 | 104 | 57 | N/A | -59 | -145 | N/A | -24 |
| Week 8 | -402 | 103 | 49 | N/A | -62 | -132 | N/A | -9 |
| Week 9 | -389 | 96 | 52 | N/A | -65 | -140 | N/A | -13 |

Table 4.12: Circumferential Strains at Center Cross Section in Test 2

| Description | Strain (Micro Strain, με) | | | | | | | |
|---|---|---|---|---|---|---|---|---|
| | Crown | 45 | SL | 135 | Invert | 225 | SL | 315 |
| Initial | 0 | 0 | 0 | 0 | 0 | 0 | 0 | 0 |
| Layer 1 | 5 | N/A | 4 | 2 | -7 | 5 | 2 | N/A |
| Layer 2 | 5 | N/A | 22 | 25 | -61 | 22 | -18 | N/A |
| Layer 3 | 26 | N/A | 64 | -5 | -90 | 52 | -18 | N/A |
| Layer 4 | -20 | N/A | 73 | -17 | -85 | 55 | -13 | N/A |
| Layer 5 | -92 | N/A | 77 | -25 | -72 | 33 | -12 | N/A |
| Layer 6 | -147 | N/A | 86 | -32 | -59 | 12 | -8 | N/A |
| Layer 7 | -198 | N/A | 115 | -55 | -54 | -8 | -6 | N/A |
| Layer 8 | -289 | N/A | 122 | -56 | -23 | -7 | -4 | N/A |
| Layer 9 | -333 | N/A | 117 | -62 | -4 | -11 | -14 | N/A |
| Layer 10 | -293 | N/A | 123 | -71 | -5 | -9 | -15 | N/A |
| Backfill Complete | -225 | N/A | 125 | -139 | 375 | -77 | -45 | N/A |
| Week 1 | -229 | N/A | 126 | -150 | 415 | -86 | -48 | N/A |
| Week 2 | -234 | N/A | 125 | -162 | 420 | -87 | -55 | N/A |
| Week 3 | -246 | N/A | 132 | -159 | 415 | -79 | -52 | N/A |
| Week 4 | -244 | N/A | 145 | -163 | 418 | -91 | -71 | N/A |
| Week 5 | -233 | N/A | 162 | -167 | 423 | -93 | -73 | N/A |
| Week 6 | -261 | N/A | 163 | -182 | 429 | -88 | -145 | N/A |
| Week 7 | -283 | N/A | 152 | -173 | 417 | -96 | -132 | N/A |
| Week 8 | -284 | N/A | 245 | -169 | 425 | -95 | -139 | N/A |
| Week 9 | -275 | N/A | 266 | -176 | 431 | -106 | -148 | N/A |

Table 4.13: Circumferential Strains at North Cross Section in Test 2

| Description | Strain (Micro Strain, με) | | | | | | | |
|---|---|---|---|---|---|---|---|---|
| | Crown | 45 | SL | 135 | Invert | 225 | SL | 315 |
| Initial | 0 | 0 | 0 | 0 | 0 | 0 | 0 | 0 |
| Layer 1 | 4 | N/A | 5 | 1 | -1 | 18 | 40 | -9 |
| Layer 2 | -231 | N/A | -5 | 24 | -32 | -6 | 174 | -37 |
| Layer 3 | -283 | N/A | 29 | 0 | -50 | 60 | 162 | -80 |
| Layer 4 | N/A | N/A | 35 | -26 | -62 | 73 | 167 | -85 |
| Layer 5 | N/A | N/A | 52 | -38 | -57 | 48 | 153 | -42 |
| Layer 6 | N/A | N/A | 38 | -50 | -58 | 25 | 148 | -35 |
| Layer 7 | N/A | N/A | 28 | -65 | -42 | -19 | 150 | 6 |
| Layer 8 | N/A | N/A | 17 | -65 | -37 | -21 | 144 | 141 |
| Layer 9 | N/A | N/A | 11 | -71 | -34 | -30 | 138 | 142 |
| Layer 10 | N/A | N/A | 8 | -67 | -34 | -30 | 141 | 128 |
| Backfill Complete | N/A | N/A | -111 | -139 | 67 | -132 | 409 | 65 |
| Week 1 | N/A | N/A | -128 | -150 | 80 | -133 | 408 | 57 |

Table 4.13 (Continued)

| Description | Strain (Micro Strain, µε) | | | | | | | |
|---|---|---|---|---|---|---|---|---|
| | Crown | 45 | SL | 135 | Invert | 225 | SL | 315 |
| Week 2 | N/A | N/A | -135 | -148 | 82 | -139 | N/A | N/A |
| Week 3 | N/A | N/A | -133 | -153 | 85 | -138 | N/A | N/A |
| Week 4 | N/A | N/A | -139 | -162 | 83 | -134 | N/A | N/A |
| Week 5 | N/A | N/A | -144 | -165 | 90 | -140 | N/A | N/A |
| Week 6 | N/A | N/A | -151 | -155 | 87 | -145 | N/A | N/A |
| Week 7 | N/A | N/A | -142 | -158 | 94 | -146 | N/A | N/A |
| Week 8 | N/A | N/A | -146 | -161 | 91 | -142 | N/A | N/A |
| Week 9 | N/A | N/A | -148 | -159 | 93 | -141 | N/A | N/A |

Note: Strain Gages are located with crown representing 0 degrees and in increment of 45 degrees in clockwise direction.
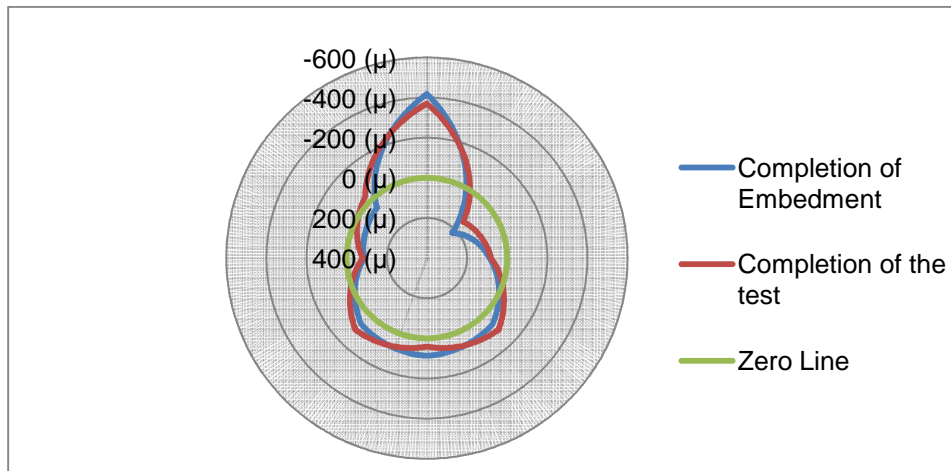


Figure 4.8: Plotted Strain Data for South Cross Section in Test 2
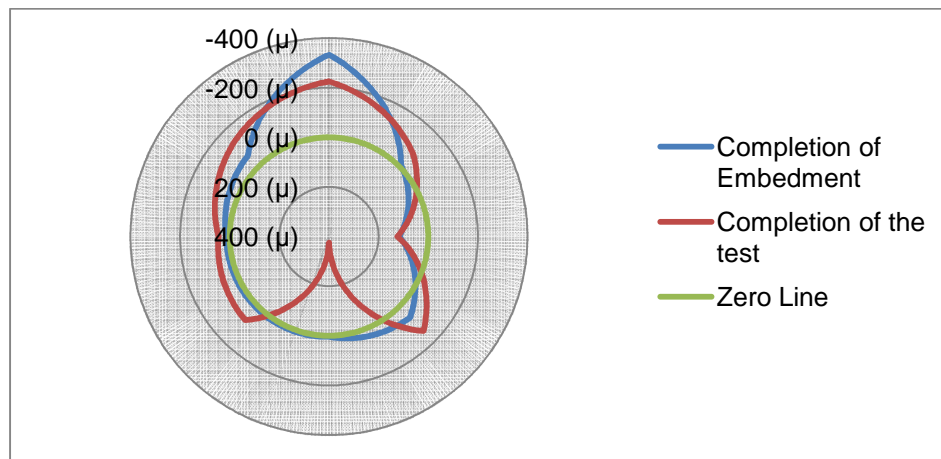


Figure 4.9: Plotted Strain Data for Center Cross Section in Test 2
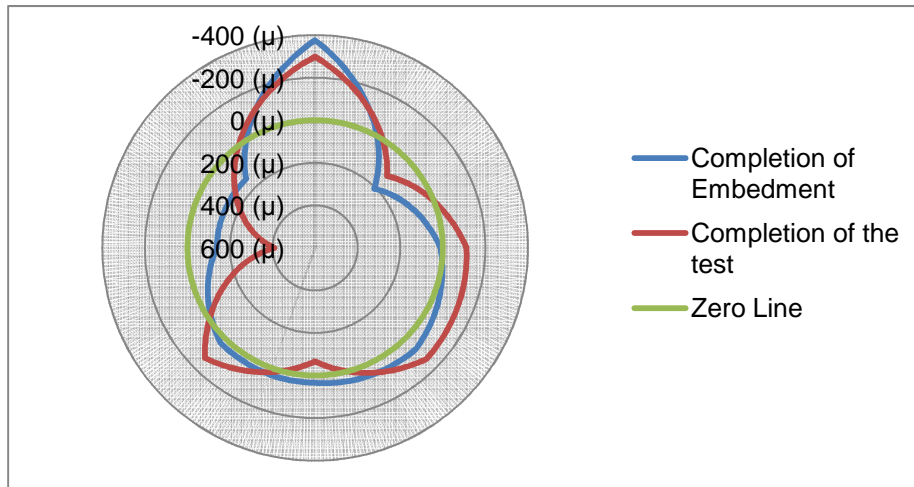
Figure 4.10: Plotted Strain Data for Center Cross Section in Test 2

### 4.6 Test 1a

4.6.1 Embedment Layers

Nine layers of embedment were placed during Test 1a to cover the pipe. Densities of these layers were measured by nuclear density gage. Table 4.14 presents thicknesses, and compaction densities of these layers.

Table 4.14: Embedment Layer Densities for Test 1a

| Layer No. | Average Layer Thickness in. | Embedment Height in. | Average Dry Density (pcf) | Average Water Content (%) | Average wet Density (pcf) | Percent Compaction (%) |
|---|---|---|---|---|---|---|
| 1 | 7 | 7 | 99.5 | 18.1 | 117.5 | 92.0 |
| 2 | 8 | 15 | 98.7 | 21.8 | 120.2 | 91.3 |
| 3 | 9 | 24 | 99.7 | 19.0 | 118.7 | 91.6 |
| 4 | 9 | 33 | 100.2 | 18.2 | 118.4 | 92.7 |
| 5 | 7 | 40 | 99.7 | 18.6 | 118.2 | 92.2 |
| 6 | 8 | 48 | 100.7 | 16.4 | 117.2 | 93.2 |
| 7 | 10 | 58 | 99.8 | 15.7 | 115.4 | 92.3 |
| 8 | 9 | 67 | 99.9 | 10.6 | 110.5 | 92.4 |
| 9 | 11 | 78 | 98.7 | 12.0 | 110.5 | 91.3 |

4.6.2 Pipe Deflection

Pipe deflection during Test 1a is summarized in Table 4.15. Figure 4.11 illustrates graphical representation of deflection during Test 1a. Peaking deflection (increase in vertical diameter) was

observed up to layer 9. Surcharge load of cover added after layer 9 caused deflection in pipe. During peaking deflection, horizontal and vertical deflections were approximately equal in magnitude. Horizontal deflection due to surcharge load was less than 40% of vertical deflection.

4.6.3 Earth Pressure

Earth Pressures were measured at ten locations described in Section 3.5.3. The vertical pressures were measured at center under the pipe and three locations (south, center, and north) on top of pipe. Horizontal pressures were measured at pipe springline and soil box walls. Table 4.16 presents the recorded pressures at these locations at different stages of the test. Figure 4.12 illustrates graphical representation of earth pressure cell data.

Table 4.15: Pipe Deflection in Test 1a

| Description | Vertical Deflection (in.) | | | Horizontal Deflection (in.) | | |
|---|---|---|---|---|---|---|
| | South | Center | North | South | Center | North |
| Strut Placement | 0.41 | 0.41 | 0.38 | -0.39 | -038 | -0.36 |
| Layer 1 | 0.41 | 0.41 | 0.38 | -0.39 | -0.38 | -0.36 |
| Layer 2 | 0.41 | 0.41 | 0.38 | -0.39 | -0.38 | -0.36 |
| Layer 3 | 0.83 | 0.85 | 0.74 | -0.8 | -0.87 | -0.72 |
| Layer 4 | 1.13 | 1.12 | 1.03 | -1.15 | -1.09 | -1.07 |
| Layer 5 | 1.57 | 1.51 | 1.33 | -1.66 | -1.59 | -1.48 |
| Layer 6 | 1.82 | 1.75 | 1.59 | -2.00 | -1.88 | -1.75 |
| Layer 7 | 2.08 | 2.09 | 1.86 | -2.20 | -2.04 | -1.96 |
| Layer 8 | 2.17 | 2.13 | 1.95 | -2.20 | -2.06 | -1.96 |
| Layer 9 | 2.22 | 2.17 | 1.99 | -2.20 | -2.05 | -1.95 |
| Backfill Complete | 1.84 | 1.73 | 1.57 | -2.07 | -1.99 | -1.78 |
| Week 1 | 1.75 | 1.65 | 1.48 | -2.03 | -1.94 | -1.75 |
| Week 2 | 1.72 | 1.62 | 1.46 | -2.02 | -1.94 | -1.74 |
| Week 3 | 1.71 | 1.61 | 1.45 | -2.02 | -1.93 | -1.73 |
| Week 4 | 1.72 | 1.61 | 1.45 | -2.02 | -1.93 | -1.72 |
| **Immediate Deflections Due to Surcharge Load** | **-0.38** | **-0.44** | **-0.42** | **0.13** | **0.06** | **0.17** |
| **Total Deflections Due to Surcharge Load** | **-0.5** | **-0.56** | **-0.54** | **0.18** | **0.12** | **0.23** |

Note: Refer to Figure 3.15 for North, Center, and South Locations
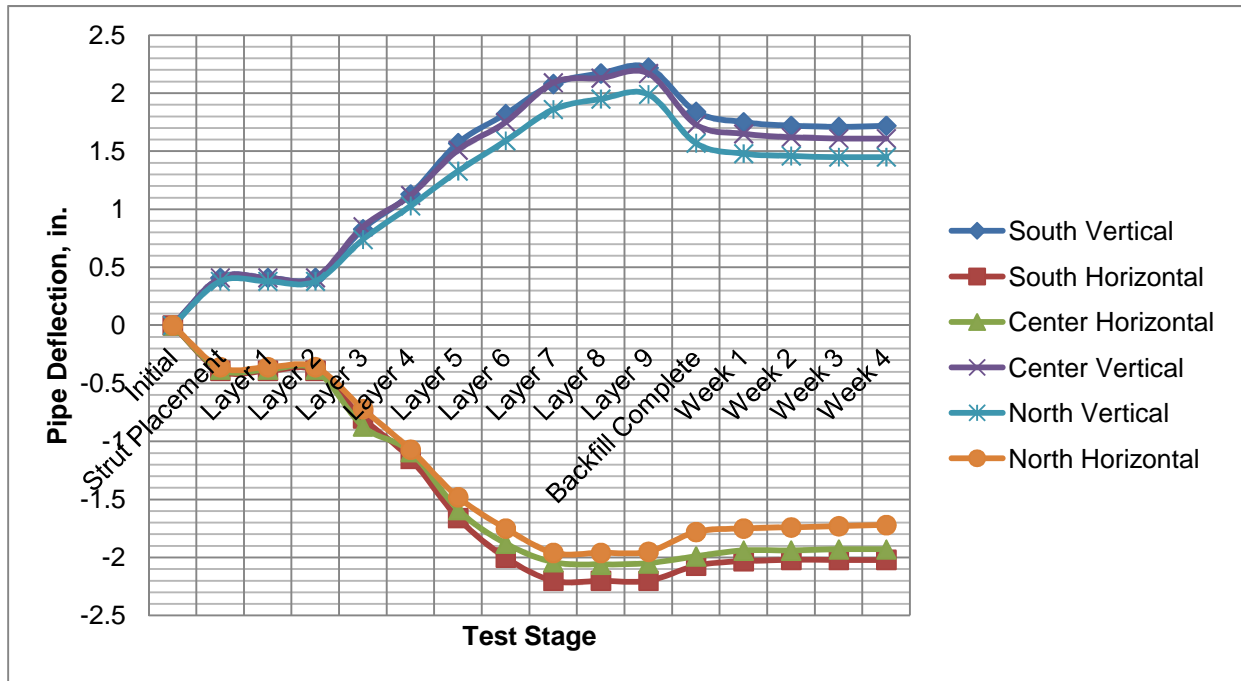
Figure 4.11: Deflection of Pipe in Test 1a

Table 4.16: Earth Pressure Cell Data for Test 1a

| Description | Horizontal/Vertical (Springline) Pressures, psi | | | | | | | | | |
| | Pipe South | Pipe Center | | | | | | Pipe North | Soil-box Walls | |
| | Top | Bottom | Sprin. East | East Wall | Spring. West | West Wall | Top | Top | South | North |
| Initial | N/A | 27.7 | N/A | N/A | N/A | N/A | N/A | N/A | N/A | N/A |
| Layer 1 | N/A | 26.8 | N/A | N/A | N/A | N/A | N/A | N/A | N/A | N/A |
| Layer 2 | N/A | 24.5 | N/A | N/A | N/A | N/A | N/A | N/A | N/A | N/A |
| Layer 3 | N/A | 23.3 | N/A | N/A | N/A | N/A | N/A | N/A | N/A | N/A |
| Layer 4 | N/A | 21.6 | N/A | N/A | N/A | N/A | N/A | N/A | N/A | N/A |
| Layer 5 | N/A | 21.6 | 3.7 | 1.4 | 2.8 | 0.8 | N/A | N/A | 0.4 | 0.5 |
| Layer 6 | N/A | 21.3 | 3.8 | 1.5 | 2.1 | 0.8 | N/A | N/A | 0.4 | 0.5 |
| Layer 7 | N/A | 21.2 | 3.1 | 1.1 | 0.5 | 0.7 | N/A | N/A | 0.6 | 0.4 |
| Layer 8 | N/A | 21.3 | 1.5 | 0.9 | 0.8 | 0.5 | N/A | N/A | 0.6 | 0.4 |
| Layer 9 | N/A | 21.3 | 2.1 | 0.9 | 1.3 | 0.6 | N/A | N/A | 0.6 | 0.4 |
| Backfill Complete | 15.5 | 24.7 | 4.9 | 2.5 | 5.4 | 2.2 | 9.6 | 9.2 | 1.1 | 0.7 |
| Week 1 | 13.0 | 24.8 | 4.1 | 2.8 | 5.4 | 2.7 | 8.8 | 8.9 | 1.5 | 1.1 |
| Week 2 | 12.5 | 25.4 | 3.6 | 2.6 | 5.2 | 2.5 | 8.7 | 8.9 | 1.4 | 0.9 |
| Week 3 | 12.8 | 25.6 | 3.4 | 2.5 | 5.3 | 2.5 | 8.9 | 9.1 | 1.5 | 0.9 |
| Week 4 | 9.4 | 25.7 | 2.9 | 2.1 | 5.3 | 2.2 | 6.8 | 8.8 | 1.3 | 0.8 |
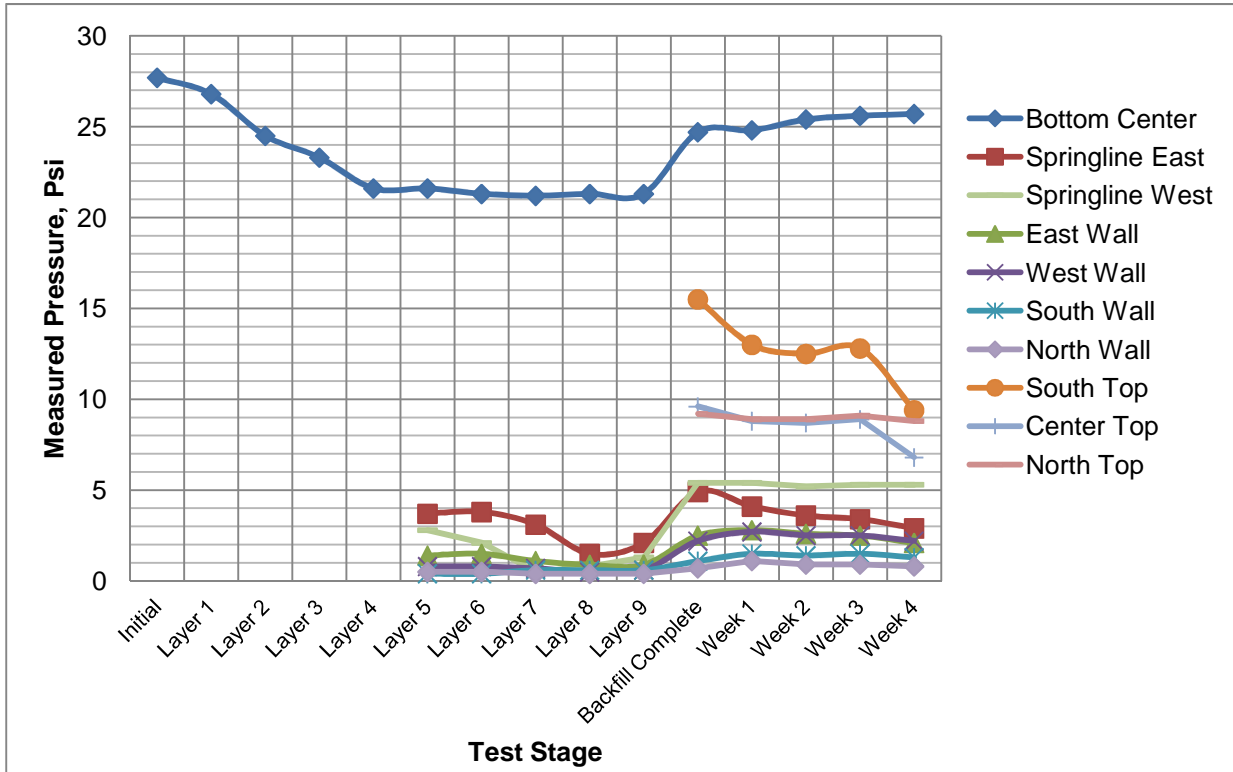
Figure 4.12: Earth Pressures at Different Stages of Test 1a

4.6.4 Pipe Wall Strains

Strain gages were installed at thirty-six points circumferentially, as described in Section 3.5.3; strains were measured successfully at thirty-two points. Tables 4.17 to 4.22 present strains on pipe wall at different stages of Test 1a. Figures 4.12, 4.13 and 4.14 illustrate graphical representation of pipe wall strain data. The strain data are so plotted in order to show exaggerated shape of pipe deformation.

Table 4.17: Strains at South Cross Section Interior Wall in Test 1a

| Description | Strain (Micro Strain, µε) | | | | | | | | |
|---|---|---|---|---|---|---|---|---|---|
| | Crown | 45 | SL | 135 | Invert | 225 | SL | 315 | Crown Long |
| Initial/Strut Placement | -96 | 11 | 72 | 5 | -101 | 25 | 58 | 41 | -396 |
| Layer 1 | -56 | -2 | 61 | 75 | -144 | 75 | 51 | 29 | -363 |
| Layer 2 | -15 | -7 | 45 | 123 | -177 | 128 | 48 | 10 | -316 |
| Layer 3 | -90 | -37 | 125 | 47 | -222 | 87 | 132 | 0 | -366 |
| Layer 4 | -133 | -59 | 159 | 31 | -263 | 58 | 213 | 6 | -368 |
| Layer 5 | -243 | -80 | 331 | -32 | -283 | 26 | 329 | 6 | -357 |
| Layer 6 | -330 | -64 | 424 | -74 | -291 | 14 | 329 | 29 | -344 |
| Layer 7 | -477 | -43 | 391 | -99 | -276 | -6 | 260 | 243 | -345 |

80

Table 4.17 (Continued)

| Description | Strain (Micro Strain, µε) | | | | | | | | |
|---|---|---|---|---|---|---|---|---|---|
| | Crown | 45 | SL | 135 | Invert | 225 | SL | 315 | Crown Long |
| Layer 8 | -591 | 110 | 369 | -116 | -250 | -15 | 257 | 338 | -350 |
| Layer 9 | -639 | 128 | 359 | -128 | -224 | -24 | 260 | 338 | -242 |
| Backfill Complete | -242 | 80 | 382 | -257 | 86 | -152 | 255 | 262 | N/A |
| Week 1 | -426 | 80 | 372 | -278 | 133 | -201 | 250 | 259 | N/A |
| Week 2 | -586 | 79 | 369 | -283 | 141 | -197 | 250 | 259 | N/A |
| Week 3 | -585 | 77 | 360 | -289 | 151 | -209 | 247 | 257 | N/A |
| Week 4 | -581 | 76 | 354 | -295 | 169 | -204 | 245 | 261 | N/A |

Table 4.18: Strain at South Cross Section Exterior Wall in Test 1a

| Description | Strain (Micro Strain, µε) | | |
|---|---|---|---|
| | SL | Top | SL |
| Initial/Strut Placement | -65 | 97 | -62 |
| Layer 1 | -51 | 68 | -46 |
| Layer 2 | -69 | 79 | -73 |
| Layer 3 | -80 | 112 | -123 |
| Layer 4 | -165 | 154 | -175 |
| Layer 5 | N/A | 262 | -404 |
| Layer 6 | N/A | 355 | N/A |
| Layer 7 | N/A | 517 | N/A |
| Layer 8 | N/A | 642 | N/A |
| Layer 9 | N/A | 672 | N/A |
| Backfill Complete | N/A | 515 | N/A |
| Week 1 | N/A | 507 | N/A |
| Week 2 | N/A | 506 | N/A |
| Week 3 | N/A | 504 | N/A |
| Week 4 | N/A | 499 | N/A |

Table 4.19: Strains at Center Cross Section Interior Wall in Test 1a

| Description | Strain (Micro Strain, µε) | | | | | | | | |
|---|---|---|---|---|---|---|---|---|---|
| | Crown | 45 | SL | 135 | Invert | 225 | SL | 315 | Crown Long |
| Initial/Strut Placement | -75 | 7 | 70 | 14 | -85 | 27 | 65 | 27 | 6 |
| Layer 1 | -83 | -8 | 81 | 16 | -108 | 37 | 67 | 22 | 7 |
| Layer 2 | -90 | -15 | 57 | 22 | -126 | 42 | 86 | 3 | 9 |
| Layer 3 | -99 | -37 | 132 | 31 | -209 | 55 | 129 | 1 | 4 |
| Layer 4 | -107 | -72 | 180 | 52 | -369 | 70 | 205 | -1 | 8 |
| Layer 5 | -217 | -93 | 352 | -11 | -389 | 38 | 321 | -1 | 19 |
| Layer 6 | -304 | -77 | 445 | -53 | -397 | 26 | 321 | 22 | 32 |
| Layer 7 | -451 | -56 | 412 | -78 | -382 | 6 | 252 | 236 | 31 |
| Layer 8 | -565 | 97 | 390 | -95 | -356 | -3 | 249 | 331 | 26 |
| Layer 9 | -613 | 115 | 380 | -107 | -330 | -12 | 252 | 331 | 134 |
| Backfill Complete | -506 | -18 | 372 | -216 | -258 | 168 | 268 | 272 | 60 |
| Week 1 | -516 | -16 | 366 | -236 | -260 | 221 | 268 | 273 | 64 |
| Week 2 | -509 | -16 | 363 | -239 | -258 | 230 | 268 | 273 | 60 |
| Week 3 | -503 | -15 | 362 | -244 | -260 | 242 | 265 | 275 | 63 |
| Week 4 | -501 | -15 | 354 | -249 | -261 | 264 | 264 | 276 | 59 |

Table 4.20: Strains at Center Cross Section Exterior Wall in Test 1a

| Description | Strain (Micro Strain, µε) | | |
|---|---|---|---|
| | SL | Top | SL |
| Initial/Strut Placement | -62 | 96 | -50 |
| Layer 1 | -46 | 83 | -35 |
| Layer 2 | -53 | 77 | -50 |
| Layer 3 | -115 | 101 | -86 |
| Layer 4 | -215 | 143 | -135 |
| Layer 5 | -373 | 232 | -304 |
| Layer 6 | -372 | 318 | -419 |
| Layer 7 | -297 | 490 | -375 |
| Layer 8 | -298 | 591 | -361 |
| Layer 9 | -295 | 634 | -354 |
| Layer 10 | -306 | 602 | -368 |
| Backfill Complete | -317 | 499 | -383 |
| Week 1 | -312 | 498 | -377 |
| Week 2 | -311 | 495 | -373 |
| Week 3 | -311 | 493 | -371 |
| Week 4 | -307 | 499 | -361 |

Table 4.21: Strains at North Cross Section Interior Wall in Test 1a

| Description | Strain (Micro Strain, με) | | | | | | | | |
|---|---|---|---|---|---|---|---|---|---|
| | Crown | 45 | SL | 135 | Invert | 225 | SL | 315 | Crown Long |
| Initial/Strut Placement | -91 | 9 | 69 | 12 | -92 | 26 | 65 | 102 | -11 |
| Layer 1 | -56 | -2 | 61 | 75 | -144 | 75 | 51 | 29 | -363 |
| Layer 2 | -15 | -7 | 45 | 123 | -177 | 128 | 48 | 10 | -316 |
| Layer 3 | -90 | -37 | 125 | 47 | -222 | 87 | 132 | 0 | -366 |
| Layer 4 | -111 | -72 | 174 | 54 | -289 | 67 | 194 | 53 | -9 |
| Layer 5 | -221 | -93 | 346 | -9 | -309 | 35 | 310 | 53 | 2 |
| Layer 6 | -308 | -77 | 439 | -51 | -317 | 23 | 310 | 76 | 15 |
| Layer 7 | -455 | -56 | 406 | -76 | -302 | 3 | 241 | 290 | 14 |
| Layer 8 | -569 | 97 | 384 | -93 | -276 | -6 | 238 | 385 | 9 |
| Layer 9 | -617 | 115 | 374 | -105 | -250 | -15 | 241 | 385 | 117 |
| Backfill Complete | -534 | 47 | 391 | -325 | 232 | -178 | 273 | 242 | -18 |
| Week 1 | -532 | 51 | 382 | -348 | 283 | -198 | 269 | 239 | -13 |
| Week 2 | -531 | 53 | 382 | -352 | 292 | -201 | 269 | 240 | -12 |
| Week 3 | -535 | 52 | 375 | -358 | 304 | -206 | 263 | 253 | -11 |
| Week 4 | -533 | 57 | 372 | -366 | 326 | -215 | 260 | 260 | -9 |

Table 4.22: Strains at South Cross Section Exterior Wall in Test 1a

| Description | Strain (Micro Strain, με) | | |
|---|---|---|---|
| | SL | Top | SL |
| Initial/Strut Placement | -54 | 81 | -619 |
| Layer 1 | -38 | 68 | -604 |
| Layer 2 | -45 | 62 | -619 |
| Layer 3 | -107 | 86 | -655 |
| Layer 4 | -158 | 104 | -548 |
| Layer 5 | -316 | 193 | -717 |
| Layer 6 | -315 | 279 | -832 |
| Layer 7 | -240 | 451 | -788 |
| Layer 8 | -241 | 552 | -774 |
| Layer 9 | -238 | 595 | -767 |
| Backfill Complete | -361 | 510 | N/A |
| Week 1 | -359 | 518 | N/A |
| Week 2 | -357 | 518 | N/A |
| Week 3 | -353 | 523 | N/A |
| Week 4 | -351 | 526 | N/A |
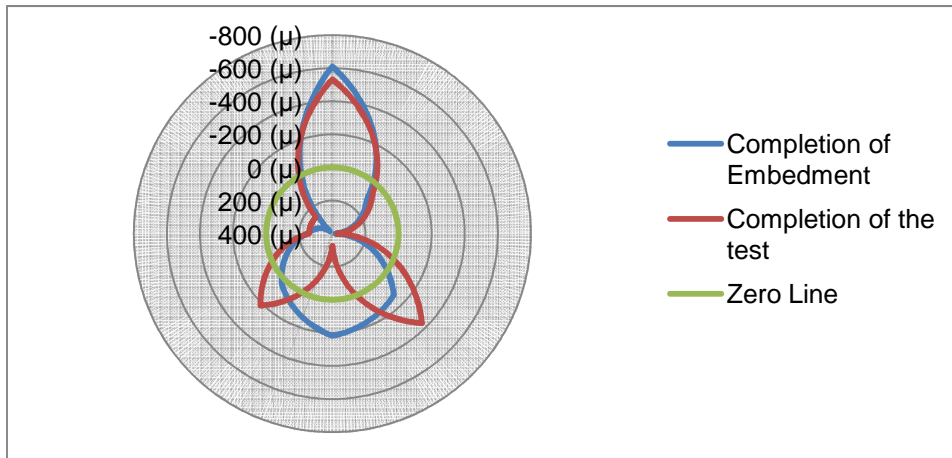
Figure 4.13: Strain at South Cross Section in Test 1a
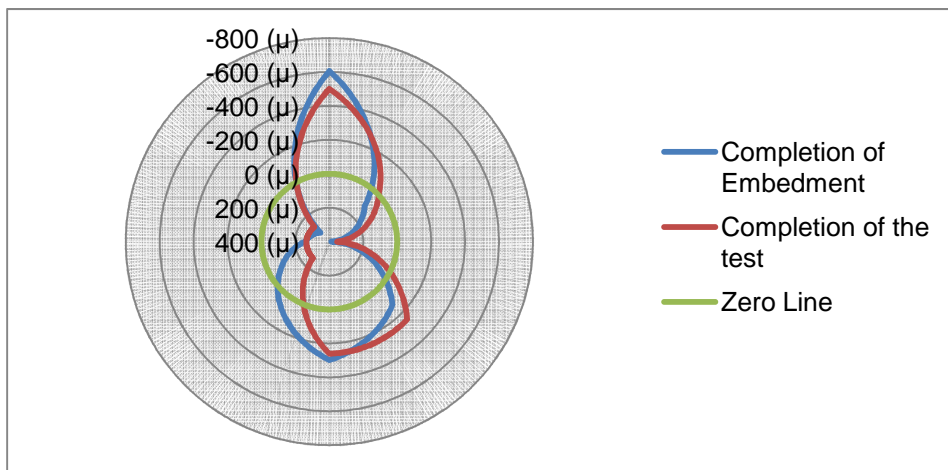


Figure 4.14: Strain at Center Cross Section in Test 1a
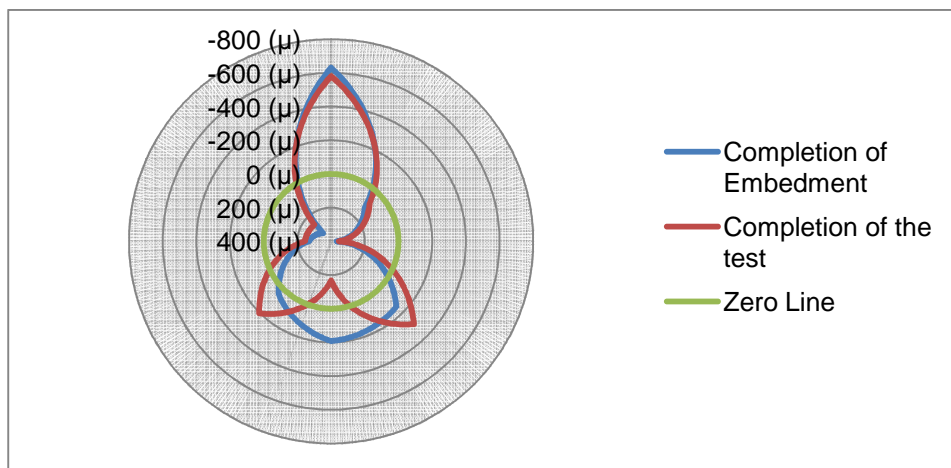


Figure 4.15: Strain at North Cross Section in Test 1a

## 4.7.1 Embedment Layers

       Six layers of crushed limestone embedment were placed during Test 3 to cover the pipe. Table 4.23 presents thicknesses of these layers.

## 4.7.2 Pipe Deflection

       Pipe deflection during Test 3 is summarized in Table 4.24. Figure 4.16 illustrates graphical representation of deflection during Test 3. Peaking deflection (increase in vertical diameter) was observed up to layer 6. Surcharge load of cover added after layer 9 caused deflection in pipe. During peaking deflection, horizontal and vertical deflections were approximately equal in magnitude. Horizontal deflection due to surcharge load was approximately 67% of vertical deflection.

Table 4.23: Embedment Layer Densities for Test 3

| Layer No. | Average Layer Thickness (in.) | Embedment Height (in.) |
|-----------|-------------------------------|------------------------|
| 1 | 18 | 18 |
| 2 | 18 | 36 |
| 3 | 12 | 48 |
| 4 | 12 | 60 |
| 5 | 12 | 72 |
| 6 | 12 | 84 |

## 4.7.3 Earth Pressure

       Earth Pressures were measured at ten locations described in Section 3.5.4. The vertical pressures were measured at center under the pipe and three locations (south, center, and north) on top of pipe. Horizontal pressures were measured at pipe springline and soil box walls. Table 4.25 presents the recorded pressures at these locations at different stages of the test. Figure 4.17 illustrates graphical representation of earth pressure cell data.

Table 4.24: Pipe Deflection in Test 3

| Description | Vertical Deflection (in.) | | | Horizontal Deflection (in.) | | |
|---|---|---|---|---|---|---|
| | South | Center | North | South | Center | North |
| Struts Placement | 0.16 | 0.24 | 0.29 | -0.19 | -0.23 | -0.30 |
| Layer 1 | 0.16 | 0.24 | 0.29 | -0.19 | -0.23 | -0.3 |
| Layer 2 | 0.16 | 0.24 | 0.29 | -0.19 | -0.23 | -0.3 |
| Layer 3 | 0.28 | 0.4 | 0.38 | -0.35 | -0.37 | -0.43 |
| Layer 4 | 0.34 | 0.41 | 0.46 | -0.37 | -0.41 | -0.49 |
| Layer 5 | 0.34 | 0.42 | 0.46 | -0.37 | -0.4 | -0.48 |
| Layer 6 | 0.36 | 0.43 | 0.47 | -0.37 | -0.4 | -0.49 |
| Backfill Complete | 0.31 | 0.35 | 0.33 | -0.33 | -0.36 | -0.42 |
| Week 1 | 0.3 | 0.34 | 0.32 | -0.32 | -0.35 | -0.41 |
| Week 2 | 0.3 | 0.34 | 0.31 | -0.32 | -0.35 | -0.4 |
| Week 3 | 0.29 | 0.34 | 0.31 | -0.31 | -0.35 | -0.4 |
| Week 4 | 0.29 | 0.34 | 0.31 | -0.31 | -0.35 | -0.4 |
| **Immediate Deflections Due to Surcharge Load** | -0.05 | -0.08 | -0.14 | 0.04 | 0.04 | 0.07 |
| **Total Deflections Due to Surcharge Load** | -0.07 | -0.06 | -0.16 | 0.06 | 0.05 | 0.09 |

Note: Refer to Figure 3.16 for North, Center, and South Locations
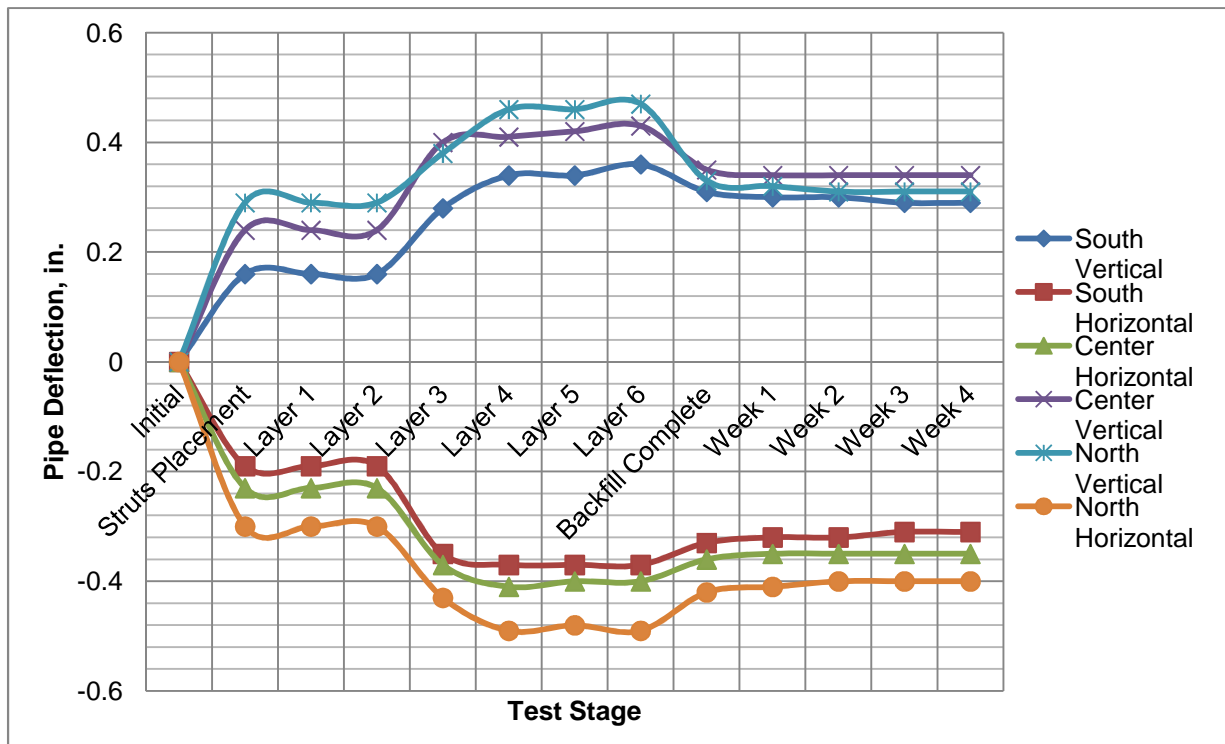


Figure 4.16: Deflection of Pipe in Test 3

Table 4.25: Earth Pressure Cell Data for Test 3

| Description | Horizontal/Vertical (Springline) Loads, psi | | | | | | | | | |
| --- | --- | --- | --- | --- | --- | --- | --- | --- | --- | --- |
| | South | Center | | | | | | North | Walls | |
| | Top | Bottom | SL East | East Wall | SL West | West Wall | Top | Top | South | North |
| Initial | N/A | 8.0 | N/A | N/A | N/A | N/A | N/A | N/A | N/A | N/A |
| Layer 1 | N/A | 7.7 | N/A | N/A | N/A | N/A | N/A | N/A | N/A | N/A |
| Layer 2 | N/A | 7.6 | N/A | N/A | N/A | N/A | N/A | N/A | N/A | N/A |
| Layer 3 | N/A | 7.6 | 0.5 | 0.4 | 0.4 | 0.3 | N/A | N/A | 0.4 | 0.5 |
| Layer 4 | N/A | 8.1 | 0.5 | 0.4 | 0.4 | 0.3 | N/A | N/A | N/A | 0.4 |
| Layer 5 | N/A | 8.9 | 0.6 | 0.4 | 0.4 | 0.3 | N/A | N/A | N/A | 0.3 |
| Layer 6 | 1.6 | 9.0 | 0.7 | 0.8 | 0.5 | 0.4 | 1.5 | 1.5 | N/A | 0.3 |
| Backfill Complete | 7.5 | 17.8 | 1.0 | 4.1 | 0.9 | 1.0 | 3.0 | 7.4 | N/A | 0.5 |
| Week 1 | 7.5 | 20.4 | 1.2 | 4.3 | 1.0 | 1.3 | 2.9 | 7.6 | N/A | 0.5 |
| Week 2 | 7.5 | 20.4 | 1.2 | 4.3 | 1.1 | 1.3 | 2.9 | 7.6 | N/A | 0.6 |
| Week 3 | 7.5 | 20.4 | 1.2 | 4.3 | 1.0 | 1.3 | 2.9 | 7.6 | N/A | 0.5 |
| Week 4 | 7.5 | 20.4 | 1.2 | 4.3 | 1.0 | 1.3 | 2.9 | 7.6 | N/A | 0.5 |
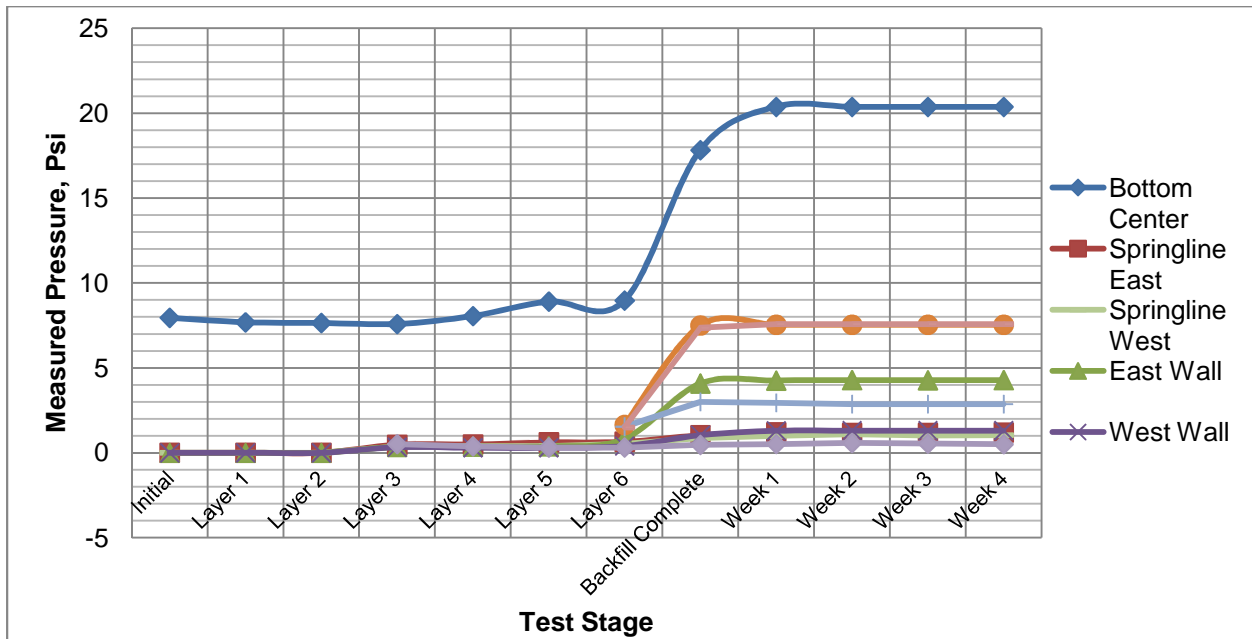


Figure 4.17: Earth Pressures at Different Stages of Test 3

### 4.7.4 Pipe Wall Strains

Strain gages were installed at thirty-six points circumferentially, as described in Section 3.5.3; strains were measured successfully at thirty-two points. Tables 4.26 to 4.31 present strains on pipe wall at different stages of Test 3. Figures 4.18, 4.19 and 4.20 illustrate graphical representation of pipe wall strain data. The strain data are so plotted in order to show exaggerated shape of pipe deformation.

Table 4.26: Strains at South Cross Section Interior Wall in Test 3

| Description | Strain (Micro Strain, µε) | | | | | | | | |
|---|---|---|---|---|---|---|---|---|---|
| | Crown | 45 | SL | 135 | Invert | 225 | SL | 315 | Crown Long |
| Initial/Strut Placement | -38 | 23 | 7 | -9 | -28 | 1 | 2 | 5 | -10 |
| Layer 1 | -28 | 12 | 10 | -3 | -33 | 9 | -1 | -5 | -11 |
| Layer 2 | -27 | 12 | 44 | -4 | -16 | 4 | 24 | -3 | -6 |
| Layer 3 | -21 | 17 | 55 | -15 | 6 | 4 | 42 | -14 | -5 |
| Layer 4 | -109 | 107 | 37 | -39 | 25 | -22 | 85 | 10 | -12 |
| Layer 5 | -108 | 108 | 38 | -37 | 27 | -19 | 87 | 11 | -13 |
| Layer 6 | -126 | 78 | 22 | -23 | 74 | -5 | 64 | -8 | -20 |
| Backfill Complete | -130 | 66 | 14 | -13 | 283 | 2 | 41 | -19 | -3 |
| Week 1 | -130 | 67 | 15 | -13 | 275 | 2 | 41 | -19 | -8 |
| Week 2 | -130 | 63 | 14 | -16 | 271 | 1 | 39 | -21 | -16 |
| Week 3 | -130 | 66 | 16 | -12 | 308 | 4 | 41 | -18 | -14 |
| Week 4 | -130 | 61 | 23 | -5 | 379 | 8 | 39 | -17 | -13 |

Table 4.27: Strains at South Cross Section Exterior Wall in Test 3

| Description | Strain (Micro Strain, µε) | | |
|---|---|---|---|
| | SL | Top | SL |
| Initial/Strut Placement | -30 | 45 | -26 |
| Layer 1 | -32 | 29 | -37 |
| Layer 2 | -25 | 24 | -52 |
| Layer 3 | N/A | N/A | -53 |
| Layer 4 | N/A | N/A | -61 |
| Layer 5 | N/A | N/A | -69 |
| Layer 6 | N/A | N/A | -57 |
| Backfill Complete | N/A | N/A | -27 |
| Week 1 | N/A | N/A | -32 |
| Week 2 | N/A | N/A | -30 |
| Week 3 | N/A | N/A | -26 |
| Week 4 | N/A | N/A | -23 |

Table 4.28: Strain at Center Cross Section Interior Wall in Test 3

| Description | Strain (Micro Strain, µε) | | | | | | | | |
|---|---|---|---|---|---|---|---|---|---|
| | Crown | 45 | SL | 135 | Invert | 225 | SL | 315 | Crown Long |
| Initial/Strut Placement | -32 | 7 | 23 | 14 | -21 | 0 | 19 | 4 | -8 |
| Layer 1 | -18 | 0 | 26 | 19 | -36 | 11 | 18 | -6 | -8 |
| Layer 2 | -22 | 4 | 45 | 21 | -53 | 8 | 34 | -13 | -2 |
| Layer 3 | -28 | 9 | 64 | 10 | -36 | 10 | 51 | -20 | -1 |
| Layer 4 | -121 | 75 | 52 | -9 | -14 | -1 | 93 | -26 | -20 |
| Layer 5 | -123 | 74 | 52 | -8 | -14 | -1 | 93 | -24 | -20 |
| Layer 6 | -136 | 86 | 48 | -8 | -13 | 1 | 88 | -15 | -32 |
| Backfill Complete | -53 | 42 | -3 | 7 | 50 | 46 | 28 | -78 | -12 |
| Week 1 | -54 | 40 | -7 | 6 | 50 | 46 | 24 | -79 | -19 |
| Week 2 | -52 | 41 | -7 | 7 | 50 | 47 | 24 | -78 | -18 |
| Week 3 | -53 | 41 | -7 | 7 | 51 | 46 | 23 | -79 | -16 |
| Week 4 | -47 | 42 | -9 | 14 | 55 | 54 | 22 | -78 | -11 |

Table 4.29: Strain at Center Cross Section Exterior Wall in Test 3

| Description | Strain (Micro Strain, µε) | | |
|---|---|---|---|
| | SL | Top | SL |
| Initial/Strut Placement | -21 | 36 | -25 |
| Layer 1 | -21 | 26 | -32 |
| Layer 2 | -29 | 25 | -44 |
| Layer 3 | -33 | N/A | -45 |
| Layer 4 | -47 | N/A | -63 |
| Layer 5 | -83 | N/A | -50 |
| Layer 6 | -77 | N/A | -47 |
| Backfill Complete | -42 | N/A | -18 |
| Week 1 | -40 | N/A | -17 |
| Week 2 | -40 | N/A | -17 |
| Week 3 | -39 | N/A | -16 |
| Week 4 | -31 | N/A | -12 |

Table 4.30: Strains at North Cross Section Interior Wall in Test 3

| Description | Strain (Micro Strain, µε) | | | | | | | | |
|---|---|---|---|---|---|---|---|---|---|
| | Crown | 45 | SL | 135 | Invert | 225 | SL | 315 | Crown Long |
| Initial/Strut Placement | -31 | 10 | 50 | 14 | -33 | 2 | 80 | 9 | 8 |
| Layer 1 | -22 | 10 | 75 | 12 | -49 | 11 | 102 | -11 | 5 |
| Layer 2 | -7 | 0 | 98 | 12 | -64 | 17 | 108 | -17 | 9 |
| Layer 3 | -5 | 0 | 88 | 12 | -65 | 18 | 108 | -17 | 12 |
| Layer 4 | -22 | -3 | 132 | -7 | -52 | 19 | 112 | -32 | 29 |
| Layer 5 | -67 | 56 | 116 | -32 | -25 | 8 | 145 | 2 | 43 |
| Layer 6 | -61 | 22 | 97 | -5 | 42 | 35 | 128 | -58 | 48 |
| Backfill Complete | -15 | -15 | 41 | 32 | 200 | 83 | 99 | -97 | 52 |
| Week 1 | -22 | -11 | 83 | 33 | 206 | 84 | 99 | -79 | 49 |
| Week 2 | -24 | -13 | 82 | 33 | 206 | 86 | 99 | -77 | 48 |
| Week 3 | -26 | -13 | 77 | 32 | 207 | 85 | 99 | -75 | 46 |
| Week 4 | -67 | -6 | -247 | 33 | 217 | 78 | 99 | -59 | 56 |

Table 4.31: Strain at North Cross Section Exterior Wall in Test 3

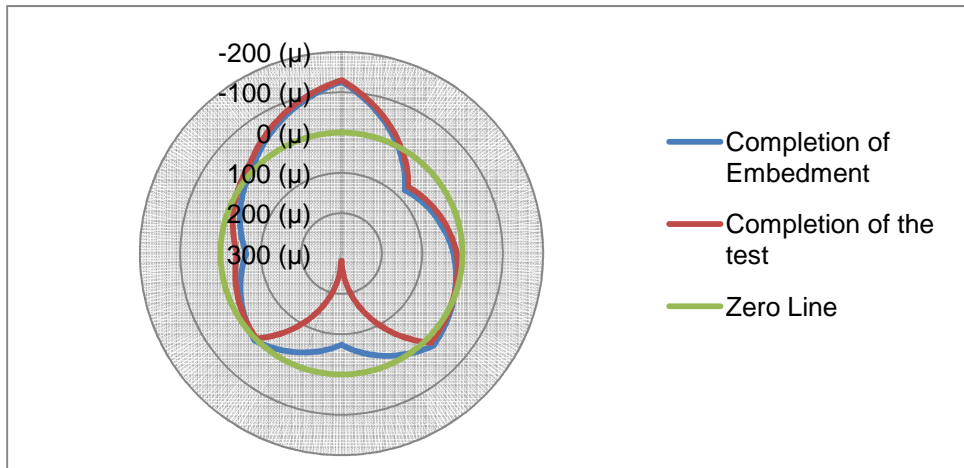| Description | Strain (Micro Strain, µε) | | |
|---|---|---|---|
| | SL | Top | SL |
| Initial/Strut Placement | -62 | 69 | -43 |
| Layer 1 | -75 | 29 | -53 |
| Layer 2 | -75 | 29 | -54 |
| Layer 3 | -71 | 35 | -53 |
| Layer 4 | -85 | 45 | -76 |
| Layer 5 | N/A | 107 | -72 |
| Layer 6 | N/A | 112 | -71 |
| Backfill Complete | N/A | 14 | -40 |
| Week 1 | N/A | 16 | -37 |
| Week 2 | N/A | 12 | -37 |
| Week 3 | N/A | 12 | -36 |
| Week 4 | N/A | 12 | -21 |

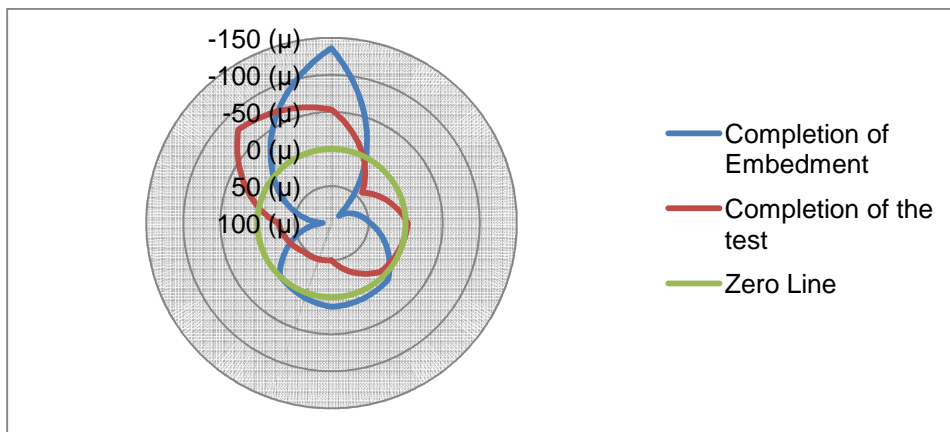Figure 4.18: Strains at South Cross Section in Test 3



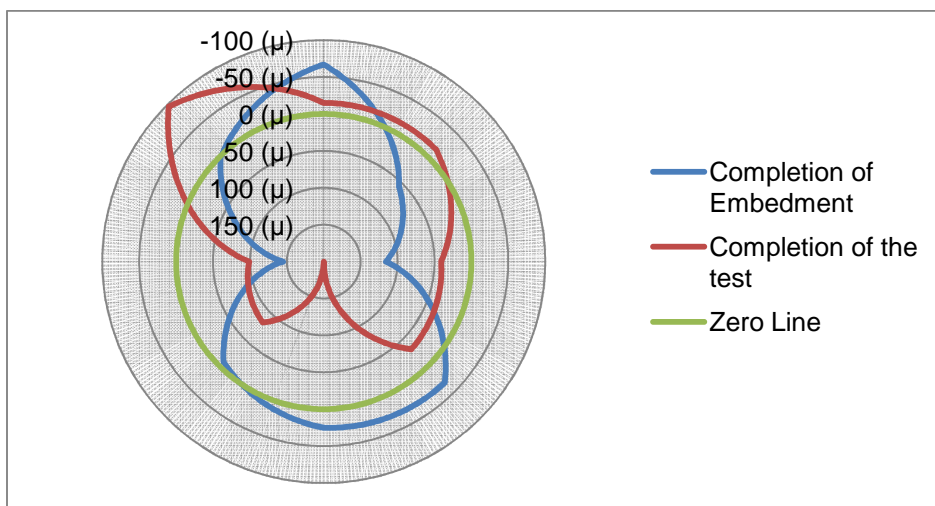Figure 4.19: Strains at Center Cross Section in Test 3



Figure 4.20: Strains at North Cross Section in Test 3

## 4.8 Test 4

### 4.8.1 Embedment Layers

One layer of crushed limestone embedment and seven layers of native clay were placed during Test 4 to cover the pipe. Density of native clay was measured by nuclear density gage. Table 4.23 presents thicknesses, and densities of these embedment layers.

Table 4.32: Embedment Layer Densities for Test 3

| Layer No. | Average Layer Thickness in. | Embedment Height in. | Average Dry Density (pcf) | Average Water Content (%) | Average wet Density (pcf) | Percent Compaction (%) |
|---|---|---|---|---|---|---|
| 1 | 23 | 23 | Crushed Limestone | | | |
| 2 | 6 | 29 | 102.3 | 20.7 | 123.5 | 94.6 |
| 3 | 6 | 35 | 102.0 | 22.9 | 125.4 | 94.4 |
| 4 | 7 | 42 | 101.3 | 22.7 | 124.3 | 93.7 |
| 5 | 7 | 49 | 103.5 | 22.1 | 126.4 | 95.7 |
| 6 | 8 | 57 | 104.3 | 20.9 | 126.1 | 96.5 |
| 7 | 9 | 66 | Density Measurements were not taken | | | |
| 8 | 9 | 75 | | | | |
| 9 | 12 | 87 | | | | |

### 4.8.2 Pipe Deflection

Pipe deflection during Test 4 is summarized in Table 4.33. Figure 4.21 illustrates graphical representation of deflection during Test 4. Peaking deflection (increase in vertical diameter) was observed up to layer 6. Surcharge load of cover added after layer 9 caused deflection in pipe. Horizontal and vertical deflections were approximately equal in magnitude throughout the test.

### 4.8.3 Earth Pressure

Earth Pressures were measured at ten locations described in Section 3.5.5. The vertical pressures were measured at center under the pipe and three locations (south, center, and north) on top of pipe. Horizontal pressures were measured at pipe springline and soil box walls. Table 4.34 presents the recorded pressures at these locations at different stages of the test. Figure 4.22 illustrates graphical representation of earth pressure cell data.

4.8.4 Pipe Wall Strains

Strain gages were installed at thirty-six points circumferentially, as described in Section 3.5.3; strains were measured successfully at twenty-five points. Tables 4.35 to 4.40 present strains on pipe wall at different stages of Test 4. Figures 4.23, 4.24 and 4.25 illustrate graphical representation of pipe wall strain data. The strain data are so plotted in order to show exaggerated shape of pipe deformation.

Table 4.33: Pipe Deflection in Test 4

| Description | Increase in Vertical Diameters (in.) | | | Decrease in Horizontal Diameters (in.) | | |
|---|---|---|---|---|---|---|
| | South | Center | North | South | Center | North |
| Struts Placement | 0.24 | 0.27 | 0.37 | -0.22 | -0.28 | -0.39 |
| Layer 1 | 0.24 | 0.37 | 0.38 | -0.22 | -0.3 | -0.42 |
| Layer 2 | 1.19 | 1.08 | 1.00 | -1.23 | -1.14 | -1.22 |
| Layer 3 | 1.86 | 1.8 | 1.78 | -1.99 | -1.95 | -1.99 |
| Layer 4 | 2.48 | 2.44 | 2.45 | -2.62 | -2.62 | -2.65 |
| Layer 5 | 2.81 | 2.77 | 2.75 | -2.82 | -2.82 | -3.05 |
| Layer 6 | 3.01 | 2.97 | 2.95 | -2.9 | -2.98 | -3.1 |
| Layer 7 | 2.99 | 2.99 | 2.99 | -2.86 | -2.95 | -3.06 |
| Layer 8 | 3.03 | 3.01 | 3.01 | -2.84 | -2.93 | -3.03 |
| Layer 9 | 3.03 | 3.00 | 3.00 | -2.81 | -2.92 | -2.99 |
| Surcharge Load | 2.95 | 2.92 | 2.88 | -2.69 | -2.79 | -2.86 |
| Week 1 | 2.92 | 2.89 | 2.86 | -2.68 | -2.76 | -2.83 |
| Week 2 | 2.91 | 2.88 | 2.85 | -2.67 | -2.75 | -2.82 |
| Week 3 | 2.9 | 2.87 | 2.84 | -2.66 | -2.75 | -2.82 |
| Week 4 | 2.89 | 2.86 | 2.83 | -2.64 | -2.74 | -2.81 |
| **Immediate Deflections Due to Surcharge Load** | -0.08 | -0.08 | -0.12 | 0.12 | 0.13 | 0.13 |
| **Total Deflections Due to Surcharge Load** | -0.14 | -0.14 | -0.13 | 0.17 | 0.18 | 0.18 |
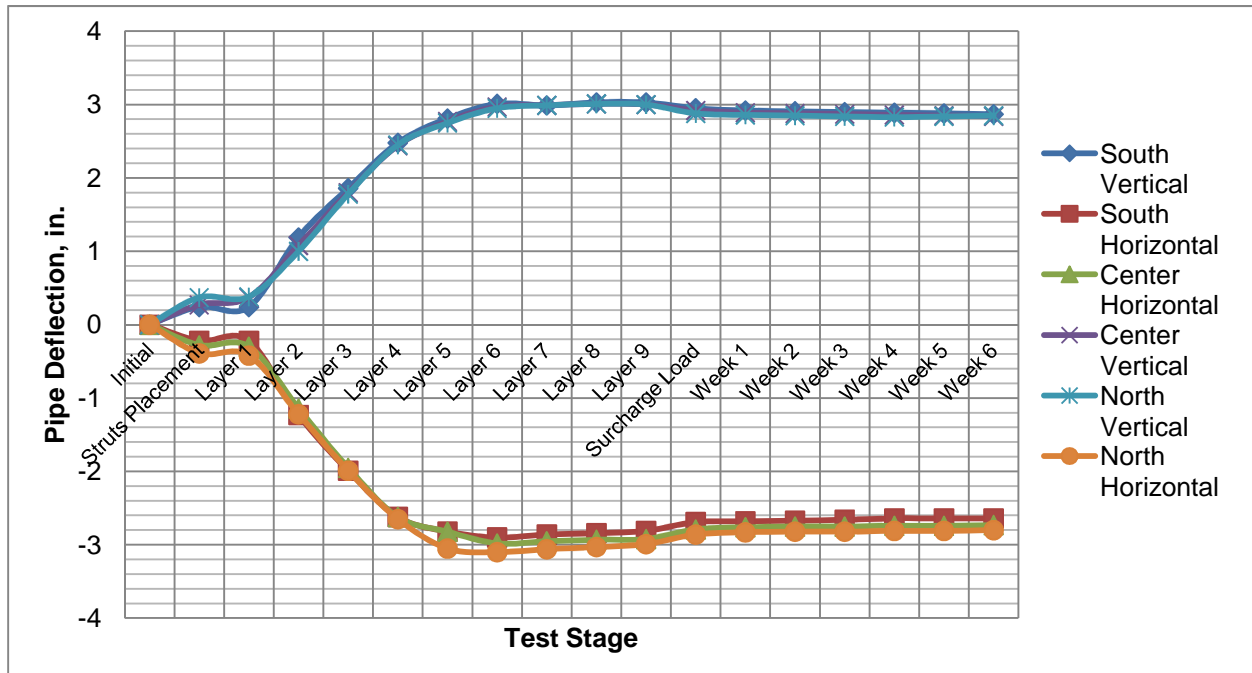
Figure 4.21: Deflection of Pipe in Test 4

Table 4.34: Earth Pressure Cell Data for Test 4

| Description | Horizontal/Vertical (Springline) Pressures, psi | | | | | | | | | |
| | Pipe South | Pipe Center | | | | | | Pipe North | Soil-box Walls | |
| | Top | Bottom | Sprin. East | East Wall | Spring. West | West Wall | Top | Top | South | North |
| Initial | N/A | 4.9 | N/A | N/A | N/A | N/A | N/A | N/A | N/A | N/A |
| Layer 1 | N/A | 4.8 | N/A | N/A | N/A | N/A | N/A | N/A | N/A | N/A |
| Layer 2 | N/A | 4.4 | N/A | N/A | N/A | N/A | N/A | N/A | N/A | N/A |
| Layer 3 | N/A | 4.5 | N/A | N/A | N/A | N/A | N/A | N/A | N/A | N/A |
| Layer 4 | N/A | 4.7 | 2.9 | 1.6 | 2.8 | 1.6 | N/A | N/A | 0.8 | 0.5 |
| Layer 5 | N/A | 4.9 | 3.1 | 1.8 | 2.6 | 1.5 | N/A | N/A | 0.7 | 0.5 |
| Layer 6 | N/A | 5.1 | 3.0 | 1.7 | 0.8 | 0.9 | N/A | N/A | 0.7 | 0.5 |
| Layer 7 | N/A | 5.4 | 1.6 | 1.1 | 0.9 | 0.9 | N/A | N/A | 0.9 | 0.4 |
| Layer 8 | N/A | 5.5 | 1.9 | 1.5 | 1.5 | 1.1 | N/A | N/A | 0.9 | 0.6 |
| Layer 9 | 1.1 | 6.7 | 2.3 | 2.1 | 1.6 | 1.2 | 0.9 | 1.1 | 1.0 | 0.6 |
| Backfill Complete | 6.4 | 13.9 | 3.8 | 4.4 | 5.5 | 3.3 | 5.5 | 6.3 | 2.1 | 0.8 |
| Week 1 | 6.4 | 13.6 | 3.2 | 4.7 | 5.7 | 3.5 | 5.4 | 6.4 | 2.0 | 0.8 |
| Week 2 | 6.5 | 13.5 | 2.6 | 4.8 | 5.6 | 3.3 | 5.2 | 6.3 | 2.0 | 0.8 |
| Week 3 | 6.4 | 13.1 | 2.3 | 4.8 | 5.9 | 3.3 | 5.1 | 6.5 | 2.0 | 0.8 |
| Week 4 | 6.3 | 12.9 | 2.2 | 4.9 | 5.8 | 3.3 | 5.2 | 6.1 | 2.0 | 0.8 |
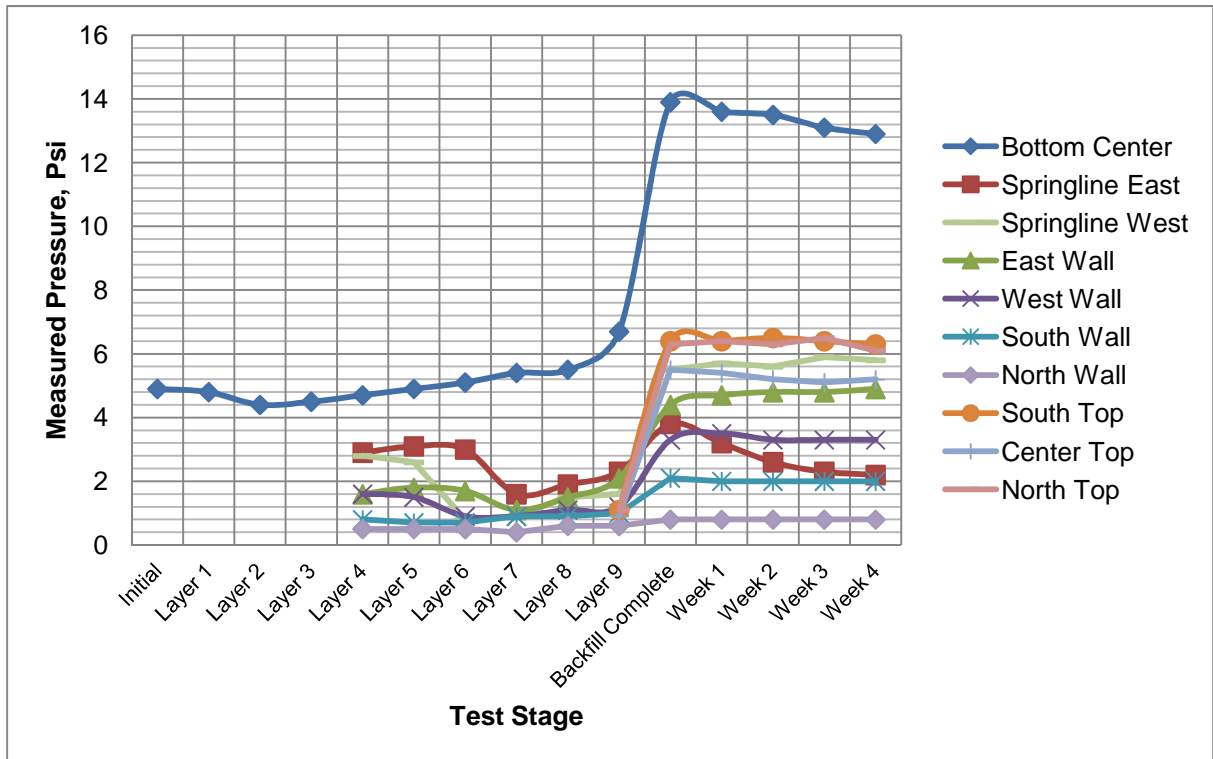
Figure 4.22: Earth Pressures at Different Stages of Test 4

Table 4.35: Strains at South Cross Section Interior Wall in Test 4

| Description | Strain (Micro Strain, με) | | | | | | | | |
|---|---|---|---|---|---|---|---|---|---|
| | Crown | 45 | SL | 135 | Invert | 225 | SL | 315 | Crown Long |
| Initial/Strut Placement | -48 | 5 | 26 | 27 | -89 | 32 | 29 | 2 | -4 |
| Layer 1 | -51 | -2 | 34 | 31 | -109 | 31 | 35 | -11 | -4 |
| Layer 2 | -176 | -17 | 249 | 40 | -270 | 126 | 165 | -68 | 5 |
| Layer 3 | -309 | 65 | 384 | 5 | -342 | 82 | 420 | -99 | 8 |
| Layer 4 | -472 | 120 | 444 | -29 | -387 | 65 | 641 | -107 | 17 |
| Layer 5 | -782 | 181 | 538 | -36 | -428 | 54 | 702 | -85 | 28 |
| Layer 6 | -825 | 232 | 582 | -45 | -436 | 25 | 723 | -42 | 32 |
| Layer 7 | -986 | 251 | 602 | -52 | -452 | 8 | 741 | -28 | 34 |
| Layer 8 | -1132 | 263 | 633 | -48 | -457 | -4 | 749 | -15 | 41 |
| Layer 9 | -1055 | 309 | 623 | -25 | -428 | 4 | 738 | 24 | 56 |
| Backfill Complete | -1052 | 502 | 326 | 45 | -325 | 52 | 489 | 203 | 77 |
| Week 1 | -1035 | 498 | 305 | 52 | -309 | 63 | 472 | 202 | 72 |
| Week 2 | -1012 | 483 | 292 | 59 | -301 | 81 | 464 | 201 | 76 |
| Week 3 | -984 | 482 | 285 | 63 | -294 | 89 | 450 | 197 | 71 |
| Week 4 | -939 | 478 | 240 | 62 | -291 | 109 | 438 | 198 | 75 |

Table 4.36: Strain at South Cross Section Exterior Wall in Test 4

| Description | Strain (Micro Strain, µε) | | |
|---|---|---|---|
| | SL | Top | SL |
| Initial/Strut Placement | -40 | 49 | -40 |
| Layer 1 | 128 | N/A | 163 |
| Layer 2 | 444 | N/A | -329 |
| Remaining layers | N/A | N/A | N/A |

Table 4.37: Strain at Center Cross Section Interior Wall in Test 4

| Description | Strain (Micro Strain, µε) | | | | | | | | |
|---|---|---|---|---|---|---|---|---|---|
| | Crown | 45 | SL | 135 | Invert | 225 | SL | 315 | Crown Long |
| Initial/Strut Placement | -36 | 4 | 39 | 3 | -53 | 21 | 45 | 38 | 12 |
| Layer 1 | -43 | -6 | 42 | -16 | -67 | 30 | 52 | 47 | 0 |
| Layer 2 | -118 | -35 | 225 | -88 | -214 | 78 | 161 | 114 | 6 |
| Layer 3 | -256 | -4 | 355 | -152 | -286 | 56 | 428 | 56 | 15 |
| Layer 4 | -388 | 19 | 558 | -208 | -361 | 11 | 638 | 31 | 21 |
| Layer 5 | -626 | 56 | 635 | -261 | -413 | 2 | 762 | 14 | 29 |
| Layer 6 | -738 | 82 | 692 | -345 | -452 | -12 | 803 | 6 | 35 |
| Layer 7 | -829 | 105 | 703 | -266 | -486 | -18 | 821 | -11 | 43 |
| Layer 8 | -989 | 122 | 715 | -152 | -501 | -23 | 836 | -32 | 51 |
| Layer 9 | -995 | 156 | 684 | -143 | -428 | -3 | 793 | -15 | 75 |
| Backfill Complete | -901 | 291 | 358 | 32 | -256 | 78 | 452 | 106 | 98 |
| Week 1 | -892 | 293 | 324 | 35 | -249 | 76 | 436 | 93 | 105 |
| Week 2 | -905 | 305 | 284 | 31 | -242 | 71 | 421 | 95 | 109 |
| Week 3 | -916 | 324 | 256 | 24 | -241 | 70 | 413 | 98 | 118 |
| Week 4 | -923 | 334 | 243 | 29 | -236 | 66 | 405 | 102 | 114 |

Table 4.38: Strain at Center Cross Section Exterior Wall in Test 4

| Description | Strain (Micro Strain, µε) | | |
|---|---|---|---|
| | SL | Top | SL |
| Initial/Strut Placement | | | |
| Layer 1 | -49 | 52 | -51 |
| Remaining layers | N/A | N/A | N/A |

Table 4.39: Strain at North Cross Section Interior Wall in Test 4

| Description | Strain (Micro Strain, με) | | | | | | | | |
|---|---|---|---|---|---|---|---|---|---|
| | Crown | 45 | SL | 135 | Invert | 225 | SL | 315 | Crown Long |
| Initial/Strut Placement | -79 | 2 | 48 | 39 | 45 | 44 | 42 | 3 | 4 |
| Layer 1 | -86 | -6 | 54 | 46 | 27 | 56 | 56 | -3 | 5 |
| Layer 2 | -123 | -30 | 192 | 87 | -132 | 197 | 191 | -71 | 5 |
| Layer 3 | -289 | -16 | 356 | 39 | -205 | 183 | 426 | -109 | 2 |
| Layer 4 | -442 | -1 | 525 | 26 | -294 | 178 | 697 | -141 | -4 |
| Layer 5 | -863 | 6 | 709 | 22 | -400 | 143 | 739 | -98 | 6 |
| Layer 6 | -985 | 25 | 740 | 3 | -452 | 126 | 786 | -46 | 15 |
| Layer 7 | -1249 | 32 | 753 | -6 | -482 | 109 | 798 | -25 | 22 |
| Layer 8 | -1382 | 54 | 783 | -17 | -496 | 98 | 805 | 4 | 23 |
| Layer 9 | -1356 | 92 | 620 | 2 | -402 | 142 | 632 | 52 | 28 |
| Backfill Complete | -1235 | 201 | 346 | 85 | -144 | 240 | 495 | 130 | 68 |
| Week 1 | -1288 | 236 | 289 | 92 | -93 | 232 | 478 | 128 | 63 |
| Week 2 | -1294 | 250 | 245 | 94 | -85 | 231 | 469 | 126 | 69 |
| Week 3 | -1279 | 260 | 232 | 99 | -62 | 222 | 458 | 119 | 71 |
| Week 4 | -1273 | 266 | 227 | 102 | -40 | 226 | 463 | 115 | 68 |

Table 4.40: Strain at South Cross Section Exterior Wall in Test 4

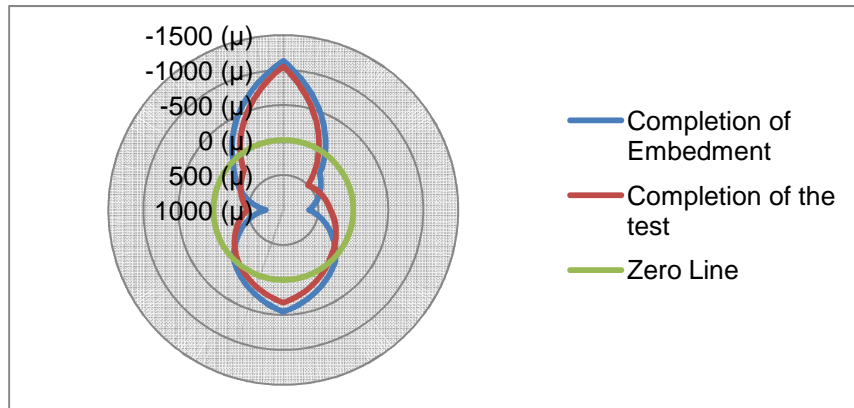| Description | Strain (Micro Strain, με) | | |
|---|---|---|---|
| | SL | Top | SL |
| Initial/Strut Placement | -55 | N/A | -51 |
| Layer 1 | -60 | N/A | -61 |
| Layer 2 | -221 | N/A | -176 |
| Layer 3 | -423 | N/A | -452 |
| Layer 4 | -501 | N/A | -645 |
| Layer 5 | N/A | N/A | -723 |
| Layer 6 | N/A | N/A | -772 |
| Layer 7 | N/A | N/A | -793 |
| Layer 8 | N/A | N/A | -809 |
| Layer 9 | N/A | N/A | -822 |
| Backfill Complete | N/A | N/A | -524 |
| Week 1 | N/A | N/A | -496 |
| Week 2 | N/A | N/A | -435 |
| Week 3 | N/A | N/A | -419 |
| Week 4 | N/A | N/A | -392 |

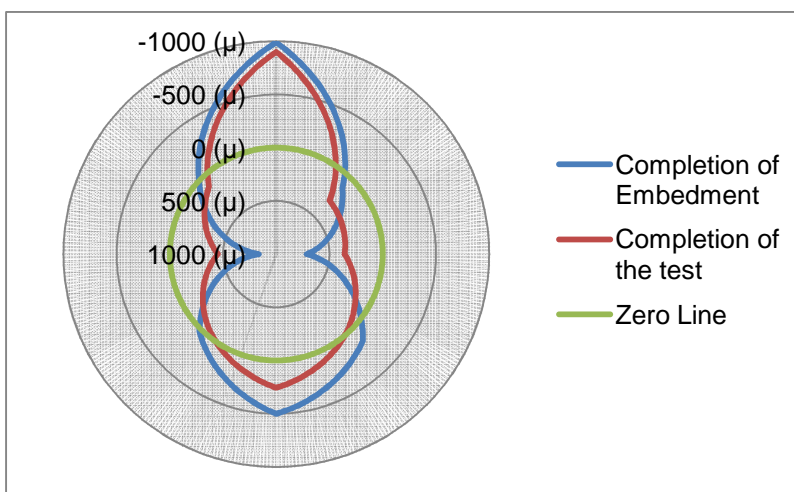Figure 4.23: Strains at South Cross Section in Test 4



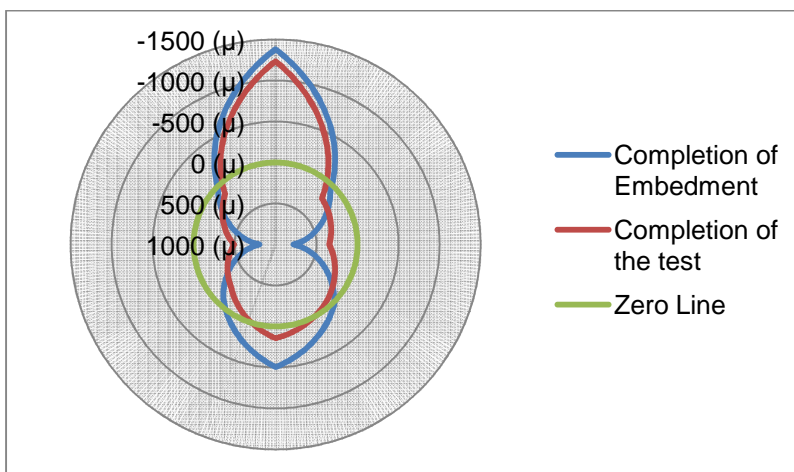Figure 4.24: Strains at Center Cross Section in Test 4



Figure 4.25: Strains at North Cross Section in Test 4

## 4.9 Summary

This chapter presented the results of the full scale laboratory tests. The data acquired and the key observations from the tests were presented. The key data included deflection results, earth pressure readings, and pipe wall strains.

Chapter 5

Discussion of Test Results

5.1 Introduction

This chapter presents the discussion of the results of the full scale laboratory tests. The key observations including deflection ratio (ratio of horizontal deflection to vertical), bedding angle (as described in Spangler's model), lateral earth pressure coefficient and Modulus of soil reaction value obtained by fitting test parameters to modified Iowa equation and Bureau of reclamation equation are discussed. The calculations of these values are also shown.

5.2 Pipe Deflection Due to Self-Weight

The test pipe (pipe sample) was delivered to CUIRE with two sets of struts placed inside the pipe to provide stiffness against handling stresses. During preparation for Test 1, test pipe was instrumented with the convergence meters with struts inside the pipe. Struts were removed from inside of the pipe to record deflection of pipe due to removal of struts (due to self-weight of pipe).

Expected pipe deflection due to self-weight was calculated by using modified Iowa equation as shown below:

$\Delta x$ = Predicted long term horizontal deflection of pipe

$D_l$ = Deflection lag factor = 1

K = Bedding constant = 0.1

W = Load per unit length of pipe (lb/in.) = 20.462 lb/in.

r = Pipe radius (in.) = 36.875

E = Modulus of elasticity (psi) of pipe material = 30,000,000 psi

I = Moment of inertia of pipe wall per unit length of pipe (in$^4$/in) = 0.313$^3$/12= 0.00255536 in$^4$/in

EI = 76,660.7

E' = Modulus of soil reaction (psi) = 0

$\Delta x$ = 1 * 0.1 * 20.462/(76660.7/36.875^3) = 1.34 in.

Expected deflection as per above calculation is 1.34 in. Calculated expected deflection due to self-weight was more than two times the deflection actually observed due to removal of struts. Therefore,

there is need to evaluate shape that pipe is molded during manufacture in order to evaluate deflection due to self-weight of pipe. However, argument can be made that bedding constant is reduced when there is no soil around the pipe, hence reducing predicted pipe deformation due to self-weight.

<div align="center">5.3 Deflection Ratio</div>

Deflection ratio, in this dissertation, is defined as absolute value of ratio of horizontal deflection to vertical deflection. Iowa equation was derived with an assumption that deflection ratio is close to one. Therefore, it is important to investigate if that assumption holds true. Also, Howard (1973) defined ring-stiffness factor of pipe ($EI/r^3$) as the ratio of the load on the ring to its deflection which can be determined from a parallel plate test or a three-edge bearing test. Pipe ring-stiffness factor is given by equations 5.1 and 5.2.

$$EI/r^3 = 0.149\ P/\Delta y \dots\dots\dots\dots\dots (5.1)$$

$$EI/r^3 = 0.136\ P/\Delta x \dots\dots\dots\dots\dots (5.2)$$

$\Delta x$ = Horizontal deflection of pipe (in.)

$\Delta y$ = Vertical deflection of pipe (in.)

P = Load per unit length of pipe (lb/in.)

r = Pipe radius (in.)

E = Modulus of elasticity (psi) of pipe material

I = Moment of inertia of pipe wall per unit length of pipe ($in^4/in$)

From equation 5.1 and 5.2, it can be concluded that if the pipe ring-stiffness is maintained in embedded condition, deflection ratio ($\Delta x/\Delta y$) is equal to (0.136/0.149) = 0.912.

Deflection ratios for each of the tests were calculated at three stages, at completion of embedment, at completion of test and due to surcharge load only. Calculations and discussion of deflection ratios of each of the tests are presented below.

5.3.1 Test 1

Deflection ratios for Test 1 were calculated as follows. Figure 5.1 presents the graphical representation of deflection ratio results.

At completion of Embedment:

Average vertical deflection, $\Delta y$ = (1.32 + 1.19 + 1.07)/3 = 1.19

Average horizontal deflection, $\Delta x$ = - (1.33 + 1.14 + 0.99)/3 = - 1.15

Deflection Ratio, $\Delta x/\Delta y$ = **0.97**

At completion of Test:

Average vertical deflection, $\Delta y$ = (0.75 + 0.44 + 0.35)/3 = 0.51

Average horizontal deflection, $\Delta x$ = - (1.18 + 0.94 + 0.72)/3 = - 0.95

Deflection Ratio, $\Delta x/\Delta y$ = **1.84**

Due to surcharge load only:

Average vertical deflection, $\Delta y$ = - (0.57 + 0.75 + 0.72)/3 = 0.68

Average horizontal deflection, $\Delta x$ = (0.15 + 0.20 + 0.27)/3 = 0.21

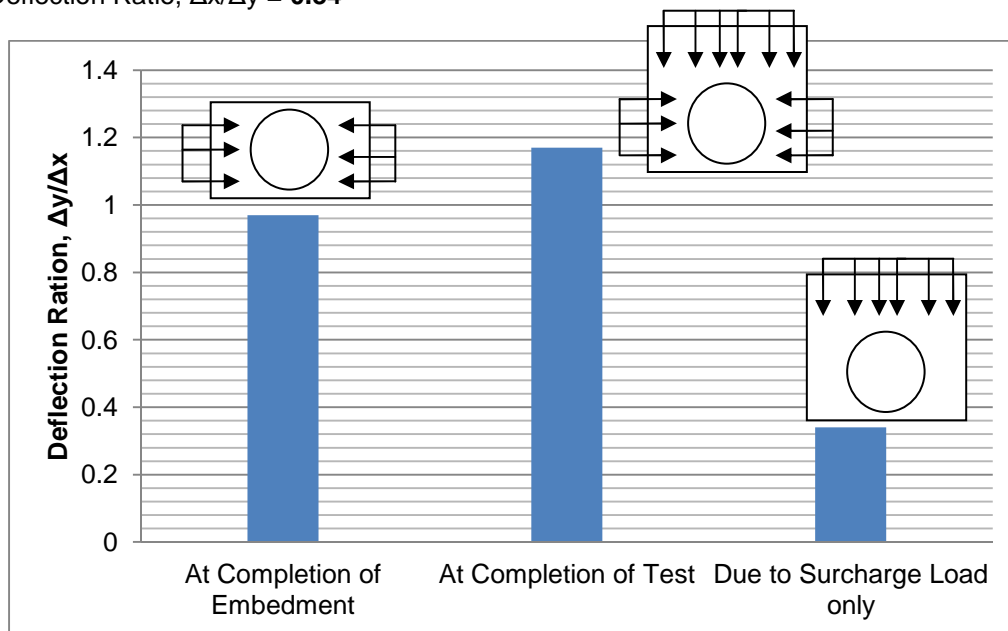Deflection Ratio, $\Delta x/\Delta y$ = **0.30**
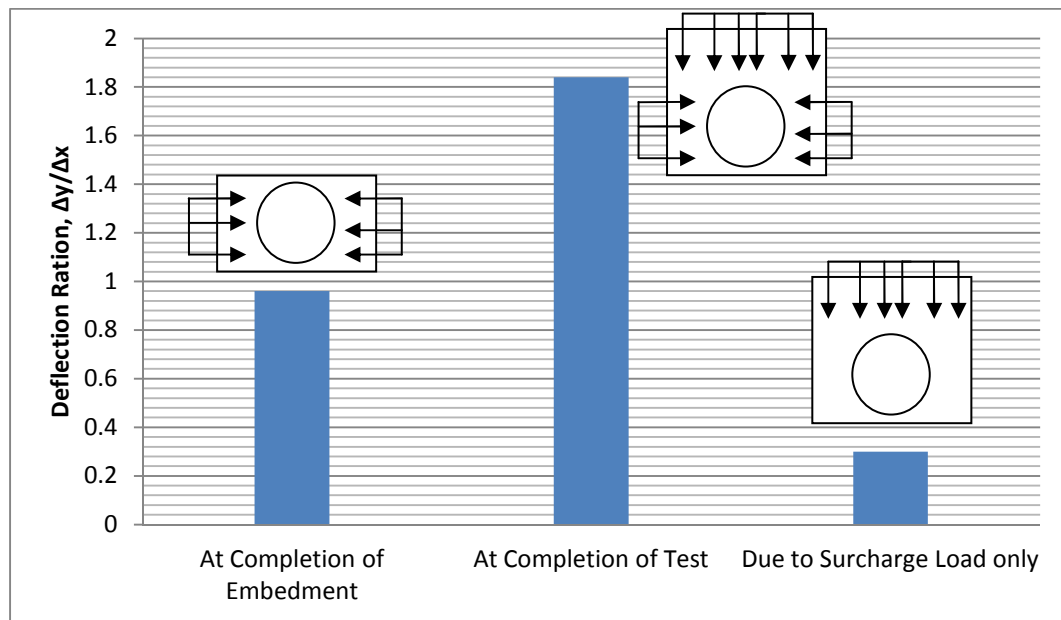


Figure 5.1: Deflection Ratios for Test 1

5.3.2 Test 2

Deflection ratios for Test 2 were calculated as follows. Figure 5.2 presents the graphical representation of deflection ratio results.

At completion of Embedment:

Average vertical deflection, Δy = (1.14 + 1.24 + 1.13)/3 = 1.17

Average horizontal deflection, Δx = - (1.24 + 1.26 + 1.13)/3 = - 1.21

Deflection Ratio, Δx/Δy = **1.03**

At completion of Test:

Average vertical deflection, Δy = (0.89 + 0.94 + 0.90)/3 = 0.91

Average horizontal deflection, Δx = - (1.16 + 1.13 + 1.03)/3 = - 1.11

Deflection Ratio, Δx/Δy = **1.22**

Due to surcharge load only:

Average vertical deflection, Δy = - (0.25 + 0.30 + 0.23)/3 = 0.26

Average horizontal deflection, Δx = (0.08 + 0.13 + 0.10)/3 = 0.10
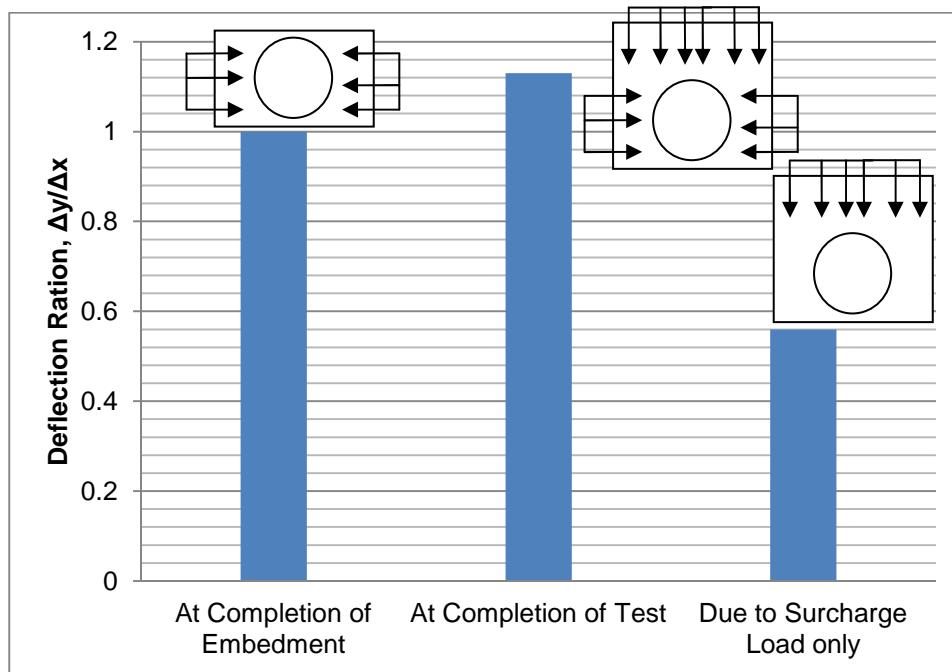
Deflection Ratio, Δx/Δy = **0.40**
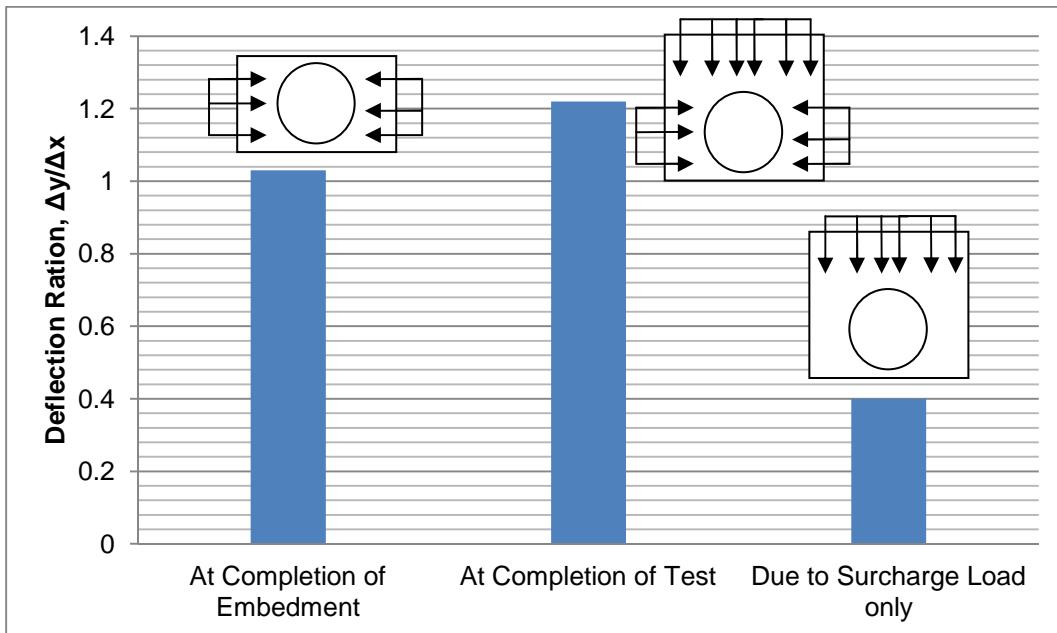


Figure 5.2: Deflection Ratios for Test 2

5.3.3 Test 1a

Deflection ratios for Test 1a were calculated as follows. Figure 5.3 presents the graphical representation of deflection ratio results.

At completion of Embedment:

Average vertical deflection, $\Delta y = (2.22 + 2.17 + 1.99)/3 = 2.13$

Average horizontal deflection, $\Delta x = - (2.2 + 2.05 + 1.95)/3 = - 2.07$

Deflection Ratio, $\Delta x/\Delta y = $ **0.97**

At completion of Test:

Average vertical deflection, $\Delta y = (1.72 + 1.65 + 1.45)/3 = 1.61$

Average horizontal deflection, $\Delta x = - (2.02 + 1.93 + 1.72)/3 = - 1.89$

Deflection Ratio, $\Delta x/\Delta y = $ **1.17**

Due to surcharge load only:

Average vertical deflection, $\Delta y = - (0.5 + 0.56 + 0.54)/3 = 0.53$

Average horizontal deflection, $\Delta x = (0.18 + 0.12 + 0.23)/3 = 0.18$

Deflection Ratio, $\Delta x/\Delta y = $ **0.34**



Figure 5.3: Deflection Ratios in Test 1a

## 5.3.4 Test 3

Deflection ratios for Test 3 were calculated as follows. Figure 5.4 presents the graphical representation of deflection ratio results.

At completion of Embedment:

Average vertical deflection, $\Delta y$ = (0.36 + 0.43 + 0.47)/3 = 0.42

Average horizontal deflection, $\Delta x$ = - (0.37 + 0.40 + 0.49)/3 = - 0.42

Deflection Ratio, $\Delta x/\Delta y$ = **1.00**

At completion of Test:

Average vertical deflection, $\Delta y$ = (0.29 + 0.34 + 0.31)/3 = 0.31

Average horizontal deflection, $\Delta x$ = - (0.31 + 0.35 + 0.4)/3 = - 0.35

Deflection Ratio, $\Delta x/\Delta y$ = **1.13**

Due to surcharge load only:

Average vertical deflection, $\Delta y$ = - (0.05 + 0.08 + 0.14)/3 = - 0.09

Average horizontal deflection, $\Delta x$ = (0.04 + 0.04 + 0.07)/3 = 0.05
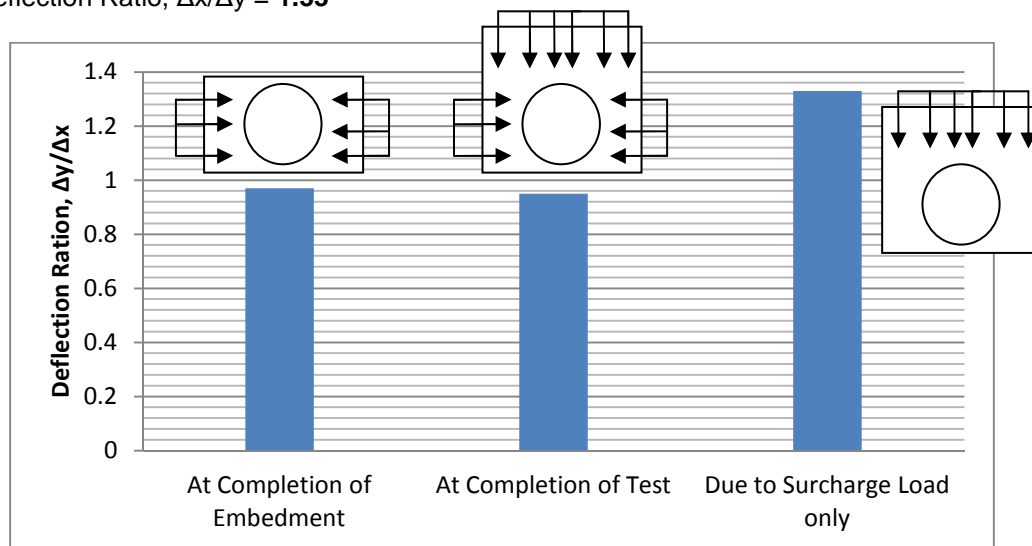
Deflection Ratio, $\Delta x/\Delta y$ = **0.56**



Figure 5.4: Deflection Ratios in Test 3

5.3.5 Test 4

Deflection ratios for Test 4 were calculated as follows. Figure 5.5 presents the graphical representation of deflection ratio results.

At completion of Embedment:

105

Average vertical deflection, $\Delta y = (3.03 + 3 + 3)/3 = 3.01$

Average horizontal deflection, $\Delta x = - (2.81 + 2.92 + 2.99)/3 = - 2.91$

Deflection Ratio, $\Delta x/\Delta y =$ **0.97**

At completion of Test:

Average vertical deflection, $\Delta y = (2.89 + 2.86 + 2.83)/3 = 2.86$

Average horizontal deflection, $\Delta x = - (2.64 + 2.74 + 2.81)/3 = - 2.73$

Deflection Ratio, $\Delta x/\Delta y =$ **0.95**

Due to surcharge load only:

Average vertical deflection, $\Delta y = - (0.08 + 0.08 + 0.12)/3 = - 0.09$

Average horizontal deflection, $\Delta x = (0.12 + 0.12 + 0.13)/3 = 0.12$

Deflection Ratio, $\Delta x/\Delta y =$ **1.33**



Figure 5.5: Deflection Ratios in Test 4

5.3.6 Comparison of Deflection Ratios

During embedment construction, horizontal and vertical deflections were approximately equal in magnitude to each other for all of the tests. This indicates that the ring-stiffness of the pipe was maintained during the embedment construction. For Tests 1, 2, 1a and 3, the horizontal deflections of pipe, when only deflections due to surcharge loads were considered, ranged from 30% to 60% of the vertical deflections. This indicates "squaring of the pipe" as defined by Howard (1996). For Test 4,

horizontal deflection was more than vertical deflection. However, the deflections due to surcharge loads recorded for Test 4 were very minimal to draw a definitive conclusion regarding deflection ratio for Test 4. The ratios of horizontal to vertical deflections due to surcharge load are compared in Figure 5.6.
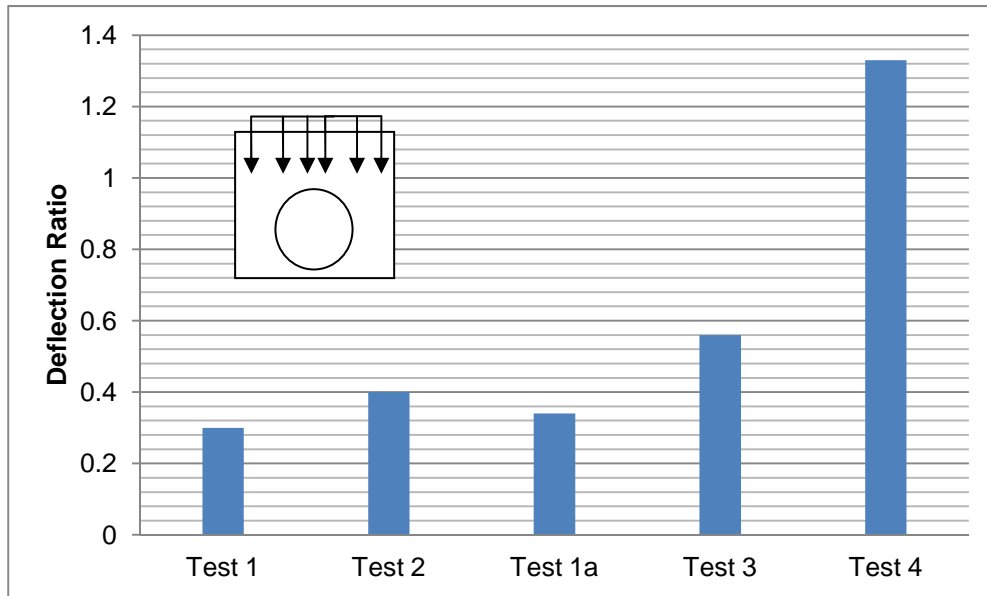


Figure 5.6: Comparison of Deflection Ratios due to Surcharge Loads

### 5.4 Bedding Angle

Spangler's model presented in Figure 1.2 provides the concept of bedding angle. Bedding angle represents the angle subtended by the lower arc of the pipe which is subjected to the reaction force from bedding. Larger bedding angle indicates better distribution of surcharge load to the bedding. When bedding angle is less, the surcharge load is concentrated at smaller area of the bedding, potentially causing settlement problems. Calculations of bedding angles are presented below.

Test 1:

Average load on top of pipe = (7.9 + 7.3 + 9.0)/3 = 8.07 psi

Pressure at bottom of pipe = 45.0 psi

Pressure due to weight of pipe = (246 lb/ft x 9 in x (1/12) ft/in)/63.62 sq. in. = 2.9 psi

Bedding angle = $2 * \sin^{-1}((8.07 + 2.9)/45) = 28.2^{\circ}$

Test 2:

Average load on top of pipe = (6.8 + 5.4 + 7.5)/3 = 6.57 psi

Pressure at bottom of pipe = 51.1 psi

Pressure due to weight of pipe = (246 lb/ft x 9 in x (1/12) ft/in)/63.62 sq. in. = 2.9 psi

Bedding angle = 2 * $\sin^{-1}$((6.57 + 2.9)/51.1) = 21.4$^{\circ}$

Test 1a:

Average load on top of pipe = (15.5 + 9.6 + 9.2)/3 = 11.43 psi

Pressure at bottom of pipe = 24.7 psi

Pressure due to weight of pipe = (246 lb/ft x 9 in x (1/12) ft/in)/63.62 sq. in. = 2.9 psi

Bedding angle = 2 * $\sin^{-1}$((11.43 + 2.9)/24.7) = 70.9$^{\circ}$

Test 3:

Average load on top of pipe = (7.5 + 3 + 7.4)/3 = 5.97 psi

Pressure at bottom of pipe = 17.8 psi

Pressure due to weight of pipe = (246 lb/ft x 9 in x (1/12) ft/in)/63.62 sq. in. = 2.9 psi

Bedding angle = 2 * $\sin^{-1}$((5.97 + 2.9)/17.8) = 59.8$^{\circ}$

Test 4:

Average load on top of pipe = (6.4 + 5.5 + 6.3)/3 = 6.07 psi

Pressure at bottom of pipe = 13.9 psi

Pressure due to weight of pipe = (246 lb/ft x 9 in x (1/12) ft/in)/63.62 sq. in. = 2.9 psi

Bedding angle = 2 * $\sin^{-1}$((6.07 + 2.9)/13.9) = 80.4$^{\circ}$

Figure 5.7 compares bedding angles achieved in the tests. Highest bedding angle of 80 degrees was achieved in Test 4. Lower bedding angles were achieved in Tests 1 and 2 with native and modified clays.
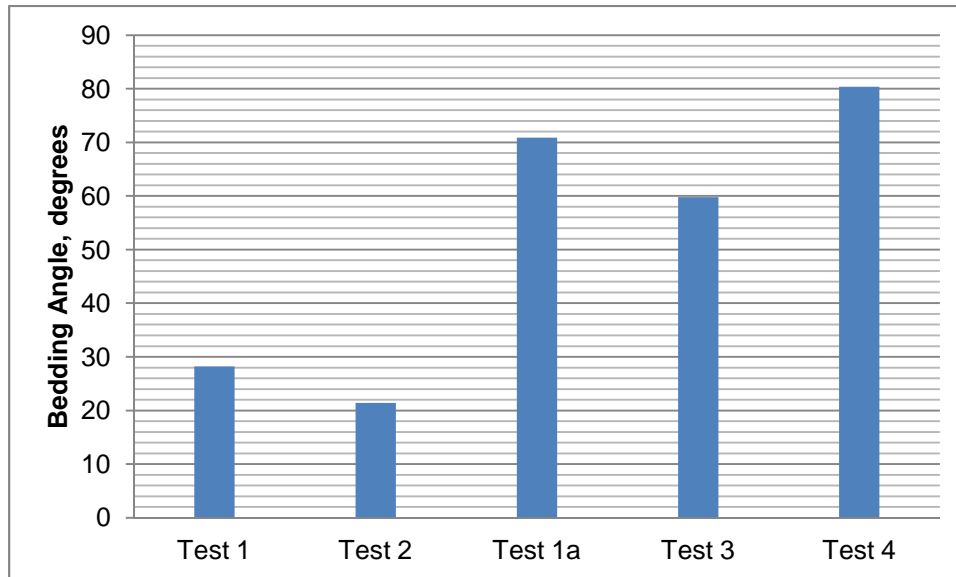
Figure 5.7: Comparison of Bedding Angles

## 5.5 Lateral Earth Pressure Coefficients

Lateral (horizontal) earth pressures at springline of the pipe were measured by earth pressure cells. Lateral earth pressure coefficients were calculated at three stages of the test: (i) immediately after placement of embedment layer above springline, (ii) at completion of embedment, and (iii) completion of backfill. Table 5.1 presents theoretical lateral earth coefficients at rest using different references. The detailed calculations of these lateral earth pressure coefficients are also presented.

Table 5.1: Lateral Earth Pressure Coefficients Using Different Theories

| Reference | Expression | Earth Pressure Coefficient at Rest | |
| --- | --- | --- | --- |
| | | Untreated B6 | Lime Stabilized B6 |
| Jaky (1944) | 1 - sin φ | 0.859 | 0.565 |
| Brooker and Ireland (1965) | 1 - sin φ | 0.809 | 0.515 |
| | 0.4 + 0.007 (PI) | 0.582 | N/A |
| Selig (1988) | N/A | 0.6 | N/A |

5.5.1 Test 1

Calculations of lateral earth pressure coefficients for Test 1 immediately after placement of embedment layer above springline, at completion of embedment, and completion of backfill are presented in Table 5.2, 5.3, and 5.4 respectively. The calculated coefficients are illustrated in Figure 5.8.

Table 5.2: Earth Pressures Immediately after Placement of Embedment Layer above Springline (Test 1)

| Location | Embedment Height (in) | Embedment Height from EPC Center (in) | Average Density of Layers above Pressure Cell (pcf) | Vertical Earth Pressure (psi) | Horizontal Pressure Recorded at EPC (psi) | Lateral Earth Pressure Coefficient |
|---|---|---|---|---|---|---|
| Springline East | 47 | 10 | 110 | 0.63 | 0.81 | 1.29 |
| Springline West | 47 | 10 | 110 | 0.63 | 0.72 | 1.14 |

Springline East (Sample calculation):

Embedment Height (in) = 47

Embedment Height from EPC Center (in) = 10

Average Density of Layers above Pressure Cell (pcf) = 110

Vertical Earth Pressure (psi) = $(110/12^3) * 14 = 0.63$

Horizontal Pressure Recorded at EPC (psi) = 0.81

Coefficient of Lateral Pressure = 0.81/0.63 = **1.29**

Table 5.3: Earth Pressures at Completion of Embedment (Test 1)

| Location | Embedment Height (in) | Embedment Height from EPC Center (in) | Average Density of Layers above Pressure Cell (pcf) | Vertical Earth Pressure (psi) | Horizontal Pressure Recorded at EPC (psi) | Lateral Earth Pressure Coefficient |
|---|---|---|---|---|---|---|
| Springline East | 77 | 40 | 104 | 2.41 | 0.8 | 0.33 |
| Springline West | 77 | 40 | 104 | 2.41 | 0.8 | 0.33 |

Table 5.4: Earth Pressures at Completion of Backfill (Test 1)

| Location | Average vertical Earth Pressure at top of pipe (psi) | Top of pipe from EPC Center (in) | Average Density of Layers above Pressure Cell (pcf) | Vertical Earth Pressure (psi) | Horizontal Pressure Recorded at EPC (psi) | Lateral Earth Pressure Coefficient |
|---|---|---|---|---|---|---|
| Springline East | 8.47 | 36 | 104 | 10.64 | 5.4 | 0.51 |
| Springline West | 8.47 | 36 | 104 | 10.64 | 5.3 | 0.50 |

Springline East (Sample)

Average vertical Earth Pressure at top of pipe (psi) = 8.47

Top of pipe from EPC Center (in) = 36

Average Density of Layers above Pressure Cell (pcf) = 104

Vertical Earth Pressure (psi) = $(104/12^3) * 36 + 8.47 = 10.64$

Horizontal Pressure Recorded at EPC (psi) = 5.4

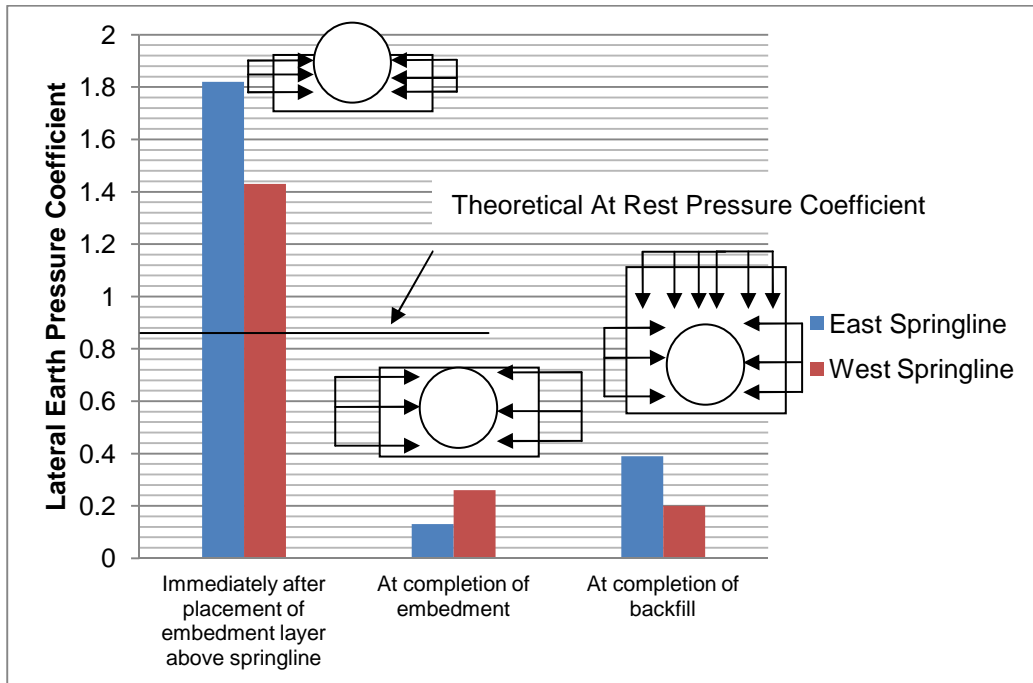Coefficient of Lateral Pressure = 5.4/10.64 = 0.51



Figure 5.8: Lateral Earth Coefficients at Different Stages of Test 1

5.5.2 Test 2

Calculations of lateral earth pressure coefficients for Test 2 immediately after placement of embedment layer above springline, at completion of embedment, and completion of backfill are presented in Table 5.5, 5.6, and 5.7 respectively. The calculated coefficients are illustrated in Figure 5.9.

5.5.3 Test 1a

Calculations of lateral earth pressure coefficients for Test 1a immediately after placement of embedment layer above springline, at completion of embedment, and completion of backfill are presented in Table 5.8, 5.9, and 5.10 respectively. The calculated coefficients are illustrated in Figure 5.10.

Table 5.5: Earth Pressures Immediately after Placement of Embedment Layer above Springline (Test 2)

| Location | Embedment Height (in) | Embedment Height from EPC Center (in) | Average Density of Layers above Pressure Cell (pcf) | Vertical Earth Pressure (psi) | Horizontal Pressure Recorded at EPC (psi) | Lateral Earth Pressure Coefficient |
|---|---|---|---|---|---|---|
| Springline East | 51 | 14 | 112 | 0.91 | 1.66 | 1.82 |
| East Wall | 51 | 14 | 112 | 0.91 | 1.30 | 1.43 |
| West Wall | 51 | 14 | 112 | 0.91 | 0.80 | 0.88 |
| South Wall | 51 | 14 | 112 | 0.91 | 0.64 | 0.70 |

Table 5.6: Earth Pressures at Completion of Embedment (Test 2)

| Location | Embedment Height (in) | Embedment Height from EPC Center (in) | Average Density of Layers above Pressure Cell (pcf) | Vertical Earth Pressure (psi) | Horizontal Pressure Recorded at EPC (psi) | Lateral Earth Pressure Coefficient |
|---|---|---|---|---|---|---|
| Springline East | 72 | 35 | 112 | 2.27 | 0.3 | 0.13 |
| East Wall | 72 | 35 | 112 | 2.27 | 0.6 | 0.26 |
| West Wall | 72 | 35 | 112 | 2.27 | 0.7 | 0.31 |
| South Wall | 72 | 35 | 112 | 2.27 | 1.1 | 0.48 |

Table 5.7: Earth Pressures at Completion of Backfill (Test 2)

| Location | Average vertical Earth Pressure at top of pipe (psi) | Top of pipe from EPC Center (in) | Average Density of Layers above Pressure Cell (pcf) | Vertical Earth Pressure (psi) | Horizontal Pressure Recorded at EPC (psi) | Lateral Earth Pressure Coefficient |
|---|---|---|---|---|---|---|
| Springline East | 6.57 | 36 | 112 | 8.9 | 3.5 | 0.39 |
| East Wall | 6.57 | 36 | 112 | 8.9 | 1.8 | 0.20 |
| West Wall | 6.57 | 36 | 112 | 8.9 | 2.6 | 0.29 |
| South Wall | 6.57 | 36 | 112 | 8.9 | 1.8 | 0.20 |
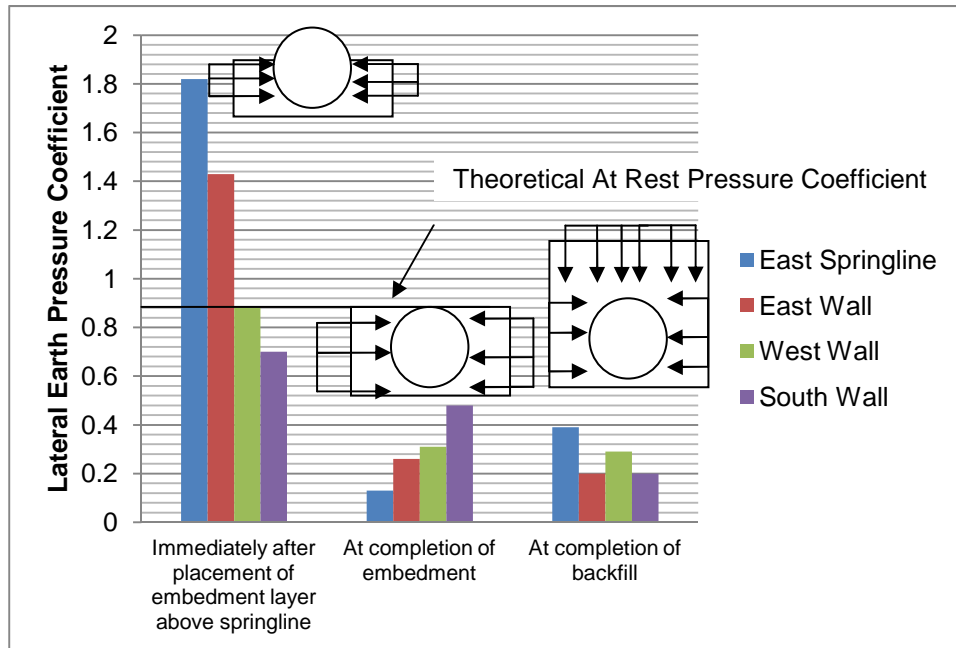
Figure 5.9: Lateral Earth Coefficients at Different Stages of Test 2

Table 5.8: Earth Pressures Immediately after Placement of Embedment Layer above Springline (Test 1a)

| Location | Embedment Height (in) | Embedment Height from EPC Center (in) | Average Density of Layers above Pressure Cell (pcf) | Vertical Earth Pressure (psi) | Horizontal Pressure Recorded at EPC (psi) | Lateral Earth Pressure Coefficient |
|---|---|---|---|---|---|---|
| Springline East | 48 | 11 | 117.7 | 0.75 | 3.8 | 5.07 |
| Springline West | 48 | 11 | 117.7 | 0.75 | 2.1 | 2.80 |
| East Wall | 48 | 11 | 117.7 | 0.75 | 1.5 | 2.00 |
| West Wall | 48 | 11 | 117.7 | 0.75 | 0.8 | 1.07 |
| South Wall | 48 | 11 | 117.7 | 0.75 | 0.4 | 0.53 |
| North Wall | 48 | 11 | 117.7 | 0.75 | 0.5 | 0.67 |

Table 5.9: Earth Pressures at Completion of Embedment (Test 1a)

| Location | Embedment Height (in) | Embedment Height from EPC Center (in) | Average Density of Layers above Pressure Cell (pcf) | Vertical Earth Pressure (psi) | Horizontal Pressure Recorded at EPC (psi) | Lateral Earth Pressure Coefficient |
|---|---|---|---|---|---|---|
| Springline East | 78 | 41 | 114.4 | 2.71 | 2.1 | 0.77 |
| Springline West | 78 | 41 | 114.4 | 2.71 | 1.3 | 0.48 |
| East Wall | 78 | 41 | 114.4 | 2.71 | 0.9 | 0.33 |
| West Wall | 78 | 41 | 114.4 | 2.71 | 0.6 | 0.22 |
| South Wall | 78 | 41 | 114.4 | 2.71 | 0.6 | 0.22 |
| North Wall | 78 | 41 | 114.4 | 2.71 | 0.4 | 0.15 |

Table 5.10: Earth Pressures at Completion of Backfill (Test 1a)

| Location | Average vertical Earth Pressure at top of pipe (psi) | Top of pipe from EPC Center (in) | Average Density of Layers above Pressure Cell (pcf) | Vertical Earth Pressure (psi) | Horizontal Pressure Recorded at EPC (psi) | Lateral Earth Pressure Coefficient |
|---|---|---|---|---|---|---|
| Springline East | 11.43 | 36 | 114.4 | 13.81 | 4.9 | 0.35 |
| Springline West | 11.43 | 36 | 114.4 | 13.81 | 5.4 | 0.39 |
| East Wall | 11.43 | 36 | 114.4 | 13.81 | 2.5 | 0.18 |
| West Wall | 11.43 | 36 | 114.4 | 13.81 | 2.2 | 0.16 |
| South Wall | 11.43 | 36 | 114.4 | 13.81 | 1.3 | 0.09 |
| North Wall | 11.43 | 36 | 114.4 | 13.81 | 0.8 | 0.06 |
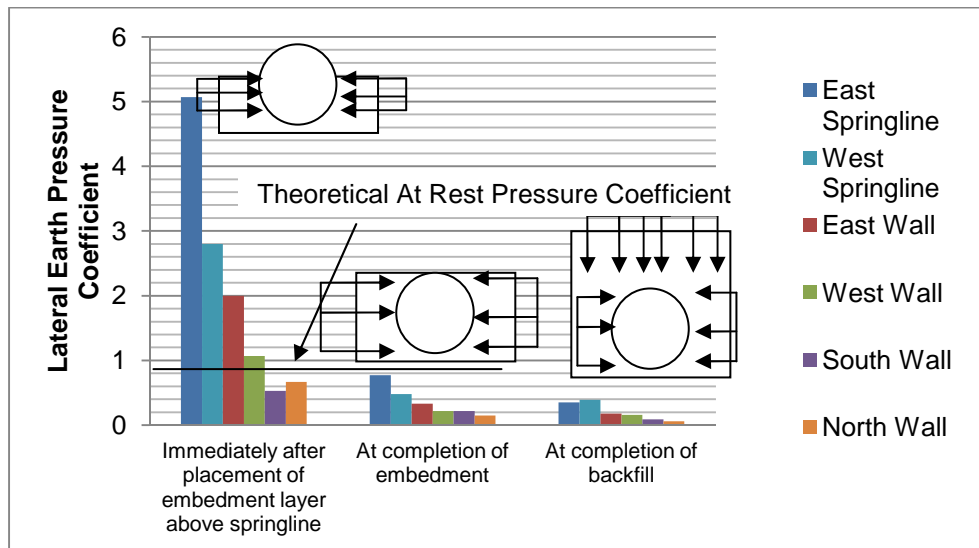
Figure 5.10: Lateral Earth Coefficients at Different Stages of Test 1a

5.5.4 Test 3

Calculations of lateral earth pressure coefficients for Test 3 immediately after placement of embedment layer above springline, at completion of embedment, and completion of backfill are presented in Table 5.11, 5.12, and 5.13 respectively. The calculated coefficients are illustrated in Figure 5.11.

Table 5.11: Earth Pressures Immediately after Placement of Embedment Layer above Springline (Test 3)

| Location | Embedment Height (in) | Embedment Height from EPC Center (in) | Average Density of Layers above Pressure Cell (pcf) | Vertical Earth Pressure (psi) | Horizontal Pressure Recorded at EPC (psi) | Lateral Earth Pressure Coefficient |
|---|---|---|---|---|---|---|
| Springline East | 48 | 11 | 120 | 0.76 | 0.5 | 0.66 |
| Springline West | 48 | 11 | 120 | 0.76 | 0.4 | 0.53 |
| East Wall | 48 | 11 | 120 | 0.76 | 0.4 | 0.53 |
| West Wall | 48 | 11 | 120 | 0.76 | 0.3 | 0.39 |
| North Wall | 48 | 11 | 120 | 0.76 | 0.4 | 0.53 |

5.5.5 Test 4

Calculations of lateral earth pressure coefficients for Test 4 immediately after placement of embedment layer above springline, at completion of embedment, and completion of backfill are presented in Table 5.14, 5.15, and 5.16 respectively. The calculated coefficients are illustrated in Figure 5.12.

Table 5.12: Earth Pressures at Completion of Embedment (Test 3)

| Location | Embedment Height (in) | Embedment Height from EPC Center (in) | Average Density of Layers above Pressure Cell (pcf) | Vertical Earth Pressure (psi) | Horizontal Pressure Recorded at EPC (psi) | Lateral Earth Pressure Coefficient |
|---|---|---|---|---|---|---|
| Springline East | 78 | 41 | 120 | 2.85 | 0.7 | 0.25 |
| Springline West | 78 | 41 | 120 | 2.85 | 0.5 | 0.18 |
| East Wall | 78 | 41 | 120 | 2.85 | 0.8 | 0.28 |
| West Wall | 78 | 41 | 120 | 2.85 | 0.4 | 0.14 |
| North Wall | 78 | 41 | 120 | 2.85 | 0.3 | 0.11 |

Table 5.13: Earth Pressures at Completion of Backfill (Test 3)

| Location | Average vertical Earth Pressure at top of pipe (psi) | Top of pipe from EPC Center (in) | Average Density of Layers above Pressure Cell (pcf) | Vertical Earth Pressure (psi) | Horizontal Pressure Recorded at EPC (psi) | Lateral Earth Pressure Coefficient |
|---|---|---|---|---|---|---|
| Springline East | 5.97 | 36 | 120 | 8.47 | 1.0 | 0.12 |
| Springline West | 5.97 | 36 | 120 | 8.47 | 0.9 | 0.11 |
| East Wall | 5.97 | 36 | 120 | 8.47 | 4.1 | 0.48 |
| West Wall | 5.97 | 36 | 120 | 8.47 | 1.0 | 0.12 |
| North Wall | 5.97 | 36 | 120 | 8.47 | 0.5 | 0.06 |
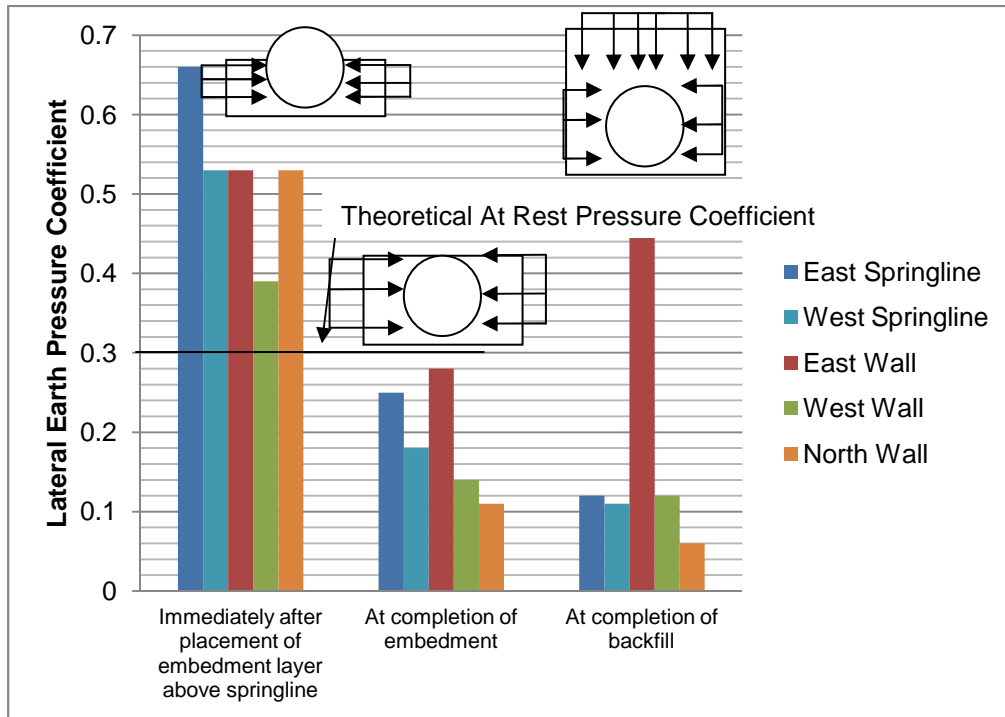
Figure 5.11: Lateral Earth Coefficients at Different Stages of Test 3

Table 5.14: Earth Pressures Immediately after Placement of Embedment Layer above Springline (Test 4)

| Location | Embedment Height (in) | Embedment Height from EPC Center (in) | Average Density of Layers above Pressure Cell (pcf) | Vertical Earth Pressure (psi) | Horizontal Pressure Recorded at EPC (psi) | Lateral Earth Pressure Coefficient |
|---|---|---|---|---|---|---|
| Springline East | 49 | 12 | 125.4 | 0.87 | 3.1 | 3.56 |
| Springline West | 49 | 12 | 125.4 | 0.87 | 2.6 | 2.99 |
| East Wall | 49 | 12 | 125.4 | 0.87 | 1.8 | 2.07 |
| West Wall | 49 | 12 | 125.4 | 0.87 | 1.5 | 1.72 |
| South Wall | 49 | 12 | 125.4 | 0.87 | 0.7 | 0.80 |
| North Wall | 49 | 12 | 125.4 | 0.87 | 0.5 | 0.57 |

Table 5.15: Earth Pressures at Completion of Embedment (Test 4)

| Location | Embedment Height (in) | Embedment Height from EPC Center (in) | Average Density of Layers above Pressure Cell (pcf) | Vertical Earth Pressure (psi) | Horizontal Pressure Recorded at EPC (psi) | Lateral Earth Pressure Coefficient |
|---|---|---|---|---|---|---|
| Springline East | 87 | 50 | 124 | 3.59 | 2.3 | 0.64 |
| Springline West | 87 | 50 | 124 | 3.59 | 1.6 | 0.45 |
| East Wall | 87 | 50 | 124 | 3.59 | 2.1 | 0.58 |
| West Wall | 87 | 50 | 124 | 3.59 | 1.2 | 0.33 |
| South Wall | 87 | 50 | 124 | 3.59 | 1.0 | 0.28 |
| North Wall | 87 | 50 | 124 | 3.59 | 0.6 | 0.17 |

Table 5.16: Earth Pressures at Completion of Backfill (Test 4)

| Location | Average vertical Earth Pressure at top of pipe (psi) | Top of pipe from EPC Center (in) | Average Density of Layers above Pressure Cell (pcf) | Vertical Earth Pressure (psi) | Horizontal Pressure Recorded at EPC (psi) | Lateral Earth Pressure Coefficient |
|---|---|---|---|---|---|---|
| Springline East | 6.07 | 36 | 124.0 | 8.65 | 3.8 | 0.44 |
| Springline West | 6.07 | 36 | 124.0 | 8.65 | 5.5 | 0.64 |
| East Wall | 6.07 | 36 | 124.0 | 8.65 | 4.4 | 0.51 |
| West Wall | 6.07 | 36 | 124.0 | 8.65 | 3.3 | 0.38 |
| South Wall | 6.07 | 36 | 124.0 | 8.65 | 2.1 | 0.24 |
| North Wall | 6.07 | 36 | 124.0 | 8.65 | 0.8 | 0.09 |
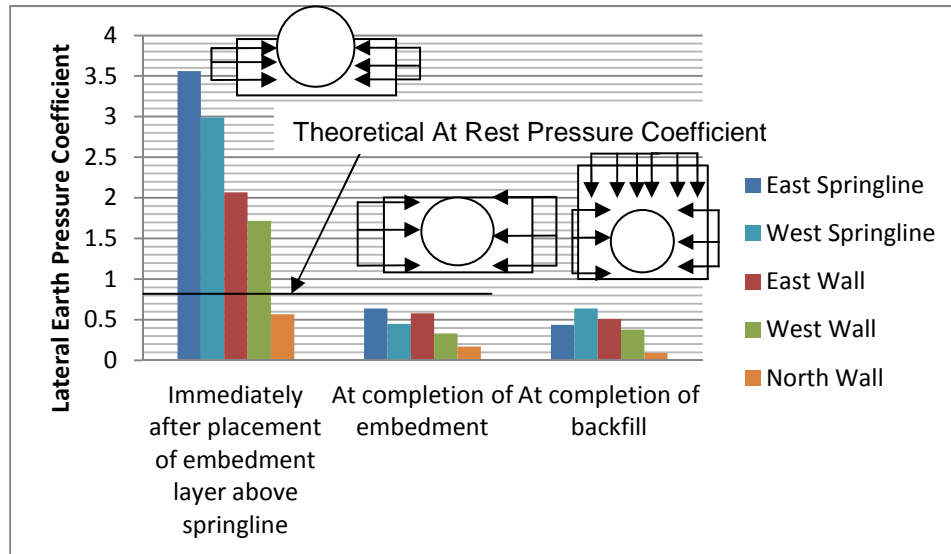
Figure 5.12: Lateral Earth Coefficients at Different Stages of Test 4

When measured lateral earth pressure coefficients immediately after placement of embedment layer above springline (or earth pressure cells) are compared with the theoretical at rest pressure values, the measured values are higher. This shows that the residual energy from compaction is also recorded.

### 5.6 Back-Calculation of E'

The maximum deflections recorded in the laboratory tests were used to fit the Modified Iowa Equation and Bureau of Reclamation Equation in order to back calculate Modulus of soil reaction (E') values. Calculations of these values are presented below.

5.6.1 Test 1

Modified Iowa Equation

$\Delta x$ = Immediate horizontal deflection of pipe = 0.65 (Vertical deflection used)

$D_l$ = Deflection lag factor = 1 (Since Immediate deflection is used)

K = Bedding constant = 0.1

W = Load per unit length of pipe (lb/in.) = {(8 + 7.6 + 9.8)/3} psi x 73.75 in. = 624.6 lb/in.

r = Pipe radius (in.) = 36.875

E = Modulus of elasticity (psi) of pipe material = 30,000,000 psi

I = Moment of inertia of pipe wall per unit length of pipe (in$^4$/in) = 0.313$^3$/12 = 0.00255 in$^4$/in

EI = 76,660.7

E' = Modulus of soil reaction (psi)         = $(0.1 \times 624.6/0.65 - 76660.7/36.875^3)/0.061$

**= 1,550 psi**

Bureau of Reclamation Equation

$\Delta Y$ = Predicted long term horizontal deflection of pipe in percentage = (0.65/73.75) = 0.88%

$T_f$ = Time lag factor = 1

$\gamma$ = Density of Soil (pcf)

h = Height of cover (ft)

$\gamma \cdot h$ = 8.47 psi = 1,219.68 psf

r = Pipe radius (in.) = 36.875

E = Modulus of elasticity (psi) of pipe material = 30,000,000 psi

I = Moment of inertia of pipe wall per unit length of pipe ($in^4$/in) = $0.313^3/12$ = 0.00255 $in^4$/in

EI = 76,660.7

$EI/r^3$ = 1.53

$F_d$ = Design Factor = 0.67

S = Soil support factor = 1.8 (from Howard (1996) table 14-3)

E' = Modulus of soil reaction (psi)         = $(0.07*1219.68*1/0.88 - 1.53)/(0.061*0.67*1.8)$

**= 1,298 psi**

5.6.2 Test 2

Modified Iowa Equation

$\Delta x$ = Immediate horizontal deflection of pipe = 0.25 (Vertical deflection used)

$D_l$ = Deflection lag factor = 1 (Since Immediate deflection is used)

K = Bedding constant = 0.1

W = Load per unit length of pipe (lb/in.) = {(6.8 + 5.4 + 7.5)/3} psi x 73.75 in. = 484.3 lb/in.

r = Pipe radius (in.) = 36.875

E = Modulus of elasticity (psi) of pipe material = 30,000,000 psi

I = Moment of inertia of pipe wall per unit length of pipe ($in^4$/in) = $0.313^3/12$ = 0.00255 $in^4$/in

EI = 76,660.7

E' = Modulus of soil reaction (psi)          = $(0.1 \times 484.3/0.25 - 76660.7/36.875^3)/0.061$

                                                                   **= 3,151 psi**

Bureau of Reclamation Equation

$\Delta Y$ = Predicted long term horizontal deflection of pipe in percentage = (0.25/73.75) = 0.34%

$T_f$ = Time lag factor = 1

$\gamma$ = Density of Soil (pcf)

h = Height of cover (ft)

$\gamma . h$ = 6.57 psi = 945.6 psf

r = Pipe radius (in.) = 36.875

E = Modulus of elasticity (psi) of pipe material = 30,000,000 psi

I = Moment of inertia of pipe wall per unit length of pipe ($in^4$/in) = $0.313^3/12$ = 0.00255 $in^4$/in

EI = 76,660.7

$EI/r^3$ = 1.53

$F_d$ = Design Factor = 0.67

S = Soil support factor = 1.8 (from Howard (1996) table 14-3)

E' = Modulus of soil reaction (psi)          = $(0.07*945.6*1/0.34 - 1.53)/(0.061*0.67*1.8)$

                                                                   **= 2,626 psi**

### 5.6.3 Test 1a

Modified Iowa Equation

$\Delta x$ = Immediate horizontal deflection of pipe = 0.44 (Vertical deflection used)

$D_l$ = Deflection lag factor = 1 (Since Immediate deflection is used)

K = Bedding constant = 0.1

W = Load per unit length of pipe (lb/in.) = {(15.5 + 9.6 + 9.2)/3} psi x 73.75 in. = 843.2 lb/in.

r = Pipe radius (in.) = 36.875

E = Modulus of elasticity (psi) of pipe material = 30,000,000 psi

I = Moment of inertia of pipe wall per unit length of pipe (in$^4$/in) = $0.313^3/12$ = 0.00255 in$^4$/in

EI = 76,660.7

E' = Modulus of soil reaction (psi)　　　 = $(0.1 \times 843.2/0.44 - 76660.7/36.875^3)/0.061$

**= 3,117 psi**

Bureau of Reclamation Equation

ΔY = Predicted long term horizontal deflection of pipe in percentage = (0.44/73.75) = 0.60%

$T_f$ = Time lag factor = 1

γ = Density of Soil (pcf)

h = Height of cover (ft)

γ. h = 11.43 psi = 1,646.4 psf

r = Pipe radius (in.) = 36.875

E = Modulus of elasticity (psi) of pipe material = 30,000,000 psi

I = Moment of inertia of pipe wall per unit length of pipe (in$^4$/in) = $0.313^3/12$ = 0.00255 in$^4$/in

EI = 76,660.7

EI/r$^3$ = 1.53

$F_d$ = Design Factor = 0.67

S = Soil support factor = 1.8 (from Howard (1996) table 14-3)

E' = Modulus of soil reaction (psi)　　　 = $(0.07*1646.4*1/0.6 - 1.53)/(0.061*0.67*1.8)$

**= 2,590 psi**

5.6.4 Test 3

Modified Iowa Equation

Δx = Immediate horizontal deflection of pipe = 0.14 (Vertical deflection used)

$D_l$ = Deflection lag factor = 1 (Since Immediate deflection is used)

K = Bedding constant = 0.1

W = Load per unit length of pipe (lb/in.) = 5.97 psi x 73.75 in. = 440.3 lb/in.

r = Pipe radius (in.) = 36.875

E = Modulus of elasticity (psi) of pipe material = 30,000,000 psi

I = Moment of inertia of pipe wall per unit length of pipe (in$^4$/in) = $0.313^3/12$ = 0.00255 in$^4$/in

EI = 76,660.7

E' = Modulus of soil reaction (psi)     = $(0.1 \times 440.3/0.14 - 76660.7/36.875^3)/0.061$

**= 5,131 psi**

Bureau of Reclamation Equation

ΔY = Predicted long term horizontal deflection of pipe in percentage = (0.14/73.75) = 0.19%

$T_f$ = Time lag factor = 1

γ = Density of Soil (pcf)

h = Height of cover (ft)

γ. h = 5.97 psi = 859.7 psf

r = Pipe radius (in.) = 36.875

E = Modulus of elasticity (psi) of pipe material = 30,000,000 psi

I = Moment of inertia of pipe wall per unit length of pipe (in$^4$/in) = $0.313^3/12$ = 0.00255 in$^4$/in

EI = 76,660.7

EI/r$^3$ = 1.53

$F_d$ = Design Factor = 1

S = Soil support factor = 1.8 (from Howard (1996) table 14-3)

E' = Modulus of soil reaction (psi)     = $(0.07*859.7*1/0.19 - 1.53)/(0.061*1*1.8)$

**= 2,871 psi**

5.6.5 Test 4

Modified Iowa Equation

Δx = Immediate horizontal deflection of pipe = 0.13

$D_l$ = Deflection lag factor = 1 (Since Immediate deflection is used)

K = Bedding constant = 0.1

W = Load per unit length of pipe (lb/in.) = 6.07 psi x 73.75 in. = 447.7 lb/in.

r = Pipe radius (in.) = 36.875

E = Modulus of elasticity (psi) of pipe material = 30,000,000 psi

I = Moment of inertia of pipe wall per unit length of pipe (in$^4$/in) = $0.313^3/12$ = 0.00255 in$^4$/in

EI = 76,660.7

E' = Modulus of soil reaction (psi)          = $(0.1 \times 447.7/0.13 - 76660.7/36.875^3)/0.061$

**= 5,621 psi**

Bureau of Reclamation Equation

ΔY = Predicted long term horizontal deflection of pipe in percentage = (0.13/73.75) = 0.18%

$T_f$ = Time lag factor = 1

γ = Density of Soil (pcf)

h = Height of cover (ft)

γ. h = 6.07 psi = 874.1 psf

r = Pipe radius (in.) = 36.875

E = Modulus of elasticity (psi) of pipe material = 30,000,000 psi

I = Moment of inertia of pipe wall per unit length of pipe (in$^4$/in) = $0.313^3/12$ = 0.00255 in$^4$/in

EI = 76,660.7

$EI/r^3$ = 1.53

$F_d$ = Design Factor = 0.67

S = Soil support factor = 1.8 (from Howard (1996) table 14-3)

E' = Modulus of soil reaction (psi)          = $(0.07*874.1*1/0.18 - 1.53)/(0.061*0.67*1.8)$

**= 4,600 psi**

5.6.6 Comparison Modulus of Soil Reaction (E')

Back-calculation of E' value achieved in each of tests was carried out. Calculated E' values are compared in Figure 5.13.
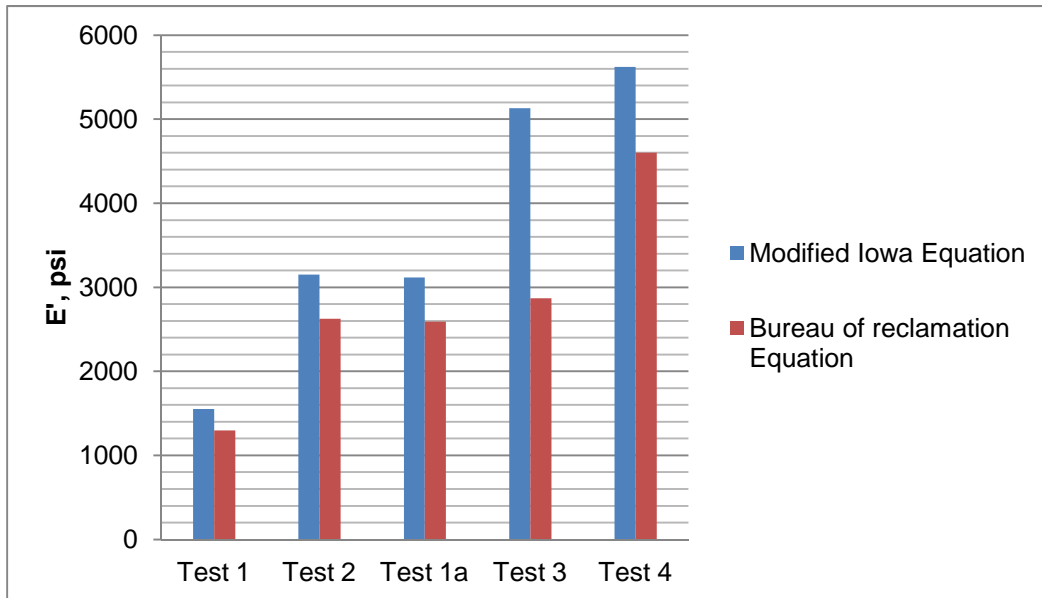
Figure 5.13: Calculated E' Values for Tests

5.7 Peaking Deflection

Maximum peaking deflection (vertical elongation during embedment construction) occurred during Test 4. Such deflection occurred during compaction of native clay. Test 1a had the next highest peaking deflections. In both of these tests, professional contractors were used to compact native clay. During Test 4, both sides were compacted simultaneously which is one possible reason for higher peaking deflection in Test 4. Tests 1 and 2 had similar peaking deflections. Test 3 had the minimum peaking deflection because vibratory plate compactor was used to compact crushed limestone as opposed to tamping foot compactor used to compact native and modified clays. Also, crushed limestone proved lesser lateral force due to higher angle of friction. Figure 4.14 compares peaking behavior of pipe during the tests. Figure 4.15 illustrates peaking of pipe during Test 4.
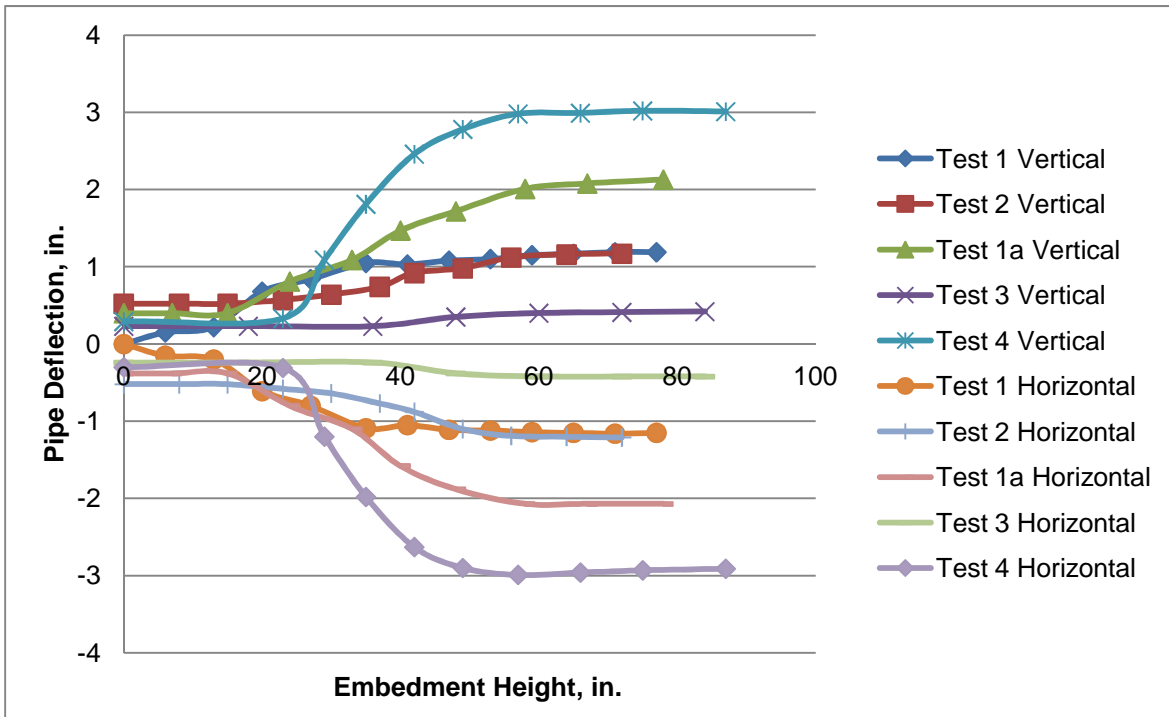
Figure 5.14: Comparison of Peaking Deflections



Figure 5.15: Peaking of Pipe during Test 4

## 5.8 Summary

This chapter presented the discussion of the results of the full scale laboratory tests. The key observations including deflection ratio (ratio of horizontal deflection to vertical), bedding angle (as described in Spangler's model), lateral earth pressure coefficient and Modulus of soil reaction value obtained by fitting test parameters to modified Iowa equation and Bureau of reclamation equation were discussed. The calculations of these values were also shown.

Chapter 6

Calibration of Soil Constitutive Model Parameters

<u>6.1 Introduction</u>

Two basic concepts in modeling soil behavior by finite element analysis are (i) effective stress analysis, and (ii) total stress analysis. Effective stress analysis treats soil and water as two distinct materials in the soil system. The examples are cam clay model, modified cam clay model, hardening soil (HS) model, etc. However, total stress analysis considers the soil system consisting solids, water and air as a single material. The examples of total stress analysis are Mohr-Coulomb model, undrained soft clay model, Drucker-Prager model, Duncan and Selig model, etc. Unsaturated soils were used for the tests; therefore it is appropriate to take total stress analysis approach.

Mohr-Coulomb model is one of the more commonly used methods to analyze soil behavior. It is simple to use, is easy to calibrate and effectively predicts the failure stresses. Figure 6.1 calibrations of Mohr-Coulomb parameters with the UU test performed by the Geotechnical team. Initial tangential Modulus of elasticity was used for the Modulus of elasticity. Therefore, the model is effective in predicting low strains but as it gets to higher strains, the strain prediction is compromised. It is still very effective in prediction the failure stresses. Other modulii like 50% secant Modulus and 100% secant Modulus may be used with Mohr-Coulomb model, but the model does not efficiently predict strains at all stress states.

Duncan and Selig model is a hyperbolic model which is more robust in prediction of strains at all levels of stresses within Mohr-Coulomb failure criteria. It uses five parameters to define Young's Modulus of elasticity at any given stress state. The parameters are listed and defined in Table 6.1. The parameters listed in Table 6.1 were calibrated for both untreated and lime treated native soil based on the UU triaxial test results obtained from the Geotechnical Team.
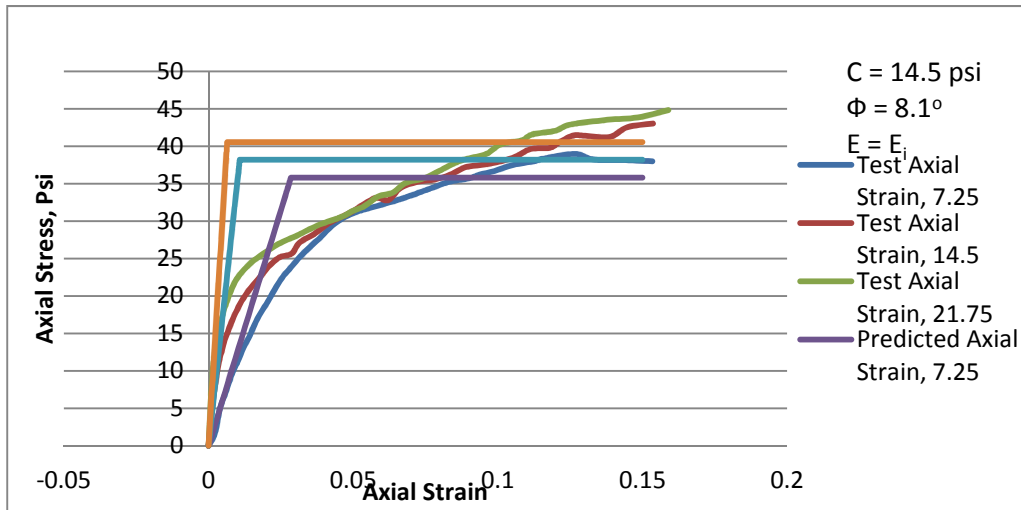
Figure 6.1: Calibration of Mohr-Coulomb Model Parameters

Table 6.1: Parameters for Duncan Model for Modulus of Elasticity

| Parameter | Definition |
|-----------|------------|
| $R_f$ | Failure Ratio |
| K | Dimensionless Parameter |
| n | Dimensionless Parameter |
| C | Cohesive Strength |
| Φ | Internal Angle of Friction |

### 6.2 Calibration of Untreated Native Soil for Duncan Hyperbolic Model Parameters

6.2.1 Calibration of $R_f$ and $E_i$:

During UU triaxial test, test soil is placed in the cylindrical triaxial cell and confined by a hydrostatic pressure of $\sigma_3$. Then, the soil is subject to deviator stress, q = until shear failure of the sample. This is illustrated in Figure 6.2.

The hyperbolic function representing the stress-strain relationship from the triaxial test is given by Equation 6.1.

$$q = \varepsilon/(1/E_i + \varepsilon/q_u) \dotfill (6.1)$$

Where,

$E_i$ = Initial tangential Modulus (psi)

$q_u$ = Ultimate deviator stress at large strain (psi)

$\varepsilon$ = Axial strain (unit-less)

Equation 4.1 can be written in the form:

$$\varepsilon/q = 1/E_i + \varepsilon/q_u \dots\dots\dots\dots\dots\dots\dots\dots\dots\dots\dots\dots\dots\dots\dots(6.2)$$

Equation 6.2 represents equation of the straight line when $\varepsilon/q$ is plotted against $\varepsilon$. The data from the UU Triaxial test carried out by the geotechnical team were plotted as illustrated in Figures 6.3, 6.4 and 6.5.
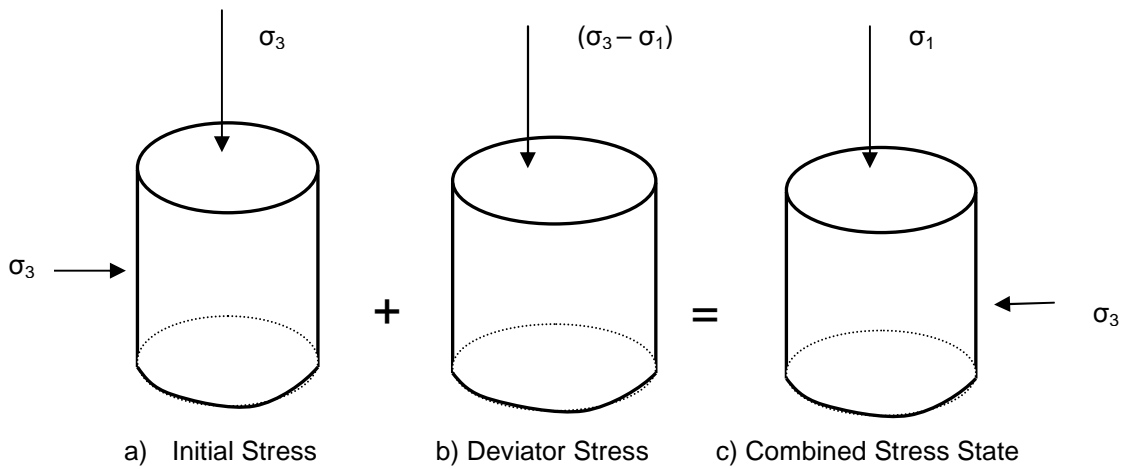


Figure 6.2: Triaxial Test Stresses
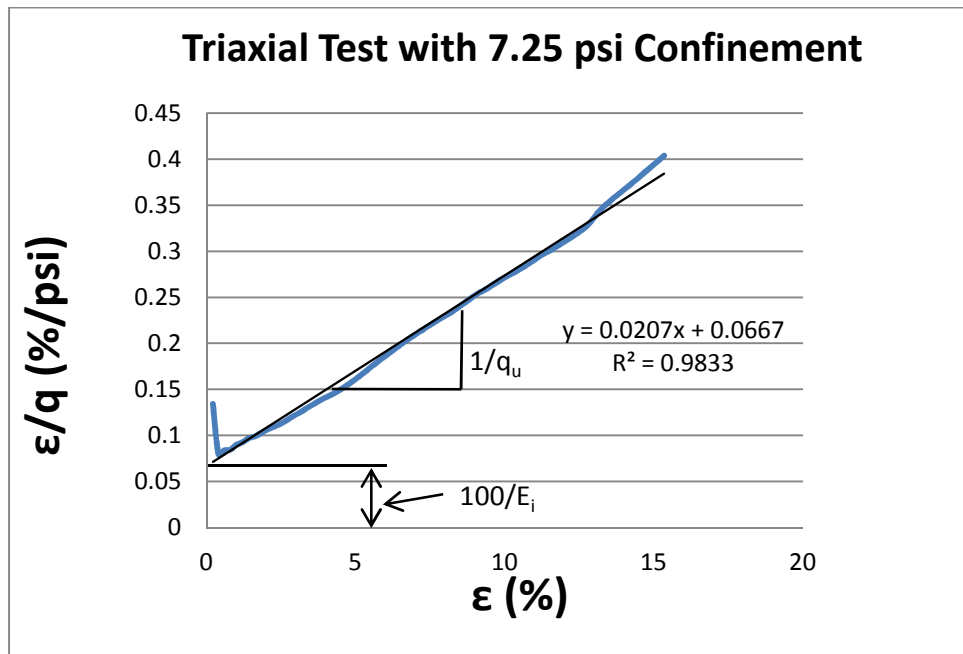


Figure 6.3: Calibration of $E_i$ and $q_u$

The failure ratio, $R_f$ is one of the parameters used in Duncan-Selig Model. $R_f$ is given by Equation A.3.

$$R_f = q_f/q_u \dots\dots\dots\dots\dots\dots\dots\dots\dots\dots\dots\dots\dots\dots\dots\dots\dots\dots\dots(6.3)$$

Where,

$q_f$ = Deviator stress at failure obtained from the triaxial test

Summary of Calibrated Data is presented in Table 6.2.
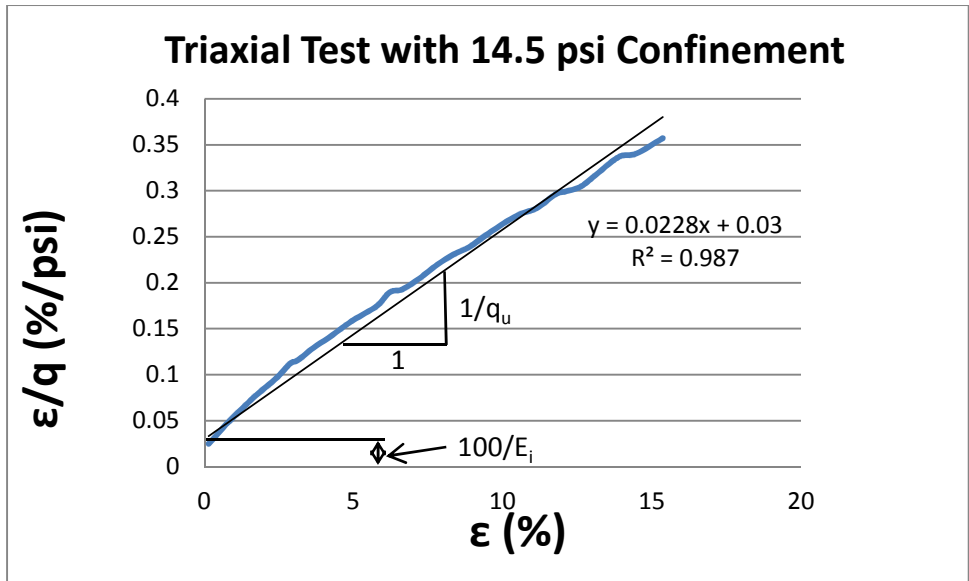


Figure 6.4: Calibration of $E_i$ and $q_u$
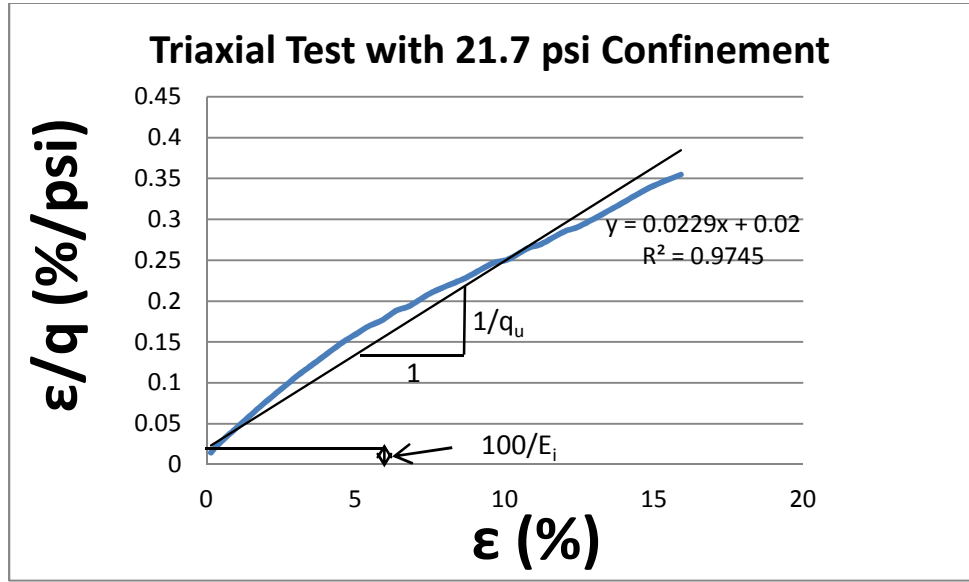


Figure 6.5: Calibration of $E_i$ and $q_u$

Table 6.2: Calibration Data for Untreated Soil

| Parameter | 7.25 psi Confinement | 14.5 psi Confinement | 21.75 psi confinement | Average |
|---|---|---|---|---|
| $E_i$ | 1,499 psi | 3,333 psi | 5,000 psi | |
| $q_u$ | 48.31 psi | 43.86 psi | 43.67 psi | |
| $q_f$[1] | 38.98 psi | 43.04 psi | 44.82 psi | |
| $R_f$ | 0.81 | 0.98 | 1 | 0.93 |

[1]$q_f$ taken as stress at 10% strain.

6.2.2 Calibration of K and n

Duncan-Selig Model assumes that the initial tangential Modulus of elasticity increases with confining pressure and this increase is illustrated by equation 6.4.

$$E_i = K\, P_a\, (\sigma_3/P_a)^n \dots\dots\dots\dots\dots\dots\dots\dots\dots\dots\dots\dots\dots\dots\dots\dots\dots\dots(6.4)$$

Where,

$E_i$ = Initial Tangential Modulus of Elasticity (psi)

K and n are model parameters

$\sigma_3$ = Confining pressure (psi)

$P_a$ = Atmospheric pressure = 14.696 psi

Equation (6.4) can be simplified as:

$$\ln (E_i/P_a) = \ln K + n \ln (\sigma_3/P_a) \dots\dots\dots\dots\dots\dots\dots\dots\dots\dots\dots\dots\dots\dots(6.5)$$

Equation (6.5) is an equation of a straight line in slope-intercept form. Parameters K and n can be calibrated by plotting data from the UU test carried out by the Geotechnical Team. The plotted data is presented in Table 6.3 and plot is illustrated in Figure 6.6.

Table 6.3: Data for Calibration of K and n

| $\sigma_3$ | $E_i$ | $\ln(E_i/P_a)$ | $\ln(\sigma_3/P_a)$ |
|---|---|---|---|
| 7.252 | 1,499 | 4.625 | − 0.706 |
| 14.504 | 3,333 | 5.424 | − 0.013 |
| 21.756 | 5,000 | 5.830 | 0.392 |
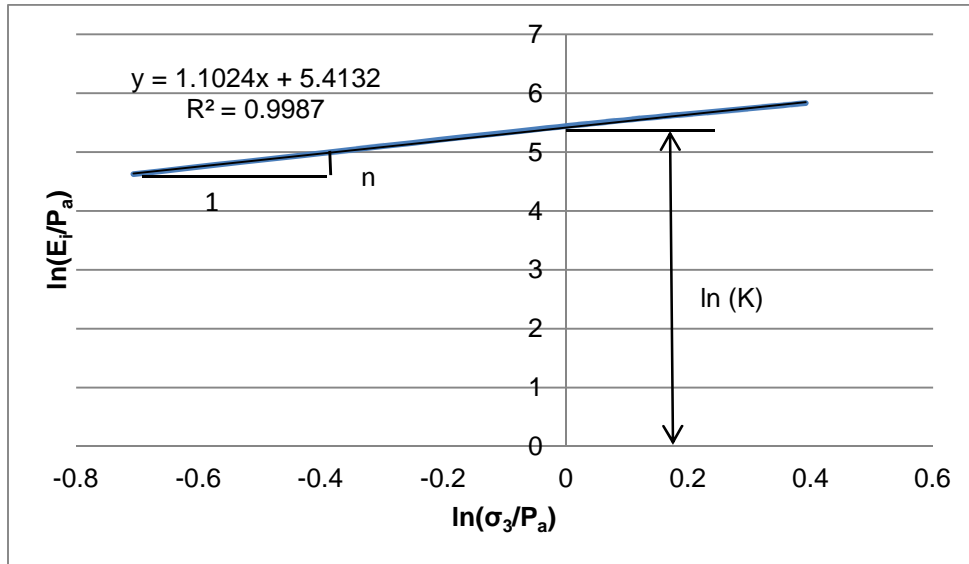
Figure 6.6: Calibration of K and n

The Equation of the straight line plotted from the test data is:

$$y = 1.1024x + 5.4132 \quad \dots\dots\dots\dots\dots\dots\dots\dots\dots\dots\dots\dots\dots\dots\dots\dots\dots\dots\dots\dots\dots\dots\dots(6.6)$$

Therefore,

n = 1.1024

$K = e^{5.4904} = 224$

Parameters cohesive strength, C and internal angle of friction, Φ, were calibrated by the Geotechnical team.

A model to predict results of a triaxial tests using Duncan-Selig model was created in MS Excel. This model was used with above calibrated parameters to predict stress-strain curve a UU triaxial test. The predicted results are compared with actual test results in Figures 6.7, 6.8 and 6.9.

$$E_t = [1 - R_f (1 - \sin \Phi) \, q/(2 \, C \cos \Phi + 2 \, \sigma_3 \sin \Phi)]^2 \, K \, P_a \, (\sigma_3/P_a)^n \dots\dots\dots\dots\dots(6.7)$$
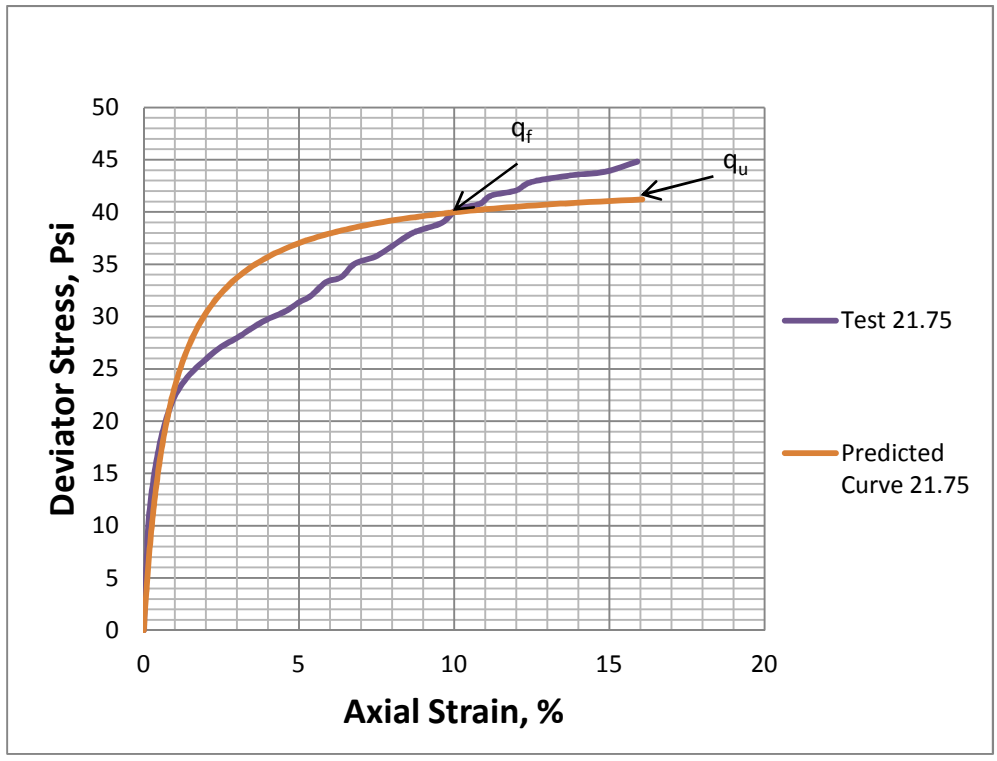
Figure 6.7: Comparison of Duncan-Selig Model Prediction with Actual Test (Untreated 21.75 psi confinement)
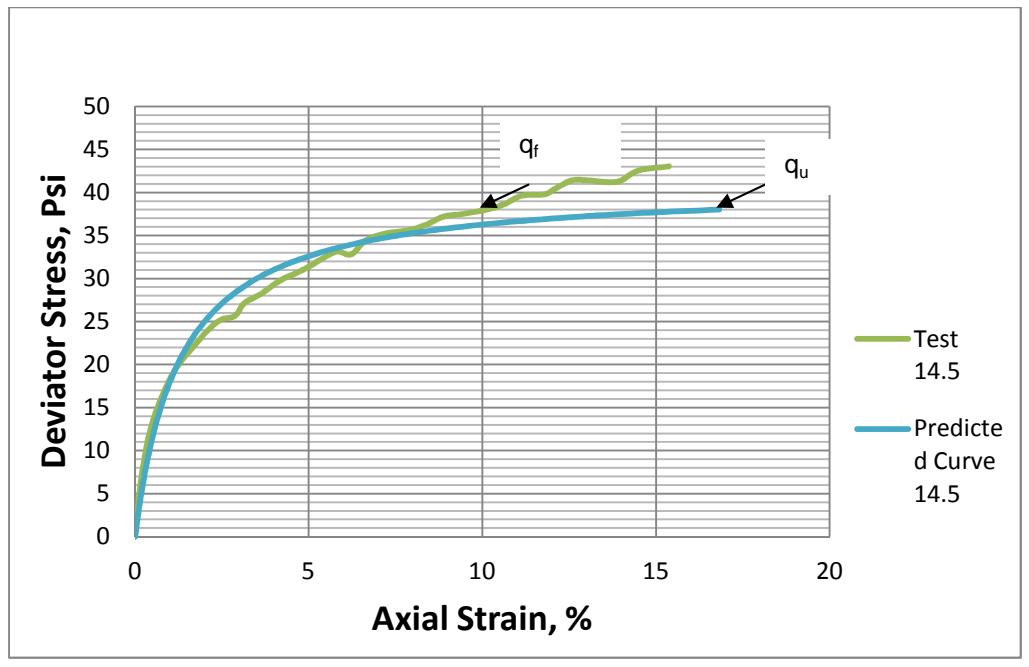


Figure 6.8: Comparison of Duncan-Selig Model Prediction with Actual Test (Untreated 14.5 psi confinement)
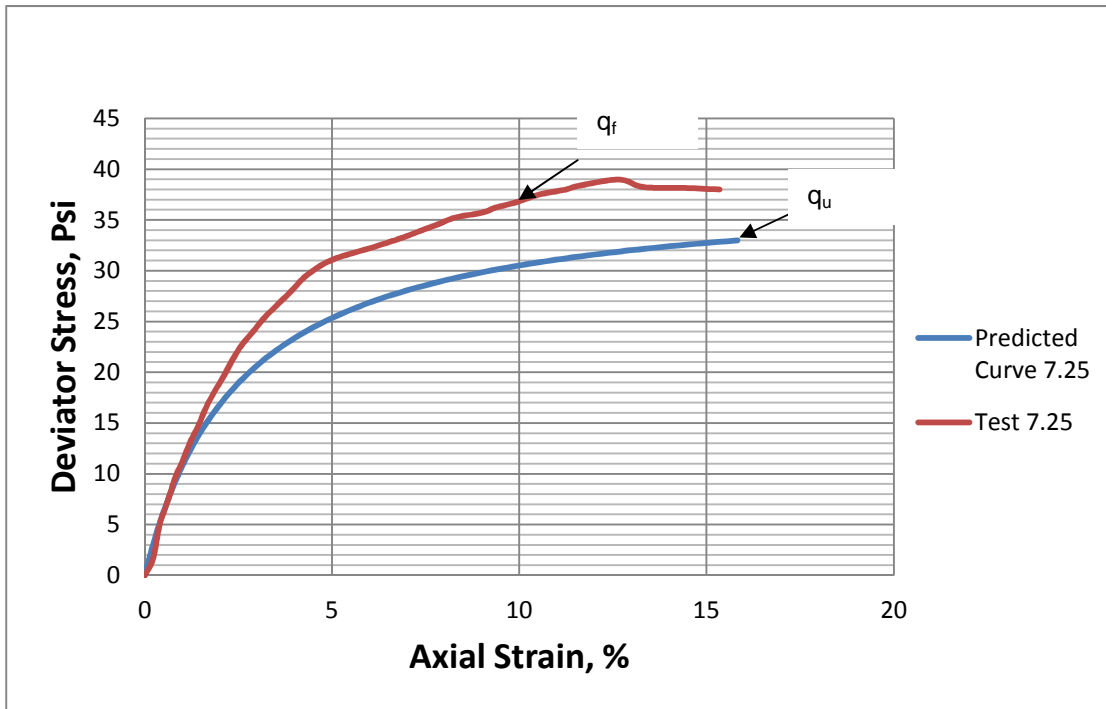
Figure 6.9: Comparison of Duncan-Selig Model Prediction with Actual Test (Untreated 7.25 psi confinement)

Table 6.4: Duncan Selig Model Parameters for Untreated Native Soil

| Parameter | Value |
|-----------|-------|
| $R_f$ | 0.93 |
| K | 224 |
| n | 1.1024 |
| C | 14.50 |
| Φ | 8.1° |

6.3 Calibration of 6% Lime-Treated Native Soil for Duncan Hyperbolic Model Parameters

Lime-treated native soil was calibrated to Duncan-Selig model parameters by similar procedure as untreated native soil. The parameter values calibrated are presented in Table 6.5.

Table 6.5: Duncan-Selig Model Parameters for 6% Lime Treated Native Soil

| Parameter | Value |
|-----------|-------|
| $R_f$ | 0.7 |
| K | 1319 |
| n | 1.0679 |
| C | 23.2 |
| Φ | 25.8° |

135

Figures 6.10 through 6.13 illustrate plots leading to the parameter values presented in Table 6.5.
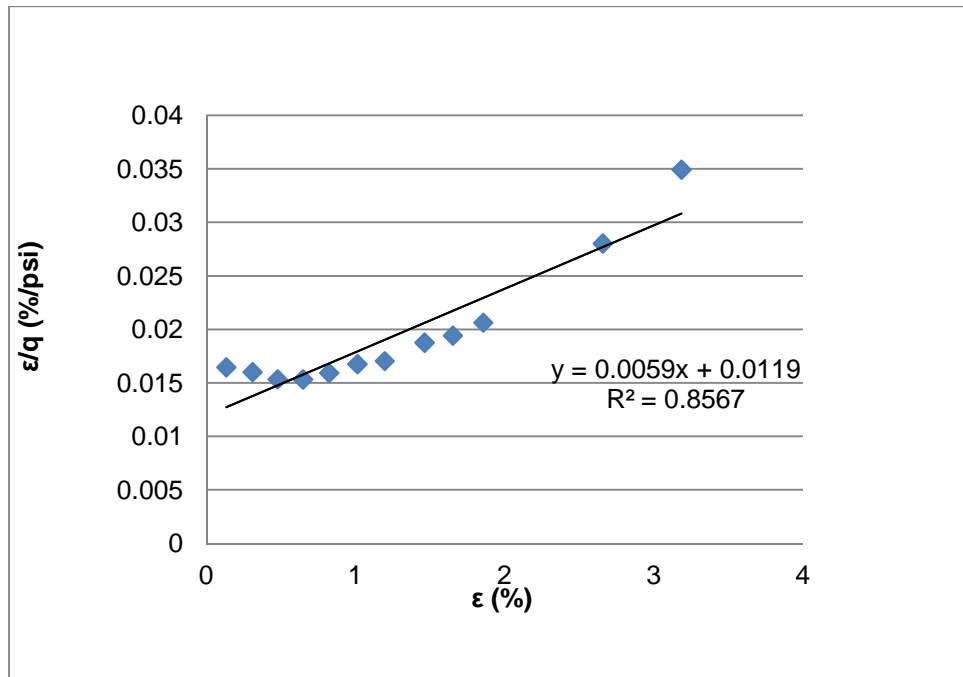


Figure 6.10: Calibration of Ei and qu
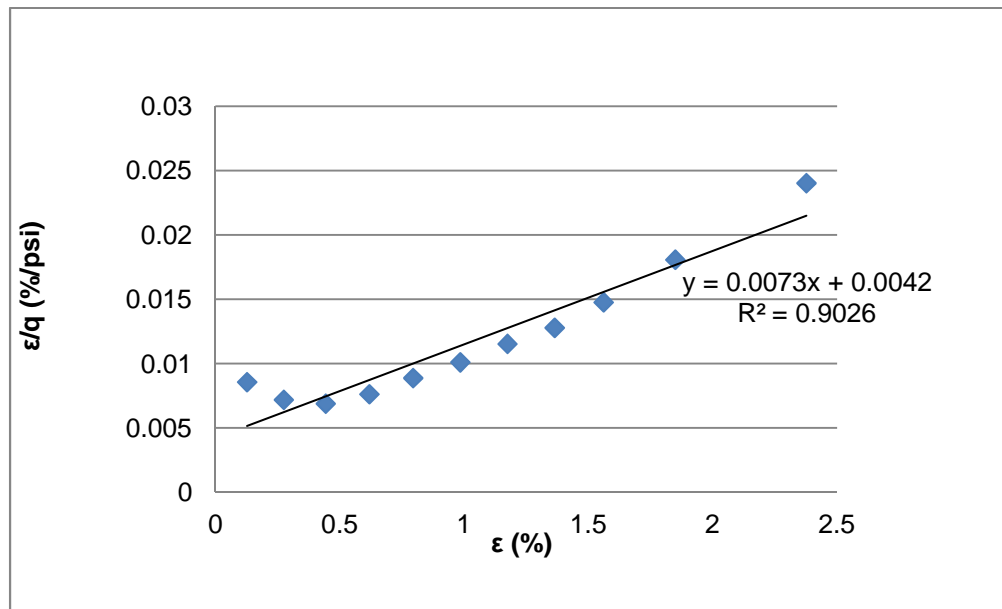


Figure 6.11: Calibration of Ei and qu
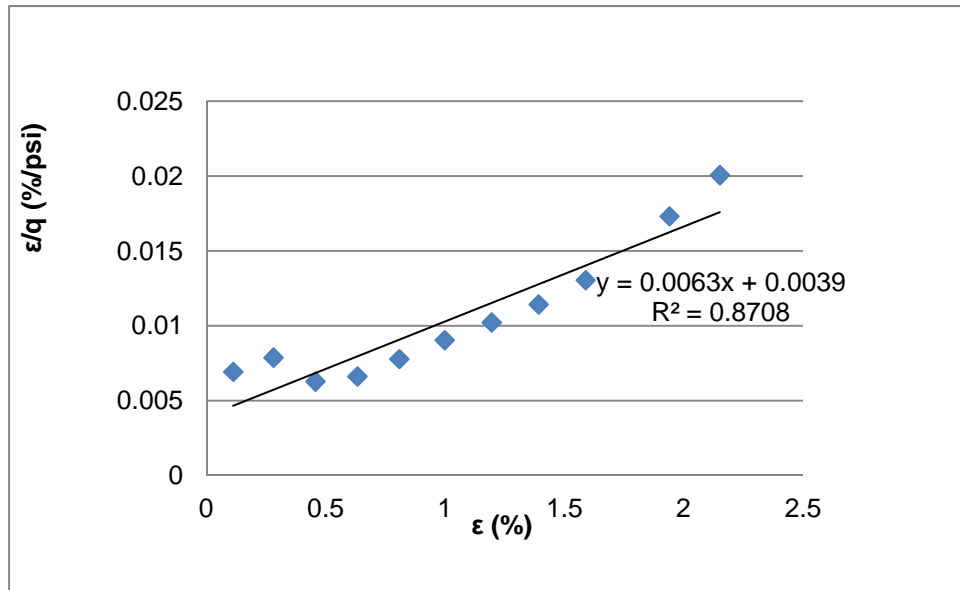
Figure 6.12: Calibration of Ei and qu
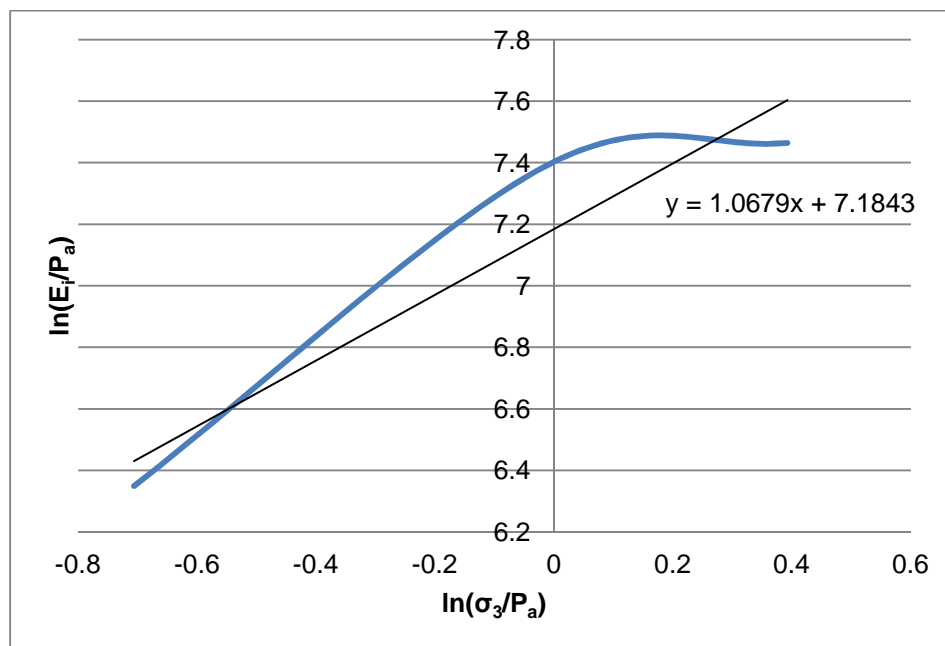


Figure 6.13: Calibration of K and n

The UU Triaxial test results were predicted using parameters presented in Table A.5 and Compared to the actual test results. Figures 6.14, 6.15 and 6.16 illustrate those comparisons.
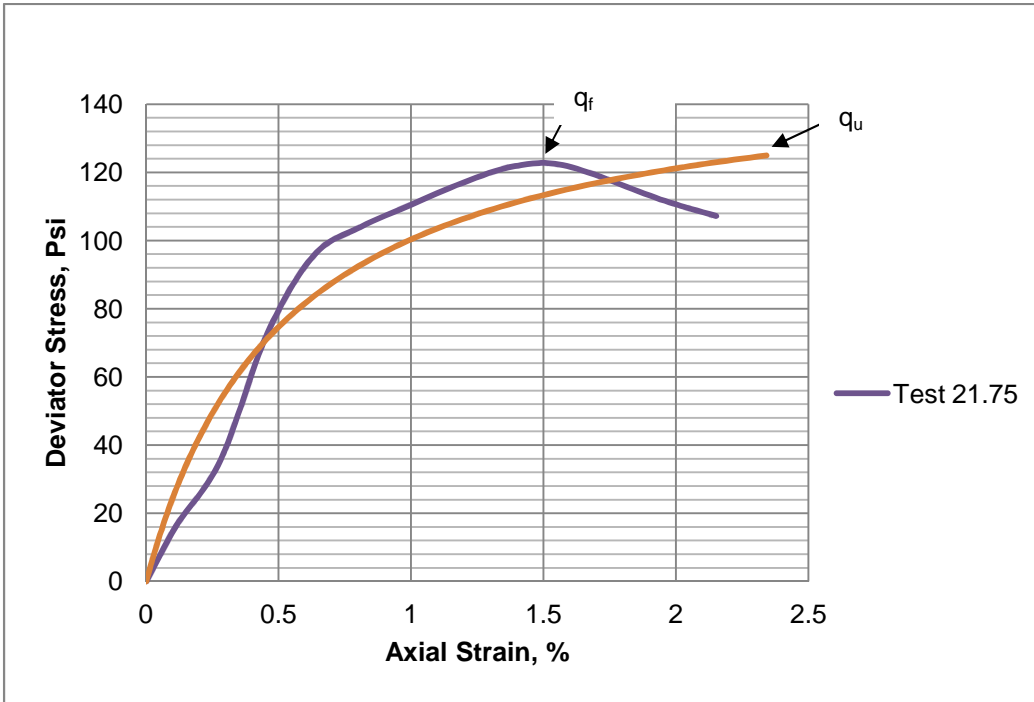
Figure 6.14: Comparison of Duncan-Selig Model Prediction with Actual Test (Treated 21.75 psi confinement)
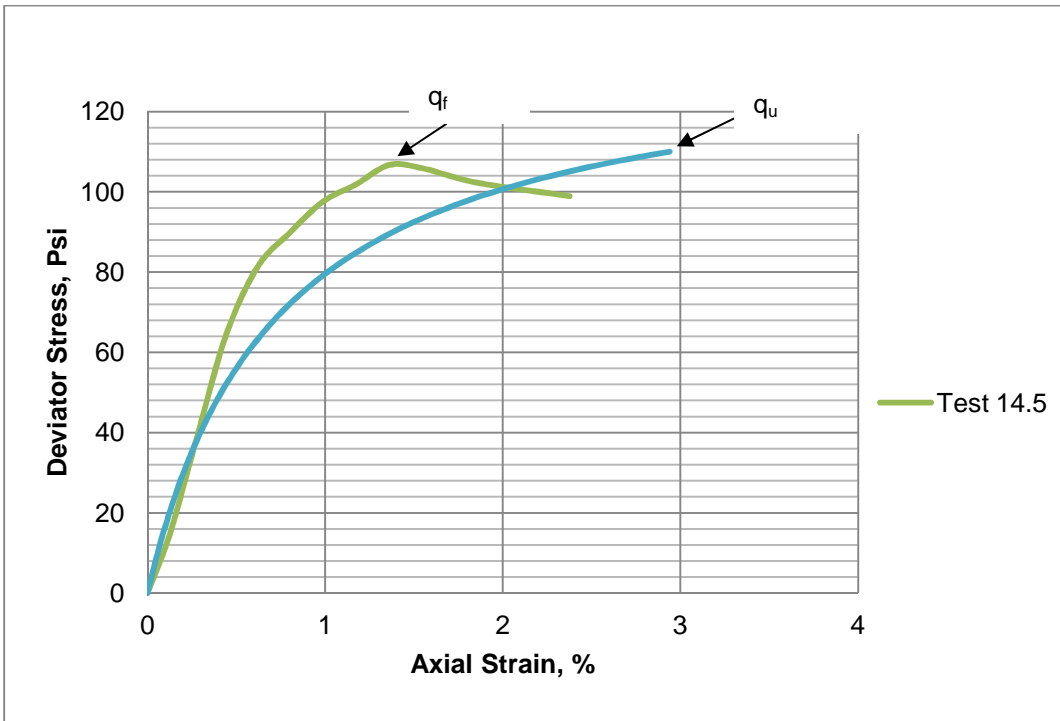


Figure 6.15: Comparison of Duncan-Selig Model Prediction with Actual Test (Treated 14.5 psi confinement)
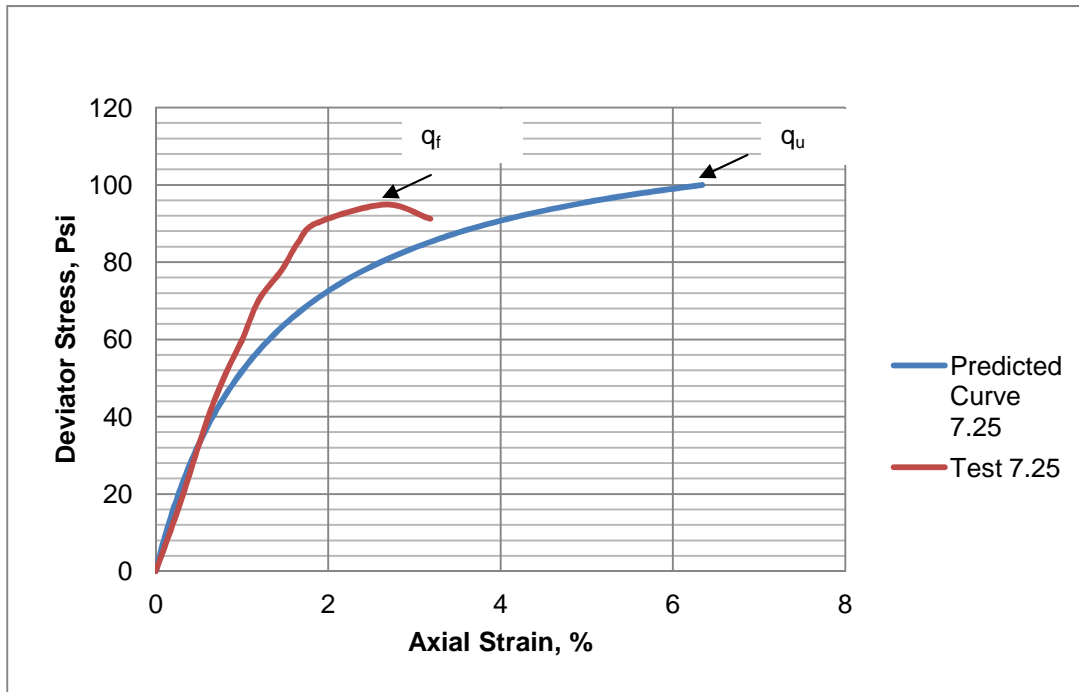
Figure 6.16: Comparison of Duncan-Selig Model Prediction with Actual Test (Treated 7.25 psi confinement)

### 6.4 Summary

Detailed procedure for calibrating the Duncan hyperbolic model parameters from the laboratory tests was discussed in this chapter. All five model parameters for native clay and modified clay were calibrated and the comparisons between actual test results and the results predicted by the hyperbolic model are illustrated. The predicted results are close to the actual results obtained from the laboratory tests.

Chapter 7

Finite Element Analysis

### 7.1 Introduction

This chapter presents the methodology and description of finite element models developed in order to model the behavior of steel pipe embedded in various backfill. The finite element models are analyzed by using PLAXIS 2D software. The results of the analysis are compared to the actual test results in order to validate the models. The validation facilitates use of finite element method to do further analyses without having to perform the actual laboratory test. Geotechnical FEA software PLAXIS 2D was used to simulate the loading of the laboratory tests. Numerous models were run with various soil properties and changes in configurations of the laboratory test. The properties and parameters of the FEA model elements, and soil and pipe models are described and the results are presented.

### 7.2 Finite Element Model

7.2.1 Assumptions

Two dimensional plane strain finite element models were used to simulate results of the laboratory tests. As per plain strain conditions, strains normal to x-y plain $\varepsilon_z$ and the shear strains $\gamma_{xz}$ and $\gamma_{yz}$ were assumed to be zero. Figure 7.1 illustrates plane strain problem for a pipe subjected to vertical load. The plane strains assumption are realistic for long bodies with constant cross-sectional area subjected to loads that act only in x and y directions and do not vary in z direction (Logan, 2012).
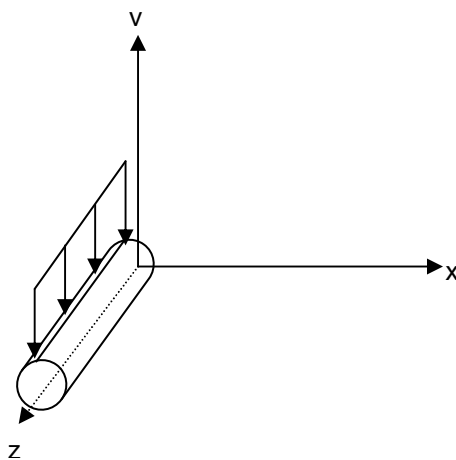


Figure 7.1: Plane Strain Condition for Pipe Subjected to Vertical Load

## 7.2.2 Pipe Element

Pipe was modeled by using plate elements (line elements) available in PLAXIS 2D software. The five node plate element illustrated in Figure 7.2 consisted of three degrees of freedom per node: two translational degrees of freedom ($U_x$, $U_y$) and one rotational degree of freedom per node. The plate elements are based on Mindlin's plate theory that allows for plate deflections due to shearing as well as bending. The element length can also be changed when axial force is applied. Also, plate elements used can become plastic if a prescribed maximum bending moment or maximum axial force is reached. Plate element consisted of four pairs of Gaussian stress points which were used to evaluate bending moments and axial forces.
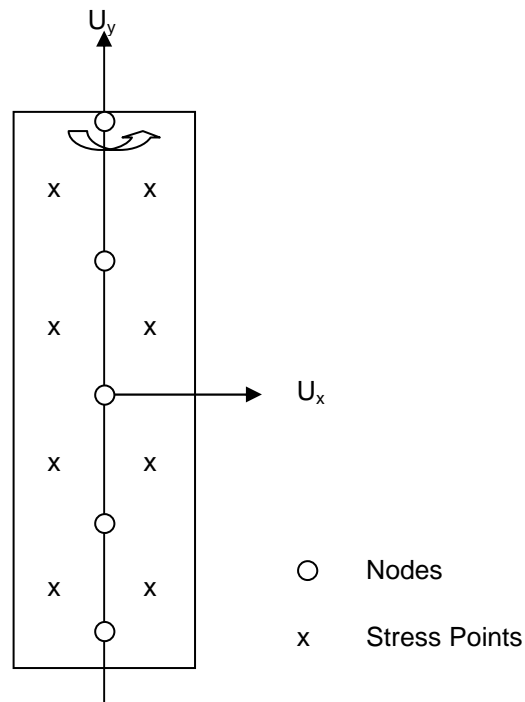


Figure 7.2: Five Node Plate Element

## 7.2.3 Soil Elements

Soil layers were modeled by using 15-node triangular elements, as shown in Figure 7.3, available in PLAXIS 2D software. The 15-node triangular elements provide fourth order interpolation for displacements and the numerical integration involves twelve Gaussian stress points. The 15-node

141

triangular elements are considered very accurate element that produces high quality stress results for difficult problems like collapse calculations for incompressible soils (PLAXIS, 2012).
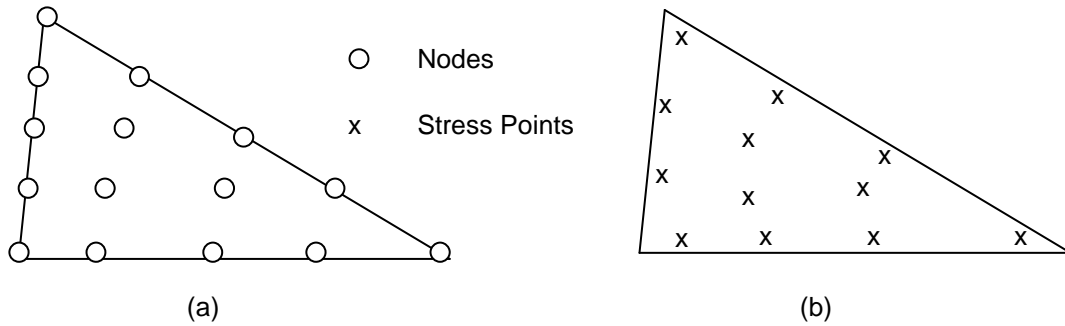


Figure 7.3: 15-node Triangular Element (a) Nodes, (b) Stress Points

7.2.4 Interface Elements

Interface elements were used at the pipe-soil interface. Interface elements were defined by five pairs of nodes as shown in Figure 7.4. Although in Figure 7.4, interface element is shown to have a finite thickness, the coordinates of each node pair are identical in the finite element formulation, and therefore the element thickness is zero. Newton Cotes integration is used to obtain the stiffness matrix for the interface elements. Five Newton Cotes stress points are positioned to coincide with the node pairs.
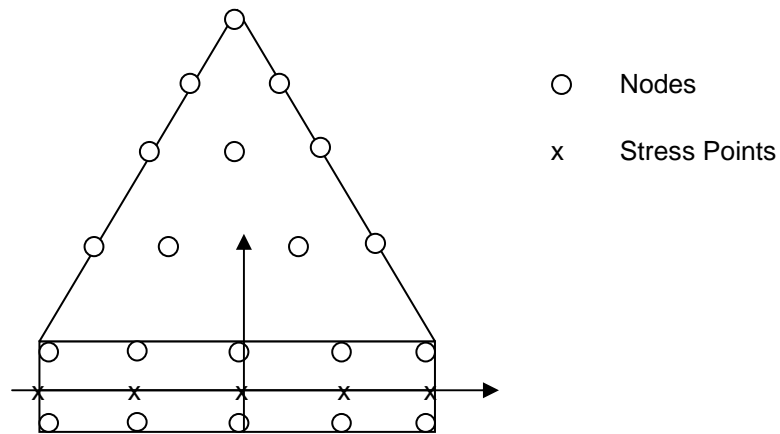


Figure 7.4: Interface Element

<u>7.3 Properties and Parameters</u>

7.3.1 Soil Constitutive Model

Hardening soil was used to model the constitutive behavior of clay and modified clay soils. Hardening soil model is a hypo-elastic model developed by Schanz et al. (1999). The parameters were calibrated from the unconsolidated undrained triaxial tests performed at the laboratory. Hardening soil model uses secant Modulus to model the stress strain relationship. This relation is given by Equations 7.1.

$$E_{50} = E_{50}^{ref} \{(\sigma_3 + c.cot\varphi)/(\sigma^{ref} + c.cot\varphi)\}^m \text{......................................................}(7.1)$$

Where,

$E_{50}$ = Confining stress dependent stiffness of primary loading (psi)

$E_{50}^{ref}$ = A reference stiffness Modulus corresponding to $\sigma^{ref}$ (psi)

$\sigma^{ref}$ = Reference stress (psi)

$\sigma_3$ = Confining pressure (psi)

m = Amount of stress dependency (unit-less)

Triaxial test was simulated by PLAXIS 2D. The screenshot of the test results is illustrated in Figure 7.5. The results compared very well with the lab test results. The secant Modulus of the soil was varied in subsequent models.

To simulate behavior of gravel and pea gravel, Mohr-Coulomb model was used. The screenshot of parameter values used for gravel are presented in Figure 7.6. Modulus of elasticity of 10,000 psi and angle of friction of 30 degrees was used for gravel.

7.3.2 Steel Pipe

Steel pipe was modeled as a linear elastic material. Modulus of elasticity of 30,000,000 psi was used and Poisson's ration of 0.3. Figure 7.7 illustrates the screenshot of steel properties used.

Table 7.1 summarizes the different types of models, elements, and constitutive relations used for the different components of the models.
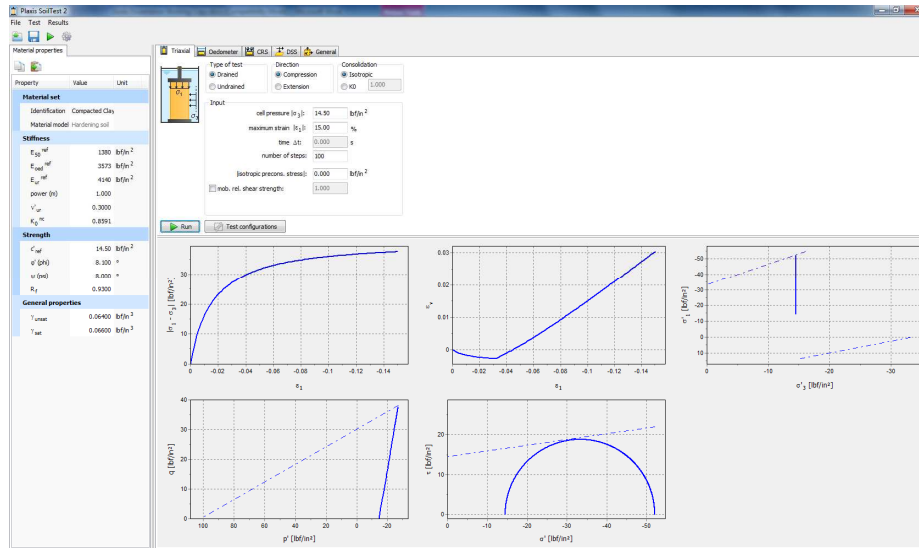
Figure 7.5: Screenshot of Triaxial Test from PLAXIS
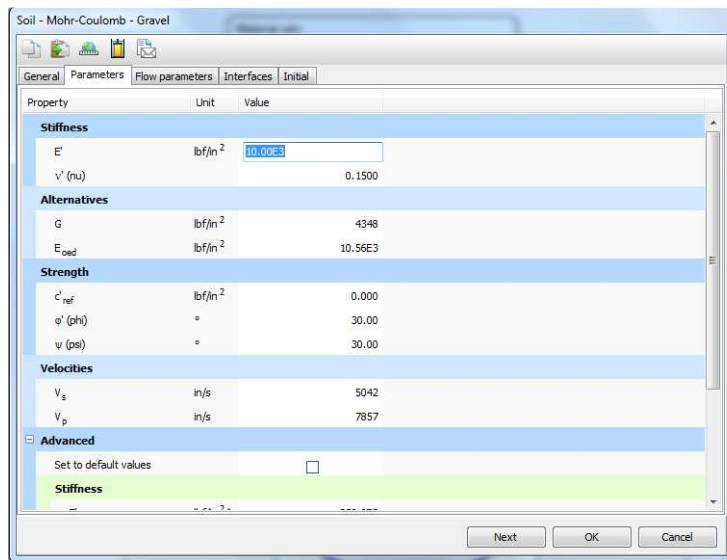


Figure 7.6: Screenshot of Gravel Properties Used

Table 7.1: Summary of Model Components

| Model Component | Material | Model | Element | Constitutive Model |
|---|---|---|---|---|
| Pipe | Steel | Plain Strain | 5-node Plate Element | Linear Elastic |
| Embedment | Clay | Plain Strain | 15-node Triangular Element | Strain Hardening Model (Uses parameters from Duncan Hyperbolic Model) |
| Embedment | Lime Treated Clay | Plain Strain | 15-node Triangular Element | Strain Hardening Model (Uses parameters from Duncan Hyperbolic Model) |
| Bedding/Embedment | Gravel | Plain Strain | 15-node Triangular Element | Mohr-Coulomb |

144
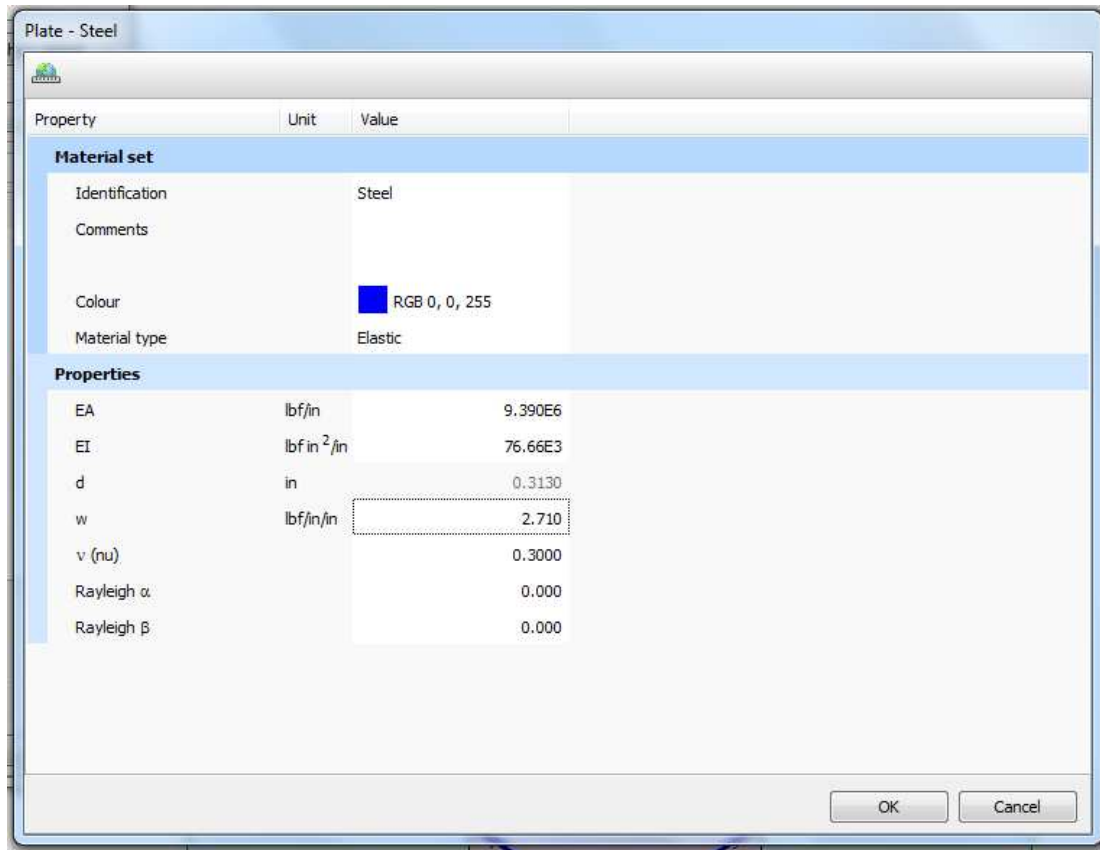
Figure 7.7: Screenshot of Steel Properties Used

<u>7.4 Simulations</u>

7.4.1 Pilot Model

Pilot model was run with the soil parameters calibrated to triaxial test results and conditions of Test 1. Trench width of 12.5 feet and height of 10 feet was used. One foot of gravel bedding was used and compacted clay was used as embedment up to top of the trench. Properties of compacted clay were based on laboratory triaxial tests with secant Modulus of 1,300 psi. 8.5 psi of uniformly distributed load was applied at the top of the trench. Screenshots of the model and displacement results are illustrated in Figure 7.7, 7.8, and 7.9. Simulation of pilot model gave vertical pipe deflection of 0.22 in and horizontal pipe deflection of 0.19 inch.

## 7.4.2 Base Model

Since the deflection obtained from the pilot model was very less compared to the laboratory test results, a second model was run by decreasing the secant Modulus of the compacted soil by 50% to 650 psi. The strength properties were not changed. Screenshots of the displacement results are illustrated in Figure 7.10, and 7.11. Simulation of the second model gave vertical pipe deflection of 0.45 in and horizontal pipe deflection of 0.41 inch. Since these values are more comparable to the laboratory test results, this model is used as base model to compare results of other simulations.
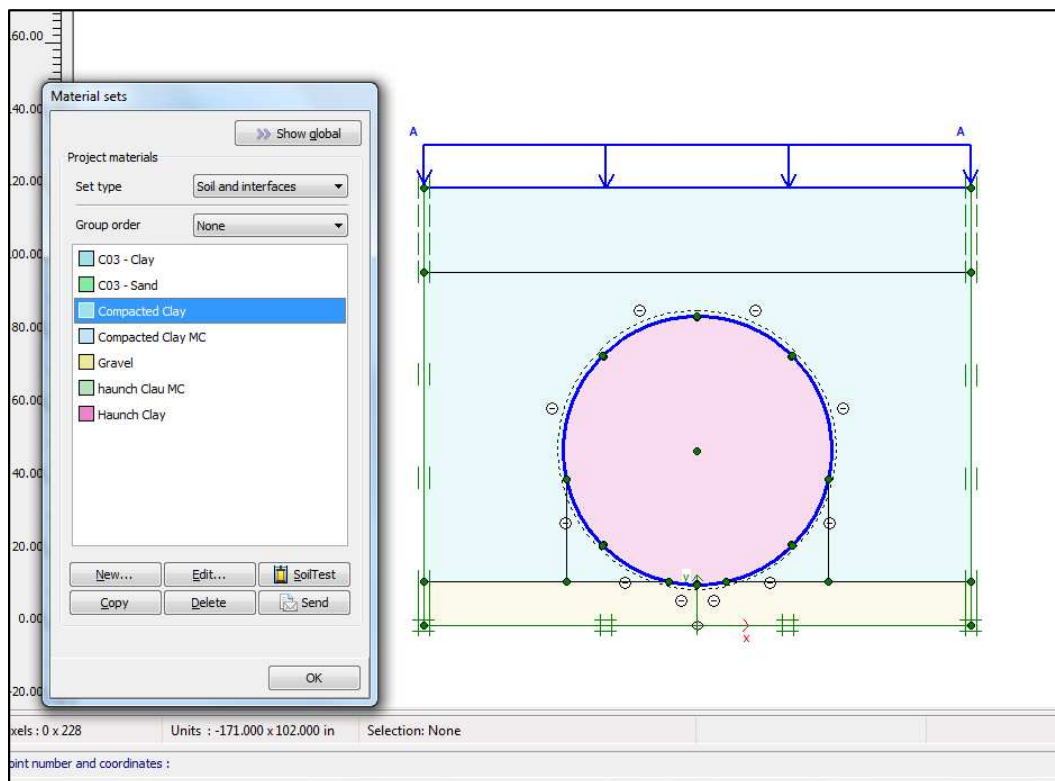


Figure 7.8: Pilot Finite Element Model
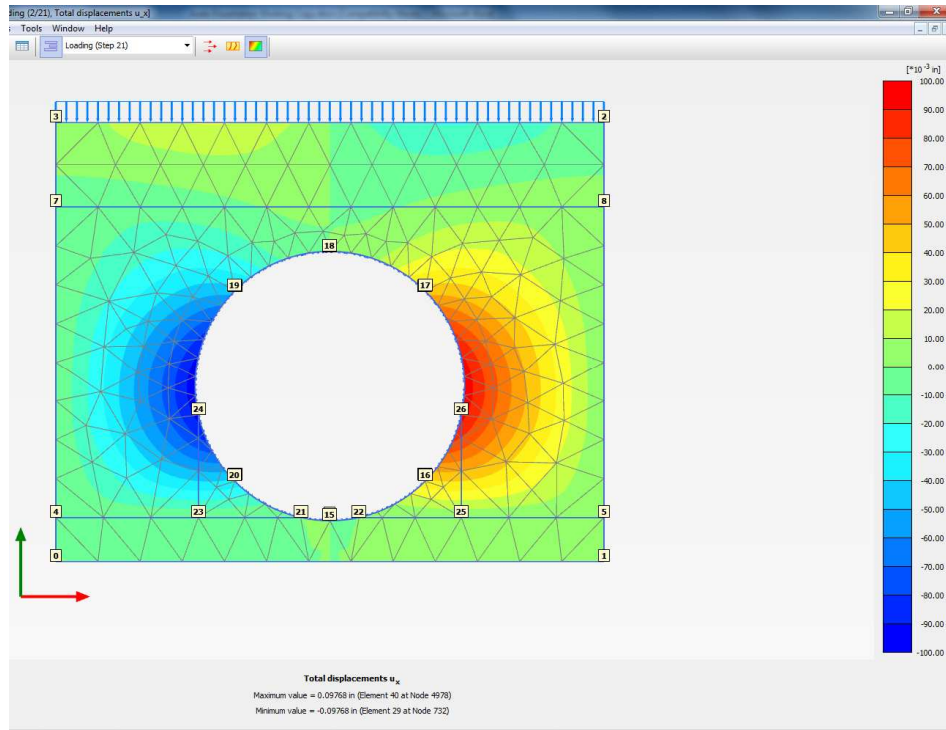
Figure 7.9: Horizontal Displacement in Pilot Model
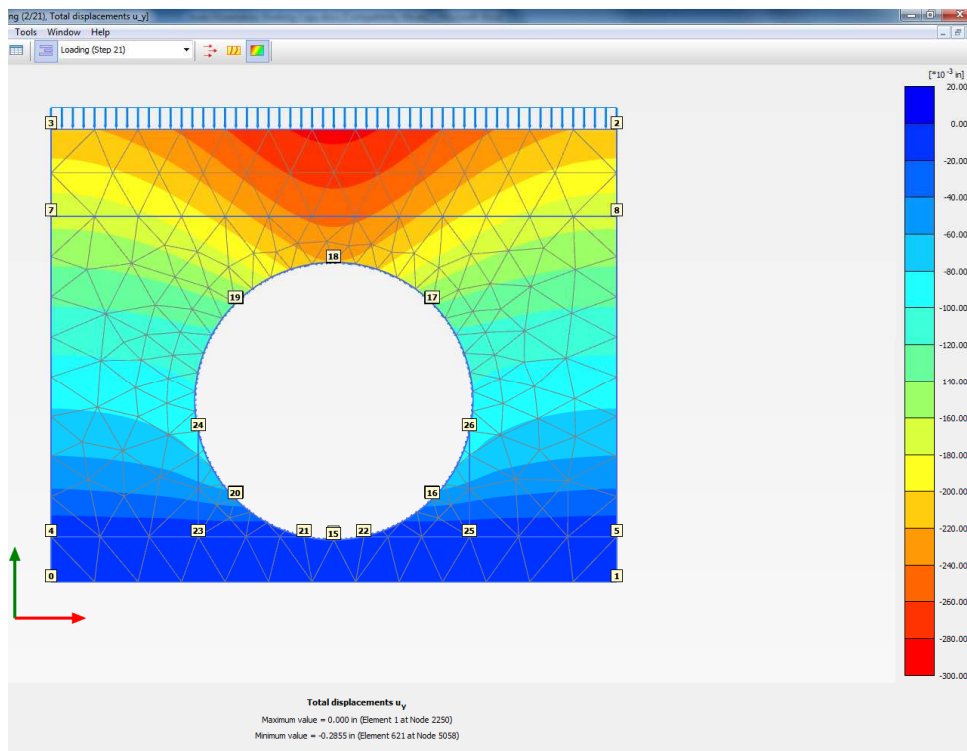


Figure 7.10: Vertical Displacement in Pilot Model
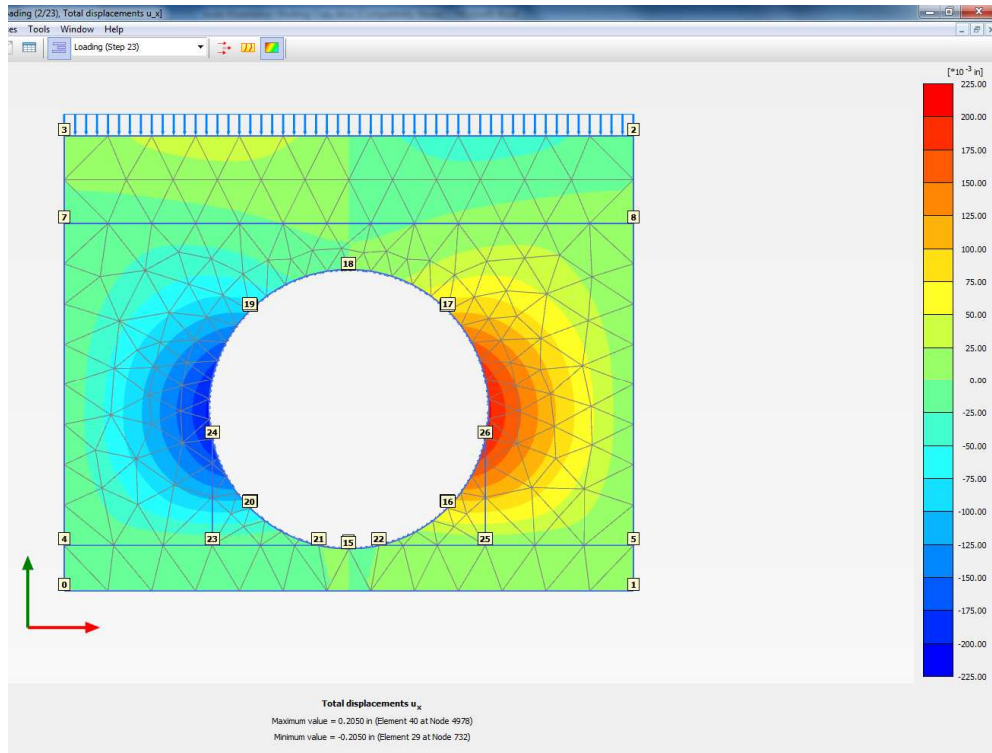
Figure 7.11: Horizontal Deflection of Base Model
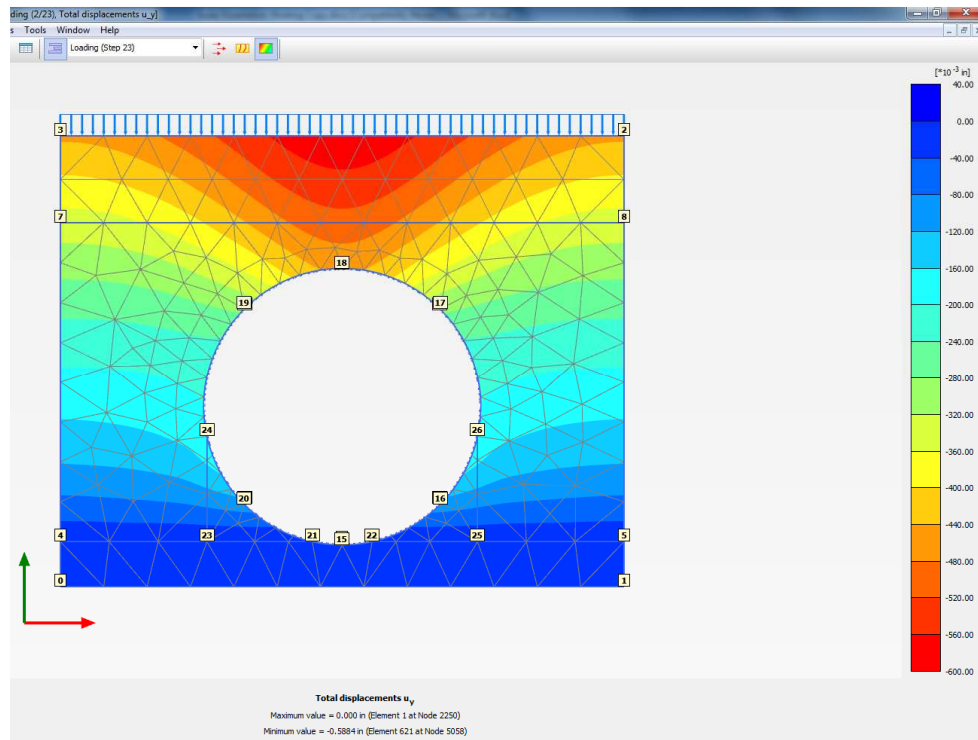


Figure 7.12: Vertical Deflection of Base Model

148

7.4.3 Sensitivity to Haunch Material Properties

Base model used same soil properties for the embedment and haunch material. The result was that the horizontal deflection of pipe was 91% of vertical deflection. During the tests, it was observed that horizontal deflection was as low as 30% of vertical deflection. In order to analyze the ratio between horizontal and vertical deflections, secant Modulus of elasticity of haunch material was reduced and models were run. Figure 7.13 illustrates the dimensions of haunch area used for this analysis. Table 7.2 provides the results of the analyses. Figure 7.13 illustrates correlation between elasticity ratio and deflection ratio. Figures 7.15 through 7.32 illustrate displacement results from these simulations.
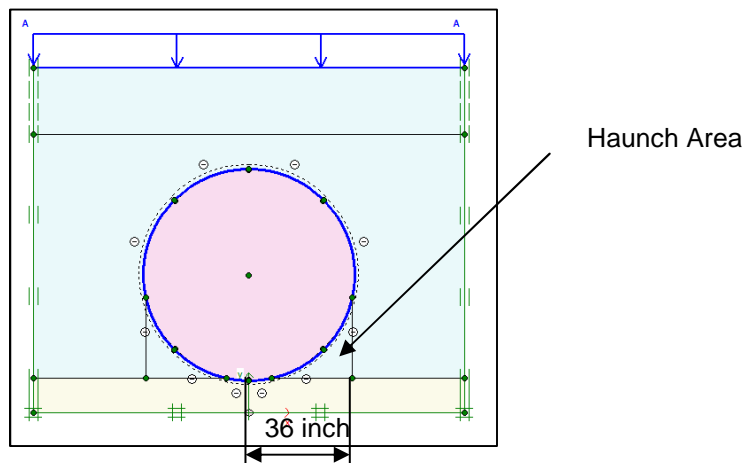


Figure 7.13: Haunch Area Dimension

Table 7.2: Deflections with Change in Haunch Material Properties

| Model No. | $E_{haunch}/E_{embedment}$ | Horizontal Deflection (in.) | Vertical Deflection (in.) | Deflection Ratio |
|-----------|-----------------------------|------------------------------|----------------------------|-------------------|
| Base | 1.0 | 0.41 | -0.45 | 0.91 |
| Model 1 | 0.9 | 0.41 | -0.48 | 0.85 |
| Model 2 | 0.8 | 0.40 | -0.48 | 0.83 |
| Model 3 | 0.7 | 0.40 | -0.49 | 0.82 |
| Model 4 | 0.6 | 0.39 | -0.50 | 0.78 |
| Model 5 | 0.5 | 0.38 | -0.51 | 0.75 |
| Model 6 | 0.4 | 0.37 | -0.52 | 0.71 |
| Model 7 | 0.3 | 0.35 | -0.54 | 0.65 |
| Model 8 | 0.2 | 0.34 | -0.58 | 0.59 |
| Model 9* | 0.2 | 0.18 | -0.28 | 0.64 |

* For model 9, secant Modulus of compacted clay was increased to 1300 psi in order to simulate

Test 1a conditions. The compaction for Test 1a was above 95% while that for Test 1 was 85-95%.
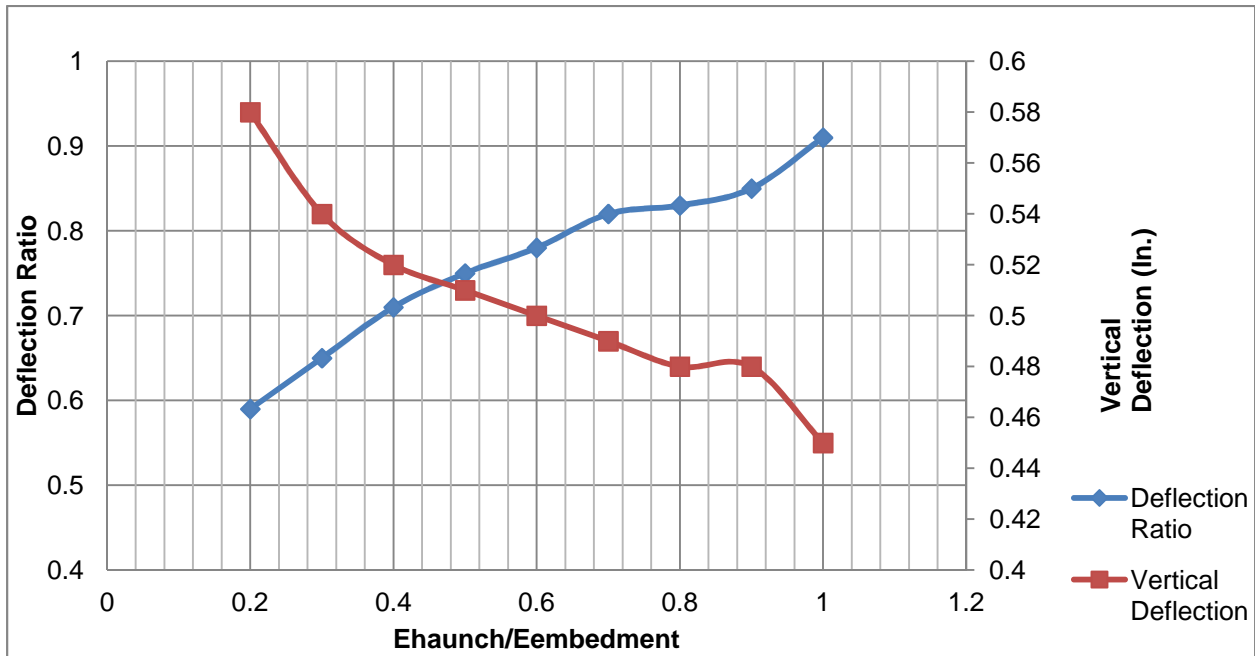
Figure 7.14: Plot of Elasticity Ratio versus Deflection Ratio
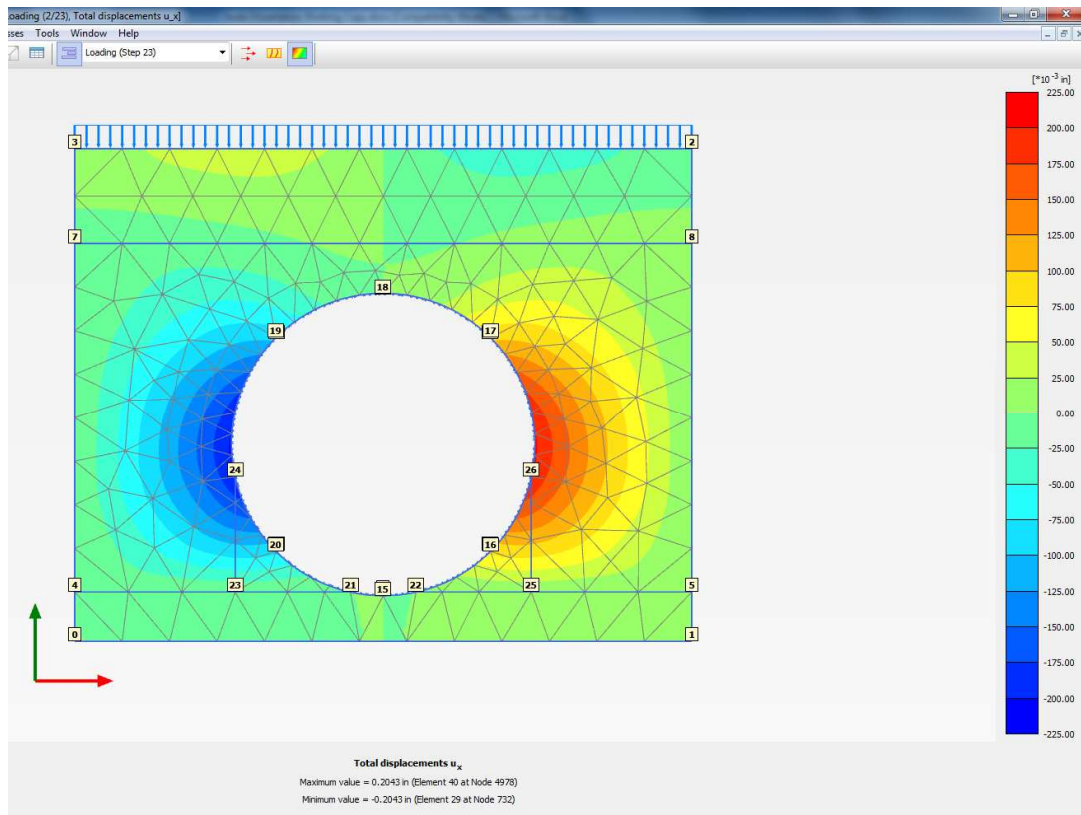


Figure 7.15: Horizontal Displacement Results: Model 1

150
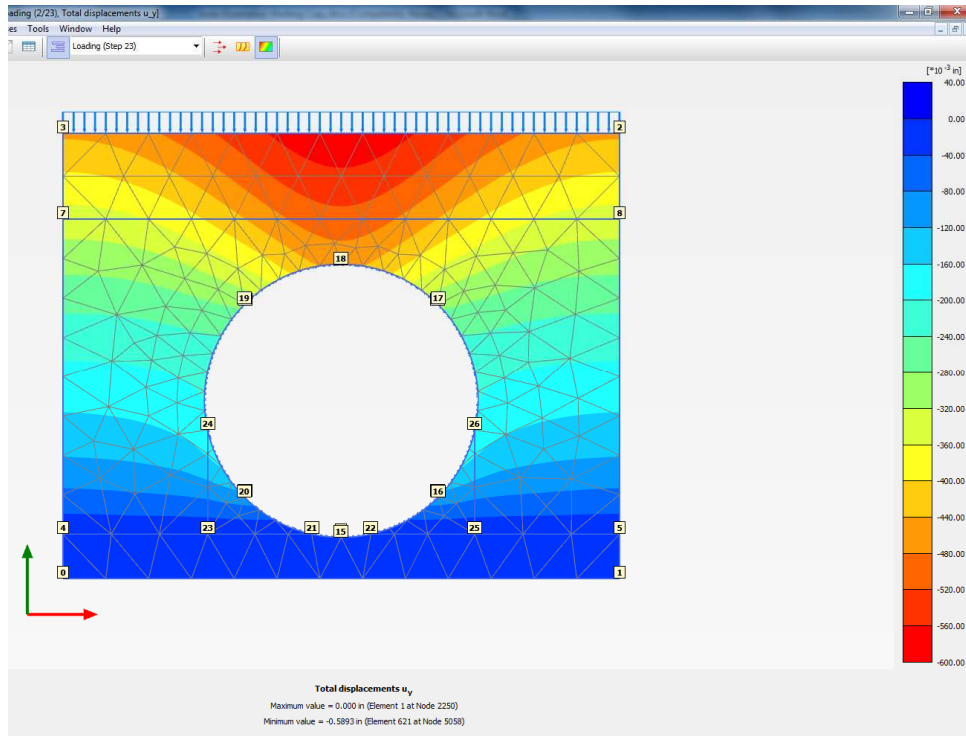
Figure 7.16: Vertical Displacement Results: Model 1
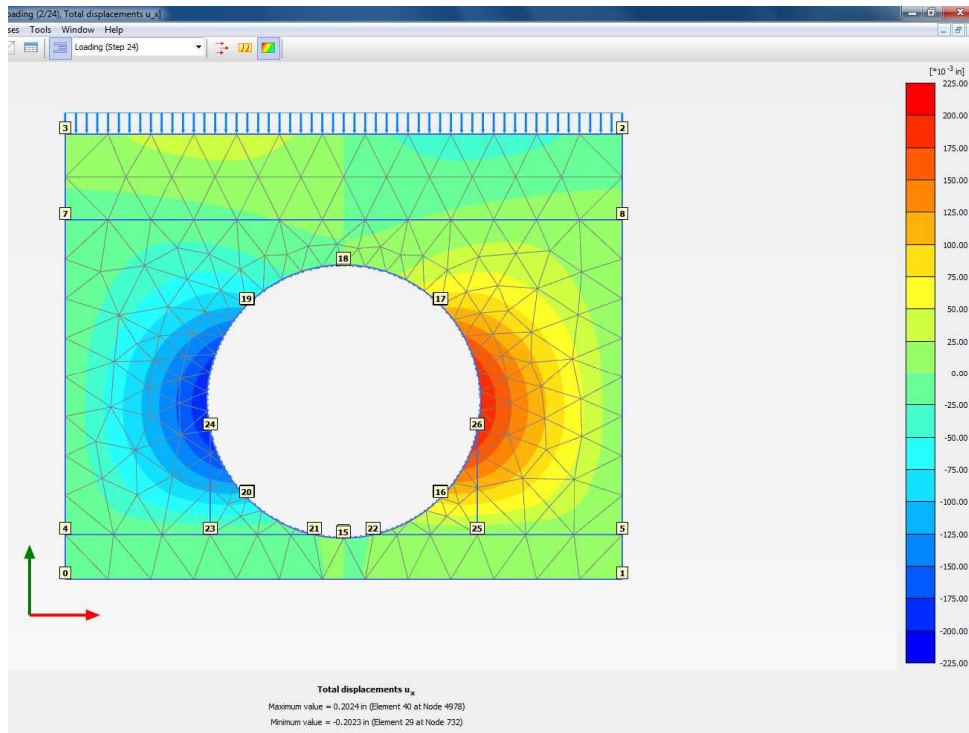


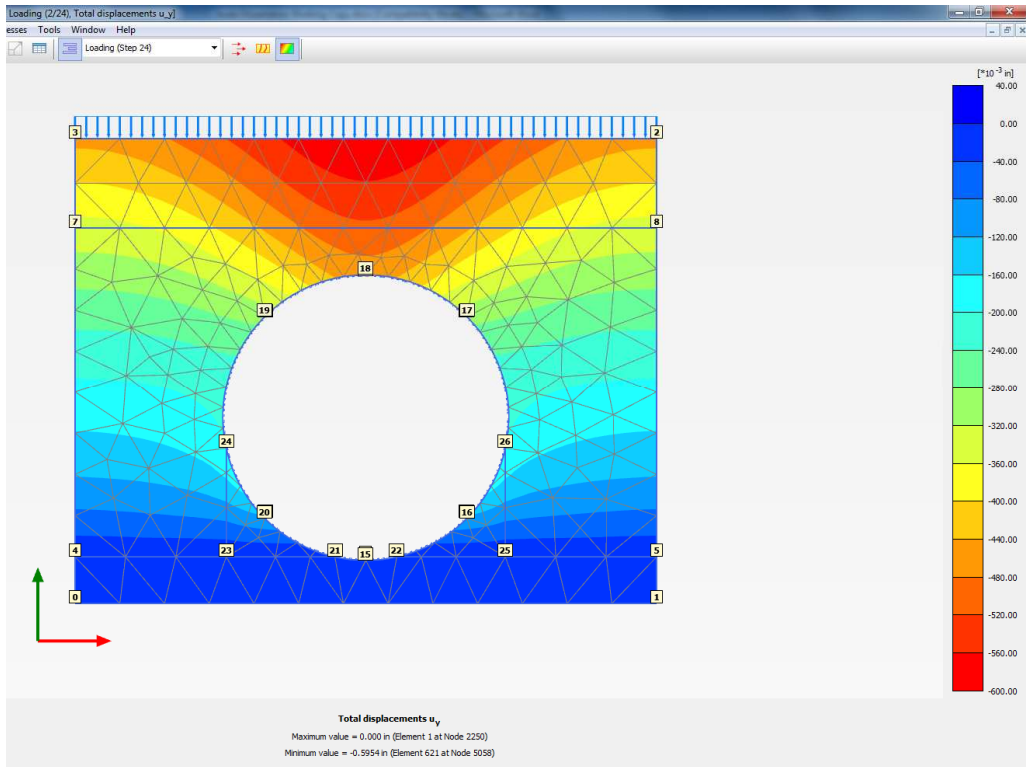Figure 7.17: Horizontal Displacement Results: Model 2

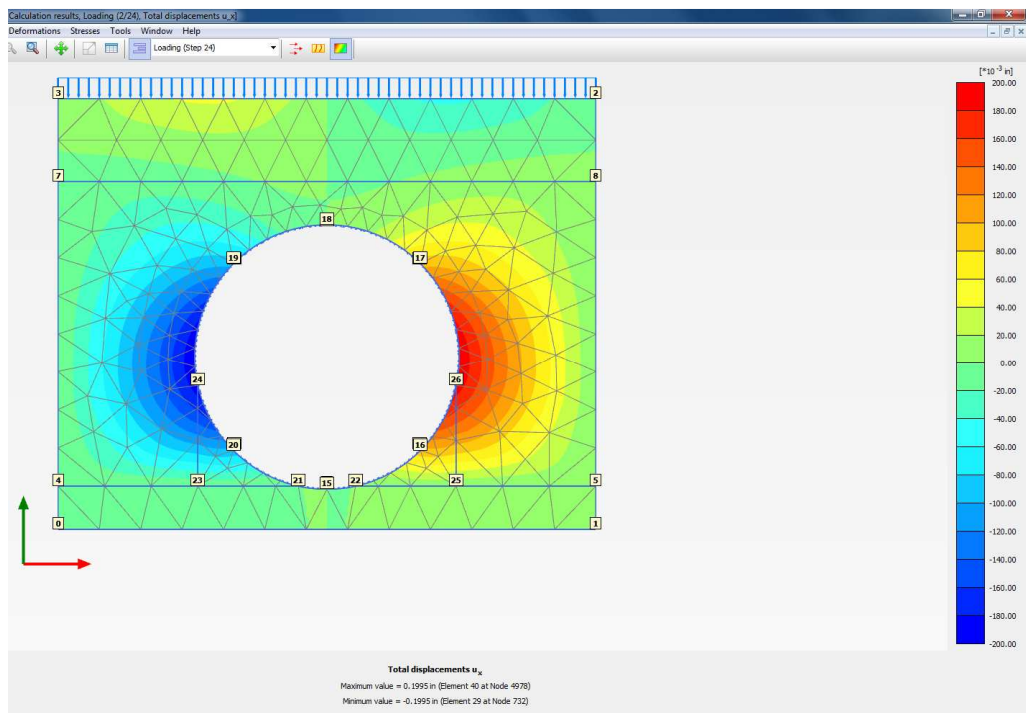Figure 7.18: Vertical Displacement Results: Model 2



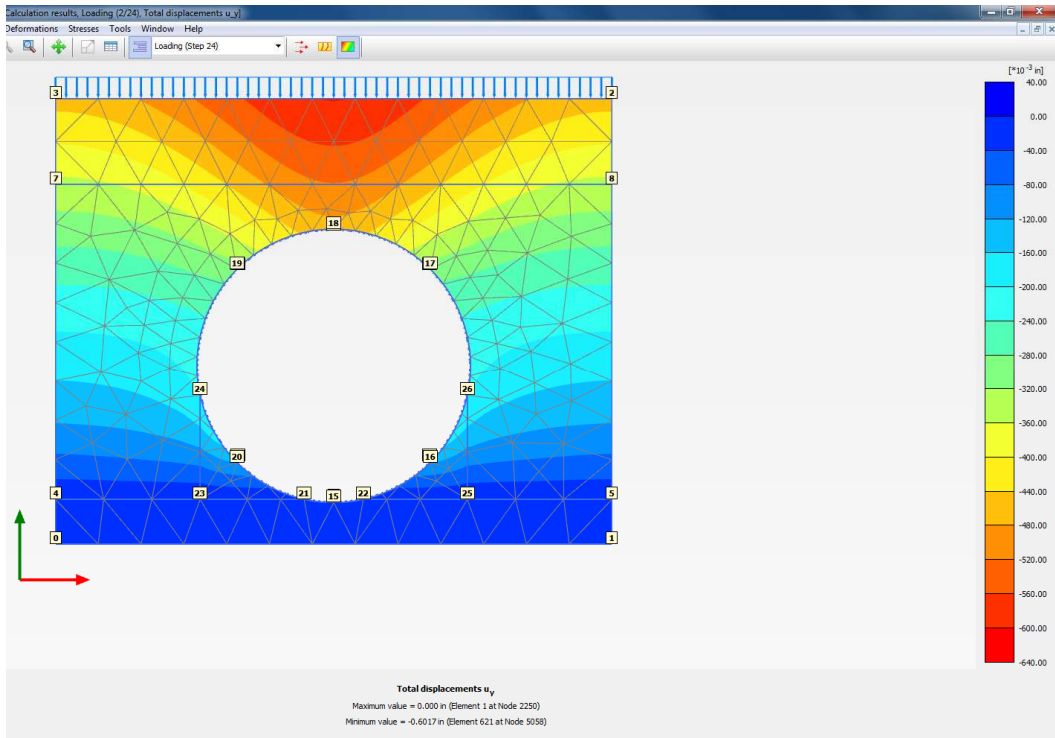Figure 7.19: Horizontal Displacement Results: Model 3

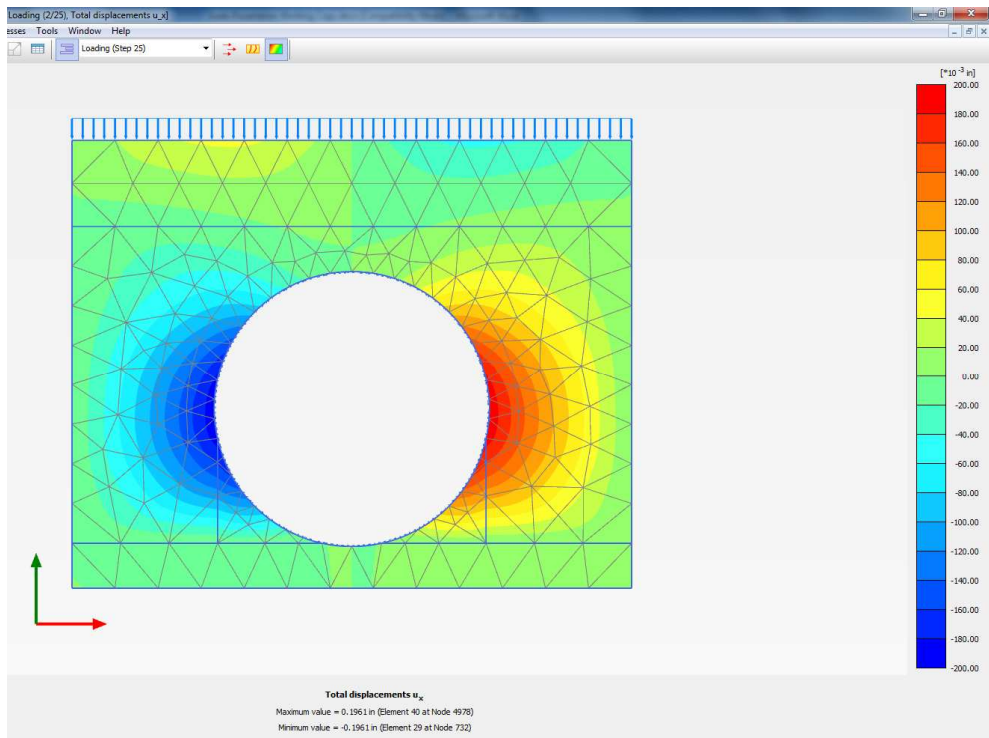Figure 7.20: Vertical Displacement Results: Model 3
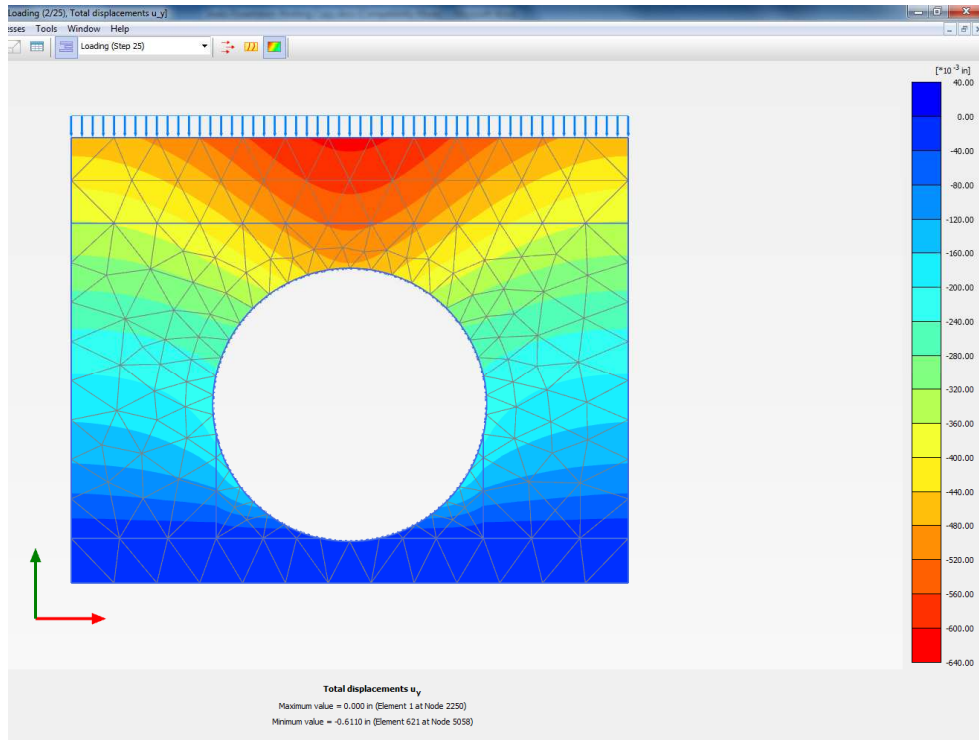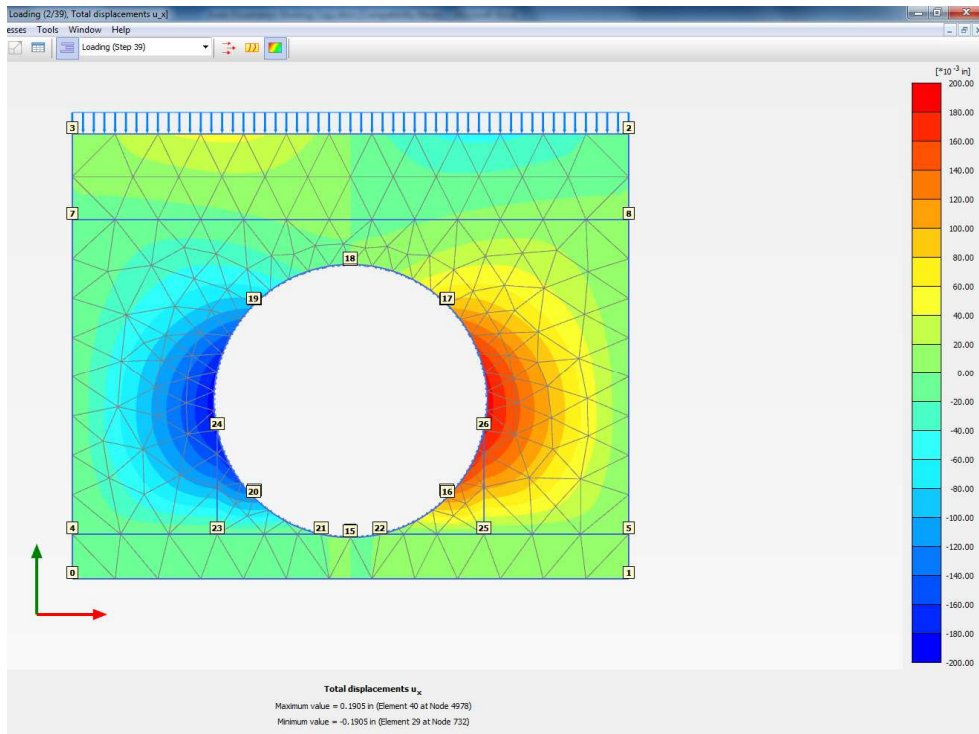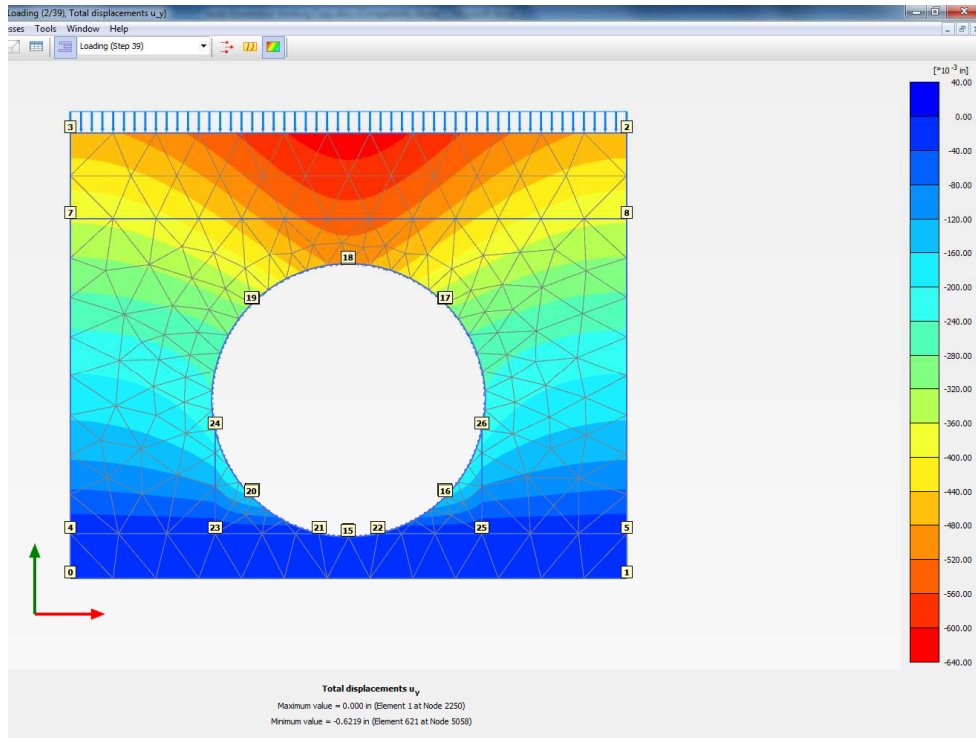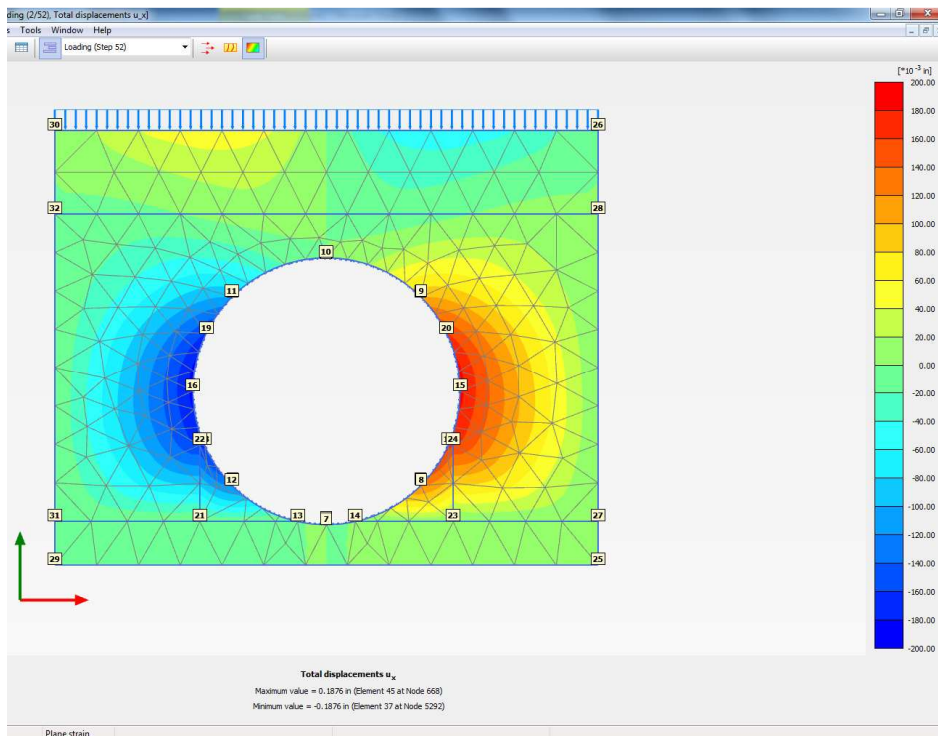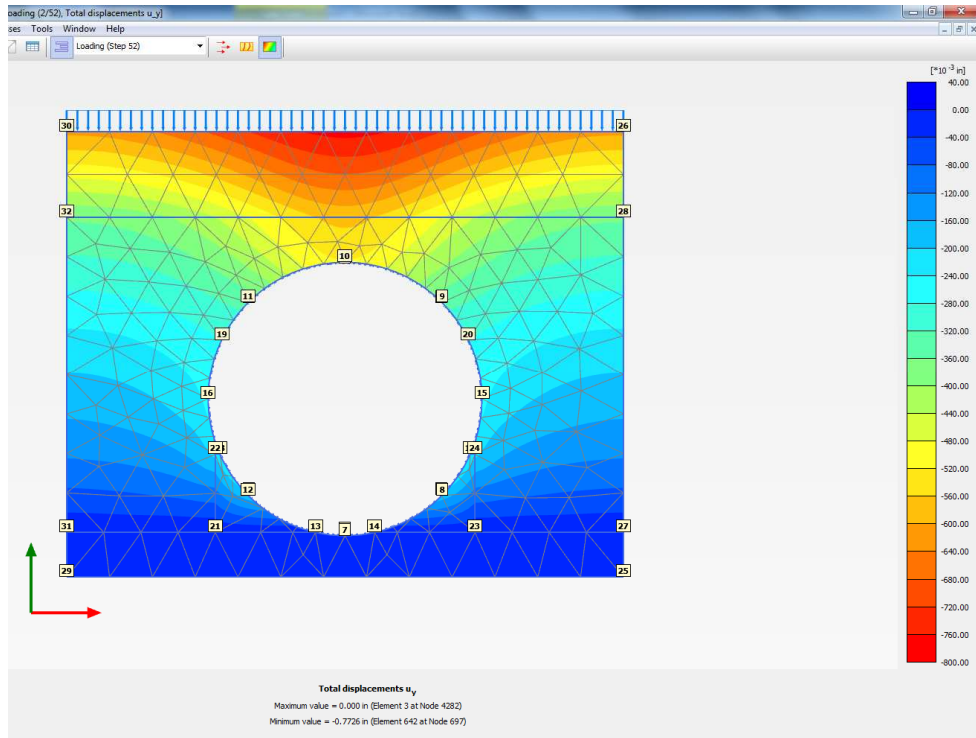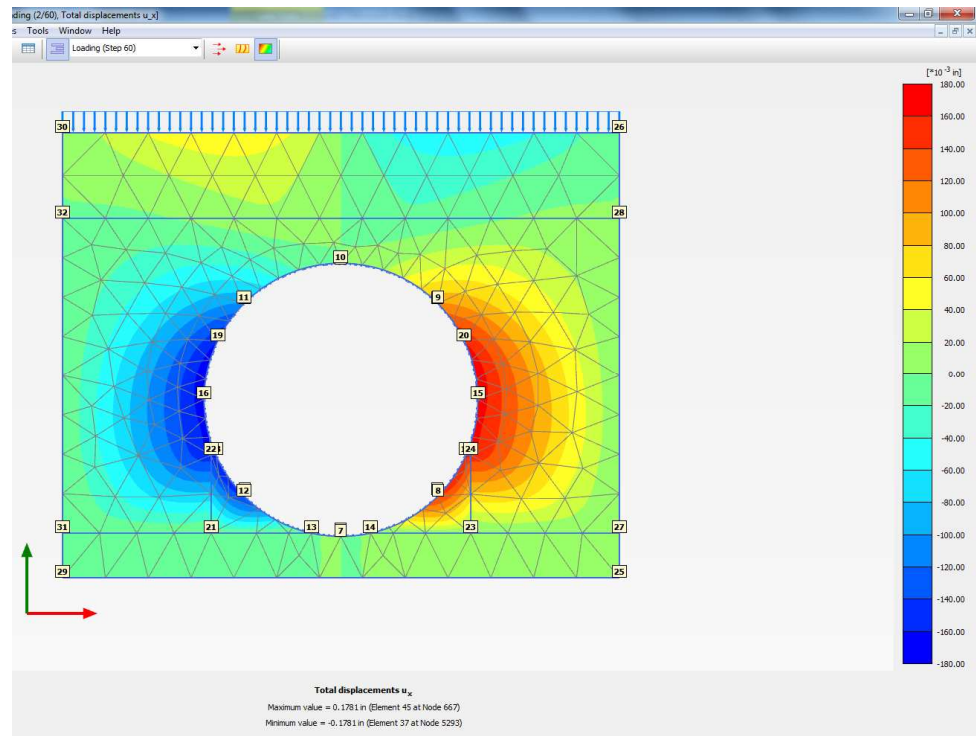


Figure 7.21: Horizontal Displacement Results: Model 4

153

Figure 7.22: Vertical Displacement Results: Model 4



Figure 7.23: Horizontal Displacement Results: Model 5

Figure 7.24: Vertical Displacement Results: Model 5



Figure 7.25: Horizontal Displacement Results: Model 6

Figure 7.26: Vertical Displacement Results: Model 6



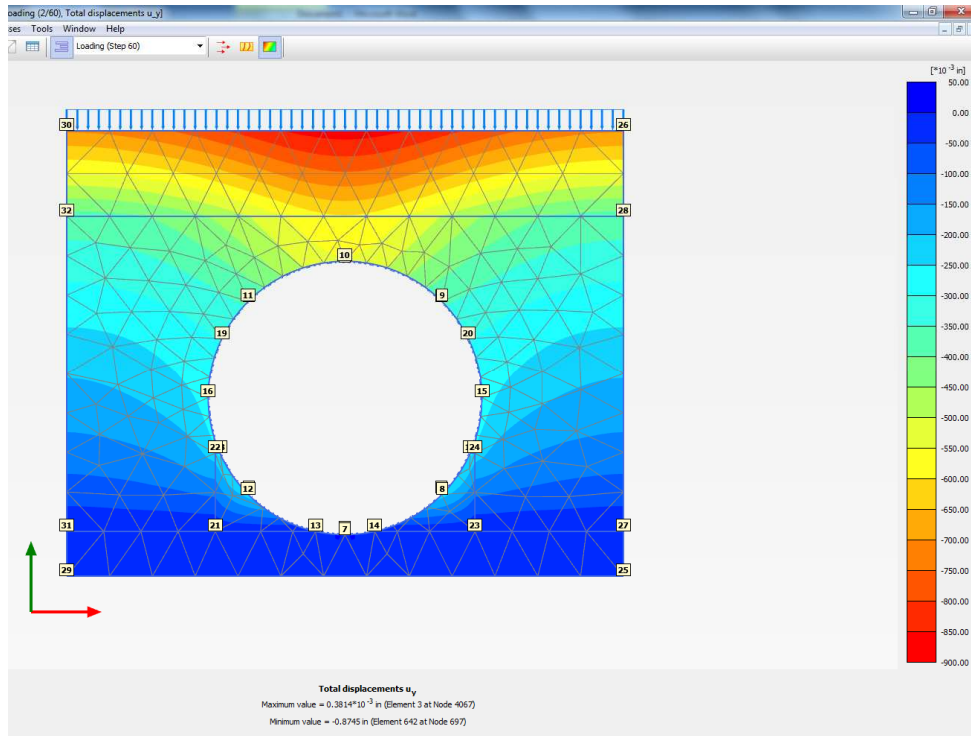Figure 7.27: Horizontal Displacement Results: Model 7

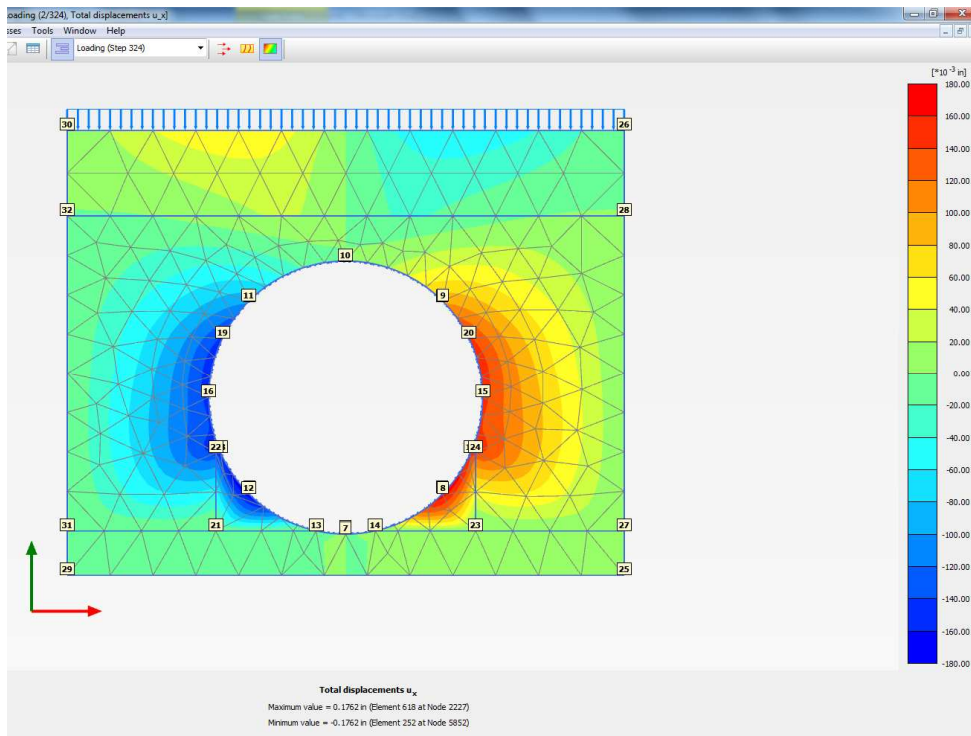Figure 7.28: Vertical Displacement Results: Model 7



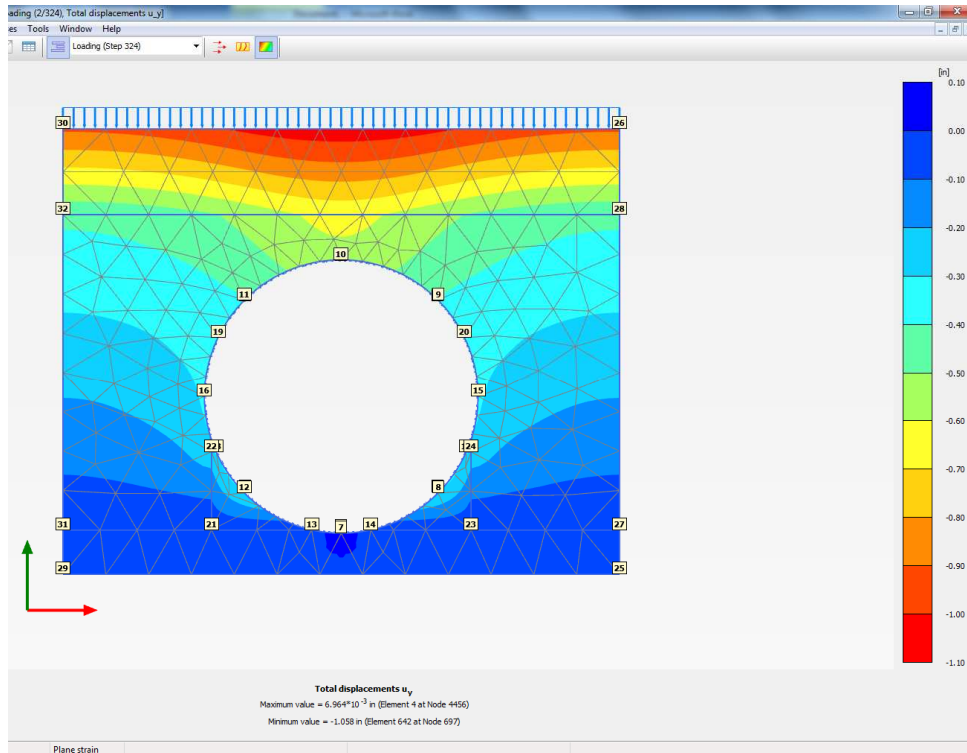Figure 7.29: Horizontal Displacement Results: Model 8

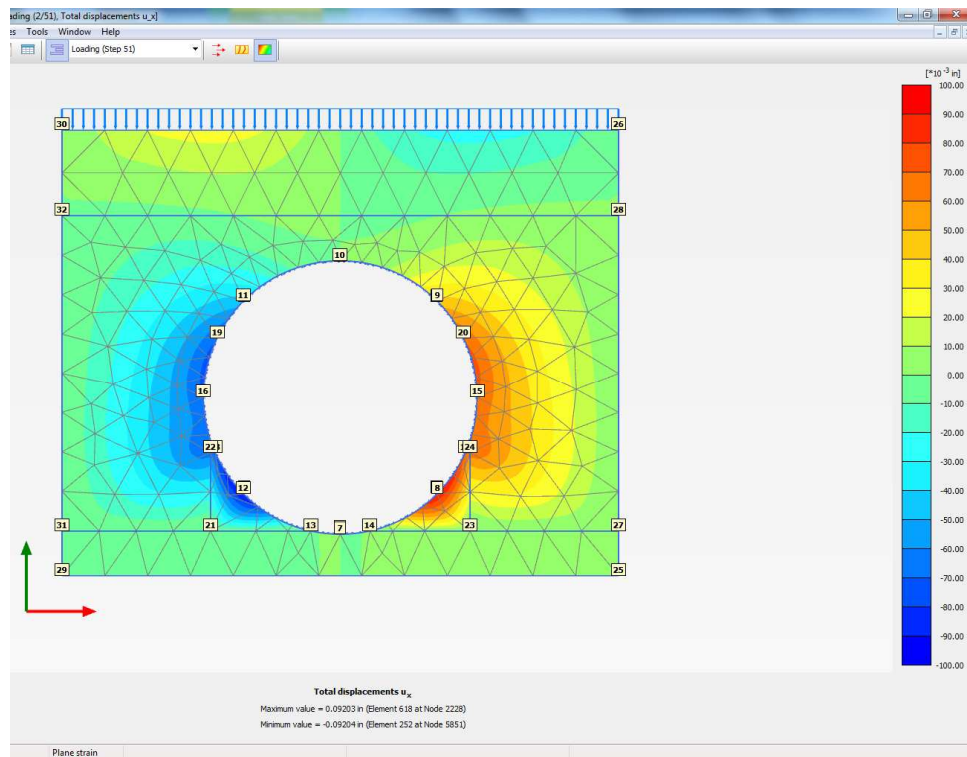Figure 7.30: Vertical Displacement Results: Model 8

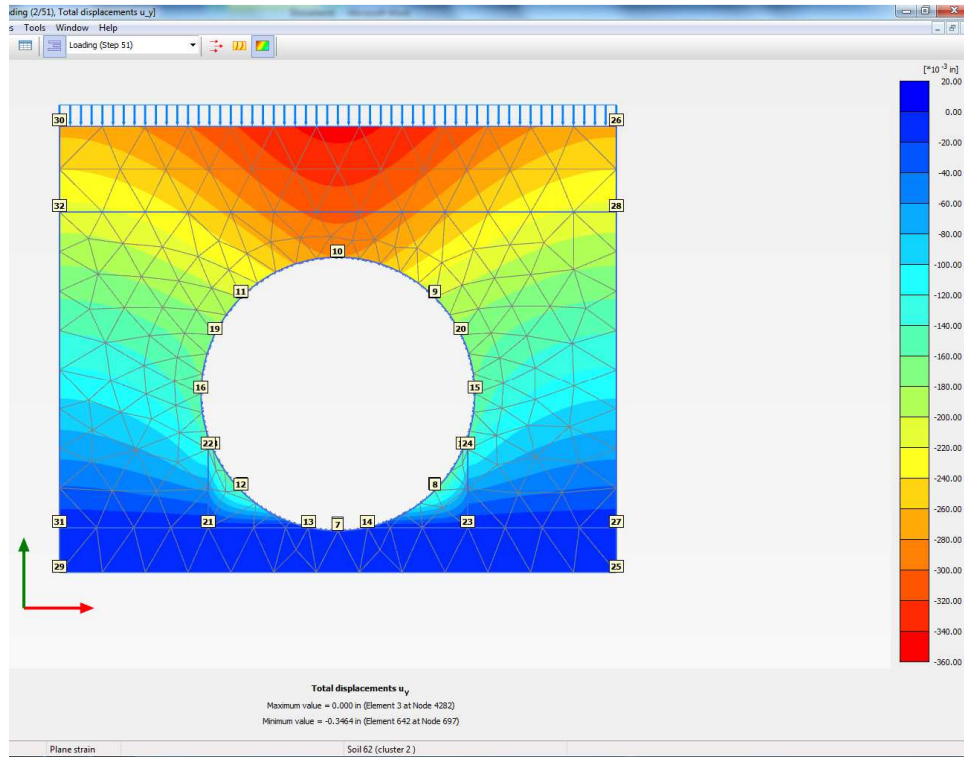Figure 7.31: Horizontal Displacement Results: Model 9



Figure 7.32: Vertical Displacement Results: Model 9

7.4.4 Sensitivity to Trench Wall Width

Two simulations were run by increasing the soil box width to see the effect of trench wall boundary conditions. The trench wall width for the laboratory tests was 12.5 feet. Simulations of the tests were run by changing the trench width to 14.5 feet and 16.5 feet. The results of these simulations are presented in Table 7.3. Figure 7.33 illustrates the effect of trench wall width on deflection ratio of the pipe. The screenshots of simulation deflection results are illustrated in Figures 7.34 through 7.39.

Table 7.3: Deflections with Change in Trench Wall Width

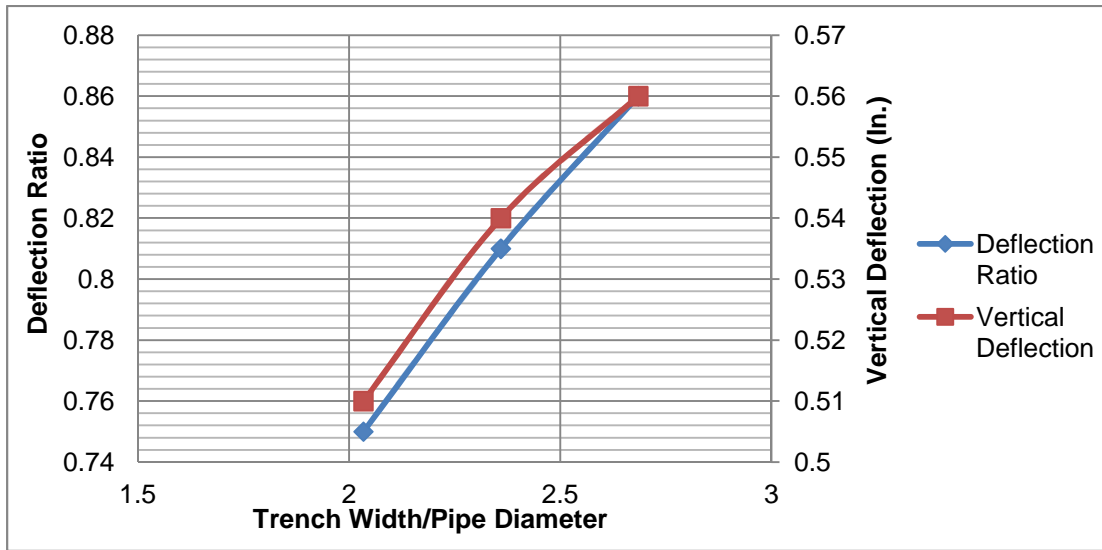| Model No. | $E_{haunch}/E_{embedment}$ | Trench Width (feet) | Horizontal Deflection (in.) | Vertical Deflection (in.) | Deflection Ratio |
|-----------|---------------------------|---------------------|-----------------------------|---------------------------|------------------|
| Model 5 | 0.5 | 12.5 | 0.38 | -0.51 | 0.75 |
| Model 10 | 0.5 | 14.5 | 0.44 | -0.54 | 0.81 |
| Model 11 | 0.5 | 16.5 | 0.48 | -0.56 | 0.86 |

Figure 7.33: Effect of Trench Wall Width on Deflection Ratio



Figure 7.34: Model 10 with 14.5 feet Wide Trench

Figure 7.35: Horizontal Displacement Results: Model 10



Figure 7.36: Vertical Displacement Results: Model 10
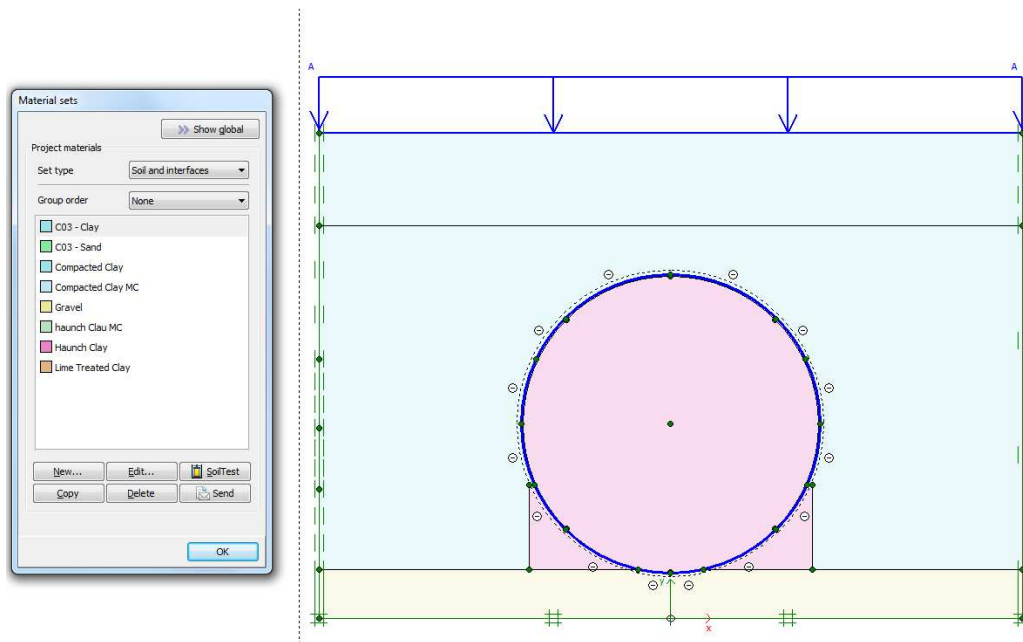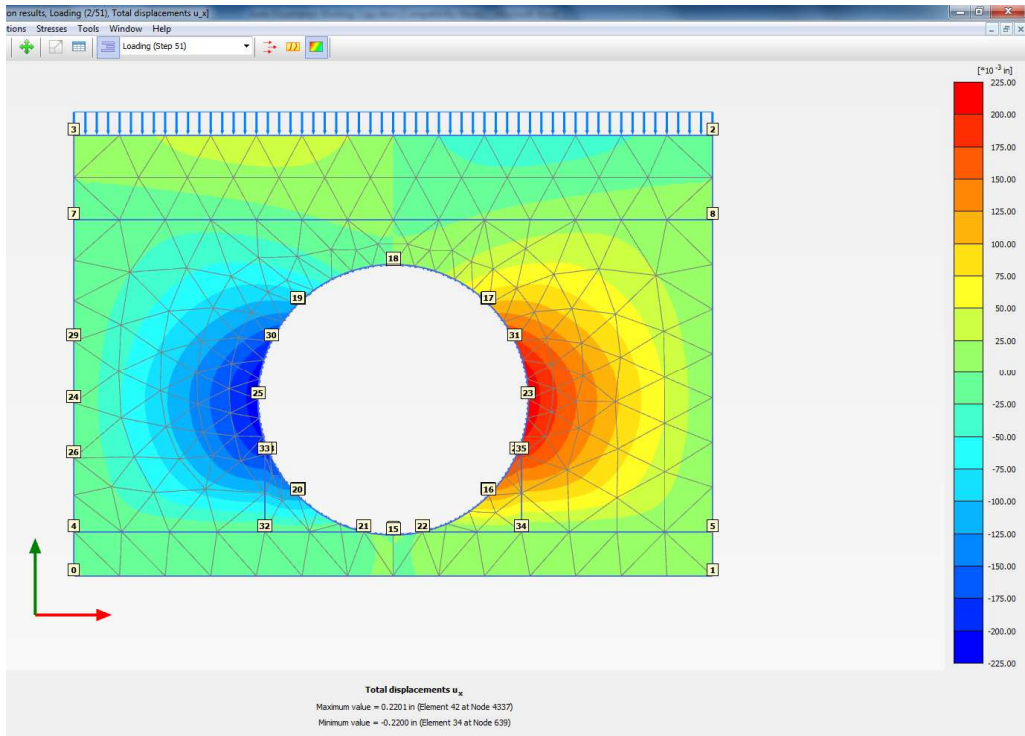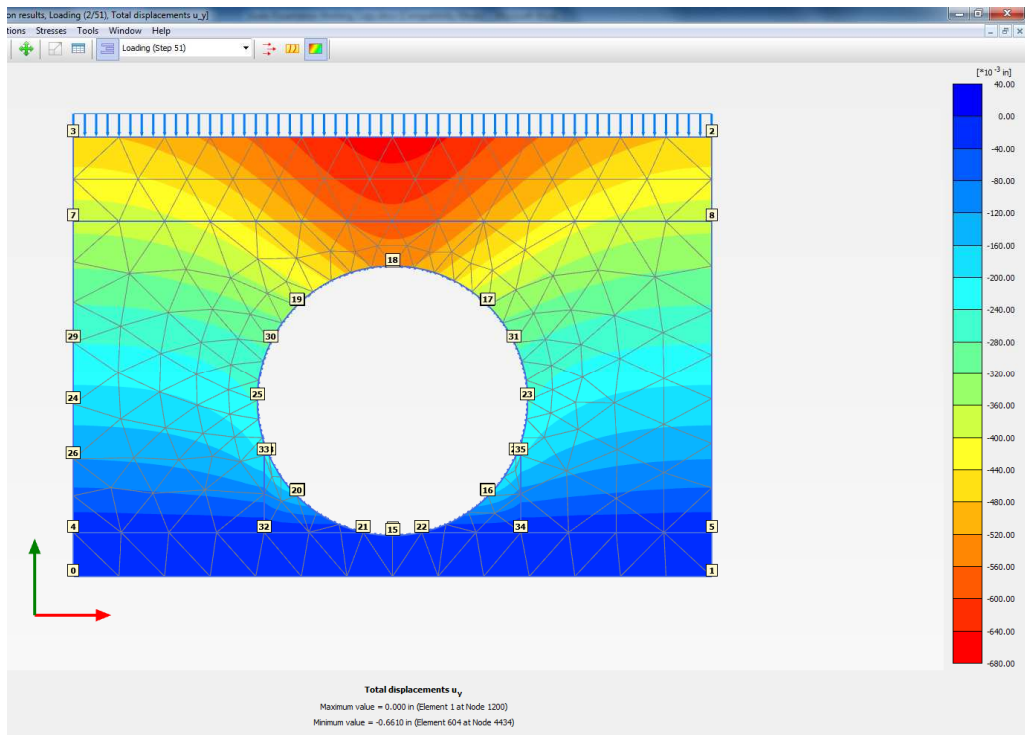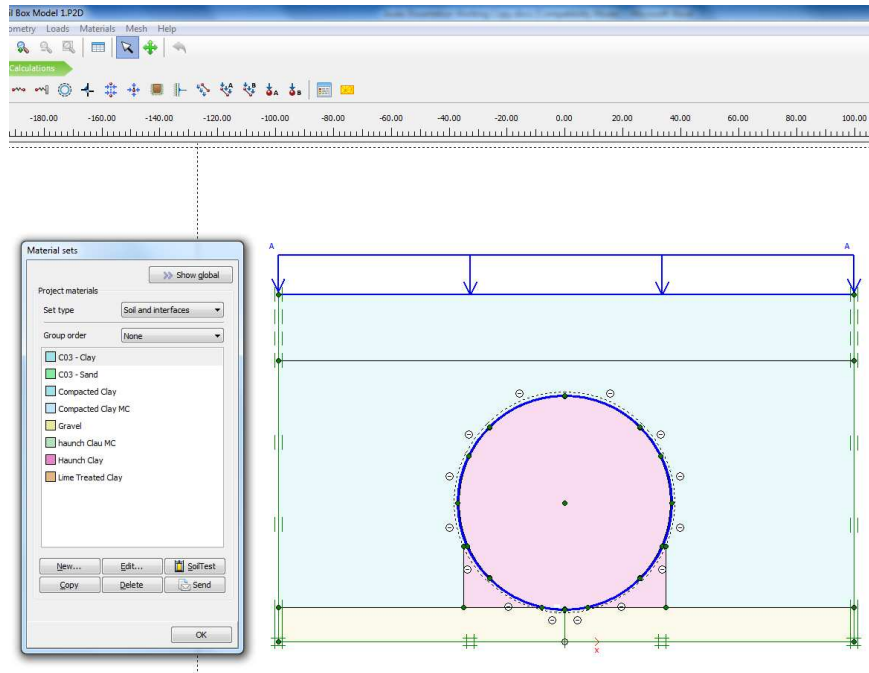
161

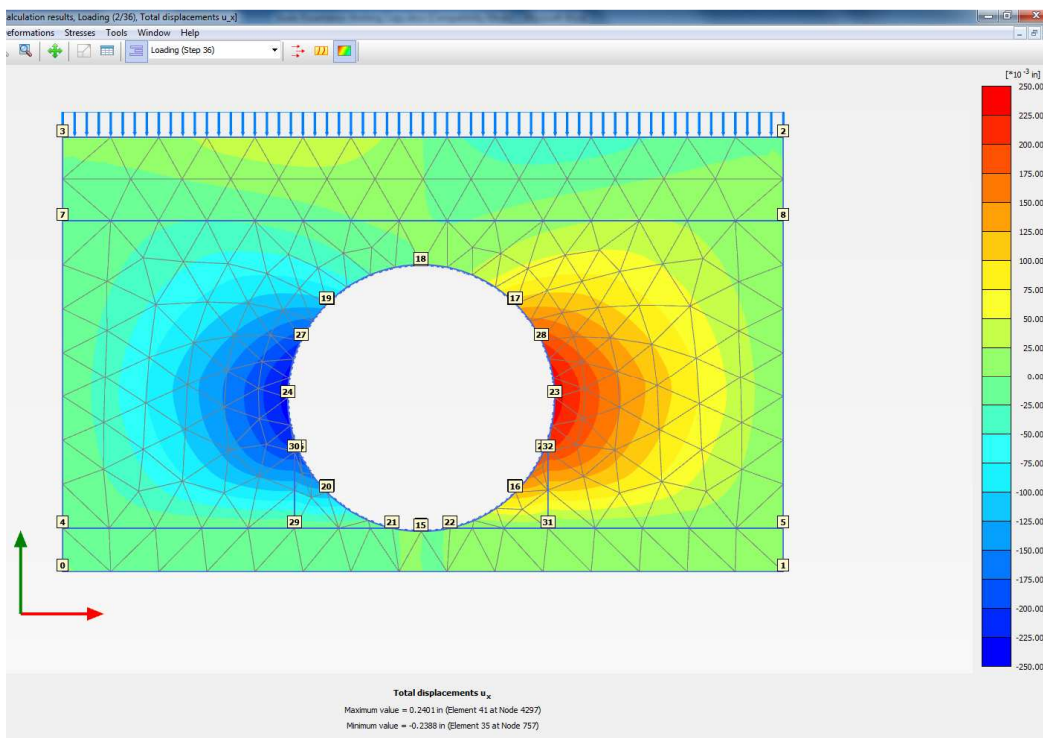Figure 7.37: Model 11 with 16.5 feet Wide Trench



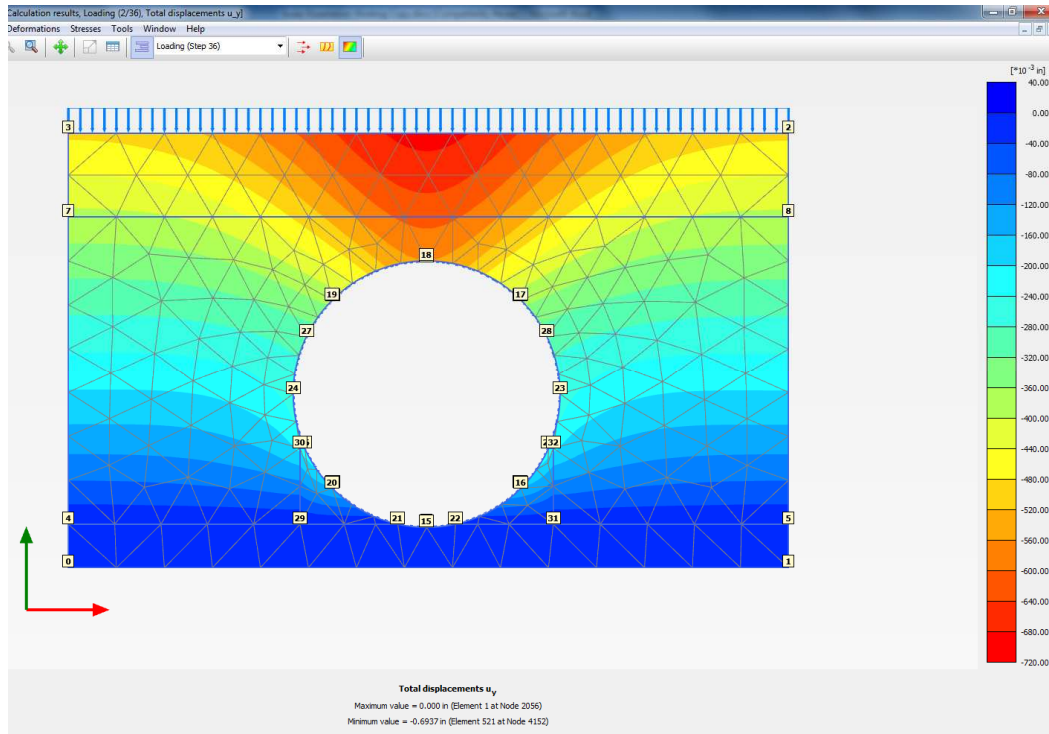Figure 7.38: Horizontal Displacement Results: Model 11

Figure 7.39: Vertical Displacement Results: Model 11

7.4.5 Haunch Area Width

The length of haunch area used for previous analyses was 36 inches on either side (72 inches total) as shown in Figure 7.13. Further analyses was run with haunch area length reduced to 33 inch, 30 inch, 27 inch, 24 inch, and 21 inch. The results of these analyses are presented in Table 7.4 and illustrated in Figure 7.40. The screenshots of simulation deflection results are illustrated in Figures 7.41 through 7.50.

Table 7.4: Deflections with Change in Haunch Width

| Model No. | $E_{haunch}/E_{embedment}$ | Haunch Width (in.) | Horizontal Deflection (in.) | Vertical Deflection (in.) | Deflection Ratio |
|-----------|------|------|------|------|------|
| Model 5 | 0.5 | 72 | 0.38 | -0.51 | 0.75 |
| Model 12 | 0.5 | 66 | 0.38 | -0.49 | 0.78 |
| Model 13 | 0.5 | 60 | 0.39 | -0.48 | 0.81 |
| Model 14 | 0.5 | 54 | 0.39 | -0.47 | 0.83 |
| Model 15 | 0.5 | 48 | 0.40 | -0.46 | 0.87 |
| Model 16 | 0.5 | 42 | 0.40 | -0.45 | 0.89 |
| Base | 1 | 0 | 0.41 | -0.45 | 0.91 |
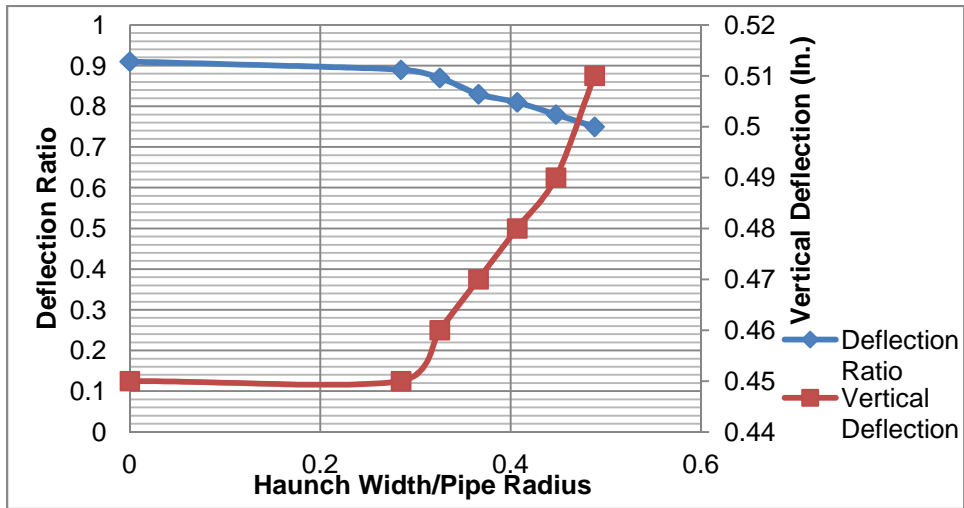
Figure 7.40: Influence of Haunch Width on Deflection



Figure 7.41: Horizontal Displacement Results: Model 12

Figure 7.42: Vertical Displacement Results: Model 12



Figure 7.43: Horizontal Displacement Results: Model 13

Figure 7.44: Horizontal Displacement Results: Model 13



Figure 7.45: Horizontal Displacement Results: Model 14
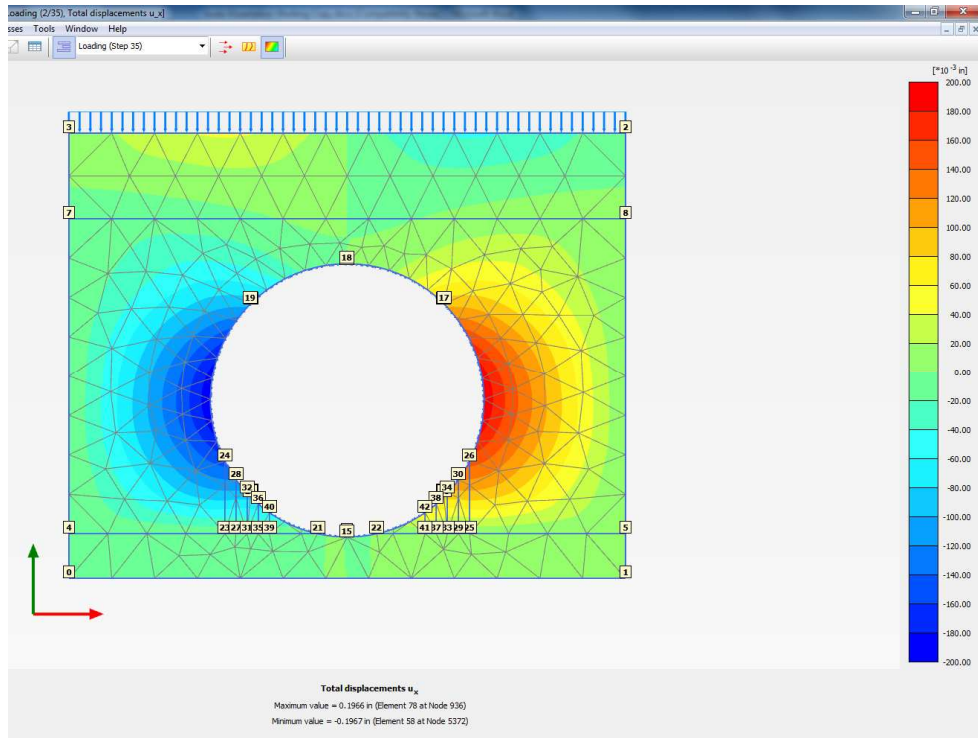
Figure 7.46: Vertical Displacement Results: Model 14



Figure 7.47: Horizontal Displacement Results: Model 15
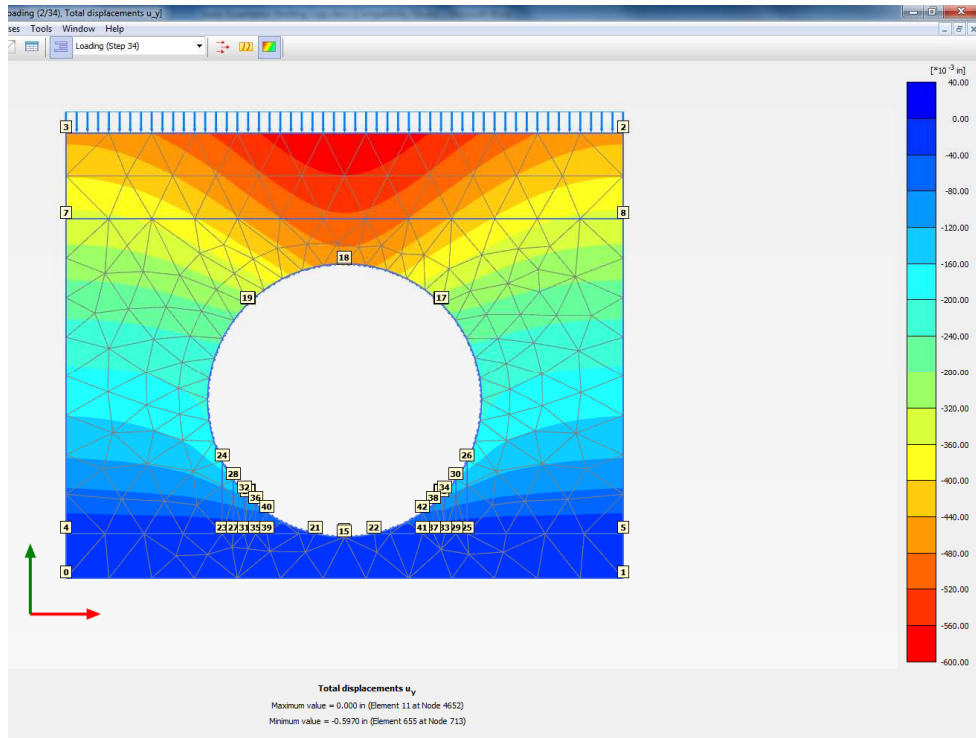
Figure 7.48: Vertical Displacement Results: Model 15
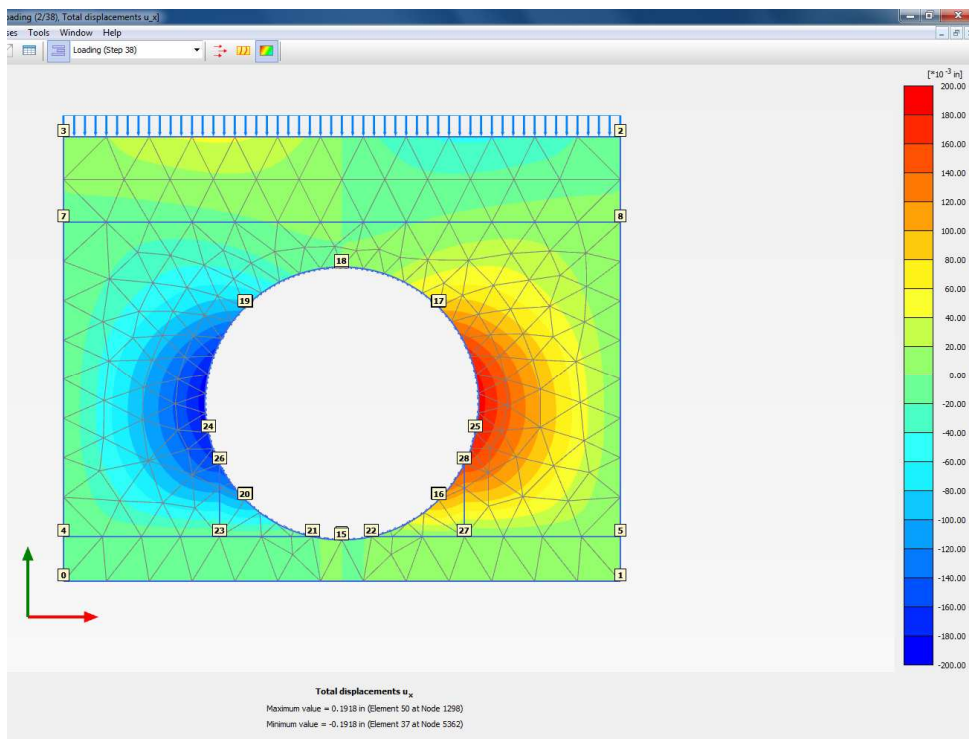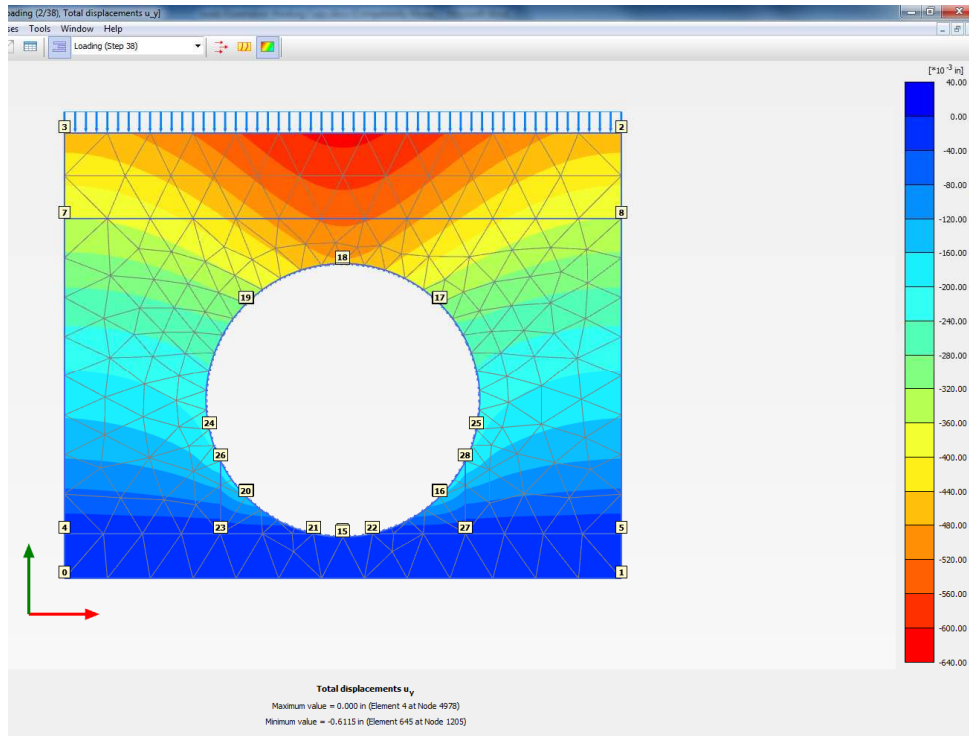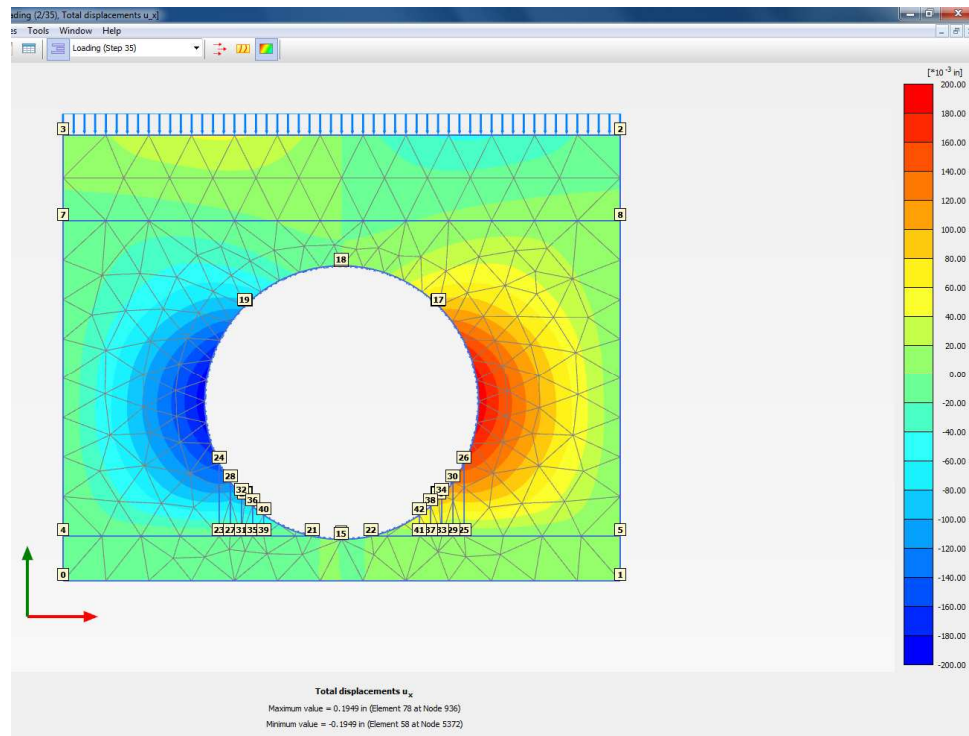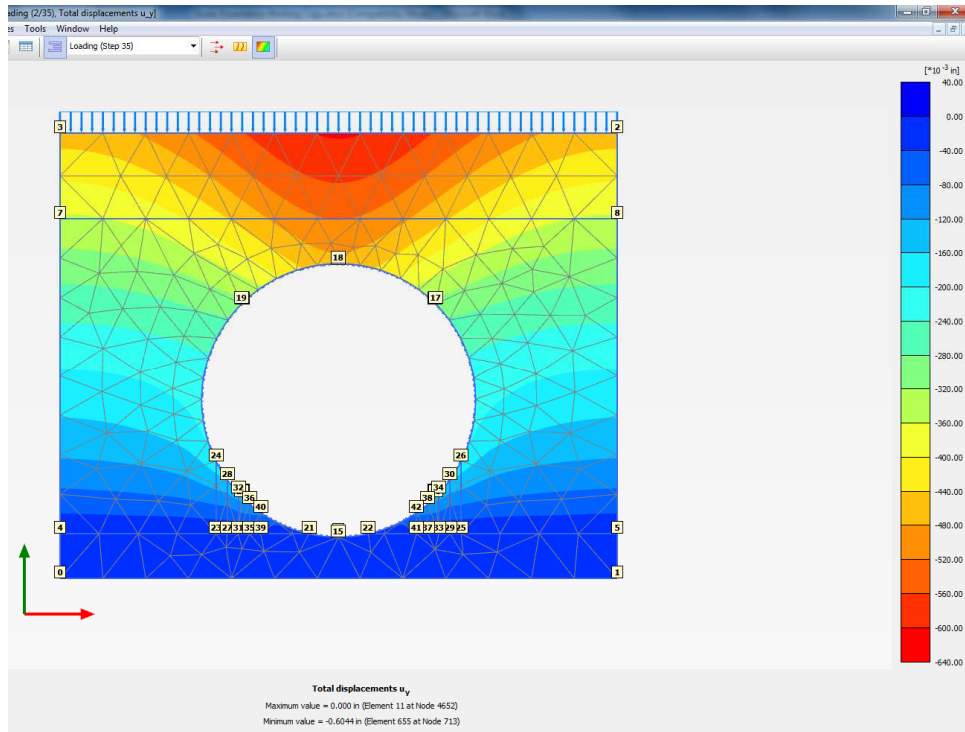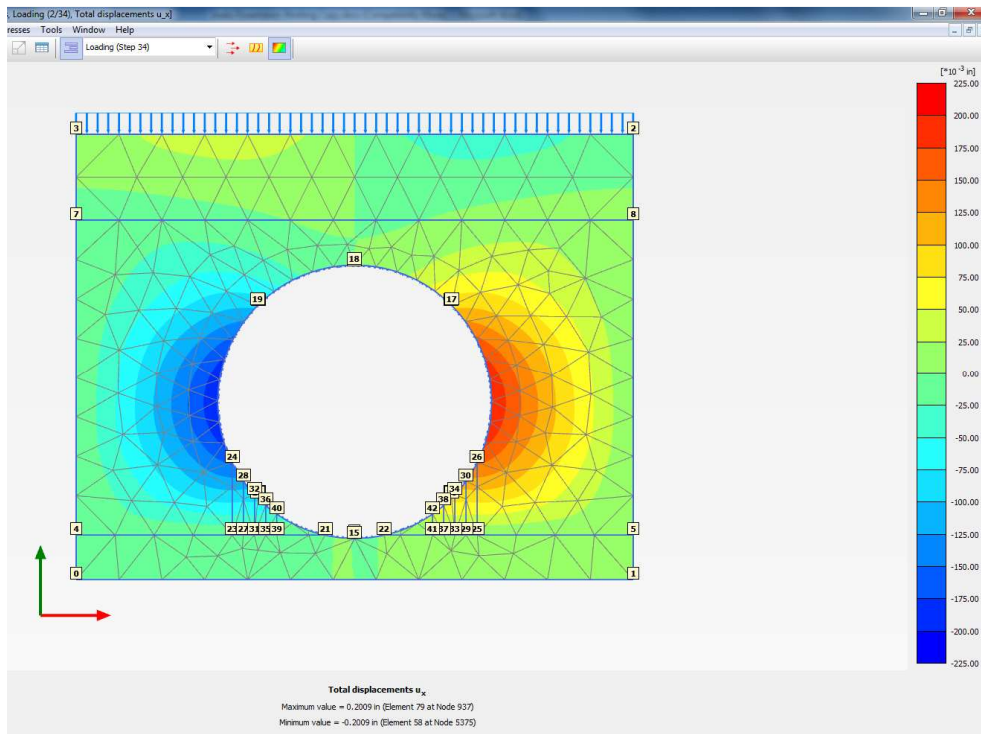


Figure 7.49: Horizontal Displacement Results: Model 16
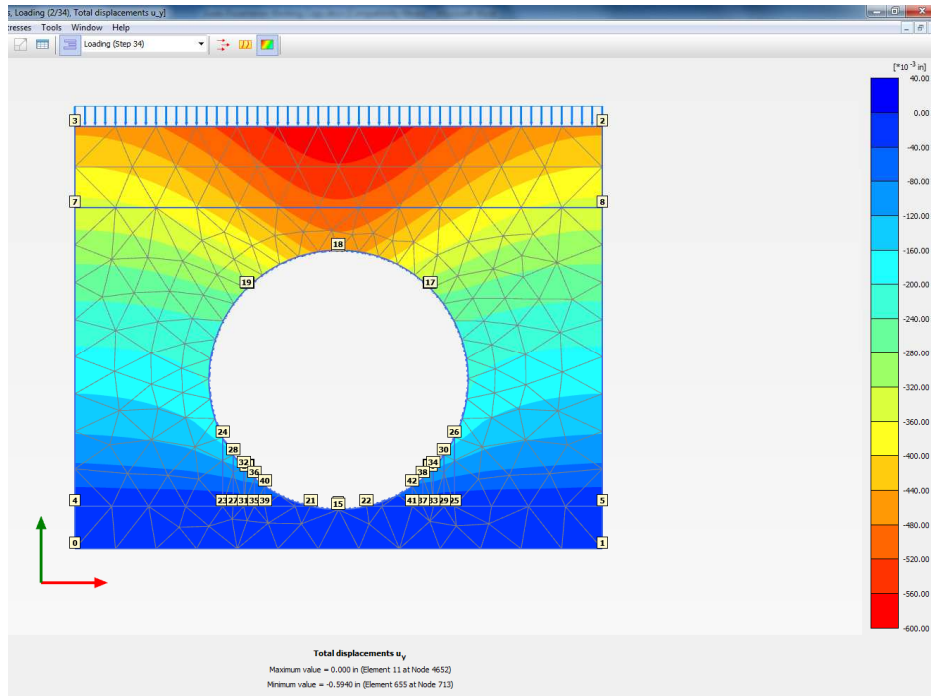
Figure 7.50: Vertical Displacement Results: Model 16

7.4.6 Test 2 Simulation

Test 2 was simulated through the model as shown in Figure 7.51. Properties of lime treated clay obtained from the laboratory test were used for embedment soil up to springline of the pipe. The screenshots of displacement results are illustrated in Figure 7.52 and 7.53. The results obtained were 0.32 inch deflection of horizontal diameter and -0.35 inch deflection of vertical diameter. The actual results from the tests were 0.13 inch maximum deflection of horizontal diameter and -0.35 inch minimum deflection of vertical diameter. Further analyses were also carried out by changing the depth of lime treated soil, and using weaker soil on haunch areas. The results are presented in Table 7.5 and the illustrations of results are presented in Figures 7.54 through 7.71.

Model 22 gave the result very comparable to the actual laboratory test. Assuming that the haunch soil was not properly mixed and compacted because of the site constraints, haunch secant Modulus was taken as 10% of the lime treated and 20% of the compacted untreated soil.

Table 7.5: Deflections for Lime Treated Soil

| Model No. | $E_{haunch}/E_{limesoil}$ | Depth of Lime Treated Embedment (in.) | Horizontal Deflection (in.) | Vertical Deflection (in.) | Deflection Ratio |
|---|---|---|---|---|---|
| Test 2 | 1 | 36 | 0.32 | -0.35 | 0.91 |
| Model 13 | 0.5 | 36 | 0.31 | -0.36 | 0.86 |
| Model 14 | 1 | 22 | 0.39 | -0.42 | 0.93 |
| Model 15 | 0.5 | 22 | 0.37 | -0.44 | 0.84 |
| Model 16 | 1 | 50 | 0.25 | -0.32 | 0.78 |
| Model 17 | 0.5 | 50 | 0.24 | -0.37 | 0.65 |
| Model 22* | 0.1 | 36 | 0.12 | -0.32 | 0.38 |
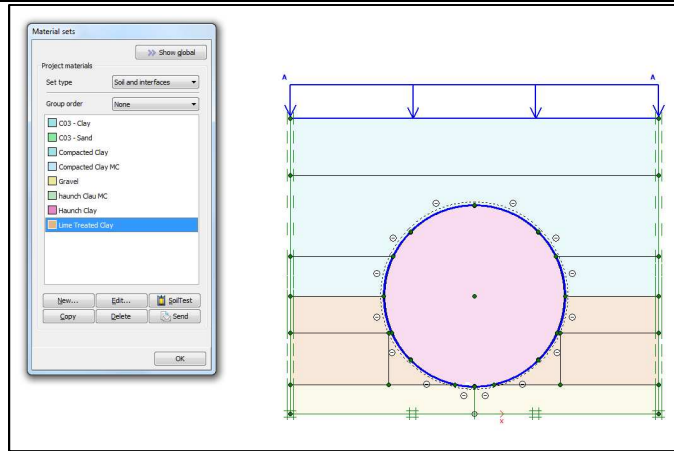


Figure 7.51: Model for Test 2 Simulation
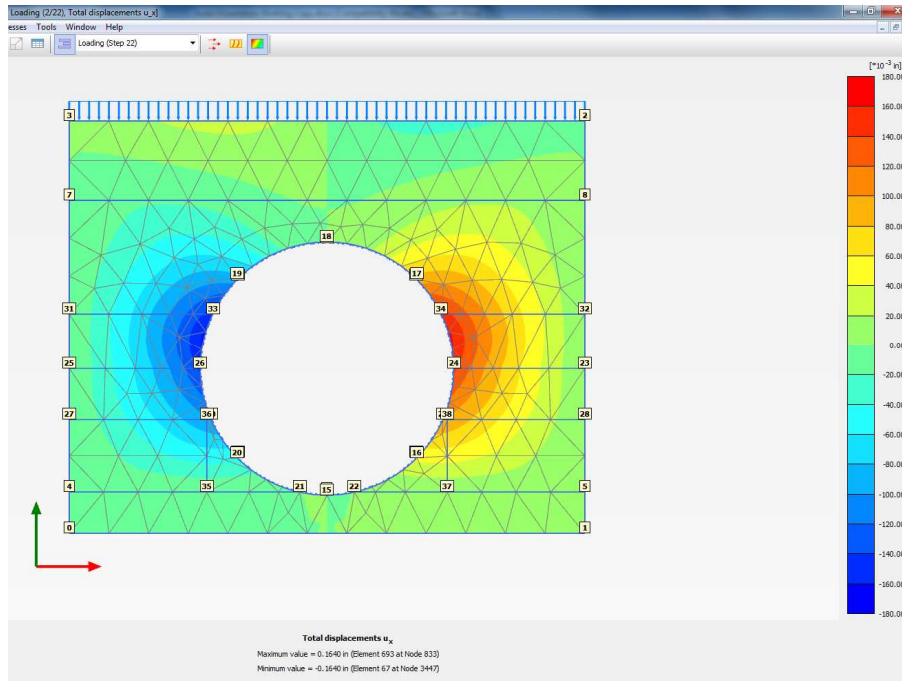


Figure 7.52: Horizontal Displacement Results for Test 2 Simulation
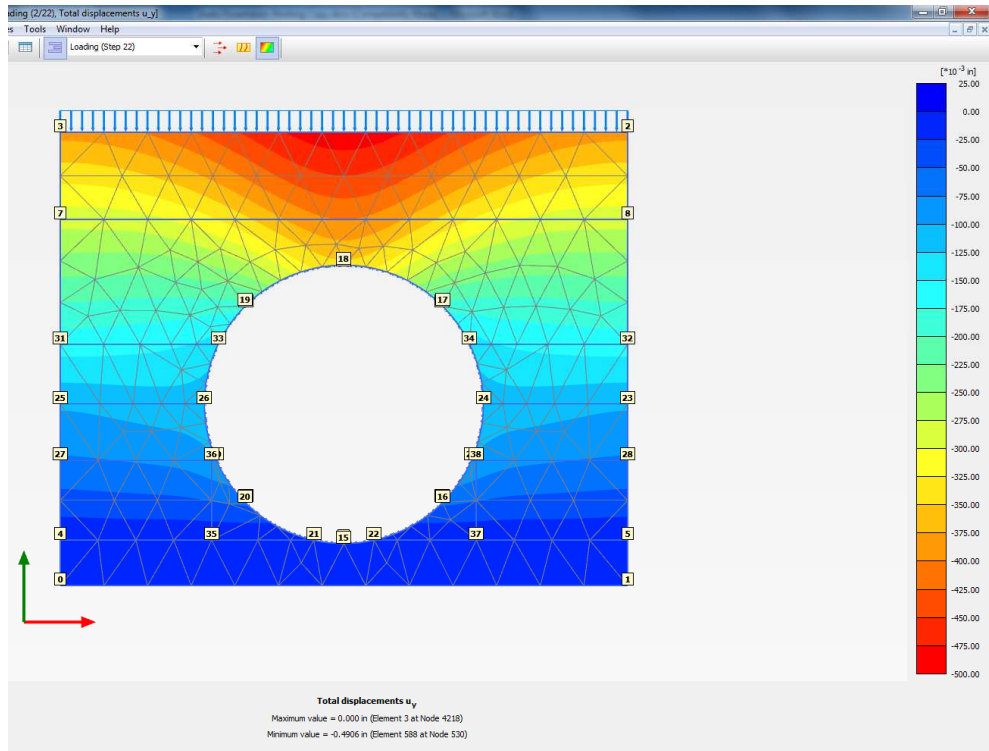
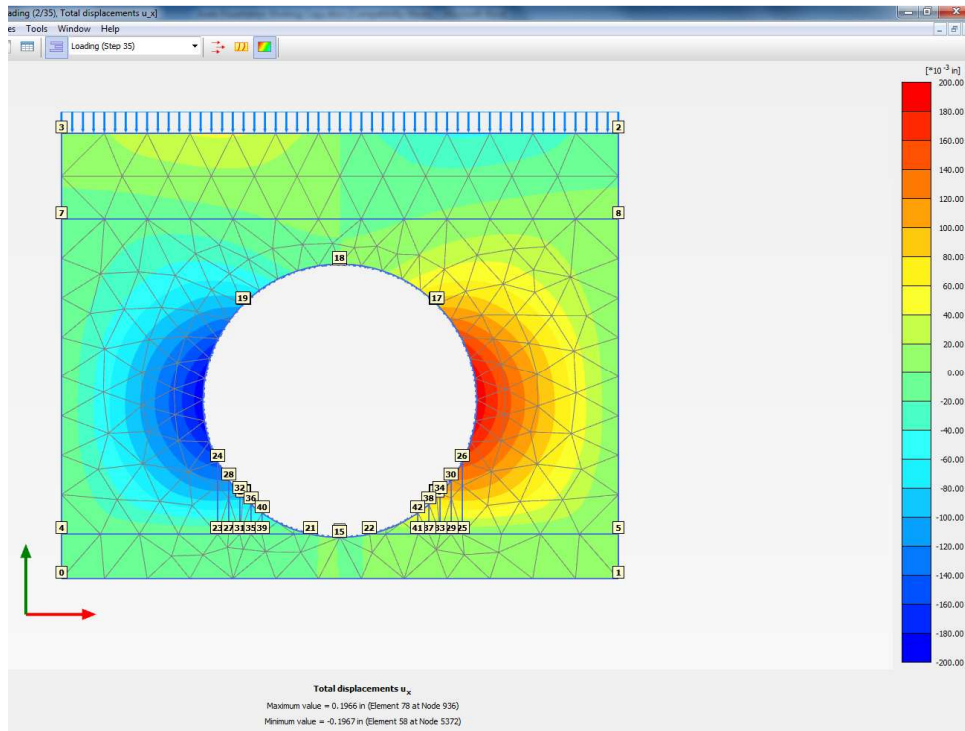Figure 7.53: Vertical Displacement Results for Test 2 Simulation
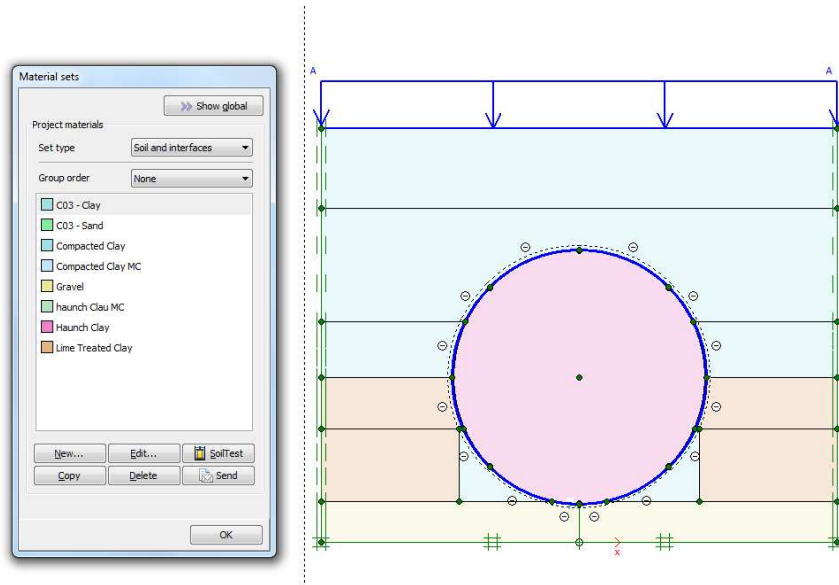


Figure 7.54: Model 17
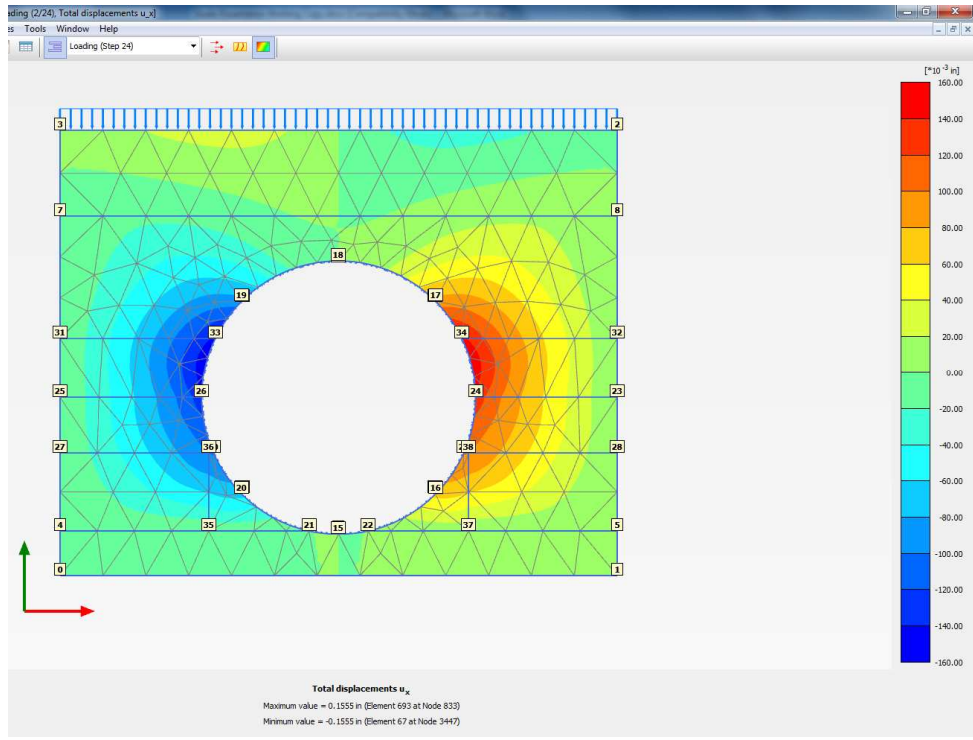
Figure 7.55: Horizontal Displacement Results: Model 17
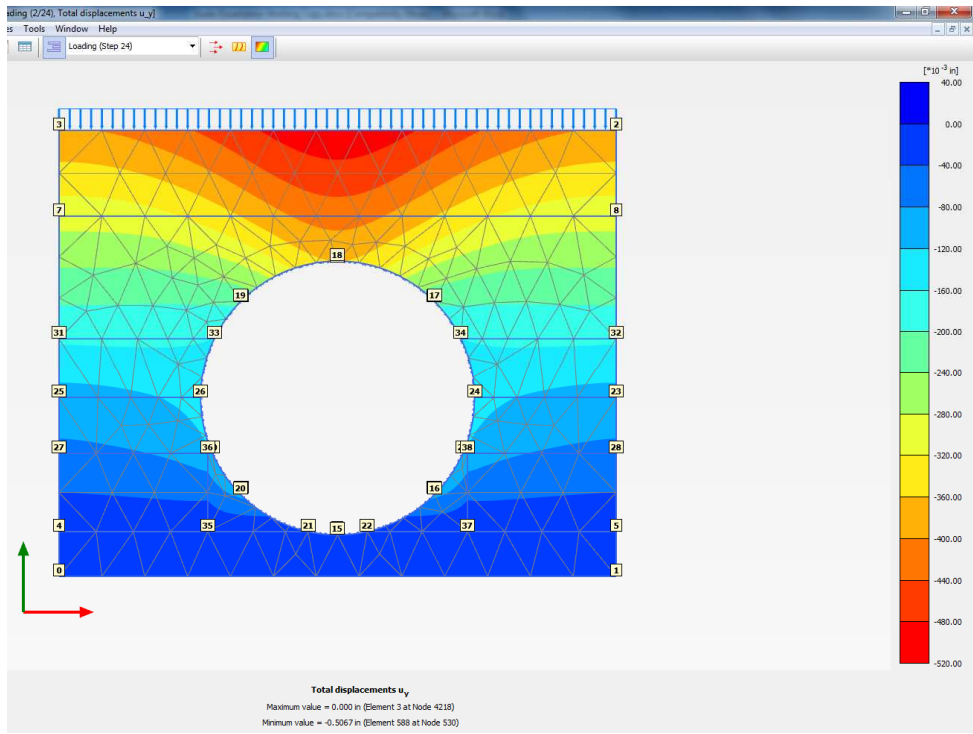


Figure 7.56: Vertical Displacement Results: Model 17
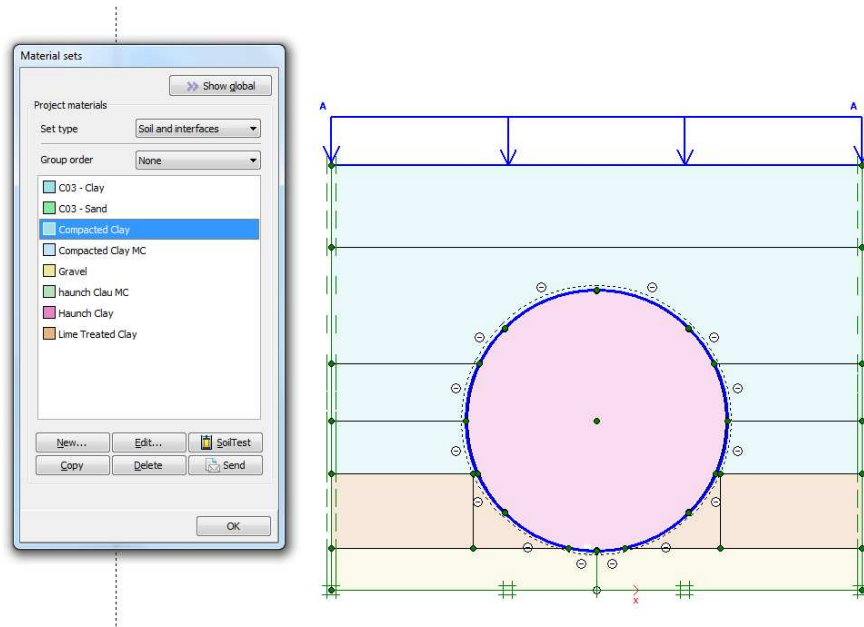
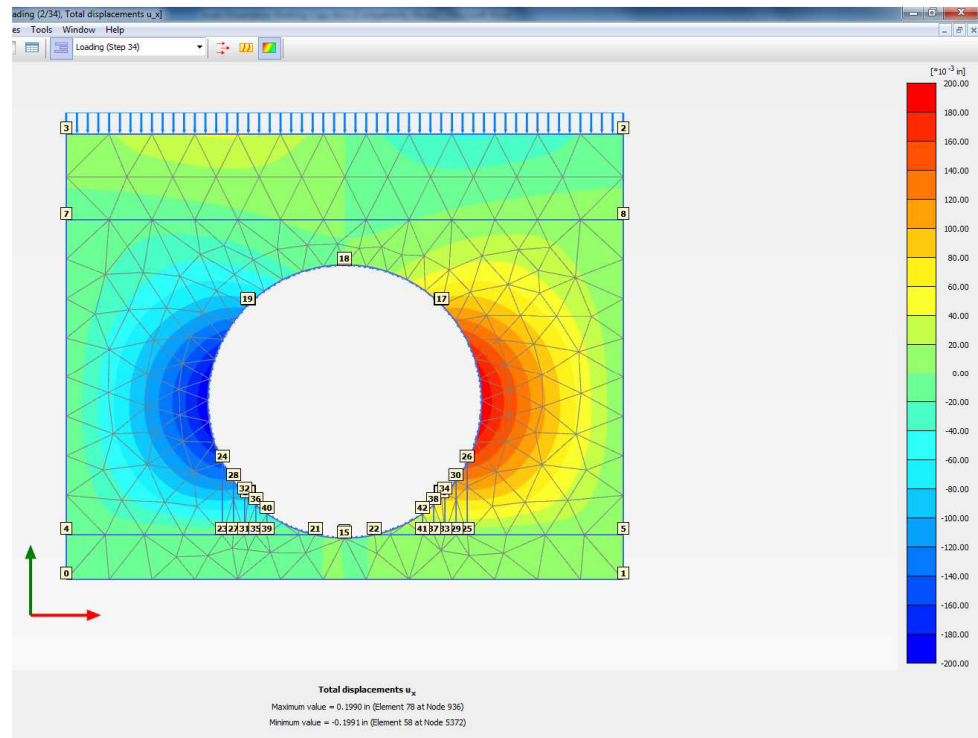Figure 7.57: Model 18
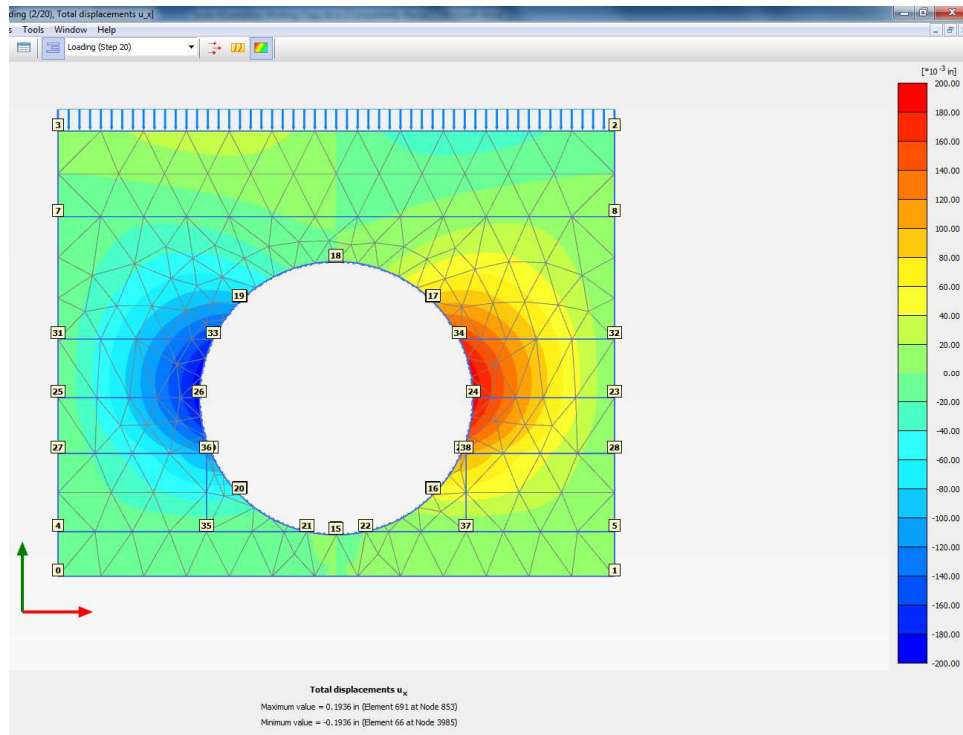


Figure 7.58: Horizontal Displacement Results: Model 18

Figure 7.59: Vertical Displacement Results: Model 18
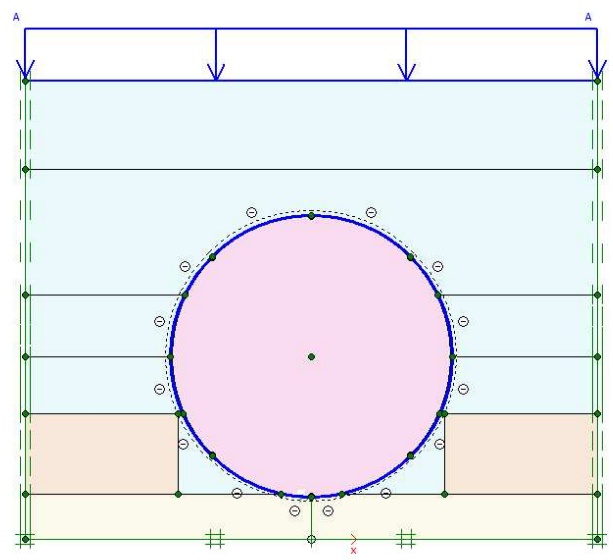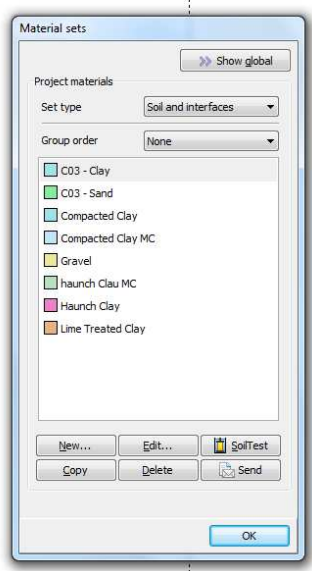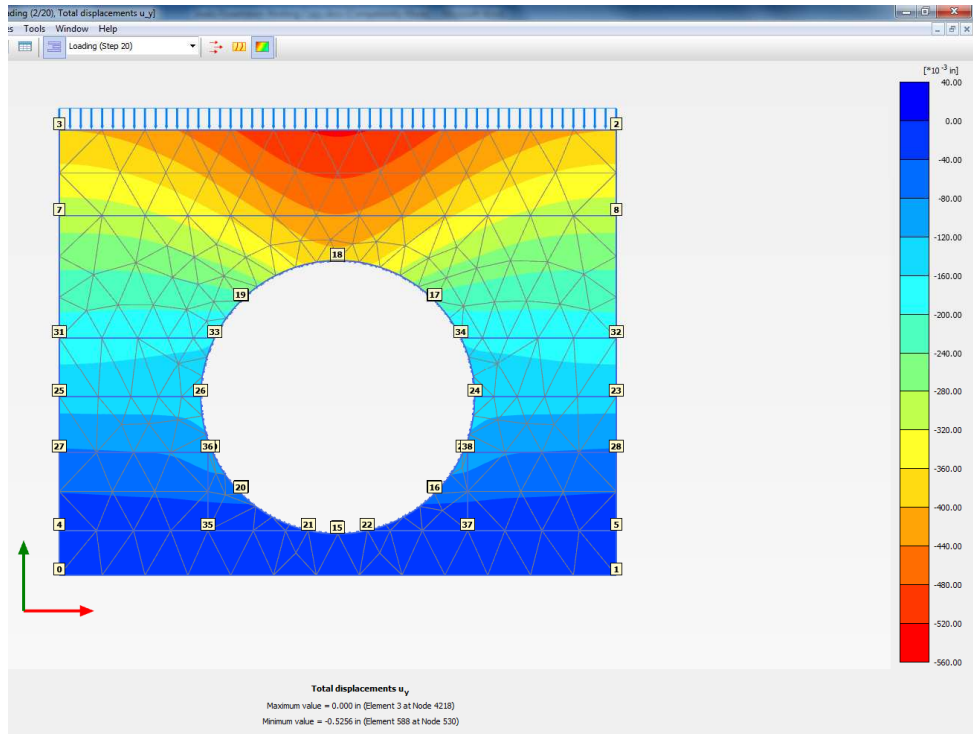


Figure 7.60: Model 19
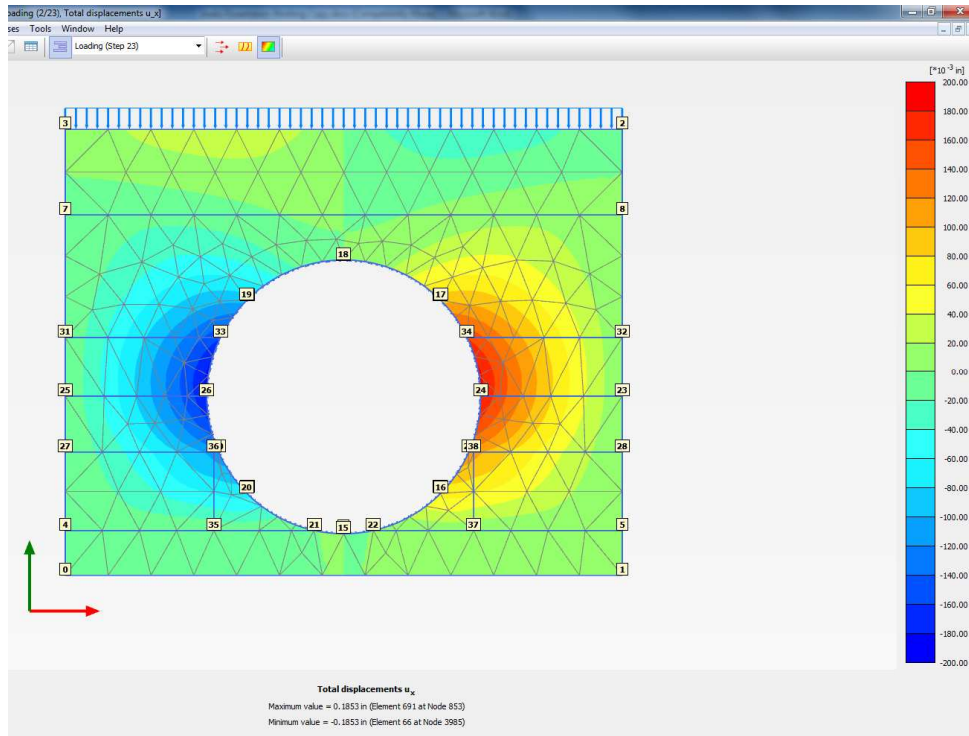
Figure 7.61: Horizontal Displacement Results: Model 19
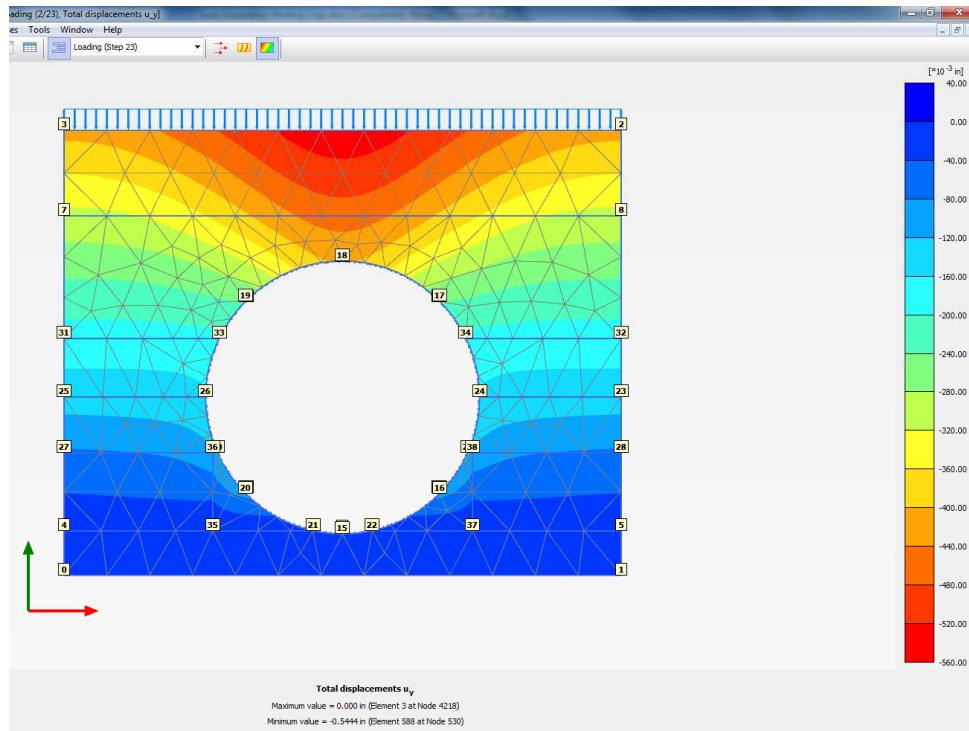


Figure 7.62: Vertical Displacement Results: Model 19
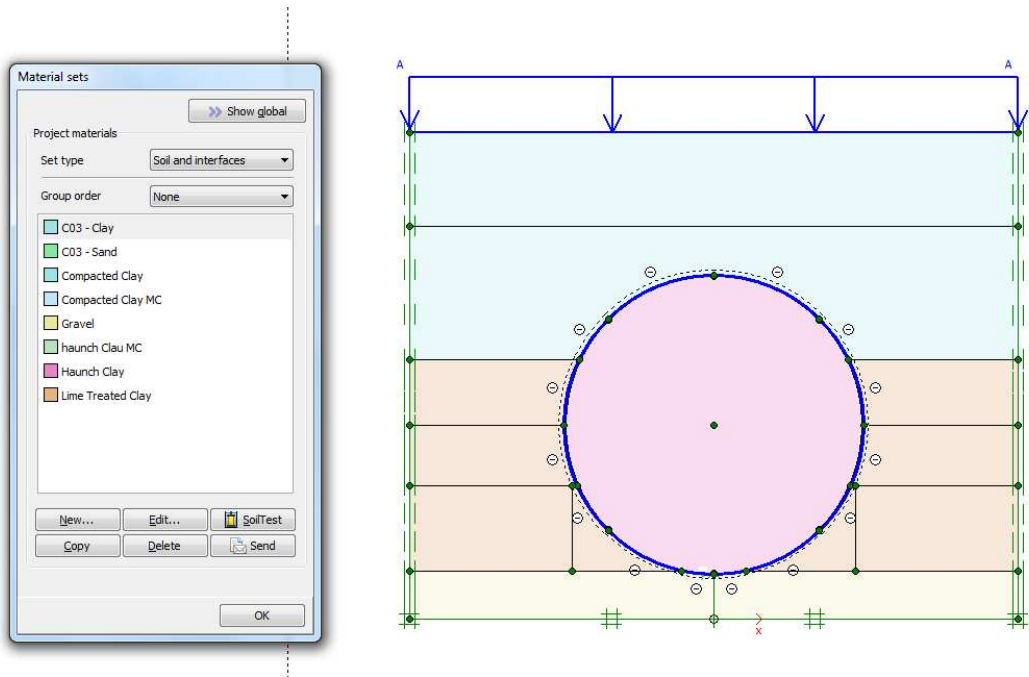
Figure 7.63: Model 20
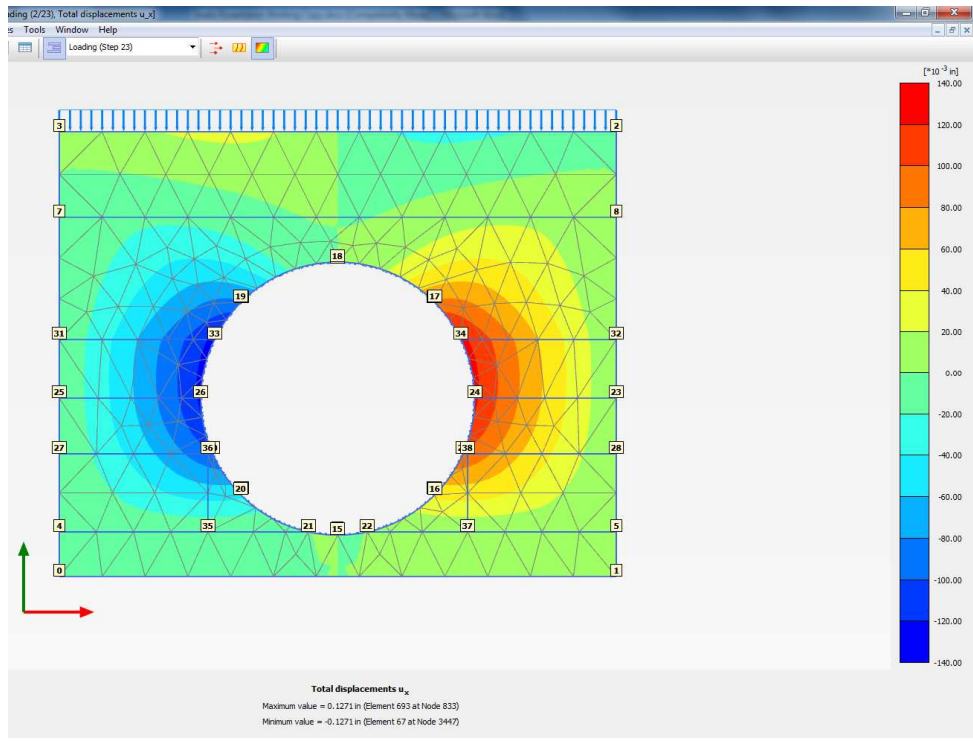


Figure 7.64: Horizontal Displacement Results: Model 20

176
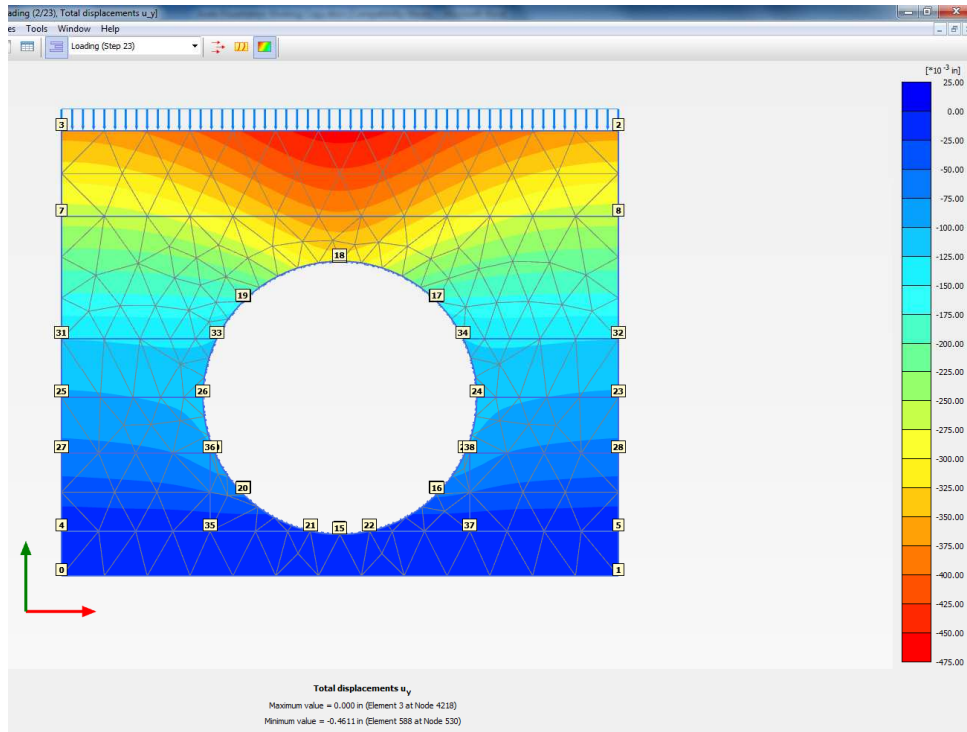
Figure 7.65: Vertical Displacement Results: Model 20
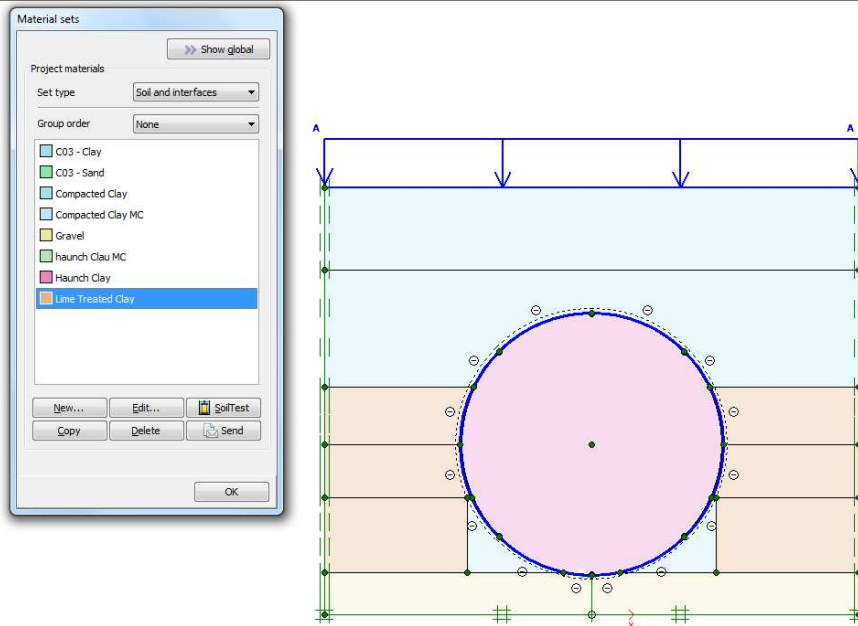


Figure 7.66: Model 21

177
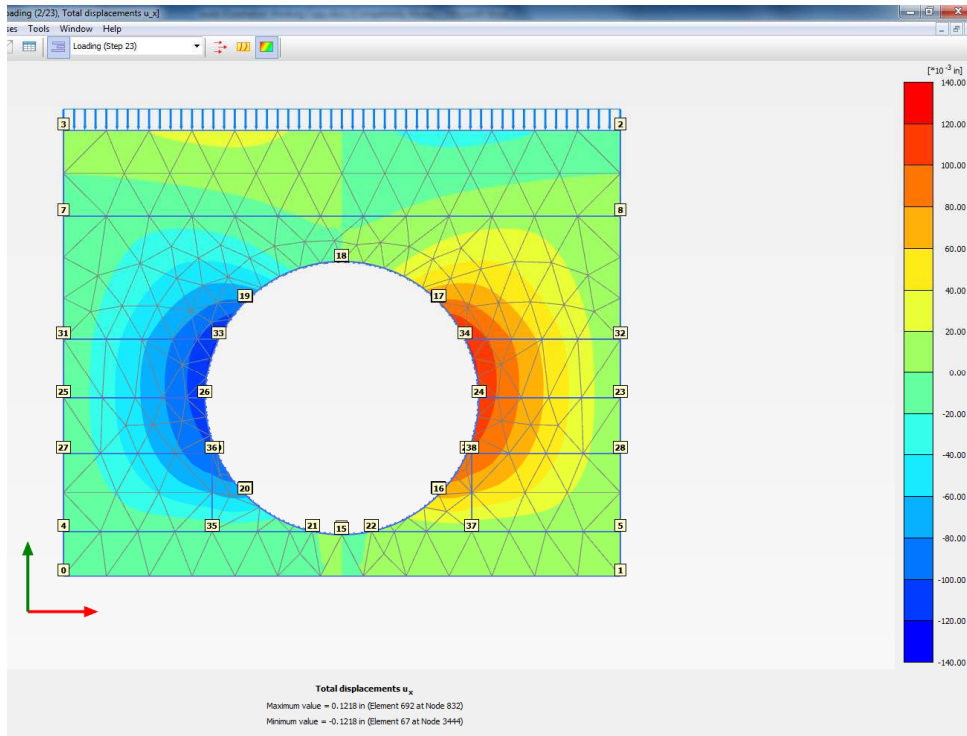
Figure 7.67: Horizontal Displacement Results: Model 21
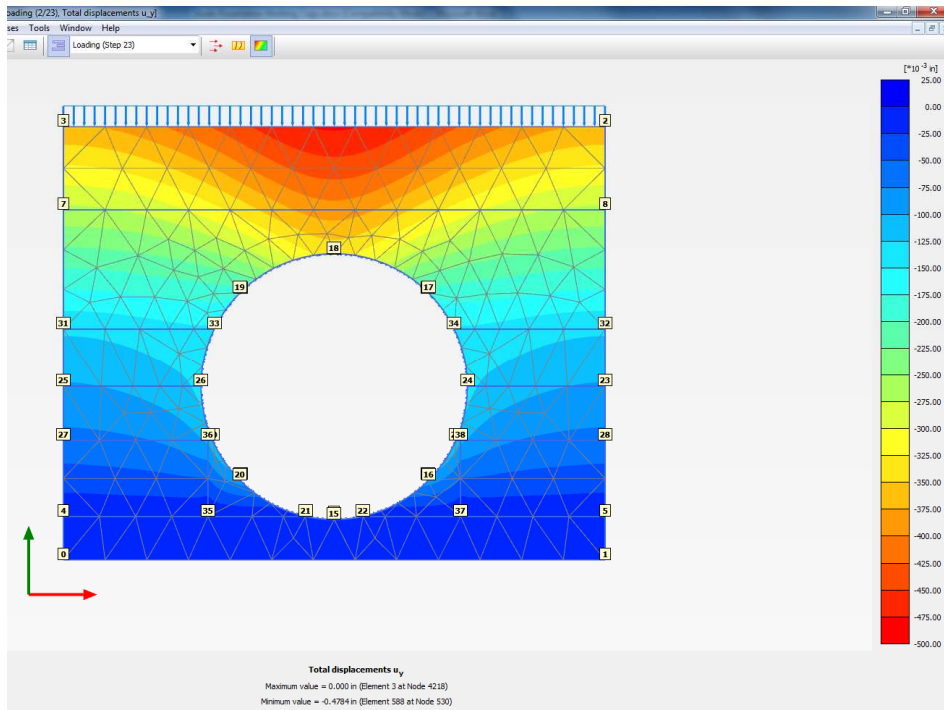


Figure 7.68: Vertical Displacement Results: Model 21
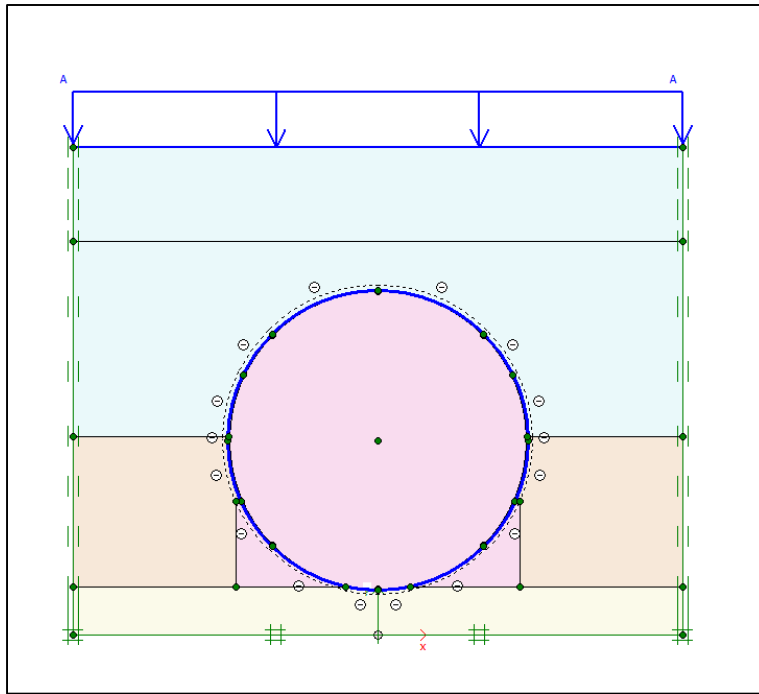
Figure 7.69: Model 22
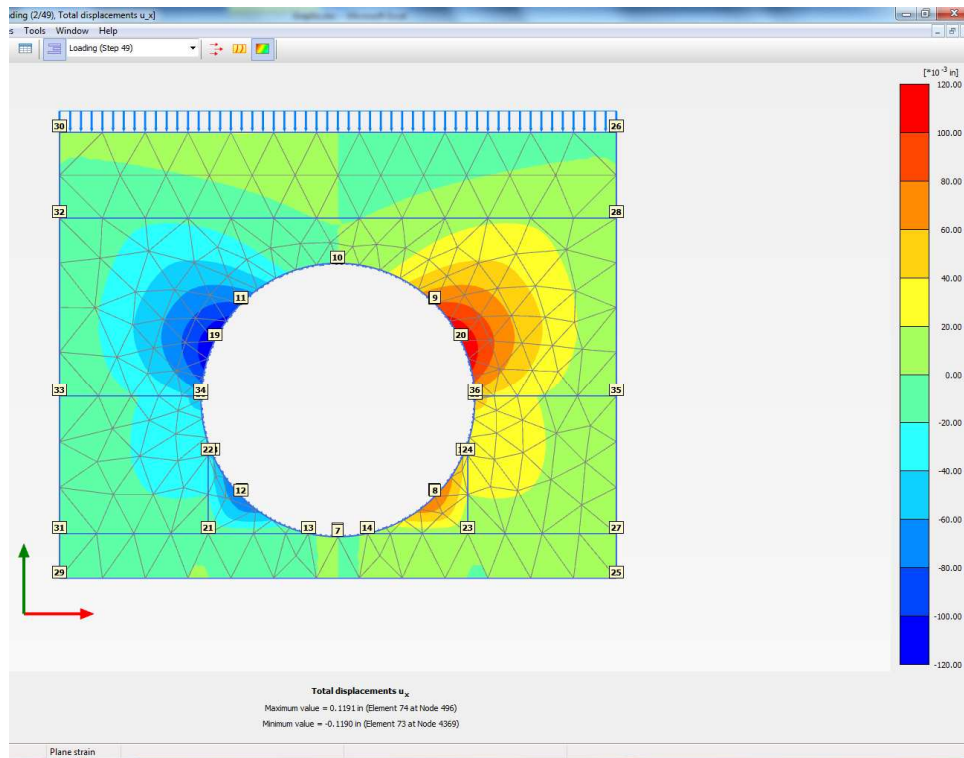


Figure 7.70: Horizontal Displacement Results: Model 22

179
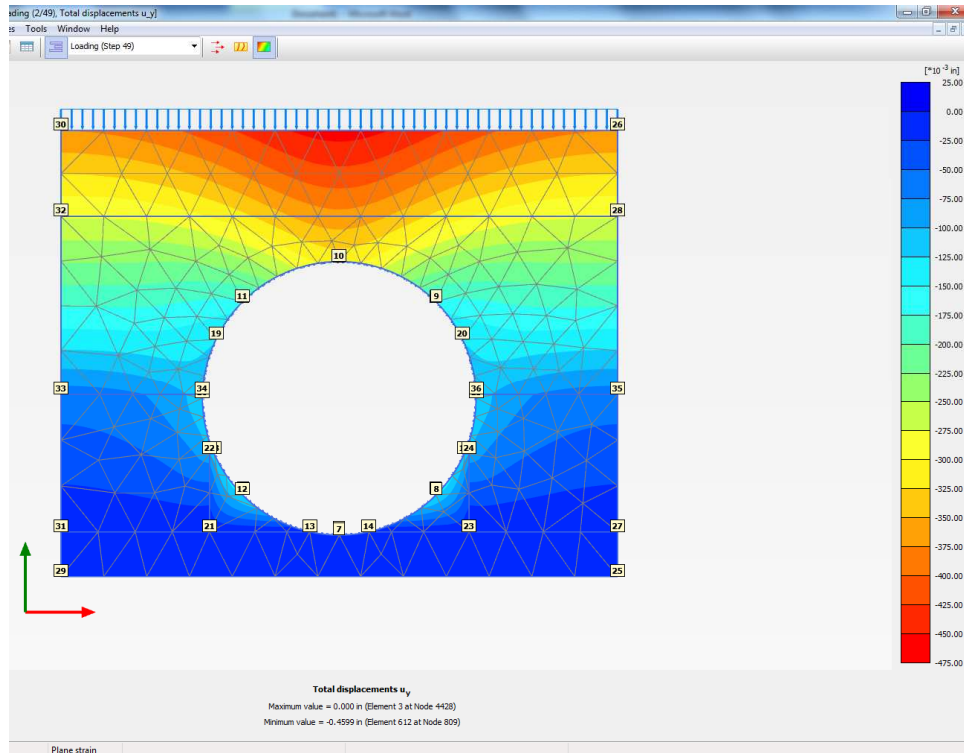
Figure 7.71: Vertical Displacement Results: Model 22

7.4.7 Gravel Embedment

Analyses were carried out by varying the depth of stiff gravel embedment. The depth of gravel embedment used for analyses were 0.3, 0.5, and 0.7 times the diameter of the pipe and one foot above the pipe. The results are presented in Table 7.6 and the illustrations of results are shown in Figures 7.72 through 7.83.

Table 7.6: Deflections for Gravel Embedment

| Model No. | Depth of Gravel Embedment (in.) | Horizontal Deflection (in.) | Vertical Deflection (in.) | Deflection Ratio |
|---|---|---|---|---|
| Model 23 (Test 4) | 22 | 0.18 | -0.20 | 0.90 |
| Model 24 | 36 | 0.12 | -0.17 | 0.71 |
| Model 25 | 50 | 0.10 | -0.15 | 0.67 |
| Model 26 (Test 3) | 84 | 0.08 | -0.13 | 0.62 |
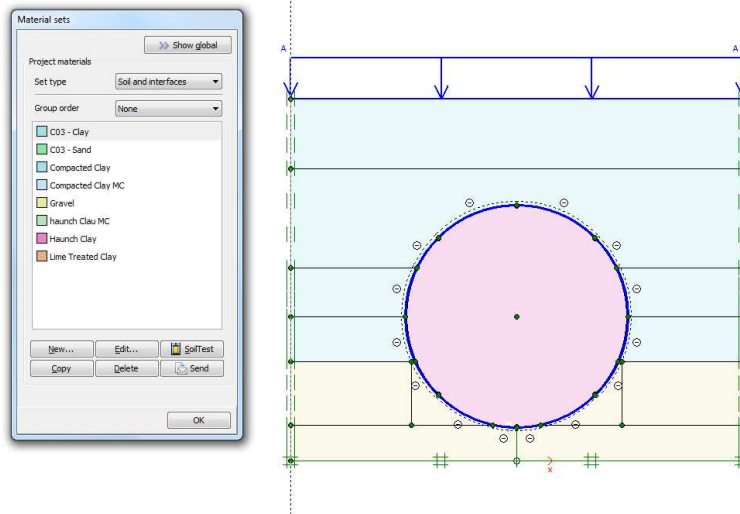
Figure 7.72: Model 23
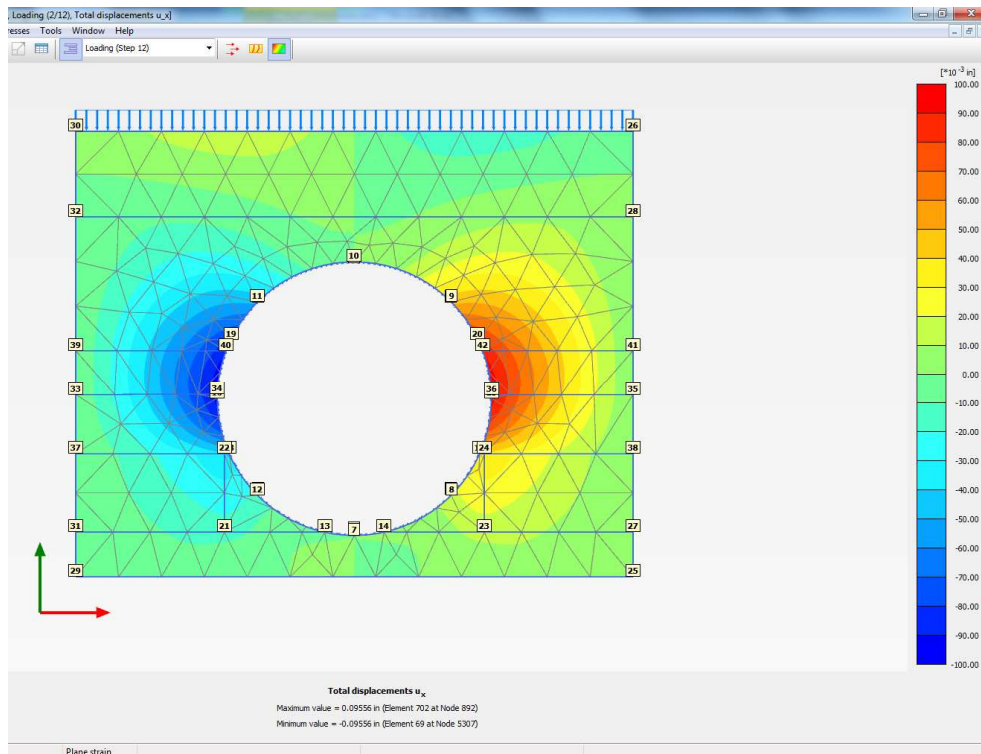


Figure 7.73: Horizontal Displacement Results: Model 23
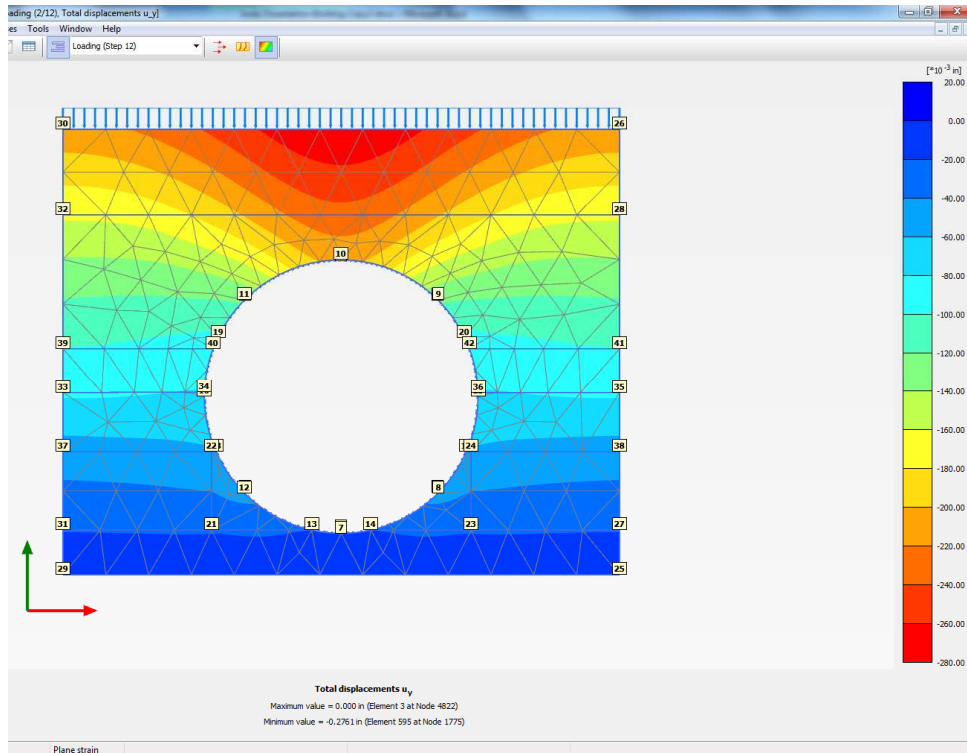
Figure 7.74: Vertical Displacement Results: Model 23
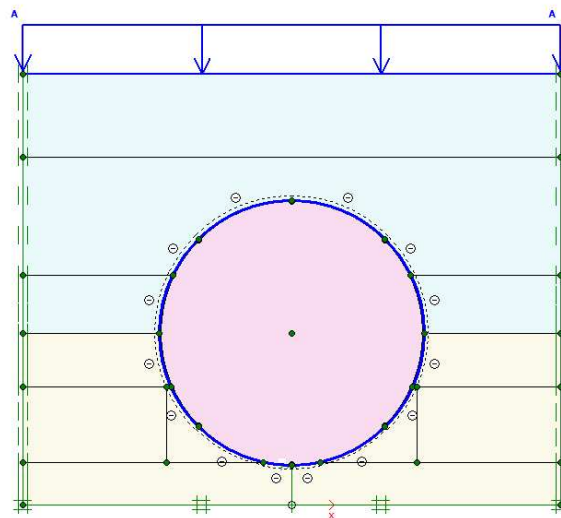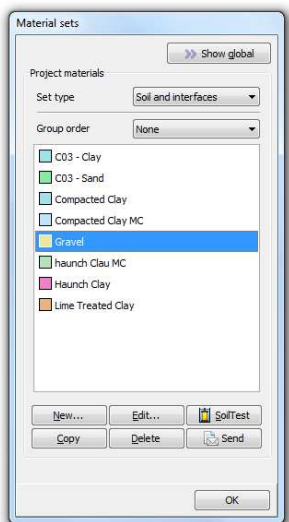


Figure 7.75: Model 24
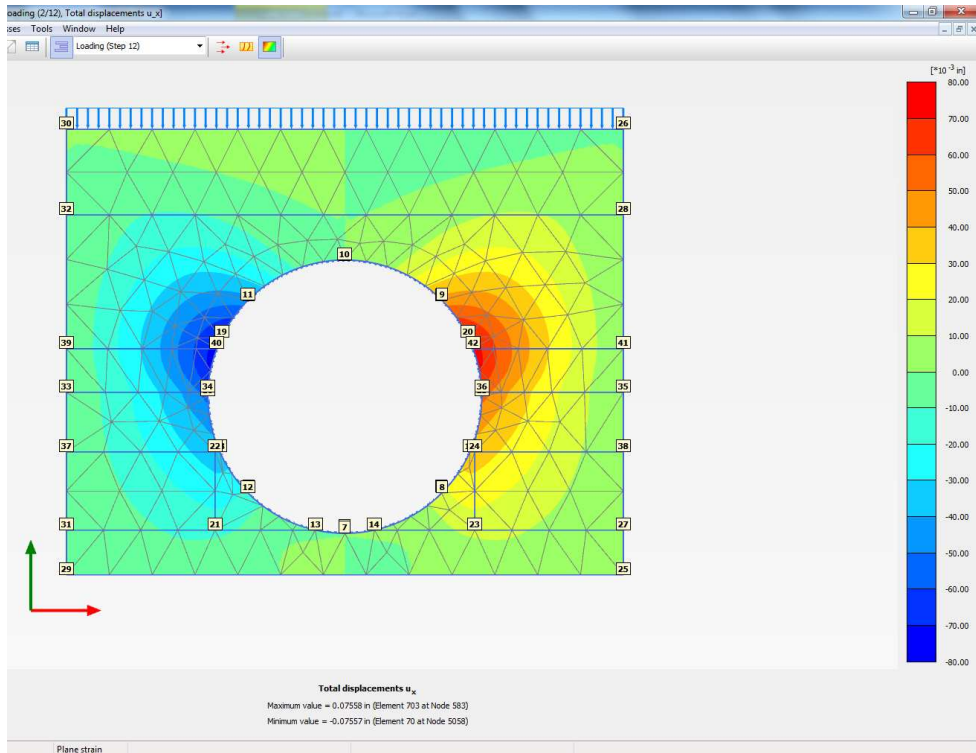
Figure 7.76: Horizontal Displacement Results: Model 24
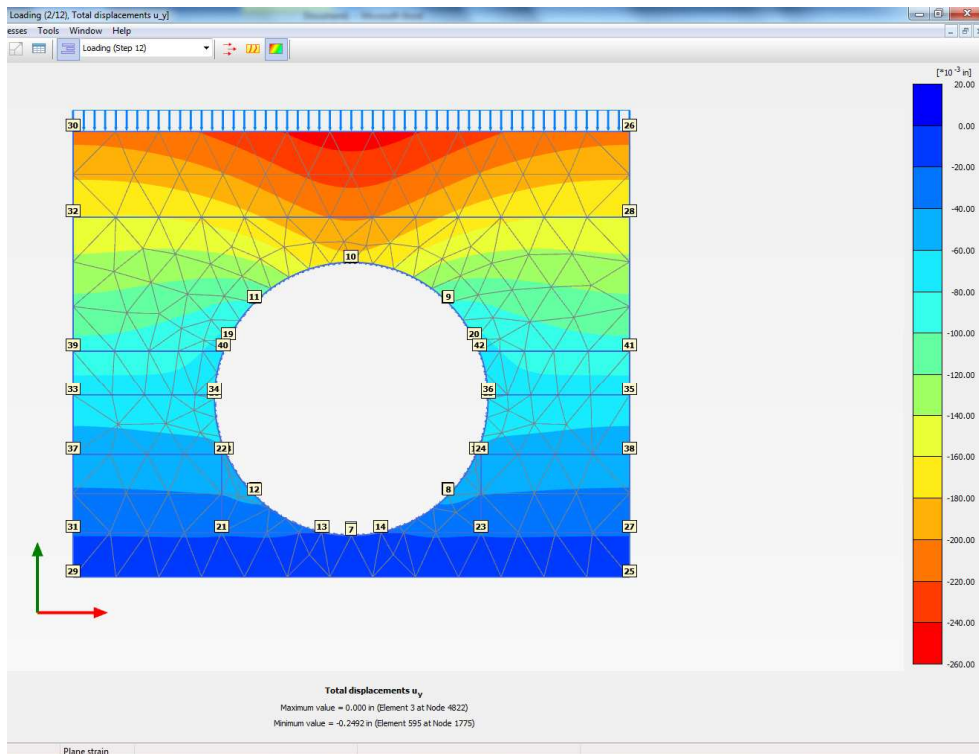


Figure 7.77: Vertical Displacement Results: Model 24
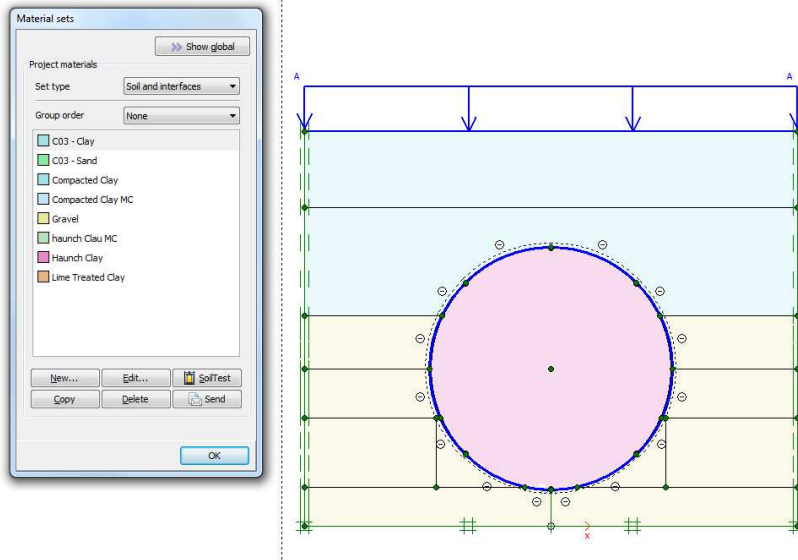
Figure 7.78: Model 25
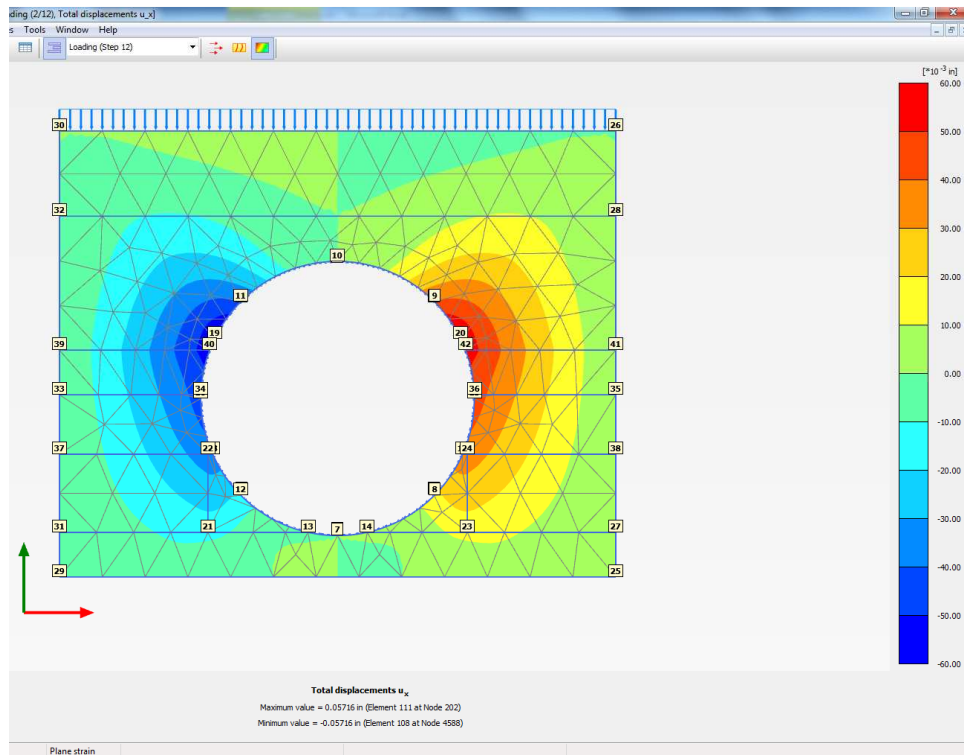


Figure 7.79: Vertical Displacement Results: Model 25
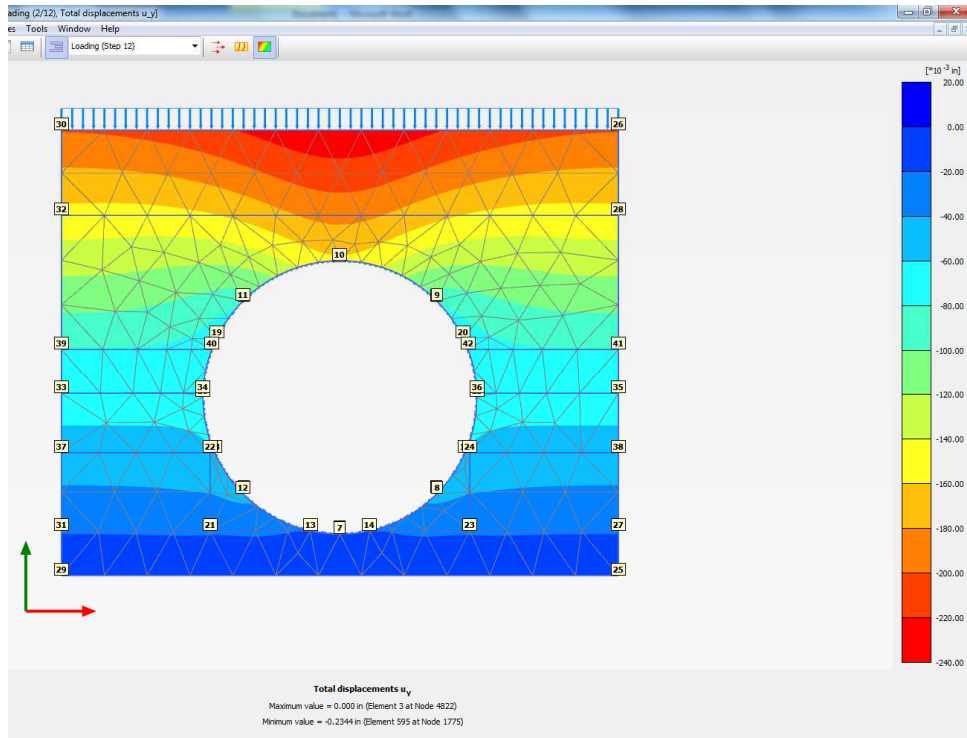
Figure 7.80: Vertical Displacement Results: Model 25
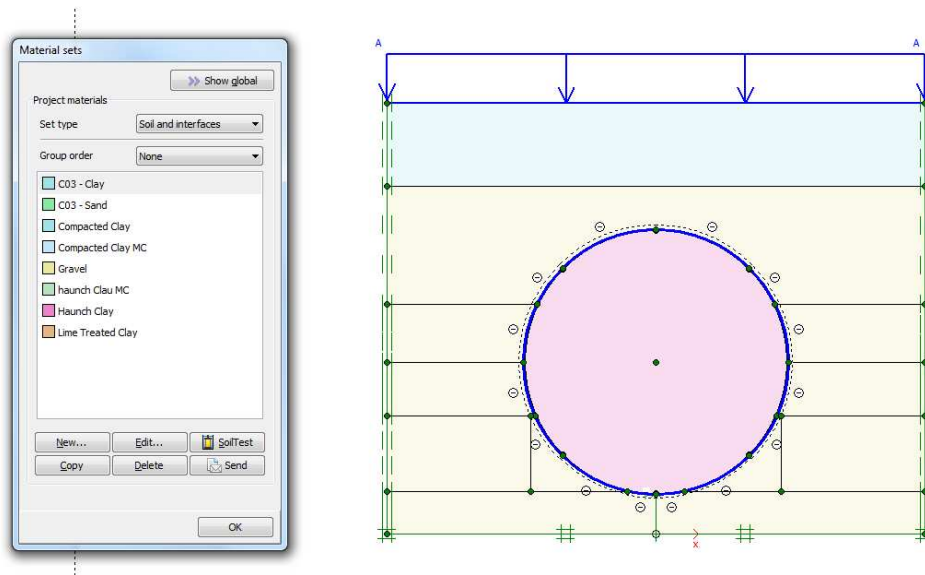


Figure 7.81: Model 26
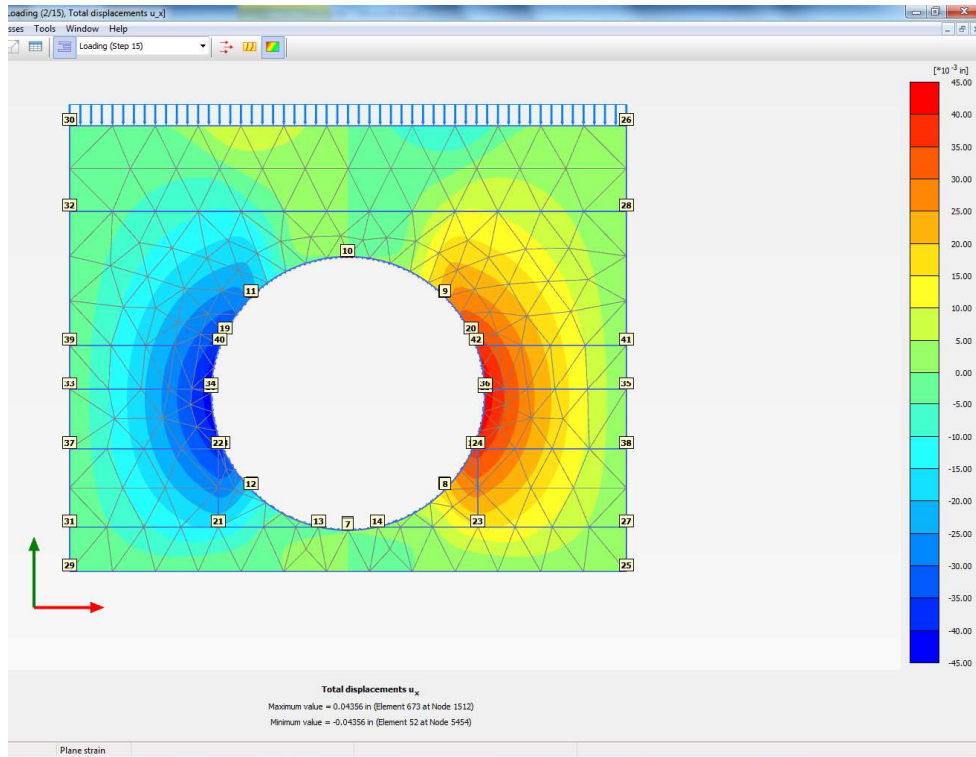
Figure 7.82: Horizontal Displacement Results: Model 26
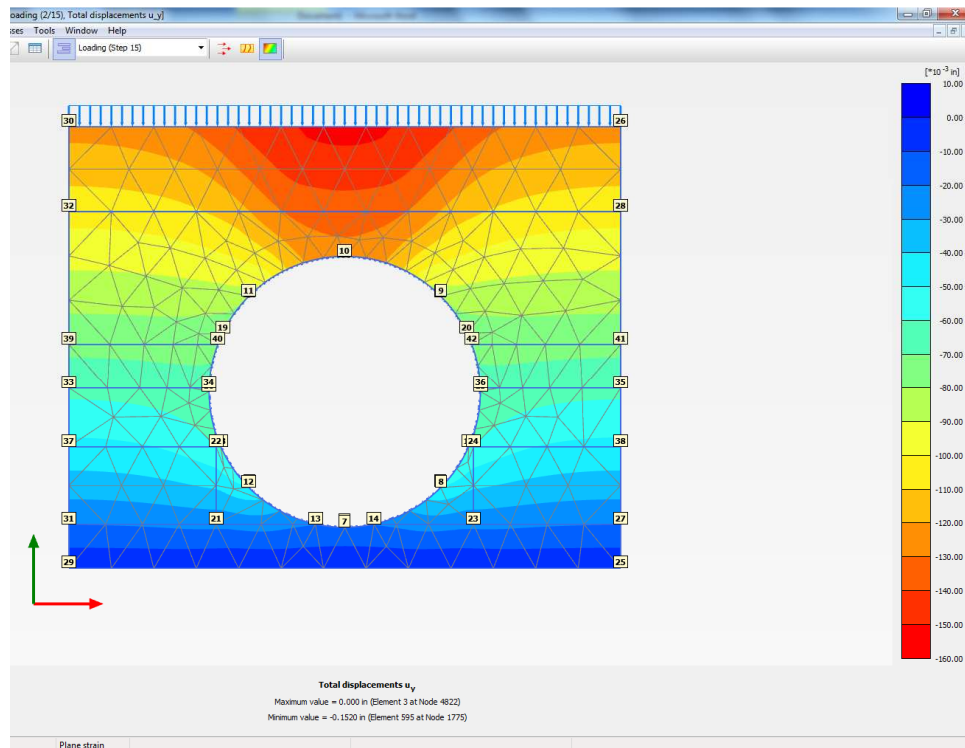


Figure 7.83: Vertical Displacement Results: Model 26

## 7.5 Comparison of Results

Figure 7.84 compares the laboratory test deflections and the deflection results obtained from finite element analyses. The closest model to the laboratory test results are compared in Table 7.7 with error in prediction.



## Chart Title

| | Test 1 | Test 1a | Pilot Model | Base Model | Model 8 | Model 9 | Test 2 | Model 22 | Test 3 | Test 3 Model | Test 4 | Test 4 Model |
|---|---|---|---|---|---|---|---|---|---|---|---|---|
| ■ Horizontal Deflection | 0.22 | 0.17 | 0.19 | 0.41 | 0.34 | 0.18 | 0.13 | 0.12 | 0.07 | 0.08 | 0.13 | 0.18 |
| ■ Vertical Deflection | 0.65 | 0.42 | 0.22 | 0.45 | 0.58 | 0.28 | 0.25 | 0.32 | 0.14 | 0.13 | 0.12 | 0.2 |
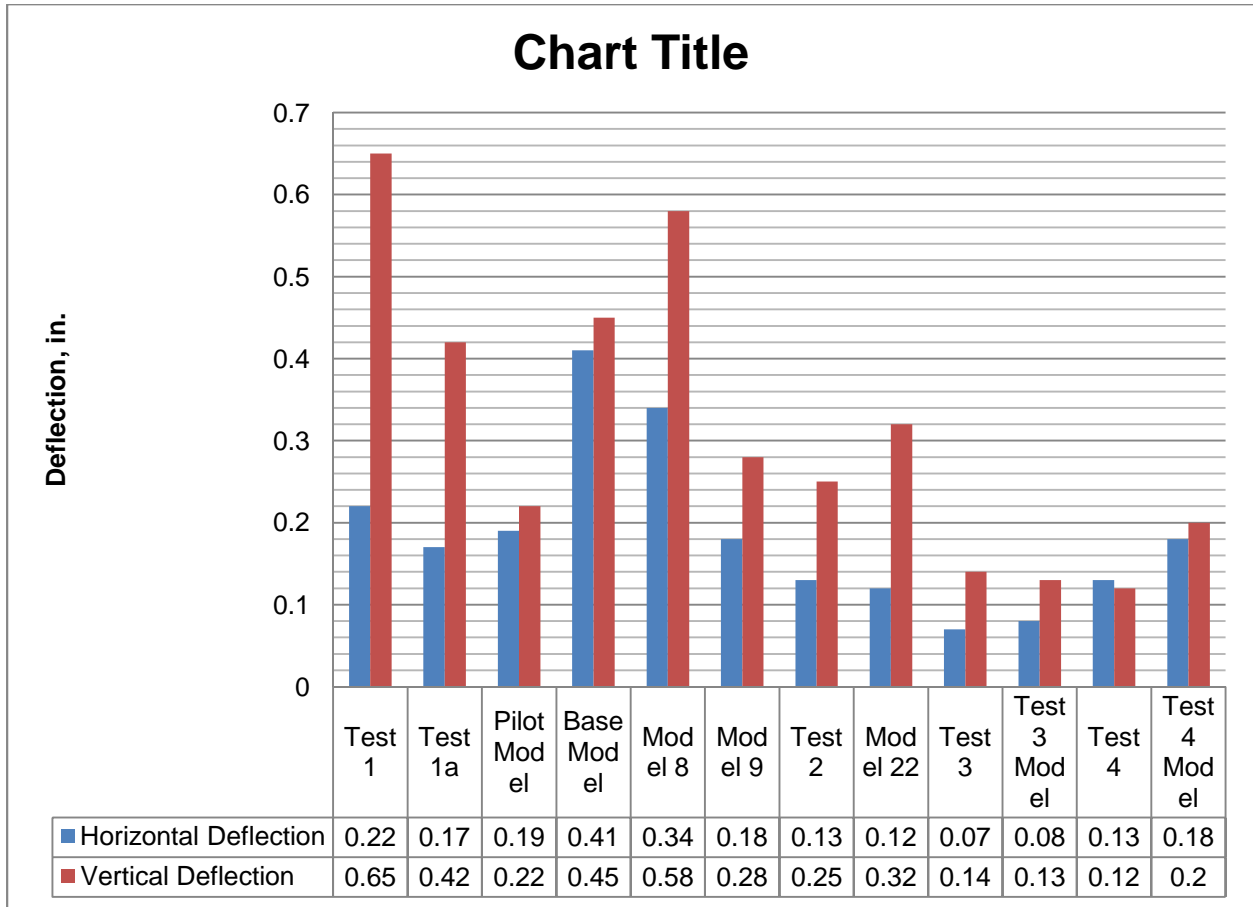
Figure 7.84: Comparison of Test Results with Finite Element Models

Table 7.7: Comparison of Test Results to Closest Models

| Laboratory Tests | Finite Element Models | Error | | | |
|---|---|---|---|---|---|
| | | Horizontal Deflection | | Vertical Deflection | |
| | | % | in. | % | in. |
| Test 1 | Model 8 | 35% | 0.12 | -12% | -0.07 |
| Test 2 | Model 22 | -8% | -0.01 | 22% | 0.07 |
| Test 1a | Model 9 | 6% | 0.01 | -50% | -0.14 |
| Test 3 | Model 23 | 12% | 0.01 | -8% | -0.01 |
| Test 4 | Model 26 | 27% | 0.05 | 40% | 0.08 |

The results of the finite element analyses are fairly close to the results obtained from the laboratory tests. Results of Test 1, Test 2, and Test 1a compared respectively to Model 8, Model 22 and Model 9 indicate that due to lack of compatibility in the haunch area, it is difficult to achieve haunch soil property identical to the compacted embedment. The errors between model prediction and laboratory test results range from -0.14 inches to 0.12 inches which translate to – 50% to 40%. These errors are acceptable because the magnitude of error is minimal and predicted deformations are within 0.9% of pipe diameter. If the model can be calibrated to predict higher magnitude of deflection, for example 2% of pipe diameter or 1.5 inch, at similar magnitude of error, the model can be considered highly effective because the percentage error will drop significantly.

### 7.6 Summary

Results of the finite element analysis performed based on soil laboratory test results and soil box tests were presented in this chapter. Further finite element analysis were carried out for other different scenarios like wider soil box width, varied width of haunch area, varied depth of embedment, and varied properties of embedment. Results of the tests were compared to that of the finite element analyses.

Chapter 8

Conclusions and Recommendations for Future Research

<u>8.1 Conclusions</u>

8.1.1 Model for Soil Pipe Interaction

One of the key assumptions in Spangler's soil pipe interaction model is that both horizontal and vertical deflections due to surcharge or backfill load are equal in magnitude. In all of the tests, it was observed that this assumption was not followed. Another key assumption in Spangler's model is that the passive soil resistances offered by embedment soil above and below the pipe springline are symmetric. This assumption is questionable from geotechnical engineering point of view, especially in case of large diameter pipes. This is because it is widely accepted principle in geotechnical engineering that lateral pressure (active, at-rest or passive) from soil is dependent on depth, with deeper soils offering higher lateral forces due to greater overburden pressures. This assumption is further invalidated in the cases where two different embedment materials are used in layers. Modified Iowa formula and Bureau of Reclamation Equation are based on Spangler's model with Modulus of soil reaction (E') values being fitted to Spangler's model. Two key concerns in using E' values in soil pipe interaction modeling are: validity of Spangler's model to large diameter pipe, and biased results from fitted E' values because the fitting of E' values were carried out based on soil classification rather than any strength parameter of soil.

In this research, finite element method was effectively used to model the soil pipe interaction for five full scale laboratory tests conducted on a steel pipe. Such models can be used for analysis of flexible pipe embedment design for layered embedment conditions.

8.1.2 Role of Haunch Area

Haunch area is the most important part of embedment. In all of the tests, deflections due to surcharge load were well within the allowable range of 3%. However, the ratio between horizontal and vertical deflection showed that the squaring of the pipe occurred. The finite element analysis results showed that the squaring of the pipe occurs when haunch soil is weak compared to the side column. Another critical observations made during the tests were stresses at the bottom of pipe and bedding angle. It is desirable that the stress due to surcharge load on top of pipe, weight of pipe, and water inside

189

the pipe be distributed uniformly across the width of bedding. It was observed in Test 1 and 2, that there was very high stress concentration at the bottom of pipe. Although, deflections of pipe were acceptable in these cases, high stress concentration in bottom of pipe can result in undesirable settlement of bedding. This concern is more pronounced when there are clay layers below bedding that exhibit consolidation settlements as stresses are increased.

8.1.3 Results

Best results against peaking deflection obtained with crushed limestone (Test 3) due to lesser lateral earth pressure coefficient and lesser energy required for compaction. Perhaps, that is the reason why peaking deflections in flexible pipe have not been studied extensively in the past. However, if clayey materials are considered, peaking deflections need to be examined closely.

Best results against deflection due to surcharge load obtained in Test 4 with mixed embedment of crushed limestone and native clay. This was the only case when horizontal deflection due to surcharge load was observed to be approximately equal to vertical deflection in magnitude. This only echoes the importance of haunch area in behavior of pipe. The haunch area consisted of flow-able crushed limestone which was also subjected to compaction energy from compaction of clay embedment above 0.3 diameter. Also, the bedding angle for Test 4 was highest of all tests. The stress at top of pipe was well distributed along the bedding of pipe which is a favorable condition for integrity of bedding.

8.1.4 Haunch Material

Despite acceptable results with native and lime treated clays in haunch area with respect to deflection behavior, it is recommended that more flow-able material be used at the haunch area. The reason for such recommendation is to avoid stress concentration at the bottom of pipe. Although well compacted native or modified clay soil columns at sides of the pipe will provide enough resistance against the deflection of the pipe, the stress concentration at the bottom of pipe is a concern. From the test results, it was found that flow-able crushed limestone was more efficient in spreading the load from the top of the pipe to the width of the bedding.

### 8.1.5 Materials above Haunches

There is a high potential of native material to be used above haunches in natural or modified form. Test 4 results showed that best performance against backfill load was achieved in Test 4 when material below 0.3 diameter of pipe was limestone and native clay compacted to 95% above that. Perhaps, the results would be different with 85% compaction. However, it is recommended that analysis be done with consideration to 85% compacted native clay above 0.3 diameter of pipe. The key reason to recommending lesser compaction effort is to avoid peaking deflection due to compaction energy.

### 8.1.6 Compaction of Native Clay

Based on test results, it is recommended that the compaction efforts be limited to 85% for native clay material. Such recommendation is made in order to avoid peaking deflection that may exceed allowable deflection for steel pipe. Also, compaction lateral forces exceeding lateral passive resistance of the in-situ trench wall can cause failure of the trench soils.

### 8.1.7 Soil-Pipe Interaction Model

It was observed that the basic assumptions of Spangler's soil-pipe interaction model were not realized in the test. The basic assumptions that were not followed include: (i) passive resistance is the only lateral force acting on pipe (at-rest and active earth pressures acting on pipe during embedment construction were ignored), (ii) vertical deflection is approximately equal to horizontal, and (iii) passive lateral pressure due to soil is symmetric about springline. There is a need to develop a new model to analyze soil-pipe interaction which takes into account shortcomings of Spangler's model mentioned above.

### 8.1.8 In-Situ Tests

It is recommended the tests be carried out to determine in-situ properties of the alignment soils. Laboratory tests on alignment soils have been carried out in remolded state. However, it is of utmost important to recognize in-situ properties of soil. One such example of usefulness of in-situ property is evaluating lateral pressure offered by embedment and/or compaction effort against passive resistance

offered by the trench walls. Risk of compaction energy is not limited to failure due to peaking deflection of pipe but factor of safety of failure of in-situ trench soils must also be considered.

<p style="text-align:center">8.2  Recommendations for Future Research</p>

### 8.2.1 Field Tests

Future research can be carried out with similar embedment/backfill conditions as the laboratory tests but in actual field conditions with in-situ soil trench walls as opposed to concrete walls. The field test results may be very similar to ones obtained in the laboratory as long as the in-situ trench-walls can offer at least equivalent passive resistance as lateral forces of embedment and compaction. In adverse situation, failure of in-situ soils may be encountered.

In this research, only one earth pressure cell was used at one particular plane of wall and pipe to measure the lateral earth pressures. Multiple earth pressure cells should be used to understand the distribution of lateral pressure on pipe and the trench walls.

### 8.2.2 Model Calibration

The errors between model prediction and laboratory test results range from -0.14 inches to 0.12 inches which translate to – 50% to 40%. These errors are acceptable because the magnitude of error is minimal and predicted deformations are within 0.9% of pipe diameter. If the model can be calibrated to predict higher magnitude of deflection, for example 2-3% of pipe diameter, at similar magnitude of error, the model can be considered highly effective because the percentage error will drop significantly. Unfortunately, laboratory tests were not conducted to such high deformations. For future research, model should be calibrated for larger deformations or deformations to failure.

### 8.2.3 Model for Predicting Peaking Deflection of Pipe

Spangler's model fails to consider peaking behavior of pipe during embedment construction. From results of Test 3, it can be concluded that the pipe does not exhibit peaking behavior when embedment offering minimal at-rest and active lateral pressure (soils with higher friction angle) with requirement of minimal compaction energy is used. However, peaking of pipe can be a concern when

clayey soil is compacted. Test 4 results show peaking deflections which are approximately 3% of diameter of the pipe.

There is a need to develop a model to predict pipe behavior due to embedment construction, especially while considering clay as potential embedment material. This model needs to consider the cycle that embedment soil goes through from at-rest condition (at the time of placement of layer), to active condition (during peaking deflection), and finally to passive condition (due to deflection of pipe).

Appendix A

Instrument Calibration Sheets

# GEOKON

48 Spencer St. Lebanon, N.H. 03766 USA

## Vibrating Wire Pressure Transducer Calibration Report

| | | | |
|---|---|---|---|
| Type: | S | Date of Calibration: | November 22, 2010 |
| Serial Number: | 1035439 | Temperature: | 24.8 °C |
| Pressure Range: | 350 kPa | †Barometric Pressure: | 1002.6 mbar |
| | | Calibration Instruction: | VW Pressure Transducers |
| | | Technician: | KRogers |

| Applied Pressure (kPa) | Gage Reading 1st Cycle | Gage Reading 2nd Cycle | Average Gage Reading | Calculated Pressure (Linear) | Error Linear (%FS) | Calculated Pressure (Polynomial) | Error Polynomial (%FS) |
|---|---|---|---|---|---|---|---|
| 0.0 | 8745 | 8745 | 8745 | 0.066 | 0.02 | -0.127 | -0.04 |
| 70.0 | 8065 | 8066 | 8066 | 70.23 | 0.06 | 70.32 | 0.09 |
| 140.0 | 7391 | 7392 | 7392 | 139.8 | -0.05 | 140.0 | 0.01 |
| 210.0 | 6715 | 6716 | 6716 | 209.6 | -0.11 | 209.8 | -0.05 |
| 280.0 | 6034 | 6032 | 6033 | 280.1 | 0.02 | 280.0 | 0.01 |
| 350.0 | 5354 | 5354 | 5354 | 350.2 | 0.05 | 350.0 | 0.00 |

(kPa) Linear Gage Factor (G): **0.1033** (kPa/ digit)  Regression Zero: **8746**

Polynomial Gage Factors: A: **-1.262E-07**  B: **-0.1015**  C: **896.9**

Thermal Factor (K): **-0.0820** (kPa/ °C)

(psi) Linear Gage Factor (G): **0.01498** (psi/ digit)

Polynomial Gage Factors: A: **-1.83039E-08**  B: **-0.01472**  C: **130.08**

Thermal Factor (K): **-0.01189** (psi/ °C)

Calculated Pressures:

$$\text{Linear, } P = G(R_0 - R_1) + K(T_1 - T_0) - (S_1 - S_0)^{**}$$

$$\text{Polynomial, } P = AR_1^2 + BR_1 + C + K(T_1 - T_0) - (S_1 - S_0)^{**}$$

†Barometric pressures are absolute. Barometric compensation is <u>not</u> required with vented and differential pressure transducers.

Factory Zero Reading:

GK-401 Pos. B or F(R_c): **8684**  Temp(T_0): **21.8** °C  †Baro(S_c): **991.3** mbar  Date: December 2, 2010

*Initial zero readings must be established in the field following the procedures described in the Instruction Manual. If the Polynomial equation is used the field value of C must be calculated by plugging the initial zero reading into the polynomial equation with the value of P set to zero.

The above instrument was found to be in tolerance in all operating ranges.
The above named instrument has been calibrated by comparison with standards traceable to the NIST, in compliance with ANSI Z540-1.
This report shall not be reproduced except in full without written permission of Geokon Inc.

195

# GEOKON
48 Spencer St. Lebanon, N.H. 03766 USA

## Vibrating Wire Pressure Transducer Calibration Report

Type: **S**

Serial Number: **1035440**

Pressure Range: **350 kPa**

Date of Calibration: **November 22, 2010**

Temperature: **24.8 °C**

†Barometric Pressure: **1002.6 mbar**

Calibration Instruction: **VW Pressure Transducers**

Technician: *[signature]*

| Applied Pressure (kPa) | Gage Reading 1st Cycle | Gage Reading 2nd Cycle | Average Gage Reading | Calculated Pressure (Linear) | Error Linear (%FS) | Calculated Pressure (Polynomial) | Error Polynomial (%FS) |
|---|---|---|---|---|---|---|---|
| 0.0 | 8734 | 8735 | 8735 | -0.086 | -0.02 | -0.045 | -0.01 |
| 70.0 | 8072 | 8072 | 8072 | 70.19 | 0.05 | 70.19 | 0.05 |
| 140.0 | 7414 | 7414 | 7414 | 140.0 | -0.01 | 140.0 | 0.00 |
| 210.0 | 6755 | 6755 | 6755 | 209.9 | -0.03 | 209.9 | -0.03 |
| 280.0 | 6094 | 6094 | 6094 | 280.0 | 0.00 | 280.0 | 0.00 |
| 350.0 | 5434 | 5433 | 5434 | 350.1 | 0.01 | 350.0 | 0.00 |

(kPa) Linear Gage Factor (G): **0.1061** (kPa/ digit)

Regression Zero: **8734**

Polynomial Gage Factors: A: **-8.580E-09**   B: **-0.1059**   C: **926.0**

Thermal Factor (K): **-0.1061** (kPa/°C)

(psi) Linear Gage Factor (G): **0.01538** (psi/ digit)

Polynomial Gage Factors: A: **-1.24439E-09**   B: **-0.01537**   C: **134.30**

Thermal Factor (K): **-0.01538** (psi/°C)

Calculated Pressures:

Linear, $P = G(R_0 - R_1) + K(T_1 - T_0) - (S_1 - S_0)$**

Polynomial, $P = AR_1^2 + BR_1 + C + K(T_1 - T_0) - (S_1 - S_0)$**

†Barometric pressures are absolute. Barometric compensation is <u>not</u> required with vented and differential pressure transducers.

Factory Zero Reading:

GK-401 Pos. B or F(R₀): **8681**   Temp(T₀): **21.9** °C   †Baro(S₀): **991.3** mbar   Date: **December 2, 2010**

*Initial zero readings must be established in the field following the procedures described in the Instruction Manual. If the Polynomial equation is used the field value of C must be calculated by plugging the initial zero reading into the polynomial equation with the value of P set to zero.

The above instrument was found to be in tolerance in all operating ranges.
The above named instrument has been calibrated by comparison with standards traceable to the NIST, in compliance with ANSI Z540-1.
This report shall not be reproduced except in full without written permission of Geokon Inc.

# GEOKON 48 Spencer St. Lebanon, N.H. 03766 USA

## Vibrating Wire Pressure Transducer Calibration Report

Type: **S**

Serial Number: **1035441**

Pressure Range: **350 kPa**

Date of Calibration: **November 22, 2010**

Temperature: **24.8 °C**

†Barometric Pressure: **1002.6 mbar**

Calibration Instruction: **VW Pressure Transducers**

Technician: *DRogers*

| Applied Pressure (kPa) | Gage Reading 1st Cycle | Gage Reading 2nd Cycle | Average Gage Reading | Calculated Pressure (Linear) | Error Linear (%FS) | Calculated Pressure (Polynomial) | Error Polynomial (%FS) |
|---|---|---|---|---|---|---|---|
| 0.0 | 8826 | 8826 | 8826 | 0.604 | 0.17 | 0.088 | -0.03 |
| 70.0 | 8216 | 8216 | 8216 | 69.70 | -0.09 | 69.80 | -0.06 |
| 140.0 | 7598 | 7598 | 7598 | 139.7 | -0.09 | 140.1 | 0.03 |
| 210.0 | 6981 | 6981 | 6981 | 209.6 | -0.12 | 210.0 | 0.00 |
| 280.0 | 6360 | 6360 | 6360 | 279.9 | -0.02 | 280.0 | 0.01 |
| 350.0 | 5737 | 5737 | 5737 | 350.5 | 0.14 | 350.0 | -0.01 |

(kPa) Linear Gage Factor (G): **0.1133** (kPa/ digit)

Regression Zero: **8831**

Polynomial Gage Factors: A: **-4.076E-07**    B: **-0.1073**    C: **979.1**

Thermal Factor (K): **-0.0452** (kPa/ °C)

---

(psi) Linear Gage Factor (G): **0.01643** (psi/ digit)

Polynomial Gage Factors: A: **-5.91199E-08**    B: **-0.01557**    C: **142.01**

Thermal Factor (K): **-0.00656** (psi/ °C)

---

Calculated Pressures:

Linear, $P = G(R_0 - R_1) + K(T_1 - T_0) - (S_1 - S_0)$**

Polynomial, $P = AR_1^2 + BR_1 + C + K(T_1 - T_0) - (S_1 - S_0)$**

†Barometric pressures are absolute. Barometric compensation is <u>not</u> required with vented and differential pressure transducers.

---

Factory Zero Reading:

GK-401 Pos. B or F(R₀): **8780**    Temp(T₀): **21.8** °C    †Baro(S₀): **991.3** mbar    Date: **December 2, 2010**

*Initial zero readings must be established in the field following the procedures described in the Instruction Manual. If the Polynomial equation is used the field value of C must be calculated by plugging the initial zero reading into the polynomial equation with the value of P set to zero.

# GEOKON 48 Spencer St. Lebanon, N.H. 03766 USA

## Vibrating Wire Pressure Transducer Calibration Report

| | | | |
|---|---|---|---|
| Type: | S | Date of Calibration: | November 22, 2010 |
| Serial Number: | 1035442 | Temperature: | 24.8 °C |
| Pressure Range: | 350 kPa | †Barometric Pressure: | 1002.6 mbar |
| | | Calibration Instruction: | VW Pressure Transducers |
| | | Technician: | K.Rogers |

| Applied Pressure (kPa) | Gage Reading 1st Cycle | Gage Reading 2nd Cycle | Average Gage Reading | Calculated Pressure (Linear) | Error Linear (%FS) | Calculated Pressure (Polynomial) | Error Polynomial (%FS) |
|---|---|---|---|---|---|---|---|
| 0.0 | 8715 | 8716 | 8716 | 0.489 | 0.14 | 0.111 | 0.03 |
| 70.0 | 8100 | 8101 | 8101 | 69.83 | -0.05 | 69.98 | -0.01 |
| 140.0 | 7482 | 7482 | 7482 | 139.6 | -0.12 | 139.9 | -0.02 |
| 210.0 | 6859 | 6859 | 6859 | 209.8 | -0.05 | 210.2 | 0.05 |
| 280.0 | 6238 | 6238 | 6238 | 279.8 | -0.04 | 279.9 | -0.02 |
| 350.0 | 5612 | 5612 | 5612 | 350.4 | 0.12 | 350.0 | 0.00 |

(kPa) Linear Gage Factor (G): 0.1128 (kPa/ digit)          Regression Zero: 8720

Polynomial Gage Factors:   A: -3.396E-07      B: -0.1079      C: 966.2

Thermal Factor (K): -0.0460 (kPa/ °C)

---

(psi) Linear Gage Factor (G): 0.01635 (psi/ digit)

Polynomial Gage Factors:   A: -4.92549E-08      B: -0.01565      C: 140.13

Thermal Factor (K): -0.00667 (psi/ °C)

---

Calculated Pressures:       Linear, $P = G(R_0 - R_1) + K(T_1 - T_0) - (S_1 - S_0)**$

Polynomial, $P = AR_1^2 + BR_1 + C + K(T_1 - T_0) - (S_1 - S_0)**$

†Barometric pressures are absolute. Barometric compensation is not required with vented and differential pressure transducers.

---

Factory Zero Reading:

GK-401 Pos. B or F(R₀): 8662      Temp(T₀): 22.1 °C      †Baro(S₀): 991.3 mbar      Date: December 2, 2010

*Initial zero readings must be established in the field following the procedures described in the Instruction Manual. If the Polynomial equation is used the field value of C must be calculated by plugging the initial zero reading into the polynomial equation with the value of P set to zero.

# GEOKON 48 Spencer St. Lebanon, N.H. 03766 USA

## Vibrating Wire Pressure Transducer Calibration Report

Type: S

Serial Number: 1035443

Pressure Range: 350 kPa

Date of Calibration: November 22, 2010

Temperature: 24.8 °C

†Barometric Pressure: 1002.6 mbar

Calibration Instruction: VW Pressure Transducers

Technician: _KRogers_

| Applied Pressure (kPa) | Gage Reading 1st Cycle | Gage Reading 2nd Cycle | Average Gage Reading | Calculated Pressure (Linear) | Error Linear (%FS) | Calculated Pressure (Polynomial) | Error Polynomial (%FS) |
|---|---|---|---|---|---|---|---|
| 0.0 | 8794 | 8793 | 8794 | 0.070 | 0.02 | -0.026 | -0.01 |
| 70.0 | 8132 | 8131 | 8132 | 69.89 | -0.03 | 69.85 | -0.04 |
| 140.0 | 7466 | 7466 | 7466 | 140.1 | 0.02 | 140.1 | 0.03 |
| 210.0 | 6803 | 6804 | 6804 | 210.0 | -0.01 | 210.0 | 0.01 |
| 280.0 | 6140 | 6140 | 6140 | 279.9 | -0.02 | 279.9 | -0.02 |
| 350.0 | 5475 | 5475 | 5475 | 350.1 | 0.02 | 350.0 | 0.01 |

(kPa) Linear Gage Factor (G): 0.1055 (kPa/ digit)     Regression Zero: 8794

Polynomial Gage Factors:     A: -2.990E-08     B: -0.1050     C: 926.0

Thermal Factor (K): -0.0840 (kPa/ °C)

(psi) Linear Gage Factor (G): 0.01530 (psi/ digit)

Polynomial Gage Factors:     A: -4.33666E-09     B: -0.01524     C: 134.31

Thermal Factor (K): -0.01219 (psi/ °C)

Calculated Pressures:     Linear, $P = G(R_0 - R_1) + K(T_1 - T_0) - (S_1 - S_0)$**

Polynomial, $P = AR_1^2 + BR_1 + C + K(T_1 - T_0) - (S_1 - S_0)$**

†Barometric pressures are absolute. Barometric compensation is not required with vented and differential pressure transducers.

**Factory Zero Reading:**

GK-401 Pos. B or F($R_0$): 8734     Temp($T_0$): 21.9 °C     †Baro($S_0$): 991.3 mbar     Date: December 2, 2010

*Initial zero readings must be established in the field following the procedures described in the Instruction Manual. If the Polynomial equation is used the field value of C must be calculated by plugging the initial zero reading into the polynomial equation with the value of P set to zero.

199

# GEOKON 48 Spencer St. Lebanon, N.H. 03766 USA

## Vibrating Wire Pressure Transducer Calibration Report

Type: ___S___

Serial Number: ___1035444___

Pressure Range: ___350 kPa___

Date of Calibration: ___November 22, 2010___

Temperature: ___24.8 °C___

†Barometric Pressure: ___1002.6 mbar___

Calibration Instruction: ___VW Pressure Transducers___

Technician: _~~KRogers~~_

| Applied Pressure (kPa) | Gage Reading 1st Cycle | Gage Reading 2nd Cycle | Average Gage Reading | Calculated Pressure (Linear) | Error Linear (%FS) | Calculated Pressure (Polynomial) | Error Polynomial (%FS) |
|---|---|---|---|---|---|---|---|
| 0.0 | 8581 | 8581 | 8581 | -0.309 | -0.09 | 0.041 | 0.01 |
| 70.0 | 8018 | 8018 | 8018 | 70.00 | 0.00 | 69.93 | -0.02 |
| 140.0 | 7455 | 7455 | 7455 | 140.3 | 0.09 | 140.0 | 0.01 |
| 210.0 | 6895 | 6895 | 6895 | 210.2 | 0.07 | 210.0 | -0.01 |
| 280.0 | 6335 | 6335 | 6335 | 280.2 | 0.05 | 280.1 | 0.03 |
| 350.0 | 5779 | 5779 | 5779 | 349.6 | -0.11 | 349.9 | -0.01 |

(kPa) Linear Gage Factor (G): ___0.1249___ (kPa/ digit)

Polynomial Gage Factors: A: ___3.335E-07___ B: ___-0.1297___ C: ___1088.2___

Regression Zero: ___8579___

Thermal Factor (K): ___-0.0638___ (kPa/ °C)

(psi) Linear Gage Factor (G): ___0.01811___ (psi/ digit)

Polynomial Gage Factors: A: ___4.83761E-08___ B: ___-0.01881___ C: ___157.83___

Thermal Factor (K): ___-0.00925___ (psi/ °C)

Calculated Pressures:

Linear, $P = G(R_0 - R_1) + K(T_1 - T_0) - (S_1 - S_0)$**

Polynomial, $P = AR_1^2 + BR_1 + C + K(T_1 - T_0) - (S_1 - S_0)$**

†Barometric pressures are absolute. Barometric compensation is <u>not</u> required with vented and differential pressure transducers.

Factory Zero Reading:

GK-401 Pos. B or F(R$_c$): ___8538___ Temp(T$_0$): ___22.1___ °C †Baro(S$_c$): ___991.3___ mbar Date: ___December 2, 2010___

*Initial zero readings must be established in the field following the procedures described in the Instruction Manual. If the Polynomial equation is used the field value of C must be calculated by plugging the initial zero reading into the polynomial equation with the value of P set to zero.

# GEOKON
48 Spencer St. Lebanon, N.H. 03766 USA

# Vibrating Wire Displacement Transducer Calibration Report

Range: 100 mm

Serial Number: 1029568

Calibration Date: November 19, 2010

Temperature: 24.9 °C

Calibration Instruction: CI-4400

Technician: *Elice*

GK-401 Reading Position B

| Actual Displacement (mm) | Gage Reading 1st Cycle | Gage Reading 2nd Cycle | Average Gage Reading | Calculated Displacement (Linear) | Error Linear (%FS) | Calculated Displacement (Polynomial) | Error Polynomial (%FS) |
|---|---|---|---|---|---|---|---|
| 0.0 | 2710 | 2710 | 2710 | -0.21 | -0.21 | -0.01 | -0.01 |
| 20.0 | 3739 | 3740 | 3740 | 20.06 | 0.06 | 20.01 | 0.01 |
| 40.0 | 4762 | 4760 | 4761 | 40.17 | 0.17 | 40.00 | 0.00 |
| 60.0 | 5777 | 5776 | 5777 | 60.16 | 0.16 | 60.00 | 0.00 |
| 80.0 | 6786 | 6784 | 6785 | 80.02 | 0.02 | 79.98 | -0.02 |
| 100.0 | 7791 | 7789 | 7790 | 99.81 | -0.19 | 100.01 | 0.01 |

(mm) Linear Gage Factor (G): 0.01969 (mm/ digit)      Regression Zero: 2721

Polynomial Gage Factors:      A: 5.94602E-08      B: 0.01906      C: -52.111

(inches) Linear Gage Factor (G): 0.0007752 (inches/ digit)

Polynomial Gage Factors:      A: 2.34095E-09      B: 0.0007506      C: -2.0516

Calculated Displacement:      Linear, $D = G(R_1 - R_0)$

Polynomial, $D = AR_1^2 + BR_1 + C$

Refer to manual for temperature correction information.

**Function Test at Shipment:**

GK-401 Pos. B : 2752      Temp($T_0$): 20.5 °C      Date: December 9, 2010

The above instrument was found to be in tolerance in all operating ranges.
The above named instrument has been calibrated by comparison with standards traceable to the NIST, in compliance with ANSI Z540-1.
This report shall not be reproduced except in full without written permission of Geokon Inc.

201

# GEOKON

48 Spencer St. Lebanon, N.H. 03766 USA

## Vibrating Wire Displacement Transducer Calibration Report

Range: 100 mm

Serial Number: 1029569

Calibration Date: November 19, 2010

Temperature: 24.9 °C

Calibration Instruction: CI-4400

Technician: _Elice_

GK-401 Reading Position B

| Actual Displacement (mm) | Gage Reading 1st Cycle | Gage Reading 2nd Cycle | Average Gage Reading | Calculated Displacement (Linear) | Error Linear (%FS) | Calculated Displacement (Polynomial) | Error Polynomial (%FS) |
|---|---|---|---|---|---|---|---|
| 0.0 | 2646 | 2644 | 2645 | -0.22 | -0.22 | -0.01 | -0.01 |
| 20.0 | 3681 | 3680 | 3681 | 20.05 | 0.05 | 20.01 | 0.01 |
| 40.0 | 4710 | 4709 | 4710 | 40.19 | 0.19 | 40.02 | 0.02 |
| 60.0 | 5730 | 5728 | 5729 | 60.14 | 0.14 | 59.98 | -0.02 |
| 80.0 | 6745 | 6745 | 6745 | 80.03 | 0.03 | 79.99 | -0.01 |
| 100.0 | 7756 | 7755 | 7756 | 99.80 | -0.20 | 100.01 | 0.01 |

(mm) Linear Gage Factor (G): 0.01957 (mm/ digit)     Regression Zero: 2656

Polynomial Gage Factors:     A: 5.92391E-08     B: 0.01896     C: -50.561

(inches) Linear Gage Factor (G): 0.0007705 (inches/ digit)

Polynomial Gage Factors:     A: 2.33225E-09     B: 0.0007463     C: -1.9906

Calculated Displacement:     Linear, $D = G(R_1 - R_0)$

Polynomial, $D = AR_1^2 + BR_1 + C$

Refer to manual for temperature correction information.

Function Test at Shipment:

GK-401 Pos. B : 2733     Temp($T_0$): 20.8 °C     Date: December 9, 2010

The above instrument was found to be in tolerance in all operating ranges.
The above named instrument has been calibrated by comparison with standards traceable to the NIST, in compliance with ANSI Z540-1.
This report shall not be reproduced except in full without written permission of Geokon Inc.

# GEOKON

48 Spencer St. Lebanon, N.H. 03766 USA

## Vibrating Wire Displacement Transducer Calibration Report

Range: 100 mm

Serial Number: 1029570

Calibration Date: November 19, 2010

Temperature: 24.9 °C

Calibration Instruction: CI-4400

Technician: *Elise*

GK-401 Reading Position B

| Actual Displacement (mm) | Gage Reading 1st Cycle | Gage Reading 2nd Cycle | Average Gage Reading | Calculated Displacement (Linear) | Error Linear (%FS) | Calculated Displacement (Polynomial) | Error Polynomial (%FS) |
|---|---|---|---|---|---|---|---|
| 0.0 | 2681 | 2678 | 2680 | -0.19 | -0.19 | 0.00 | 0.00 |
| 20.0 | 3707 | 3705 | 3706 | 20.02 | 0.02 | 19.98 | -0.02 |
| 40.0 | 4731 | 4730 | 4731 | 40.19 | 0.19 | 40.04 | 0.04 |
| 60.0 | 5744 | 5743 | 5744 | 60.14 | 0.14 | 59.99 | -0.01 |
| 80.0 | 6755 | 6751 | 6753 | 80.02 | 0.02 | 79.98 | -0.02 |
| 100.0 | 7758 | 7758 | 7758 | 99.81 | -0.19 | 100.01 | 0.01 |

(mm) Linear Gage Factor (G): 0.01969 (mm/ digit)   Regression Zero: 2689

Polynomial Gage Factors: A: 5.71046E-08    B: 0.01910    C: -51.575

(inches) Linear Gage Factor (G): 0.0007753 (inches/ digit)

Polynomial Gage Factors: A: 2.24821E-09    B: 0.0007518    C: -2.0305

Calculated Displacement:

Linear, $D = G(R_1 - R_0)$

Polynomial, $D = AR_1^2 + BR_1 + C$

Refer to manual for temperature correction information.

**Function Test at Shipment:**

GK-401 Pos. B : 2740    Temp($T_0$): 20.3 °C    Date: December 9, 2010

The above instrument was found to be in tolerance in all operating ranges.
The above named instrument has been calibrated by comparison with standards traceable to the NIST, in compliance with ANSI Z540-1.
This report shall not be reproduced except in full without written permission of Geokon Inc.

# GEOKON
48 Spencer St. Lebanon, N.H. 03766 USA

# Vibrating Wire Displacement Transducer Calibration Report

Range: 100 mm

Serial Number: 1029571

Calibration Date: November 19, 2010

Temperature: 24.9 °C

Calibration Instruction: CI-4400

Technician: *Elice*

GK-401 Reading Position B

| Actual Displacement (mm) | Gage Reading 1st Cycle | Gage Reading 2nd Cycle | Average Gage Reading | Calculated Displacement (Linear) | Error Linear (%FS) | Calculated Displacement (Polynomial) | Error Polynomial (%FS) |
|---|---|---|---|---|---|---|---|
| 0.0 | 2624 | 2624 | 2624 | -0.19 | -0.19 | -0.01 | -0.01 |
| 20.0 | 3651 | 3650 | 3651 | 20.08 | 0.08 | 20.04 | 0.04 |
| 40.0 | 4666 | 4660 | 4663 | 40.07 | 0.07 | 39.92 | -0.08 |
| 60.0 | 5681 | 5683 | 5682 | 60.18 | 0.18 | 60.04 | 0.04 |
| 80.0 | 6688 | 6688 | 6688 | 80.04 | 0.04 | 80.01 | 0.01 |
| 100.0 | 7690 | 7689 | 7690 | 99.81 | -0.19 | 99.99 | -0.01 |

(mm) Linear Gage Factor (G): 0.01974 (mm/ digit)   Regression Zero: 2633

Polynomial Gage Factors:   A: 5.18712E-08   B: 0.01921   C: -50.760

(inches) Linear Gage Factor (G): 0.0007772 (inches/ digit)

Polynomial Gage Factors:   A: 2.04217E-09   B: 0.0007561   C: -1.9984

Calculated Displacement:   Linear, $D = G(R_1 - R_0)$

Polynomial, $D = AR_1^2 + BR_1 + C$

Refer to manual for temperature correction information.

Function Test at Shipment:

GK-401 Pos. B : 2700   Temp($T_0$): 20.4 °C   Date: December 9, 2010

# GEOKON
48 Spencer St. Lebanon, N.H. 03766 USA

## Vibrating Wire Displacement Transducer Calibration Report

Range: 100 mm

Serial Number: 1029572

Calibration Date: November 19, 2010

Temperature: 24.9 °C

Calibration Instruction: CI-4400

Technician: *Elica*

GK-401 Reading Position B

| Actual Displacement (mm) | Gage Reading 1st Cycle | Gage Reading 2nd Cycle | Average Gage Reading | Calculated Displacement (Linear) | Error Linear (%FS) | Calculated Displacement (Polynomial) | Error Polynomial (%FS) |
|---|---|---|---|---|---|---|---|
| 0.0 | 2640 | 2638 | 2639 | -0.25 | -0.25 | -0.02 | -0.02 |
| 20.0 | 3672 | 3671 | 3672 | 20.06 | 0.06 | 20.02 | 0.02 |
| 40.0 | 4697 | 4696 | 4697 | 40.23 | 0.23 | 40.04 | 0.04 |
| 60.0 | 5709 | 5707 | 5708 | 60.12 | 0.12 | 59.94 | -0.06 |
| 80.0 | 6723 | 6719 | 6721 | 80.05 | 0.05 | 80.01 | 0.01 |
| 100.0 | 7727 | 7721 | 7724 | 99.78 | -0.22 | 100.01 | 0.01 |

(mm) Linear Gage Factor (G): 0.01967 (mm/ digit)        Regression Zero: 2652

Polynomial Gage Factors:    A: 6.64311E-08        B: 0.01898        C: -50.573

(inches) Linear Gage Factor (G): 0.0007744 (inches/ digit)

Polynomial Gage Factors:    A: 2.6154E-09        B: 0.0007473        C: -1.9911

Calculated Displacement:        Linear, $D = G(R_1 - R_0)$

Polynomial, $D = AR_1^2 + BR_1 + C$

Refer to manual for temperature correction information.

Function Test at Shipment:

GK-401 Pos. B: 2759        Temp($T_0$): 20.5 °C        Date: December 9, 2010

The above instrument was found to be in tolerance in all operating ranges.
The above named instrument has been calibrated by comparison with standards traceable to the NIST, in compliance with ANSI Z540-1.
This report shall not be reproduced except in full without written permission of Geokon Inc.

# GEOKON

48 Spencer St. Lebanon, N.H. 03766 USA

## Vibrating Wire Displacement Transducer Calibration Report

Range: 100 mm

Serial Number: 1029573

Calibration Date: November 19, 2010

Temperature: 24.9 °C

Calibration Instruction: CI-4400

Technician: *Elice*

GK-401 Reading Position B

| Actual Displacement (mm) | Gage Reading 1st Cycle | Gage Reading 2nd Cycle | Average Gage Reading | Calculated Displacement (Linear) | Error Linear (%FS) | Calculated Displacement (Polynomial) | Error Polynomial (%FS) |
|---|---|---|---|---|---|---|---|
| 0.0 | 2628 | 2625 | 2627 | -0.17 | -0.17 | -0.03 | -0.03 |
| 20.0 | 3658 | 3657 | 3658 | 20.08 | 0.08 | 20.05 | 0.05 |
| 40.0 | 4678 | 4676 | 4677 | 40.11 | 0.11 | 40.00 | 0.00 |
| 60.0 | 5696 | 5694 | 5695 | 60.11 | 0.11 | 60.00 | 0.00 |
| 80.0 | 6708 | 6706 | 6707 | 79.99 | -0.01 | 79.96 | -0.04 |
| 100.0 | 7720 | 7720 | 7720 | 99.89 | -0.11 | 100.03 | 0.03 |

(mm) Linear Gage Factor (G): 0.01964 (mm/digit)     Regression Zero: 2635

Polynomial Gage Factors:     A: 4.06152E-08     B: 0.01922     C: -50.801

(inches) Linear Gage Factor (G): 0.0007734 (inches/digit)

Polynomial Gage Factors:     A: 1.59902E-09     B: 0.0007568     C: -2.0000

Calculated Displacement:     Linear, $D = G(R_1 - R_0)$

Polynomial, $D = AR_1^2 + BR_1 + C$

Refer to manual for temperature correction information.

**Function Test at Shipment:**

GK-401 Pos. B: 2751     Temp($T_0$): 20.4 °C     Date: December 9, 2010

Acronyms and Abbreviations

ASCE – American Society of Civil Engineers

ASTM – American Society for Testing and Materials

AWWA – American Water Works Association

BWCCP – Bar-Wrap Concrete Cylinder Pipe

CD – Consolidated Drained

CLSM – Controlled Low Strength Material

CUIRE – Center for Underground Infrastructure Research and Education

DI – Ductile Iron

DWU – Dallas Water Utilities

EPC – Earth Pressure Cell

FEA – Finite Element Analysis

FEM – Finite Element Models

GRP – Glassfiber Reinforced Pipe

HDPE – High Density Polyethylene

IPL – Integrated Pipeline

MDD – Maximum Dry Density

MGD – Millions Gallons per Day

NWP – Northwest Pipe Company

OD – Outside Diameter

OMC – Optimum Moisture Content

PCCP – Pre-stressed Concrete Cylinder Pipe

PVC – Polyvinyl Chloride

RCP – Reinforced Concrete Pipe

SP – Steel Pipe

TRWD – Tarrant Regional Water District

UTA – The University of Texas at Arlington

VCP – Vitrified Clay Pipe

VE – Value Engineering

References

American Water Works Association (AWWA M11). (2004). "Steel Water Pipe: A Guide for Design and Installation (M11), Fourth Edition." American Water Works Association, Denver, CO.

Basudhar, P. K. and Madhav, M. R. (1980). "Simplified Passive Earth Pressure Analysis." *Journal of Geotechnical Division.* ASCE. 106 (4). 470-474.

Brooker, E. W., and Ireland, H. O. (1965). "Earth pressures at rest related to stress history." *Can. Geotech. J.*, 2 (1), 1–15.

Das, B. M. (2004). *Principles of Foundation Engineering Seventh Edition.* Global Engineering. 978-0-495-66810-7.

Drucker, D. C., Prager, W. (1952). "Soil mechanics and plastic analysis or limit design." *Quart. Appl. Math.* 10. 157-165.

Duncan, J. M., Byrne, P., Wong, K. S., Marby, P. (1980). "Strength, Stress-Strain and Bulk Modulus Parameters for Finite Element Analysis of Stresses and Movements in Soil Masses." *University of California, College of Engineering, Berkeley, California.* Report No. UCB/GT/80-1.

Greenwood, M. E. and Lang, D. C. (1990). "Vertical Deflection of Buried Flexible Pipes." *Buried Plastic Pipe Technology, ASTM STP 1093.* American Society of Testing and Materials. Philadelphia, Pa.

Hartley, J. D., and Duncan, J. M. (1987). "E prime and its variation with Depth." *J. Transp. Eng.,* 113(5), 538-553.

Howard, A. K. (1973). "Laboratory Load Tests on Buried Flexible Pipe Progress Report No. 5." July 1973. Bureau of Reclamation, Denver, Colorado.

Howard, A. K. (1976). "Modulus of Soil Reaction (E') Values for Buried Flexible Pipe." *Transportation Research Board, Session 57.*

Howard, A. K. (1996). "Pipeline Installation: A Manual for Construction of Buried Pipe." Relativity Publishing, Lakewood, CO.

Howard, A. K. (2006). "The Reclamation E' Table, 25 Years Later." *Plastics Pipe XIII International Conference.* Washington, D.C.

Hsieh, P. G., Ou, C. Y., and Lim, A. (2010). "Use of the total stress undrained model to the analysis of deep excavation." *Proceedings of the 17th Southeast Asian Geotechnical Conference*, Taipei, Taiwan.

Ingold, T.S. (1980). "Lateral Earth Pressures – A Reconsideration." *Ground Engineering*, 13 (4), 39–43.

Jaky, J. (1944). "The coefficient of earth pressure at rest." *J. Soc. Hung. Eng. Arch.*, 355–358.

Janbu, N. (1957). "Earth Pressures and Bearing Capacity Calculation by Generalized Procedure of Slices." *Proceedings of 4th International Conference on Soil Mechanics and Foundation Engineering.* 2. 207-212.

Kawabata, T., Mohri, Y., Tamura, H., Shoda, D. and Oda, T. (2006). "Field Test for Buried Large Steel Pipes with Thin Wall." *ASCE Pipelines 2006: Service to the Owner,* Chicago, IL, 1-8.

Logan, D. (2012). "A First Course in Finite Element Analysis." Global Engineering, Stamford, CT.

Marston, A. and Anderson, A. O. (1913). "The Theory of Loads on Pipes in Ditches and Tests of Cement and Clay Drain Tile and Sewer Pipe." *Bulletin 31. Ames: Iowa Engineering Experiment Station.*

Masada, T. (2000). "Modified Iowa Formula for Vertical Deflection of Buried Flexible Pipe." *Journal of Transportation Engineering.* ASCE, Reston, Va. 126 (5). 440 – 446.

Masada, T. and Sargand, S. M. (2007). "Peaking Deflections of Flexible Pipe during Initial Backfilling Process." *Journal of Transportation Engineering.* ASCE, Reston, Va. 133 (2). 105 – 111.

McKelvey III, J. A. I. (1994). "Anatomy of Soil Arching." *Geotextiles and Geomembranes.* Elsevier Applied Science. Oxford, Engl. 13 (5). 317-329.

Michalowski, R. L. (2005). "Coefficient of Earth Pressure at Rest." *Journal of Geotechnical and Geoenvironmental Engineering.* 131 (11). 1429-1433.

Miles, R. W. and Schrock, B. J. (1998). "Integrated Design Procedure for Flexible Pipe." *Proceedings of the 1998 Pipeline Division Conference.* ASCE, Reston, Va. 1 – 13.

Moser, A. P. (2001). "Buried Pipe Design*."* Third Edition, McGraw-Hill Professional, New York.

Najafi, M. (2010). "Trenchless Technology Piping: Installation and Inspection." McGraw-Hill Professional, New York. ISBN 978-0-07-148928-7.

Peurifoy, R. L., Schexnayder, C. J., Shapira, A., Schmitt, R. L. (2005). *Construction Planning, Equipment, and Methods, Seventh Edition.* McGraw-Hill, New York. 0072964200.

PLAXIS. (2012). "Plaxis 2D Reference Manual." http://www.plaxis.nl/shop/135/info/manuals/. Date Accessed: 3/3/2012.

Popa, H. and Batali, L. (2010). "Finite Element Method in Geotechnical Design. Soil Constitutive laws and Calibration of the Parameters. Retaining Wall Case Study." WSEAS *Transactions on Applied and Theoretical Mechanics.* 5 (3). 177-186.

Robinson, L. (1982). "Lateral Earth Pressure Determination in Cohesive Soils." *Proceedings of the Annual Engineering Geology and Soils Engineering Symposium.* Pocatello, Idaho. 217-229.

Roscoe K.H., Schofield A. N., Thurairajah A. (1963). "Yielding of clays in states wetter than critical." *Geotechnique.* 13. 211–240.

Roscoe K. H., Burland J. B. (1968). "On the generalized stress–strain behavior of 'wet clay'." *Engineering Plasticity, Heyman J, Leckie FA (eds). Cambridge University Press: Cambridge.* 1968; 535–609.

Schanz, T., Vermeer, P. A., and Bonnier, P. G. (1999). "The hardening soil model: Formulation and verification." *Beyond 2000 in Computational Geotechnics – 10 years PLAXIS*. Balkema, Rotterdam.

Selig, E. T. (1988). "Soil Parameters for Design of Buried Pipelines." *Proceedings of Pipeline Infrastructure.* New York, NY. 99 – 116.

Sharma, J., Najafi, M., Marshall, D., and Jain, A. (2012). "Evaluation of Statically-Loaded Large Diameter Steel Pipe Embedded with Lime Stabilized Native Clay Soils". Pipelines 2012: pp. 242-256.

Shields, D. H. and Tolunay, A. Z. (1973). "Passive Pressure Coefficients Predicted by Method of Slices." *Journal of the Soil Mechanics and Foundation Divisions.* ASCE. 99 (12) 1043-1053.

Spangler, M. G. (1941). "The structural design of flexible pipe culverts." *Iowa State Coll. Bull.*, XL (30).

Talesnick, M. and Baker, R. (1999). "Investigation of the Failure of a Concrete-lined Steel Pipe." *Journal of Geotechnical and Geological Engineering.* 17. Kluwer Academic Publishers, Netherlands. 99-121.

Vermeer P. (1982). "A Five Constant Model Unifying Well Established Concepts." *International workshop on Constitutive Behavior of Soils.* Grenoble. 175-197.

Webb, M. C., Trebicki, D. D. P., Smulders, P. A. (2002). "Field Testing and Buckling Strength of Buried Large-Diameter Thin-Walled Steel Pipes." *Proceedings of ASCE Pipelines 2002- Beneath Our Feet: Challengers and Solutions. ASC*E, Reston, VA. 69-103.

Biographical Information

Jwala Raj Sharma completed his Bachelor's Degree in Civil Engineering from Institute of Engineering, Tribhuvan University in Kathmandu, Nepal. He completed MS in Civil Engineering at the University of Texas at Arlington (UT Arlington) in Spring 2010 and continued on to Doctoral program since Fall 2010. During his time at UT Arlington, he contributed to numerous researches, and published one journal paper and presented several refereed conference papers.